Effects of the feeding functional response on phytoplankton diversity and ecosystem functioning in ecosystem models

Dissertation

zur Erlangung des Doktorgrades

der Mathematisch-Naturwissenschaftlichen Fakultät

der Christian-Albrechts-Universität

zu Kiel

vorgelegt von

Friederike Prowe

Kiel, 2011

Referent:	Prof. Dr. Andreas Oschlies
Korreferentin:	Prof. Dr. Birgit Schneider
Tag der mündlichen Prüfung:	19.12.2011
Zum Druck genehmigt:	19.12.2011
	gez. Prof. Dr. Lutz Kipp, Dekan

Contents

Summary

Ocean ecosystems are under pressure from the needs of a growing human population and from global environmental change. A concurrent loss of diversity observed across ecosystems raises the question of how diversity influences ecological and biogeochemical processes of ecosystems. Little is known about controls of diversity and its role in shaping ecosystem processes in the global pelagic ocean and biogeochemical cycles of nutrients and carbon. Bottom-up controls by nutrient availability and use have previously been investigated using a novel global ecosystem model which resolves phytoplankton diversity. Top-down effects of zooplankton feeding as an important mechanism able to promote diversity have not yet been investigated on the global scale. Also, the influence of diversity on primary production and other indicators of ecosystem functioning in the global ocean are not well understood. The present thesis aims to extend our understanding of how zooplankton feeding influences phytoplankton diversity in ecosystem models. In addition, it addresses the question of how diversity may influence ecosystem functioning and biogeochemical cycling.

The first part of the thesis examines the top-down control of zooplankton feeding on phytoplankton diversity in a global ocean ecosystem model with a self-assembling phytoplankton community. In simulations with different mathematical formulations for feeding, phytoplankton diversity differs by more than a factor of three. A sigmoidal Holling type 3 functional response implying preferential grazing on the most abundant prey creates refuges for phytoplankton at low abundances and punishes dominant types. The resulting seasonal succession is in better agreement with observations than for a type 2 functional response without preferential grazing. Simulations with different diversity also differ in primary production and net community production on the annual scale.

The second part investigates the effects of phytoplankton diversity on primary production as a basic ecosystem function in the pelagic ocean. Global simulations with different levels of diversity are complemented by idealised simulations without environmental forcing. A positive relationship between diversity and productivity is found for simulations using type 3 feeding. In these simulations, the phytoplankton community is characterised by a complementary use of resources. Higher diversity increases primary production only in temperate, but not in oligotrophic oceanic regions, indicating a potentially important influence of the nutrient supply. No effect of diversity on primary production can be identified for a type 2 feeding functional response.

The sensitivity of the simulated diversity to the feeding formulation motivates the development of an alternative zooplankton feeding model presented in the third part of this thesis. The commonly employed functional responses used in the previous parts are simplistic with regard to the feeding process and to the zooplankton community structure in the ocean. The model presented here addresses the first aspect

by taking into account metabolic constraints on the feeding process. Energy obtained from predation is optimally allocated between foraging activity and the assimilation of food to maximise net growth. The model captures experimental feeding data for different zooplankton taxa. It provides an alternative approach for representing plankton dynamics in a seasonally stratified mixed layer without an otherwise required shift in community structure.

The fourth part of this thesis complements the main model-based focus of zooplankton feeding and diversity with an experimental approach addressing the impact of feeding within a community. This study investigates herbivorous and carnivorous feeding relationships with a sea-ice community as a model system. It presents grazing experiments using natural communities of different algal taxa instead of individual predator-prey combinations, as well as predation experiments. The experiments reveal complex feeding relationships and estimate the feeding impact of sea-ice meiofauna on the sea-ice community. Similar experiments for plankton would provide valuable information for enhancing our understanding of feeding in a community context and ultimately help in developing future zooplankton feeding models.

The different aspects of zooplankton feeding and phytoplankton diversity addressed in this study demonstrate the influence of top-down controls on diversity, and indicate consequences for ecosystem functioning and biogeochemical cycling. A better understanding and representation of the complex feeding processes in the plankton will enhance our ability to model diversity in the pelagic ocean. Resolving diversity may be an important component in predicting biogeochemical cycling in a future ocean.

Zusammenfassung

Die Ökosysteme im Ozean stehen unter dem Druck einer wachsenden Weltbevölkerung und des globalen Wandels. Mit dem einhergehenden Verlust von Diversität, der in verschiedensten Ökosystemen beobachtet wird, stellt sich die Frage nach dem Einfluss von Diversität auf ökologische und biogeochemische Prozesse in Ökosystemen. Im globalen pelagischen Ozean ist wenig darüber bekannt, welche Mechanismen Diversität bedingen und welche Rolle Diversität für die Prozesse innerhalb eines Ökosystems und die biogeochemischen Nährstoff- und Kohlenstoffkreisläufe spielt. Der Einfluss von Nährstoffverfügbarkeit und -nutzung wurde in früheren Studien mit Hilfe eines neuartigen globalen Ökosystemmodells untersucht, das die Diversität des Phytoplanktons auflöst. Wie sich Zooplanktonfraß in diesem Rahmen auf Diversität auswirkt, ist bisher noch nicht untersucht worden. Ebenso ist unklar, welchen Einfluss Diversität auf die Primärproduktion und andere Indikatoren für die Ökosystemfunktion im globalen Ozean hat. Diese Studie erweitert unser Verständnis davon, wie Zooplanktonfraß die Diversität von Phytoplankton in marinen Ökosystemen bedingt. Sie wendet sich auch der Frage zu, wie Diversität die Ökosystemfunktion und die biogeochemischen Kreisläufe im Meer beeinflusst.

Der erste Teil dieser Arbeit untersucht die Wirkung von Zooplanktonfraß auf die Phytoplanktondiversität in einem globalen Ökosystemmodell für den Ozean, in dem sich die Phytoplanktongemeinschaft selbstständig zusammenfindet. In Simulationen mit verschiedenen mathematischen Funktionen für die Nahrungsaufnahme unterscheidet sich die Phytoplanktondiversität um mehr als das Dreifache. Eine sigmoide funktionelle Reaktion vom Typ Holling 3, die bevorzugtes Fressen auf den häufigsten Beutearten beinhaltet, vermindert den Wegfraß seltenerer Phytoplanktongruppen und verstärkt den Fraßdruck auf häufigere Gruppen. Die dadurch simulierte saisonale Sukzession stimmt besser mit Beobachtungen überein als dies mit einer Holling 2-Funktion der Fall ist. Simulationen mit unterschiedlicher Diversität unterscheiden sich auch im Hinblick auf die jährliche Primärproduktion und die Nettoökosystemproduktion.

Der zweite Teil untersucht den Einfluss von Phytoplanktondiversität auf Primärproduktion als grundlegende Funktion des pelagischen Ökosystems im Ozean. Globale Simulationen mit verschiedenen Diversitäten werden durch idealisierte Simulationen ohne Berücksichtigung von Umwelteinflüssen ergänzt. Eine Zunahme von Produktivität mit Diversität zeigt sich in Simulationen, die eine Fraßfunktion vom Typ 3 benutzen. In diesen Simulationen zeichnet sich die Phytoplanktongemeinschaft durch komplementäre Resourcennutzung aus. Höhere Diversität führt nur in gemäßigten Breiten, jedoch nicht in oligotrophen Gebieten, zu höherer Primärproduktion, was auf einen potentiell wichtigen Einfluss des Nährstoffeintrags hinweist. Wird eine Fraßfunktion vom Typ 2 verwendet, ist kein Effekt von Diversität auf Produktivität erkennbar.

Die Sensitivität der simulierten Diversität gegenüber der Fraßfunktion regt die Entwicklung des alternativen Fraßmodells für Zooplankton an, das im dritten Teil der Arbeit vorgestellt wird. Die häufig verwendeten Fraßfunktionen, die in den vorhergehenden Teilen eingesetzt wurden, sind stark vereinfacht im Hinblick auf den Prädationsprozess und die Struktur der Zooplanktongemeinschaft im Ozean. Das hier beschriebene Modell bezieht sich auf ersteren Aspekt, indem es den Metabolismus mit einbezieht. Die durch Nahrungsaufnahme erhaltene Energie wird zur Optimierung des Nettowachstums zwischen Nahrungssuche und Nahrungsassimilierung aufgeteilt. Das Modell kann experimentelle Daten für verschiedene Zooplanktontaxa nachvollziehen. Es bietet einen alternativen Ansatz, die Dynamik von Planktongemeinschaften in einer saisonal geschichteten Deckschicht darzustellen, ohne eine sonst notwendige Änderung der Struktur der Zooplanktongemeinschaft anzunehmen.

Der vierte Teil dieser Arbeit ergänzt den zentralen, modellbasierten Fokus von Zooplanktonfraß und Diversität um einen experimentellen Ansatz, der sich mit dem Einfluss von Prädation innerhalb einer Gemeinschaft von Organismen beschäftigt. Diese Studie untersucht sowohl herbivore als auch carnivore Nahrungsbeziehungen in einem Meereisökosystem als Modellsystem. Sie beschreibt Grazing-Experimente mit einer natürlichen Gemeinschaft von Algen anstatt von individuellen Kombinationen von Futter und Konsument, sowie Prädationsexperimente mit Beutetieren. Die Experimente decken komplexe Nahrungsbeziehungen auf und schätzen den Einfluss von Meereismeiofauna durch Fressen auf die Organismengemeinschaft im Meereis ab. Ähnliche Experimente könnten wertvolle Informationen zur Verbesserung unseres Verständnisses von Fressbeziehungen im Kontext von Planktongemeinschaften liefern, und könnten so dazu beitragen, zukünftige Fraßmodelle für Zooplankton weiter zu entwickeln.

Die verschiedenen Aspekte dieser Studie in Bezug auf Zooplanktonfraß und Phytoplanktondiversität demonstrieren den Einfluss von top-down-Mechanismen auf Diversität und zeigen Folgen für Ökosystemfunktionen und biogeochemische Kreisläufe auf. Ein besseres Verständnis und eine bessere Darstellung der komplexen Nahrungsprozesse im Plankton können dazu beitragen, Diversität im pelagischen Ozean besser zu modellieren. Im Hinblick auf die Untersuchung von biogeochemischen Kreisläufen in einem Ozean der Zukunft kann die Darstellung von Diversität in Modellen eine wichtige Rolle spielen.

1 Introduction

1.1 Motivation

Persistent growth and industrialisation are increasing the demand of humankind for space and natural resources, and enhance the pressure on ecosystems from regional to global scales. As a consequence of often ultimately anthropogenic perturbations, a loss of diversity has been observed in a variety of different ecosystems (Butchart et al., 2010). Increasing evidence suggests that such a diversity loss coincides with a reduction in ecosystem functioning, indicated for example by diminished primary production or nutrient use (Cardinale et al., 2011). At the same time, high diversity is suggested to make ecosystems less vulnerable to changing environmental conditions (Naeem and Li, 1997; Yachi and Loreau, 1999). Diversity might thus potentially aid in sustaining an ecosystem's established functioning through periods of change.

In marine ecosystems, diversity loss of fish and mammals might negatively affect the supply of goods, like fish as a food source, and other services of the ocean to the people (Worm et al., 2006). Reduced diversity of phytoplankton, in turn, is likely to directly affect higher trophic levels. Moreover, it might decrease oceanic primary production, which accounts for about half of the world's carbon fixation (Field et al., 1998). Part of this carbon is bound in organic particles and transported into the deep ocean. This biological pump contributes to an oceanic carbon sink which in total amounts to roughly one quarter of the anthropogenic emissions each year (Canadell et al., 2007). Diversity might thus affect the oceanic carbon sink via changes in the composition of the phytoplankton community driving the biological pump.

The coexistence of phytoplankton species, which controls community composition and diversity, has been investigated in both theoretical and experimental studies for decades. Many studies focus on bottom-up controls of resource use (e.g., Tilman, 1977; Huisman et al., 1999; Passarge et al., 2006). Some studies take into account top-down effects via feeding (e.g., McCauley and Briand, 1979; Hutson, 1984; Leibold, 1996; Beisner, 2001; Sarnelle, 2005). On a global scale, recent studies have started to investigate mechanisms of phytoplankton coexistence using a novel global ocean ecosystem model. This model explicitly resolves a diverse phytoplankton community and allows investigating controls and effects of phytoplankton diversity in simulated pelagic ecosystems (Follows et al., 2007). Results from this model have so far demonstrated the controls of resource use and the physical environment on phytoplankton biogeography and diversity (Dutkiewicz et al., 2009; Barton et al., 2010a; Monteiro et al., 2010). However, little is known about the consequences of diversity changes on ecosystem functions like primary production or carbon sequestration in the ocean. Furthermore, top-down controls

by zooplankton feeding in this context have not been investigated.

Predation may affect diversity via a variety of mechanisms, as known from theoretical models and experimental studies (Chesson, 2000). In addition, the dynamics of typical marine ecosystem models are influenced considerably by the representation of zooplankton as the highest trophic level resolved (Anderson et al., 2010). At the same time, commonly employed zooplankton formulations are oversimplified with respect to community structure and underlying mechanisms of feeding, growth and metabolism.

This study addresses some of the open questions concerning diversity in pelagic ecosystems. In Chapter 2 marine phytoplankton diversity is examined on the global scale, in particular with respect to effects of zooplankton feeding in a coupled global ecosystem model. In Chapter 3, the consequences of different diversity levels for the functioning of the pelagic ecosystem in terms of primary production are investigated. The significance of the zooplankton feeding formulation for phytoplankton diversity and ecosystem functioning motivates the development of a more sophisticated feeding model presented in Chapter 4. In addition to this main focus, Chapter 5 presents an example of an experimental approach aimed at investigating feeding in a community context, albeit for a sea-ice ecosystem. Similar experiments might serve to provide information to constrain future community feeding models.

In the remainder of this chapter, some background is provided on the two main fields addressed by this study, biodiversity and feeding. The first part presents what is known specifically in relation to pelagic phytoplankton diversity, in contrast to the abundant literature on terrestrial systems. The second part discusses zooplankton feeding ecology and the representation of the feeding process in aquatic ecosystem models as an important control of phytoplankton diversity.

1.2 Biodiversity

The pelagic ocean hosts a large diversity across trophic levels (e.g., Tittensor et al., 2010). Phytoplankton diversity in particular influences ecological and biogeochemical processes as it relates to the community composition which forms the basis of the pelagic food web (Duffy and Stachowicz, 2006). Experimental evidence indicates positive relationships between the diversity of primary producers and ecosystem functioning, e.g. primary production or nutrient use, across ecosystems. These findings suggest that a potential loss of phytoplankton diversity might reduce primary production in the ocean (Cardinale et al., 2011, see Section 1.2.1 for further details), thereby limiting the energy available to higher trophic levels. In more specific terms of community composition, phytoplankton community structure may affect zooplankton production and composition, and propagate up to fisheries and humans (Richardson and Schoeman, 2004; Hilligsøe et al., 2011; Ainsworth et al., 2011). The composition of the phytoplankton community may also affect the export of organic matter from the surface to the deep ocean, and thereby the uptake of atmospheric CO_2 (e.g., Arrigo et al., 1999; Finkel et al., 2010; Hilligsøe et al., 2011; Behl et al., 2011). This biological pump removes CO_2 taken up in the surface

ocean from contact with the atmosphere on time scales of hundreds of years depending on the circulation and mixing regimes (Volk and Hoffert, 1985). It maintains a gradient in dissolved inorganic carbon (DIC) from relatively low concentrations at the surface to high concentrations in the deep ocean (e.g., Falkowski et al., 2000). This gradient ultimately facilitates a significant uptake of atmospheric CO_2 on seasonal scales (Takahashi et al., 2009). It potentially affects an oceanic pool of carbon larger than the CO_2 content of the atmosphere (Riebesell et al., 2009). Small changes in the processes maintaining the DIC gradient could therefore have a large influence on atmospheric CO_2 levels.

In the future, ocean conditions are expected to change due to the increase of atmospheric CO_2 levels (Riebesell et al., 2009). Indirect effects on the ocean biosphere arise from warming and from changes in mixing and circulation. The warming atmosphere is expected to increase surface ocean temperatures and thereby increase stratification (Sarmiento et al., 2004). Stronger stratification may diminish the supply of nutrients to the surface layers, thereby affecting primary and export production. At the same time, the shoaling of the surface mixed layer may increase light availability for phytoplankton in regions with deep mixing, thereby increasing productivity. Higher temperatures in the surface layer might accelerate heterotrophic processes like remineralisation, and to a lesser degree primary production (Pomeroy and Wiebe, 2001). They might also reduce the ventilation of the deep ocean, thereby diminishing the supply of oxygen, leading to overall lower deep-ocean oxygen levels including larger oxygen minimum zones. Direct effects of rising atmospheric CO_2 include ocean acidification and higher oceanic CO_2 concentrations (carbonation).

Effects of environmental changes on organisms differ between, and probably within, key phytoplankton groups (Boyd et al., 2010), and diversity will thus play a role in shaping the pelagic ecosystem's response to ocean change. Species rare under present conditions might come to thrive in a future ocean, influencing community composition and thus ecosystem functioning and element cycles (Caron and Countway, 2009). Diversity may affect the stability of an ecosystem with respect to temporal variability and perturbations, including invasion of species, albeit in various ways depending on the aspect of stability in question (Ives and Carpenter, 2007). Temperature is expected, among other consequences, to directly or indirectly (e.g., through changes in stratification) cause shifts in distribution and change abundance and community structure (Beaugrand et al., 2002; Richardson and Schoeman, 2004; Hilligsøe et al., 2011), which in turn may affect export production, the oceanic CO_2 uptake and fisheries. Responses of organisms to ocean acidification and carbonation differ between species (e.g., Rost et al., 2008), while the community response is not known yet. These environmental changes will affect different species differently, potentially altering the outcome of competition or the dominance of key species. Diversity may therefore be influenced by, and itself influence the impact of environmental changes, even though specific consequences are not yet well understood.

In the following, the influence of diversity on pelagic primary production as one of the basic ecosystem functions will be discussed in more detail.

1.2.1 Diversity and ecosystem functioning

The notion that diversity might affect processes on the ecosystem level has been a focus of research for several decades (Schulze and Mooney, 1993). During recent years, experimental evidence is increasing that diversity influences the functioning of ecosystems in terms of primary production, total biomass, or nutrient use (Cardinale et al., 2011). These experiments typically focus on diversity of primary producers and manipulate species richness as measure of diversity. Recent experiments provide support for the idea that, averaged over different species and habitats, species loss reduces the biomass and resource-use efficiency of the primary producers, and might reduce primary productivity (Cardinale et al., 2011). These responses vary, however, in strength and direction for different types of ecosystems and different indicators of ecosystem functioning such as producer biomass, nutrient concentrations, or primary production (Hooper et al., 2005; Cardinale et al., 2011).

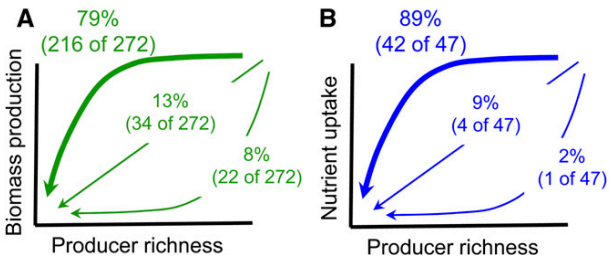

Figure 1.1: Evidence for three different relationships between diversity (as species richness) and a measure of ecosystem functioning (A: biomass production, B: nutrient uptake) across different ecosystems as % and total number of studies in a recent review. Adapted from Cardinale et al. (2011, part of their Fig. 5) with permission from the author and the American Journal of Botany.

The most commonly suggested shape of the relationship between diversity and a measure of ecosystem functioning, such as biomass or primary production, is a saturating curve as shown in Fig. 1.1 (Cardinale et al., 2011; Tilman et al., 1997). For this kind of relationship, initial diversity loss from systems with high diversity has only a minimal effect on ecosystem functioning. At some point, however, further loss of diversity results in a pronounced reduction in functioning. A positive relationship is most often thought to arise from either or both of two mechanisms: (1) the selection effect can increase functioning because a more diverse community has a higher probability of containing a highly productive species, which dominates the community (Aarssen, 1997; Huston, 1997) and which affects the performance of other species in the mixture through interactions like competition (Cardinale et al., 2004; Weis et al., 2007); (2) complementarity of species or groups through niche or resource partitioning and facilitation can increase functioning in more diverse communities by allowing the community to capture available resources more efficiently (Tilman et al., 1997; Loreau, 1998; Cardinale et al., 2002). In the classical understanding, niches arise from variability in ecological factors within the system, e.g., temperature or prey size, and can be identified by the degree of resource use along such a niche axis (Hutchinson, 1957; MacArthur and Wilson, 1967; Schoener, 1988). Distinguishing between these two mechanisms

in experimental data is not straightforward, though. The most commonly applied method is the additive partitioning equation (Loreau and Hector, 2001; Fox, 2005), which assigns complementarity and selection effects to statistical measures. The use of additive partitioning has been questioned, however, since the statistically determined complementarity and selection effects do not necessarily correspond to specific ecological mechanisms such as complementary resource use or competitive exclusion (Cardinale et al., 2011).

Experimental evidence for diversity-ecosystem functioning relationships predominantly originates from terrestrial and benthic ecosystems and the underlying mechanisms were derived mostly from these data (Hooper et al., 2005; Cardinale et al., 2011). Experimental studies on pelagic communities are still scarce (Duffy and Stachowicz, 2006; Ptacnik et al., 2010; Cardinale et al., 2011). This fact raises the question to what extent mechanisms inferred from terrestrial/benthic systems play a role in the pelagic ocean. Pelagic systems differ fundamentally from terrestrial or benthic systems (Shurin et al., 2006; Ptacnik et al., 2010, and references therein). Terrestrial and benthic systems are, to a certain degree, spatially organised. Important fractions of the community are sessile organisms which compete for space. Niches are to a large extent established along spatial environmental gradients. By comparison, the mixed surface ocean can be considered a fairly homogenous environment, where all plankton organisms can potentially interact. Short generation times and high growth rates lead to high turnover of the pelagic ecosystem. Structural biomass is of minor importance in many phytoplankton organisms, therefore allowing stronger top-down control through herbivore feeding. Niche partitioning arises from functional differences of the plankton types, which have to adapt to a high variability of environmental conditions, or from temporal patterns as apparent, for example, in seasonal succession.

Particularly for plankton communities, the classical concept of the ecological niche can thus be broadened (Ptacnik et al., 2010). Niches can arise from environmental conditions given by the number of limiting resources, variability in the physical or chemical environment, or mortality sources ("environmental dimensionality"). Species' traits concerning, for example resource uptake, tolerance width or mobility open up further niches ("trait dimensionality"). Restricted variability along any of the individual dimensionality axes constrains diversity by limiting the available number of niches. In this concept, a positive relationship between diversity and ecosystem functioning can only arise if species can coexist because of a large variability in the environment, and if their trait variability allows them to use complementary niches (Ptacnik et al., 2010).

Although indications exist that some of the mechanisms governing spatially organised ecosystems also play a role in the pelagic ocean (Duffy and Stachowicz, 2006), experimental evidence for pelagic diversity-ecosystem functioning relationships is still scarce. For phytoplankton communities, evidence stems from experiments controlling phytoplankton diversity as well as from compilations of field data from natural communities. Ptacnik et al. (2008) show that across different lakes and the Baltic Sea, nutrients are bound in phytoplankton biomass more efficiently in more diverse communities. The variability of resource use efficiency decreased with increasing diversity. One possible mechanism for the positive relationship between resource use efficiency and diversity is suggested by Striebel et al. (2009);

Behl et al. (2011). The data on assembled and natural communities of freshwater phytoplankton presented in these studies suggest that use of different photosynthetically active pigments might allow resource use complementarity in terms of light. Other studies find neutral (Gamfeldt et al., 2005) or negative (Schmidtke et al., 2010) relationships between diversity and ecosystem functioning, or more complex temporal patterns (Weis et al., 2007). In Chapter 3, the scarce observational evidence is complemented by simulations obtained with a global plankton ecosystem model. The relationship between diversity and primary production on the global and regional scale is investigated and mechanisms at play are identified.

One needs to be aware, however, that the term "diversity" in observations and in the model may refer to different measures of diversity addressing different concepts. The following section discusses a number of different diversity measures.

1.2.2 Measures of diversity

Biodiversity can be quantified on different levels. Species richness, probably the most commonly used measure of diversity, is simply the number of species present and thus depends on the taxonomic classification, which is traditionally based on morphology. It is easily determined from observations, but does not take into account, for example, dominance of individual species. The equality of relative contributions of species to the community is captured by the evenness, the opposite of dominance which can be estimated based on the relative abundances of species (Smith and Wilson, 1996). Both richness and evenness are combined in the Shannon Index H (or Shannon-Weaver Index; Shannon and Weaver, 1949)

$$H = -\sum_{j=1}^{n} p_j \ln(p_j) \quad , \quad p_j = \frac{P_j}{\sum_{r=1}^{n} P_r} \tag{1.1}$$

where P_j is the biomass or abundance for the individual phytoplankton species. This widely used index is considered the best measure of the joint effects of richness and evenness, but is also criticised because its meaning in terms of ecological diversity is not clear (see Stirling and Wilsey, 2001, for a detailed discussion).

Aside from these measures of taxonomic diversity, functional diversity gauges the variety of different effects organisms have on a particular part of the ecosystem (Tilman, 2001; Hooper et al., 2005). The impact of a species on their environment is determined by its traits, e.g., resource use characteristics. Functional diversity measures the similarity in traits of the species in a community, and thereby the range of effects on the system. Because it implicitly takes into account ecological mechanisms, functional diversity may be better suited than taxonomic diversity measures for investigating changes in ecosystem functioning (Petchey and Gaston, 2006; Longhi and Beisner, 2010; Behl et al., 2011). A major difficulty, however, arises from how to measure functional diversity, and several measures have been proposed. Rather than the choice of the measure, a key aspect appears to be the selection of traits to be considered in the assignment of organisms to functional groups (Petchey et al., 2010). In the

models used in Chapters 2 and 3, we distinguish different phytoplankton types according to particular traits regarding, such as nutrient uptake. This characterisation does not directly relate to taxonomic diversity and also reflects aspects of functional diversity. This study will use the number of coexisting phytoplankton types as simplest measure for simulated diversity. The following section presents how different phytoplankton types can coexist in the face of competition for resources.

1.2.3 Mechanisms of coexistence

Many aquatic habitats are characterised by a large number of coexisting phytoplankton species. This evident coexistence in the natural world was opposed by experiments which demonstrated that species competing for a shared resource drive each other to extinction (Gause, 1934). This effect became known as the competitive exclusion principle (Hardin, 1960), and brought up the question of how a large number of phytoplankton species can coexist on a small number of shared resources like light and nutrients (Hutchinson, 1961). In order to resolve this "paradox of the plankton" a number of hypotheses have been formulated (Sommer and Worm, 2002; Roy and Chattopadhyay, 2007), comprising equilibrium and non-equilibrium mechanisms. The following overview will concentrate on mechanisms affecting coexistence in the pelagic ocean.

Competitive exclusion can be demonstrated by looking at two phytoplankton species competing for a single abiotic resource, e.g., a nutrient R, in equilibrium. For each species P, there is a resource level, termed the critical resource level R^*, for which growth, here formulated as a Monod function for nutrient uptake, just balances mortality (Fig. 1.2):

$$\frac{\partial P}{\partial t} = P\left(\frac{\mu R}{k+R} - m\right) = 0 \Leftrightarrow \mathrm{R}^* = \frac{km}{\mu - m} \quad , \tag{1.2}$$

where μ is the maximum growth rate, k is the half-saturation concentration for nutrient uptake, and m is the mortality rate. The R^* depends on the individual growth and loss characteristics and can thus differ between the two species. In equilibrium, in the absence of other competitors each species would draw down nutrients to its R^*. If two species compete in a well-mixed and constant environment, the species with the lower R^* can persist at a lower nutrient level, and excludes the other species by drawing down nutrients to a level at which the other species cannot compensate mortality losses. In such environments, the species with the lowest R^* always wins the competition (Stewart and Levin, 1973; Tilman, 1977).

In an equilibrium system, the one resource represents one single limiting factor, and consequently allows only one species to exist (Levin, 1970). Additional limiting factors, like different nutrients, can increase the number of coexisting species. However, stable coexistence of two species on two resources in the absence of predators is possible only if each species is limited by a different resource and also consumes proportionally more of this resource than the other species (resource ratio hypothesis; Tilman, 1977). A system with three species competing for three resources can show stable coexistence, dominance of one species or coexistence through oscillations depending on the R^* values and the nutrient

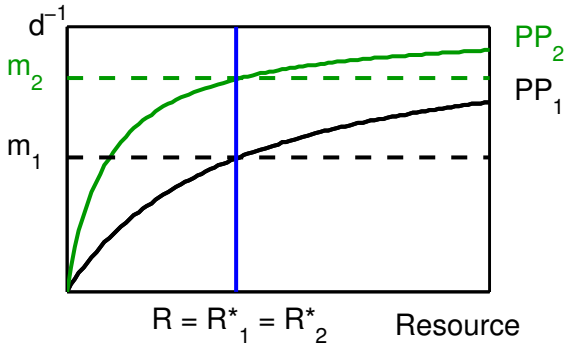

Figure 1.2: The critical resource level R* is defined as the resource concentration R where growth, here primary production PP; in units of d^{-1}, balances losses by mortality m. Rates are shown for two species with different growth and mortality, but similar R*.

consumption characteristics (Huisman and Weissing, 1999).

Within such systems, a common predator can also represent a limiting factor, in analogy to a limiting resource, depending on the grazing characteristics (see Chesson, 2000, and references therein): If, for example, grazing depends linearly on prey concentration, the species with the highest tolerance to grazing will exclude the more susceptible species through apparent competitive exclusion. In contrast, predators specialised on individual prey species can promote coexistence of prey species, as each predator acts as a limiting factor for its respective prey species. Generalist predators may enable prey species to coexist if they exhibit switching behaviour, i.e., they consume disproportionally more of the most abundant resource. This mechanism of predator-mediated coexistence is implied by grazing functional responses which, for example, depend quadratically on prey concentration, and will be the focus of Chapter 2. These bottom-up and top-down mechanisms have in common that they increase negative intraspecific interactions, i.e., between individuals of one prey type, relative to negative interspecific interactions, and are therefore considered stabilizing (Chesson, 2000). They promote systems in which intraspecific competition exceeds interspecific competition, which allows coexistence.

In contrast to these mechanisms based on equilibrium systems, in natural communities environmental conditions can vary temporally and spatially. Another line of proposed solutions for the paradox of the plankton therefore addresses non-equilibrium mechanisms and variable environmental conditions. Specifically for phytoplankton communities, pulsed supply of nutrients has been shown to increase the number of coexisting species above the number of limiting resources in laboratory chemostat cultures (Sommer, 1984). In experimental plankton systems, nutrient pulses or artificial mixing are typically used to disturb the system by changing the relative fitness of species or the competitive hierarchy (Sommer, 2002). Highest diversity is expected at intermediate frequencies and levels of disturbance (intermediate disturbance hypothesis; Connell, 1978; Sommer, 1995). At low frequencies of disturbance, competitive exclusion results in low diversity. If disturbances are too frequent, few species with other traits like a high maximum growth rate are selected for, again resulting in low diversity.

The following section describes which of the above mechanisms have so far been identified as controls of phytoplankton diversity on the global scale.

1.2.4 Global phytoplankton diversity

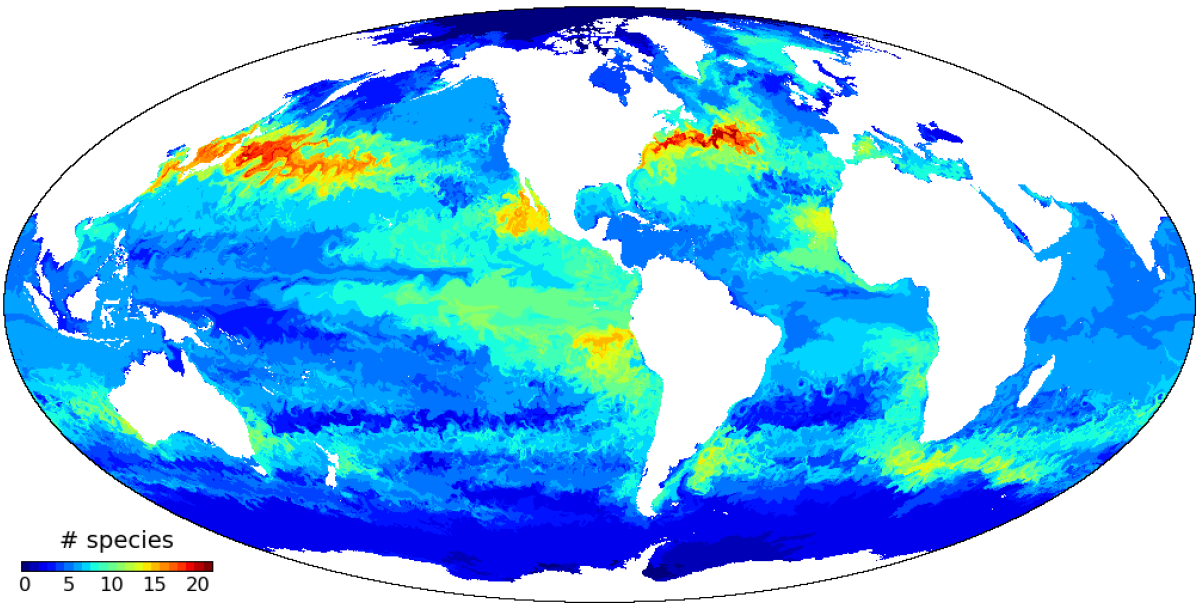

Figure 1.3: Simulated global phytoplankton diversity as number of coexisting phytoplankton model species. The model integration was performed by Oliver Jahn, Chris Hill, Stephanie Dutkiewicz and Michael Follows, Massachusetts Institute of Technology (MIT). For further details see Follows and Dutkiewicz (2011). Figure credit: Oliver Jahn, MIT.

Across oceanic regions, nutrient and mixing characteristics appear to determine pelagic diversity and community structure (Margalef, 1978). Highest phytoplankton diversity is evident in regimes with intermediate biomass, and thus productivity (Irigoien et al., 2004). Communities with high biomass tend to be dominated by a single species which might be able to escape the grazing pressure because of its size or defence mechanisms. Light limitation through shading might also reduce diversity at high phytoplankton biomass. In low biomass communities, few small phytoplankton species with higher nutrient affinity than larger species might coexist in low nutrient environments (Irigoien et al., 2004). These "gleaners" dominate in the stable low latitudes with low seasonality in global simulations with a self-assembling phytoplankton community model (Follows et al., 2007; Dutkiewicz et al., 2009). The coexisting phytoplankton types are characterised by similar critical resource levels R^*, i.e. the nutrient level required for growth to balance mortality (Barton et al., 2010a). In contrast, in the higher latitudes with variable nutrient supply by upwelling or mixing, opportunist types with high growth rates are favoured. In these complex model phytoplankton communities, the frequency of environmental fluctuations appears to select the most successful strategy, low R^* or high maximum growth rate, in each region according to the mechanisms underlying the intermediate disturbance hypothesis. Indications of highest diversity at intermediate disturbance frequencies, as observed in laboratory experiments, are less clear (Barton et al., 2010b). Phytoplankton diversity culminates in hot spot regions like the Gulf

Stream where species dominating different regions are brought together by lateral advection (Barton et al., 2010a). Simulated diversity is determined by the balance between competitive exclusion rates and replenishment of species by dispersal (MacArthur and Wilson, 1967). The local communities appear to be selected by the local environment from a large number of potential species due to high dispersal rates of phytoplankton (Cermeño et al., 2010; Ptacnik et al., 2010). These potential species can be thought of as a regional species pool (metacommunity; Leibold et al., 2004) which is selected from the global species pool by the regional environment (Ptacnik et al., 2010), so that local diversity is controlled by both local and regional environmental factors. While bottom-up controls on phytoplankton diversity by nutrient availability and use have been investigated on the global scale (Dutkiewicz et al., 2009; Barton et al., 2010a), the effect of zooplankton feeding has not been examined previously, and will be described in Chapter 2. Experimental and observational limitations here suggest the use of a global ocean ecosystem model which resolves diversity. The representation of diversity in such models is described in the following section.

1.2.5 Diversity in aquatic ecosystem models

State of the art marine ecosystem models typically represent a small number of plankton functional types (PFTs), e.g., diatoms, nitrogen fixers, small or large zooplankton (Blackford et al., 2004; Le Quéré et al., 2005). PFTs aggregate within one state variable species with a similar role in the food web or in biogeochemical cycling, such as nitrogen fixation or export of organic matter. The species implicit in one PFT, however, might have distinctly different ecology or life history and thus differ in many traits, e.g., nutrient affinity or susceptibility to grazing (Anderson, 2005). For instance, calcifiers in the ocean are found among both autotrophic and heterotrophic organisms, while in most PFT models calcifiers are exclusively autotrophs. Differences in traits and trade-offs between different trait values (i.e. improving one trait implies compromising another) govern coexistence, community dynamics and structure in marine ecosystems depending on the environmental conditions (McGill et al., 2006; Litchman et al., 2010). Representing PFTs without resolving the diversity within each PFT might thus impede a good representation of pathways within the ecosystem (Thingstad et al., 2010), and potentially of regional distributions and effects of changing environmental conditions.

Alternatives to PFT models have focused on an adaptive community structure based on traits and trade-offs. Models developed within a more theoretical context represent diversity by describing a community using a distribution of trait values for a central trait (Norberg et al., 2001; Savage et al., 2007). The community dynamics are then described by the evolution of the average and variance of the trait distribution ("moment-based approximation"). More applied plankton ecosystem models have also used a discretised trait distribution (Bruggeman and Kooijman, 2007) which can be approximated by the moment-based approach (Merico et al., 2009). These models successfully describe seasonal phytoplankton succession or chemostat predator-prey systems. In some models, sustained diversity depends on the external input of diversity, resembling migration or dispersal (Norberg et al., 2001; Bruggeman and Kooijman, 2007). In others, complementarity of two traits maintains diversity (Savage et al., 2007).

On the global scale, the Darwin model developed by Follows et al. (2007) resolves phytoplankton diversity by explicitly formulating a self-assembling community. The model is initialised with a large number (n=78) of phytoplankton types differing in traits regarding nutrient-, light- and temperature-dependent growth, sinking and susceptibility to grazing by zooplankton. Out of this seed community, the simulated physical and biological environment selects the coexisting phytoplankton types. This trait-based formulation allows to investigate mechanisms of phytoplankton coexistence and consequences of diversity for simulated biogeochemical cycling and ecosystem functioning, and is employed in Chapters 2 and 3. A detailed description of the model can be found, e.g., in Dutkiewicz et al. (2009). Diversity of other trophic levels is at present not represented in global scale models.

1.3 Zooplankton feeding

Feeding by zooplankton is an important means of how coexistence between competing phytoplankton species may be achieved (Chesson, 2000), thereby promoting diverse communities. However, predation-mediated coexistence of plankton organisms is rarely investigated experimentally, but for phytoplankton has been demonstrated only in lakes (see compilation by Hillebrand et al., 2007). On the global scale, ecosystem models have so far been employed to examine how phytoplankton diversity is controlled bottom-up, for instance by nutrient availability and use (Dutkiewicz et al., 2009; Barton et al., 2010a; Monteiro et al., 2010). Coexistence of phytoplankton mediated by zooplankton feeding, however, has not been investigated and is the focus of Chapters 2 and 3.

The term zooplankton encompasses the heterogenous assemblage of heterotrophic animals in the plankton. Zooplankton are the predominant consumers of producer biomass in pelagic food webs. They constitute the principal pathway for energy from primary producers to higher trophic-level consumers, and thereby to fisheries and humankind. Zooplankton influence phytoplankton community composition and play an important role in the recycling of nutrients for primary production and in the export of organic carbon to the deep ocean. In commonly employed large-scale ocean ecosystem models, zooplankton often represents the highest trophic level resolved and thus may govern the dynamics of the simulated ecosystem. While these models capture phytoplankton ecology in increasing detail, zooplankton formulations are typically simplistic. It is therefore important to examine zooplankton feeding formulations in models in more detail and investigate their relevance for simulated community composition, diversity and dynamics.

1.3.1 The role of zooplankton in pelagic food webs

Like other members of the plankton, zooplankton has traditionally been classified according to body size (Sieburth et al., 1978): Unicellular zooplankton, the protozoa, are mostly nano- (2-20 μm) and micro- (20-200 μm) zooplankton. Multicellular zooplankton, the metazoa, range in size from meso-

(0.2-20 mm) to macro- (2-20 cm) and even mega- (20-200 cm) zooplankton. Their prey, phytoplankton and bacterioplankton, are predominantly nano- to microplankton and picoplankton (0.2-2 μm), respectively, or include relatively smaller zooplankton.

This classification can help to generalise and assign different functions of the zooplankton in the pelagic food web and for the cycling of nutrients, energy and organic matter. Nano- and microzooplankton, e.g., flagellates and ciliates, are part of the microbial loop which is essential in the recycling of nutrients particularly in the surface mixed layers of permanently stratified, oligotrophic regions (Pomeroy, 1974; Azam et al., 1983; Fenchel, 2008). Within the microbial loop, bacteria take up dissolved organic matter and colonise particulate organic matter. Nanoflagellates consume most of the bacterial biomass and are preyed upon by ciliates, which often dominate the herbivore community (Sherr and Sherr, 2002). Together, these different trophic levels within the microbial loop make available remineralised nutrients for regenerated production in nutrient-depleted regions and seasons. Mesozooplankton, with copepods being the dominant group in the ocean, feed on the microbial loop and make organic matter and energy available to larger predators, e.g., fish. During blooms or in the productive upwelling regions of the ocean, large phytoplankton species come to dominate the community of primary producers, which can directly be consumed by mesozooplankton (Sommer et al., 2002).

Both this classical food chain from phytoplankton via zooplankton to fish and the link via microzooplankton represent important pathways of carbon to higher trophic levels (Calbet and Saiz, 2005). Zooplankton feeding can affect the abundance, biomass or productivity of several lower trophic levels with alternating effects via trophic cascades (Pace et al., 1999; Sommer, 2008; Zöllner et al., 2009). Mesozooplankton also partly facilitate the export of carbon and nutrients from the surface mixed layer into the deep ocean via vertical migration and the repackaging of biomass into fast-sinking fecal pellets (Buesseler and Boyd, 2009). At the same time, they may attenuate the vertical flux of organic matter by grazing on aggregates. They thereby affect the efficiency of the biological pump which sequesters carbon from the surface to the deep ocean (Volk and Hoffert, 1985; Steinberg et al., 2008; Jackson and Checkley, 2011).

The diverse roles of zooplankton in pelagic food webs emphasise the importance of examining the feeding process in more detail. The following section is intended illustrate the complexity and variety of constraints and trade-offs associated with zooplankton feeding.

1.3.2 The feeding process

In order to maintain a population, zooplankton face the task of obtaining food from a rather dilute suspension of a variety of prey types ranging from sinking particles to other motile plankton. In contrast to the large variety of prey items, a limited number of feeding strategies can be identified which are found across different zooplankton groups: feeding-current feeding, cruise feeding, passive and active ambush feeding, and colonisation of particles (Kiørboe, 2011). The efficiency of these strategies depends on the encounter rate between the zooplankton individual and its prey and on a successful capture. Cap-

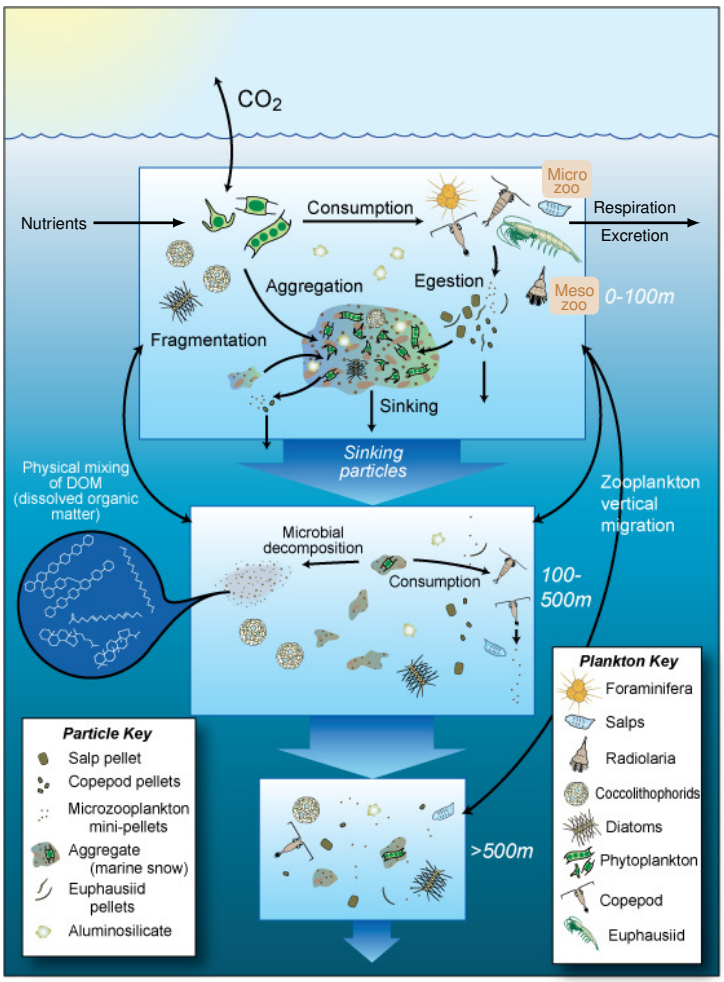

Figure 1.4: The pelagic food web and the biological pump. Figure modified from Buesseler et al. (2007, their Fig. 1.1) with permission from the author and the Journal of Marine Research.

ture is less likely to be successful if the prey can detect the zooplankton and escape by swimming or jumping (Jonsson and Tiselius, 1990; Jakobsen, 2002). The encounter rate is constrained mainly by prey motility, zooplankton size and velocity, the detection mechanism, and is affected by turbulence (Kiørboe, 2011). Size and velocity determine how the feeding process is influenced by viscous and inertial forces, as indicated by the Reynolds number Re. It is defined as $Re = ua/\nu$ where a is a linear dimension of the zooplankton organisms or prey object (e.g., the size of the capture structure) associated with the velocity u (e.g., the swimming or feeding current speed), and ν is the kinematic viscosity of water (approximately 10^{-2} cm^2 s^{-1} for seawater; Kiørboe, 2008). For a ciliate of 30 μm body length searching for food at a speed of one body length per second, $Re \approx 10^{-3} << 1$ and the water appears as a viscous medium, in which small prey particles are pushed away by the approaching predator. For larger plankton or particles and higher speeds a higher Reynolds number results. Attack jumps of larger copepods, for instance, operate at Re between 30 and 100 (Kiørboe et al., 2009), and viscosity effects are less dominant.

Apart from the feeding strategies, the ingestion also depends on the concentration of prey and zooplankton, and the selection of suitable prey by the zooplankton. The dependence of the ingestion rate on the prey concentration is named the functional response. It can be derived from feeding experiments with different prey concentration or on mechanistic concepts. Mathematical formulations of the functional response are discussed in more detail in section 1.3.3. The concentration of zooplankton might also influence the ingestion because of competition or interference between the zooplankton individuals, although the relevance of these interactions in natural plankton communities is still debated (Fussmann et al., 2005a; Kratina et al., 2009). The maximum ingestion rate appears to be governed by the size of the zooplankton according to allometric equations derived from experimental studies (Moloney and Field, 1989; Hansen et al., 1997). The size of both prey and zooplankton also is one of the main controls on the selection of prey particles (e.g., Hansen et al., 1994). A typical dome-shaped prey-size spectrum is thought to result from increasing encounter rates, but also more successful escape and more difficult handling with increasing prey size (Kiørboe, 2008). The optimum prey size differs between zooplankton groups, but the optimal predator-prey size ratio is around 10 for most groups (Hansen et al., 1994).

The following overview of different feeding strategies is based on the recent review by Kiørboe (2011) and references therein. Feeding strategies here serve as an example to illustrate the variety of factors constraining the feeding process.Trade-offs between the different strategies may arise from differences in encounter rates due to motility or size, but also from associated metabolic expenses or predation risks as zooplankton become prey, and from the need of many metazooplankton to search for mates. The trade-offs suggest that there might be an optimal feeding strategy for each zooplankton-prey combination depending on the prey environment (Kiørboe, 2011; Mariani and Visser, 2010).

Feeding-current feeding comprises mechanisms which use a feeding current from which prey particles are obtained either by direct interception, by passing through a filter, or by remote detection and subsequent capture of prey in the feeding current. Direct interception of prey particles is likely to be most important for large zooplankton, e.g., medusae because of the flow characteristics. Particles advected by the current move along the stream lines of the flow, and are only intercepted if their radius is larger than the distance of the stream line to the zooplankton. The minimum distance of the stream lines to the zooplankton decreases for higher *Re*. For large current feeders, the feeding process operates at higher *Re* than for smaller zooplankton because of their size and the speed of their feeding current. Smaller current feeders operating at smaller *Re* may directly intercept comparatively larger particles. For the latter, prey motility might play a greater role than direct interception in eliciting encounters with the prey.

Filter feeding is found among many zooplankton taxa of different size. Filter structures and mechanisms to generate the feeding current differ between taxa, yet the smallest particles retained by the filter vary only by about one order of magnitude in size. Prey motility and random motion across flow lines can facilitate retention of prey smaller than the filter mesh size. The predator-prey size ratio of filter feeders

is thus more flexible than for other feeding strategies, so that large filter feeders are less limited by the declining availability of large prey particles. Copepods use the feeding current to transport prey particles towards them, which are then detected, probably via chemical signals, and picked from the feeding current individually. Independently of the capture mechanism, feeding-current feeding is thought to be most efficient for small, non-evasive prey like bacteria or phytoplankton. In motile prey, detection of the hydrodynamic signal generated by the feeding current can trigger effective escape behaviour.

Cruise feeding is found in zooplankton swimming through the water and usually involves remote detection of the prey, as direct interception is likely to be efficient mostly for rather large, immotile particles as discussed above. Visual detection works on potentially larger length scales than other detection mechanisms (depending on the prey as well as environmental conditions), but is feasible only in larger organisms because of optical restrictions, and among the zooplankton is only found in fish larvae. Hydromechanical detection of prey is relatively more inefficient also because the cruising zooplankton itself creates a fluid disturbance that is large compared to the signal of the prey and can also warn prey of the approaching predator. Feeding on detritus particles and marine snow aggregates also requires a cruising zooplankton. Large zooplankton detect sinking particles using their chemical trail or, less efficiently, fluid disturbances. Smaller zooplankton like flagellates and ciliates appear to encounter particles largely at random while cruising.

The flow fields generated by zooplankton when stationary or cruising through the water differ in the volume of water moved past the zooplankton and thus scanned for food. Because of these differences in flow field, for copepods cruising is thought to be less efficient than stationary feeding employing a feeding current. Cruising fish larvae can scan a larger volume of water for food by using visual detection instead of other detection mechanisms. At the same time, both feeding modes generate hydrodynamic fluid disturbances which can alert a predator. The risk associated with each feeding mechanism depends on the types of predators. Because of the larger flow disturbance, stationary current feeding is more likely than cruising to alert a predator detecting hydrodynamic signals. In addition, cruising is risky towards ambush predators which rely on the movement of the zooplankton to lead to an encounter. Both feeding modes pose an equal risk towards visual cruising predators, because here the predator's speed determines the encounter rate. An effective way to reduce the predation risk is to decrease the swimming or feeding current velocity, which in its most extreme extent is ambush feeding.

Ambush feeding is the sit-and-wait strategy of a non-moving zooplankton which relies on the motility of its prey to lead to an encounter. Passive ambush feeders, e.g., hydromedusae or pteropods, wait for the prey to collide with their capture structure. Interception of sinking particles as a form of passive ambush feeding has also been termed flux feeding. Active ambush feeders detect their prey by hydrodynamical signals and actively attack it once within reach. Consequently, larger and faster swimming prey are detected at a greater distance. To enhance the volume screened for prey, active ambush feeders often have mechanoreceptors placed, for instance, on antennae that extend from the body, or they sink slowly

through the water. Still, for a given combination of predator and prey, ambush feeding can be expected to be about an order of magnitude less efficient than the more active feeding modes. The encounter rate of an ambush feeder only depends on the velocity of the prey which generally scales with body size and is therefore small compared to the speed of a feeding current or a cruise-feeding zooplankton. For the ambush feeding zooplankton, the lower encounter rate is balanced by a substantially reduced predation risk and mortality due to minimal hydrodynamic disturbances, and by lower metabolic costs.

For all mechanisms, general scaling relationships predict that across zooplankton taxa the feeding efficiency should decrease with increasing zooplankton size (Kiørboe, 2011). The relevant velocity scales with size (body length) to a power less than one. The efficiency, or volume-specific clearance rate, scales as this velocity over body size and would therefore decrease with increasing size. Besides this generally predicted tendency, a variety of characteristics is found across large taxa which might increase their feeding efficiency compared to small taxa, e.g., extended capture structures or inflated body size in ambush feeders, muscle instead of ciliary pumps in large feeding-current feeders, or visual detection in fish larvae, the large cruise feeders among the zooplankton.

1.3.3 Predation in models

Zooplankton feeding in plankton models is commonly described by the functional response, i.e. the dependence of ingestion on prey concentration. The choice of the feeding functional response has a large influence on the simulated model dynamics. In simple ecosystem models, the stability in terms of oscillations of prey (phytoplankton) and predator (zooplankton) and the existence of stable equilibrium solutions is governed by the functional response (e.g., Franks et al., 1986; Myerscough et al., 1996; Fussmann and Blasius, 2005; Gentleman and Neuheimer, 2008). In three-dimensional global ocean ecosystem models, the functional response affects phytoplankton community structure and thereby ecosystem functions, e.g., primary production and the export of organic matter to the deep ocean (Anderson et al., 2010). The many different functional responses derived mechanistically or empirically can be categorised into four general types following the work of Holling (1959a) as shown in Fig. 1.5 (Gentleman et al., 2003).

Type 1 A Holling type 1 response is characterised by a linear increase of ingestion rate with prey concentration up to a certain concentration, and a maximum ingestion rate at higher prey concentration. This type of response was suggested appropriate for some filter feeders (e.g. Frost, 1972) and implies that handling prey must require very little time or allow simultaneous search for and capture of other prey items (Jeschke et al., 2004).

Type 2 Longer handling times lead to a type 2 response which approaches saturation more gradually than the type 1 response. Holling (1959b) derived the classical type 2 response from letting his blindfolded assistant "prey" on disks laid out on a table, thus the equation is known as the "Disk equation".

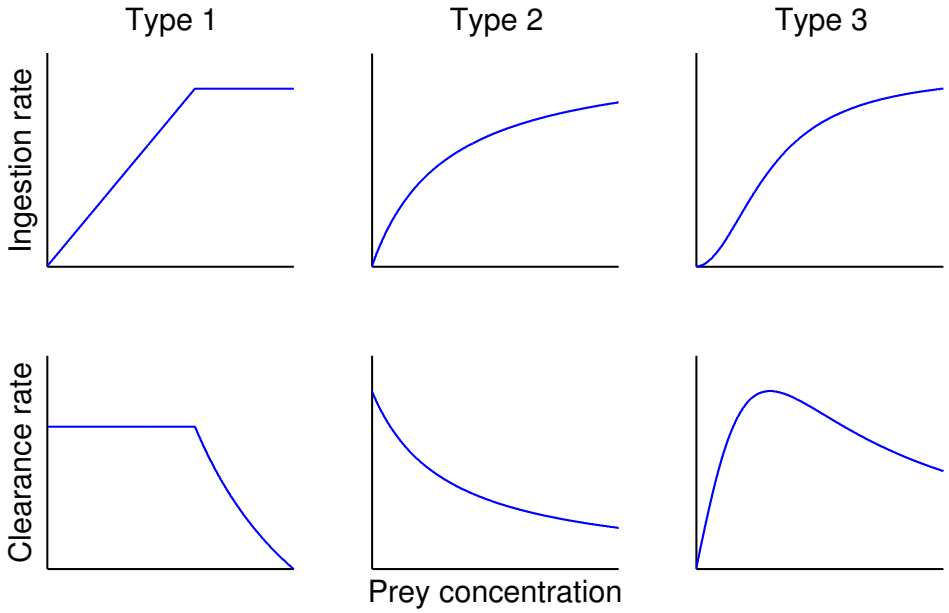

Figure 1.5: Different types of feeding functional response, i.e. the relationship between ingestion rate and prey concentration, and the corresponding clearance rate (ingestion rate divided by prey concentration) according to Holling (1959a).

Zooplankton encounter their prey at a rate $r_e = \beta P$, where P is the prey concentration (as number of prey m^{-3}), and β is the encounter rate kernel (in units of $\mathrm{m}^3\,\mathrm{d}^{-1}$). During a search time T_s, $N = r_e T_s$ prey particles are encountered, each of which requires a handling time t_H, so that the total time to ingest N prey is $T_s + N t_H$. The ingestion rate is then

$$I = \frac{N}{T_s + N t_H} = \frac{\beta P T_s}{T_s + N t_H} = \frac{\beta P}{1 + t_H \beta P} \quad . \tag{1.3}$$

The Disk equation is equivalent to the Michaelis-Menten equation for enzyme kinetics and the Monod formulation for bacterial growth (cf. Eq. 1.2) with a maximum rate of $g_{max} = 1/t_H$ and a half-saturation concentration of $\kappa_g = 1/(t_H \beta)$. At low prey concentrations, ingestion is encounter limited and the time spent on handling instead of searching does not diminish the ingestion rate. In this case, β indicates the volume of water a suspension feeder would entirely clear of prey in a given time, which is also named the clearance rate ($F = I/P$). At higher prey concentrations the handling time limits the ingestion, so that a maximum ingestion rate is approached, and the clearance rate declines (Fig. 1.5). The type 2 functional response is commonly fitted to experimental data (Jeschke et al., 2004) and used in marine ecosystem models. The so-called Ivlev formulation has a shape similar to the Disk equation, but was first obtained empirically (Gause, 1934), and derived from the assumption that a maximum uptake rate should exist (Ivlev, 1961). Its parameters cannot be explained in mechanistic terms, while for the Disk equation β is determined by feeding strategy, predator and prey size and motility, and t_H takes into account time for handling prey, but also for digestion (Jeschke et al., 2002).

Type 3 Typically, in marine ecosystem models t_H and β are taken as fixed parameters for each zooplankton type represented in the model. Experiments show, however, that the handling time and the encounter rate may depend on other factors like the prey concentration. For instance, the feeding activity might be reduced or cease at low prey concentration to reduce metabolic costs, resulting in a threshold feeding behaviour (Price and Paffenhöfer, 1986). Such a functional response, which is characterised by an increasing clearance rate at low prey concentrations before it declines again at higher prey concentrations, is classified as a Holling type 3 response (Gentleman et al., 2003). Chapter 4 presents a mechanistic model which leads to a type 3 threshold functional response through optimal allocation of energy between feeding activity and assimilation of food.

If different kinds of prey are available, some zooplankton switch to a different feeding strategy in response to changes in the relative concentrations of the prey types. In experimental studies, copepods, for example, switch from current feeding to ambush feeding if the concentration of ciliates relative to diatoms in a food mixture increases, because the offered ciliates are more motile and able to escape a feeding current (Landry, 1981; Jonsson and Tiselius, 1990; Kiørboe et al., 1996; Gismervik and Andersen, 1997). Encounter rates differ between the two feeding strategies, and the functional response therefore becomes a function of the prey environment. Switching between similar types of prey was observed for some microzooplankton taxa (Strom and Loukos, 1998). Switching can also lead to a type 3 response (Murdoch et al., 1975; Gismervik and Andersen, 1997).

In models, no commonly accepted mechanistic formulation of a type 3 response due to switching between multiple prey types exists. Mechanisms proposed to explain the emergence of a type 3 response in experiments mostly imply a behavioural change of the predator, like the change in feeding strategy or reduced feeding activity at low prey concentrations as described above.This change in behaviour identifies active selection by the predator depending on the relative concentrations of different prey types, and is therefore called "active switching". In contrast, "passive switching" implies passive selection arising purely from different prey characteristics like size or motility, which would cause different functional responses for different prey types, and not from an active behavioural change of the predator (Gentleman et al., 2003). Both types of switching are indicated by a disproportionally higher ingestion of a prey becoming more abundant compared to one becoming less abundant. In models, active switching can be formulated by introducing variable preferences, the selectivities σ_i, for each prey i where a constant preference ρ_i of the zooplankton for prey i is scaled by the ratio of prey i to the total available food (Fasham et al., 1990)

$$\sigma_i = \frac{\rho_i P_i}{\sum_r \rho_r P_r} \quad . \tag{1.4}$$

This formulation leads to a quadratic dependence on prey concentration causing the sigmoid shape of the functional response. Due to the implied active behavioural change, the selection of any particular prey type depends on the other prey available, and the functional response cannot be predicted from single-prey experiments.

The type 3 active switching response with prey-ratio based preferences was interpreted in models as a parameterisation of the unresolved zooplankton community in the model, assuming that predators

specialised on different kinds of prey covary with their prey (Fasham et al., 1990). In plankton models with low vertical resolution, a type 3 response can emerge if zooplankton are assumed to actively relocate to layers with high food concentration (Morozov, 2010), suggesting that a type 3 response can emerge from vertical movement of zooplankton in the natural environment despite a type 2 response being evident in laboratory experiments (Morozov et al., 2008).

Type 4 A Holling type 4 functional response is similar to a type 2 response, but decreases at higher prey concentration. It is thought to reflect prey toxicity or predator confusion.

The representation of zooplankton feeding in plankton ecosystem models necessarily simplifies the feeding process described in the previous section. The simplifications concern various aspects of the feeding process, community composition and pathways of energy and organic matter (Fig. 1.4). Carnivory, common in mesozooplankton ambush feeders feeding on microzooplankton when phytoplankton prey is rare (Landry, 1981; Calbet and Saiz, 2005), is implemented only in some of the large-scale ecosystem models (e.g. Buitenhuis et al., 2006; Yool et al., 2011). Mixotrophy is only beginning to be recognised in models as a potentially important strategy (Hammer and Pitchford, 2005; Flynn and Mitra, 2009; Ward et al., 2011). The most common functional responses omit any potential influence of predator abundance on the feeding process, e.g., competition or interference, although a number of different predator-dependent formulations can be found in the literature (Skalski and Gilliam, 2001). Basic effects of body size on prey selectivity are implemented in many large-scale models, e.g. as different functional groups with different parameters and pathways. More detailed formulations are found only in size-based smaller-scale models (Armstrong, 1999; Fuchs and Franks, 2010; Banas, 2011). Size effects on feeding efficiency and on the benefits and trade-offs of different strategies have not yet been addressed in plankton models (Kiørboe, 2011). Few models capture the trade-offs of the different feeding strategies related to predation risk or metabolic expenses, which define an optimal behaviour depending on the predator and prey environment (Visser, 2007; Visser et al., 2009; Mariani and Visser, 2010). Effects like these can be captured in models by formulations based on trade-offs and optimal behaviour. Chapter 4 presents one such approach, where a feeding-current feeder allocates the energy available from ingested prey to either feeding activity or assimilation of food depending on the optimal strategy for growth.

Furthermore, most plankton ecosystem models represent the zooplankton community by a small number of state variables, typically one or two, with fixed parameters. This simplification omits diversity in feeding strategies, associated prey spectra, costs and risks, and with it adaptive behaviour as described above. Such a rather "static" feeding formulation might thus let the zooplankton community appear as a single or homogeneous limiting force in the dynamics of the simulated plankton system. As the number of limiting factors governs phytoplankton diversity (see section 1.2.3), the choice of feeding formulation can influence simulated phytoplankton diversity. The alternative, however, of explicitly formulating a diverse zooplankton community with different feedings strategies and constraints requires a large number of parameter values, most of which are not well known, and implies high computational

costs if applied to larger scales. Chapter 2 contrasts a "static" functional response with a formulation that parameterises the effect of a zooplankton community to avoid the disadvantages of an explicit representation. It reveals the effects of the two formulations on phytoplankton diversity, community structure and dynamics in a global ocean ecosystem model.

1.4 Overview of the thesis and author contributions

Concurrent with other environmental changes, a loss of diversity has been observed in recent decades. In the ocean, changes in phytoplankton diversity may affect ecosystem functioning like primary production and the oceanic sink for atmospheric CO_2. On the global scale, the magnitude and underlying mechanisms of such potential effects of diversity are not well known. Controls of phytoplankton diversity, however, have been identified in terms of resource availability and use. One important control of phytoplankton diversity, which has not been investigated, is zooplankton feeding. Different aspects of zooplankton feeding include the feeding mode, the feeding functional response, and the selection between different food sources. Many ecosystem models used to investigate ocean ecosystem processes employ simplified feeding formulations, though, which capture these aspects to a limited degree. The following chapters attempt to improve our understanding of these topics using ecosystem models of different scale.

Chapter 2 examines different feeding functional responses in a global ocean ecosystem model which resolves phytoplankton diversity. The results reveal considerable effects of the zooplankton feeding functional response on phytoplankton diversity and community structure. They indicate an influence of diversity on ecosystem functions like primary production. This chapter is a submitted manuscript entitled "Top-down control of marine phytoplankton diversity in a global ecosystem model" by A. E. F. Prowe, M. Pahlow, S. Dutkiewicz, M. Follows, and A. Oschlies. FP developed the design of the experiments based on the initial idea provided by AO and MF. She modified the existing model and performed all experiments, calculations and analyses, with guidance provided by the co-authors. All co-authors contributed to the discussion. FP wrote the manuscript, with comments provided by all co-authors.

Chapter 3 investigates the effects of different diversity levels for global primary production. It examines the underlying mechanisms using a simplified 0-dimensional model. For one class of functional responses, the results reveal an increase in primary production with increasing diversity. This positive relationship between diversity and productivity is evident in oceanic regions with high nutrient supply. This chapter is also a submitted manuscript entitled "Controls on the diversity-productivity relationship in a marine ecosystem model" by A. E. F. Prowe, M. Pahlow, and A. Oschlies. FP conceived the idea and designed the experiments. She wrote the simplified 0-D model and performed all experiments, calculations and analyses. All co-authors provided guidance during analyses and contributed to the discussion of the results. FP wrote the manuscript, with comments provided by the co-authors.

The effect of feeding on diversity motivates the development of a mechanistic model of one zooplankton feeding mode presented in Chapter 4. This model assumes an optimal allocation of energy between obtaining and assimilating food. It suggests that changes in feeding behaviour may change the zooplankton contribution to export of organic matter into the deep ocean. This chapter is published in the journal *Marine Ecology Progress Series* (Citation: M. Pahlow and A. E. F. Prowe (2010). Model of optimal current feeding in zooplankton. Marine Ecology Progress Series 403:129-144, doi:10.3354/meps08466). FP contributed to reconstructing the Implicit Microbial Loop (IML) model by Steele (1998). She performed simulations comparing the IML model and the newly developed model and contributed to writing the manuscript.

In addition to this main focus, Chapter 5 presents an experimental approach investigating the complex feeding relationships between sea-ice meiofauna and its algal, ciliate, and meiofauna prey. Although this study addresses a different ecosystem, similar data for the pelagic ocean may be useful for validating future zooplankton feeding models. This chapter is a manuscript in preparation. FP contributed to the analysis and presentation of the data with Matlab and to writing the manuscript.

In Chapter 6, the main results of the thesis are summarised. The influence of diversity on export production, which is relevant for the oceanic carbon sink, and its sensitivity to changes in nutrient supply is investigated as outlook on future research.

2 Top-down control of marine phytoplankton diversity in a global ecosystem model

This chapter is a submitted manuscript by A. E. F. Prowe, M. Pahlow, S. Dutkiewicz, M. Follows, and A. Oschlies.

Abstract The potential of marine ecosystems to adapt to ongoing environmental change is largely unknown, making prediction of consequences for nutrient and carbon cycles particularly challenging. Realizing that biodiversity might influence the adaptation potential, recent model approaches have identified bottom-up controls on patterns of phytoplankton diversity regulated by nutrient availability and seasonality. Top-down control of biodiversity, however, has not been considered in depth in such models. Here we demonstrate how zooplankton predation with prey-ratio based food preferences can enhance phytoplankton diversity in a ecosystem-circulation model with self-assembling community structure. Simulated diversity increases more than three-fold under preferential grazing relative to standard density-dependent predation, and yields better agreement with observed distributions of phytoplankton diversity. The variable grazing pressure creates refuges for less competitive phytoplankton types, which reduces exclusion and improves the representation of seasonal phytoplankton succession during blooms. The type of grazing parameterization also has a significant impact on primary and net community production. Our results demonstrate how a simple parameterization of a zooplankton community response affects simulated phytoplankton community structure, diversity and dynamics, and motivates development of more detailed representations of top-down processes essential for investigating the role of diversity in marine ecosystems.

2.1 Introduction

Evidence is increasing that biodiversity influences productivity and stability of ecosystems across trophic levels in both marine and terrestrial realms (Worm et al., 2006; Ptacnik et al., 2008). Theoretical considerations indicate that higher species richness can increase ecosystem stability (Tilman et al., 1997; Yachi and Loreau, 1999). However, experimental observations demonstrating diversity effects in marine pelagic ecosystems are scarce and the role of diversity for these ecosystems is not well known (Duffy and Stachowicz, 2006; Ptacnik et al., 2010). In light of anticipated changes in marine

phytoplankton community structure (Moran et al., 2010; Boyd and Doney, 2002; Worm et al., 2002; Cardinale et al., 2006) and its effects on ecosystem structure and functioning (Bopp et al., 2005; Manizza et al., 2010), what shapes marine phytoplankton diversity is becoming a central research question.

Diversity is linked to differences in traits, e.g. optimal temperature for growth, within a community of species. One approach to capturing diversity in models is to formulate trade-offs between the different traits, which allows the system to emerge adaptively from environmental conditions (Norberg, 2004). This adaptive dynamics approach has been applied to models of local ecosystems only (Bruggeman and Kooijman, 2007; Merico et al., 2009). On the global scale, prognostic models have made efforts to resolve some of the functional diversity of phytoplankton by increasing the number of plankton functional types (e.g. Le Quéré et al., 2005). With a stronger focus on traits, an alternative approach has employed an explicit community consisting of a large number of phytoplankton types (Follows et al., 2007) differing randomly in size, optimal temperature, growth parameters, and sinking speed (Section 2.2.1).

Recent studies using the Follows et al. (2007) model have demonstrated how distinct phytoplankton communities emerge in a global ocean model through bottom-up control by resource availability, where the emergent communities differed in their competitiveness for resources in different environments (Dutkiewicz et al., 2009; Barton et al., 2010a). Besides bottom-up control, however, top-down mechanisms by consumers (predators) can shape diversity and ecosystem structure (Chesson, 2000; Worm et al., 2002; Chase et al., 2002). In models, structure and functioning of the simulated ecosystem are very sensitive to the choice of predation formulation (Anderson et al., 2010). In the previous studies based on the Follows et al. (2007) self-assembling ecosystem model, zooplankton predation was modeled in a simplistic way using two zooplankton types with similar Holling type II grazing responses and fixed preferences for each phytoplankton type. Here we show how a more flexible representation of the predation process can help to better understand the emergence of phytoplankton diversity via top-down controls in a global ecosystem-circulation model.

2.2 Methods

2.2.1 The ecosystem model

The model used in this study is the Massachusetts Institute of Technology general circulation model (MITgcm) with the "Darwin" ecosystem module (Follows et al., 2007). The latter comprises prognostic equations of state for four nutrients (phosphorus, nitrogen, iron and silica), 78 phytoplankton types, one large and one small zooplankton type, dissolved and particulate organic matter. Phosphorus is used as the main currency of the model. Temperature-dependent phytoplankton growth takes into account limitation by light, including effects of self shading, and by a Liebig-type limitation by the most limiting nutrient according to a Michaelis-Menten formulation. Phytoplankton losses include a linear mortality, sinking and zooplankton predation, which is formulated as a Holling type II functional

response. Both zooplankton types have the same maximum grazing rate and half-saturation concentration for grazing. Their grazing rates differ only in the preferences for the different phytoplankton types, which are assigned according to size and palatability. The export of organic matter to depth occurs mainly via particulate organic matter produced by phytoplankton mortality, sloppy feeding and zooplankton egestion and mortality. Sinking of phytoplankton plays a minor role. At the start of the simulation, the model ocean is seeded with the different phytoplankton types each characterized by a set of randomly assigned trait parameters. Phytoplankton types differ in cell size (small or large), nutrient requirements, half-saturation concentrations for nutrient uptake, light-limited growth, optimal temperature, and sinking speed (see Dutkiewicz et al. (2009) for equations and a detailed list of phytoplankton parameter ranges). The standard model setup in this study is identical to the one used by Dutkiewicz et al. (2009, Table A1) except for a reduced zooplankton mortality of $m^Z = 0.0125$ d^{-1}, which is not expected to result in qualitative differences to the preceding studies. Three additional configurations employ modified predation formulations (see Sections 2.2.2 and 2.3.1, and Table 2.1). For each model configuration an ensemble of five integrations with different random phytoplankton parameter sets are performed. Here, we are using five of the random parameter sets also used by Dutkiewicz et al. (2009) for better comparability.

The physical model is forced offline by the ECCO-GODAE state estimates (Wunsch and Heimbach, 2007). The coupled ecosystem-circulation model is integrated on a global grid of 1° resolution with 24 depth levels for 10 years, by which time it mostly displays a repeating annual cycle in nutrients and primary production. Results are presented as the average of the ensemble of five integrations (see Appendix 2.6.2, Fig. 2.9), averaged over 0-55 m depth in the 10th year (unless noted otherwise).

2.2.2 High/low grazing configuration

The Holling type II predation formulation describes the grazing process in terms of two compound parameters, namely the maximum grazing rate (g_{max}) and the half-saturation concentration for grazing (κ_k^P), which by themselves cannot be directly interpreted in mechanistic terms. In this study, we investigate the sensitivity of the model results to changes in the grazing formulation by using two parameterizations characterized by high and low grazing rates (the *high grazing* and *low grazing* setups, respectively). For the *high grazing* setup, we derive g_{max} and κ_k^P from a size-based mechanistic feeding-strategy model describing encounter and capture between a suspension feeder and its immotile phytoplankton prey (see Appendix 2.6.1 for a detailed description). In the simplest configuration this mechanistic model reduces to a type II formulation that is structurally identical to the type II formulation used previously (Dutkiewicz et al., 2009; Barton et al., 2010a). However, this approach allows us to determine g_{max} and κ_k^P from biologically meaningful parameters describing the grazing process. The mechanistic model results in notably higher g_{max} and lower κ_k^P than the original parameterization, and is thus referred to as *high grazing* setup in contrast to the *low grazing* standard configuration.

Table 2.1: Model configurations. Parameter values of maximum grazing rate (g_{max}) and half-saturation concentration for grazing (κ_k^P). Global annual average and maximum phytoplankton diversity as Shannon Index and as number of phytoplankton types exceeding threshold concentration P_{th} for $P_{th} = 10^{-8}$ mmol P m^{-3} (default), $P_{th} \cdot 10$ and $P_{th}/10$. Global annual average total phytoplankton biomass (0-55 m), primary production (PP) and net community production (NCP; both 0-100 m).

configuration		LGNS *low grazing & no switching*	LGAS *low grazing & active switching*	HGNS *high grazing & no switching*	HGAS *high grazing & active switching*
switching		no	active	no	active
κ_k^P	mmol P m^{-3}	0.1	0.1	0.027	0.027
g_{max}	d^{-1}	0.5	0.5	1.0	1.0
ave. diversity	no. types	6.5	10.5	4.6	21.3
ave. diversity ($P_{th} \cdot 10$)	no. types	5.8	9.4	4.1	19.1
ave. diversity ($P_{th}/10$)	no. types	7.0	11.3	5.0	23.0
max. diversity	no. types	15.9	37.4	10.4	55.3
max. diversity ($P_{th} \cdot 10$)	no. types	14.3	35.0	9.1	52.2
max. diversity ($P_{th}/10$)	no. types	16.9	38.8	11.1	59.4
ave. Shannon Index		0.7	1.1	0.6	2.0
max. Shannon Index		1.5	2.6	1.3	3.3
ave. total phytoplankton	10^{-3} mmol P m^{-3}	8.4	11.5	1.92	5.7
ave. PP	g C m^{-2} d^{-1}	0.18	0.21	0.09	0.16
ave. NCP	g C m^{-2} d^{-1}	0.09	0.11	0.04	0.09

2.2.3 Diversity measures

We define the metric "diversity" to be the number of phytoplankton types that exceed a low threshold biomass concentration of $P_{th} = 10^{-8}$ mmol m^{-3} (in units of phosphorus; following Barton et al., 2010a). Since phytoplankton types in the model are distinguished by functional traits such as maximum growth rates, the modeled functional diversity does not necessarily compare quantitatively to observational measures of (taxonomic) species richness. The modeled diversity depends to a limited extent on the number of phytoplankton types initialized (as indicated by related simulations with different numbers of phytoplankton types) as well as on the chosen threshold concentration. Therefore we also calculated the Shannon Index (H) from the biomass concentrations (P) of all phytoplankton types

$$H = -\sum_j^n p_j ln(p_j) \quad , \quad p_j = \frac{P_j}{\sum_r P_r} \quad . \tag{2.1}$$

Though not intuitively related to ecological diversity, H considers the joint influence of species richness and evenness (Stirling and Wilsey, 2001) and takes into account all phytoplankton types without the need of a threshold concentration. It is also less sensitive to changes in the initial number of phytoplankton types than diversity measured as the number of types.

2.3 Grazing parameterizations

2.3.1 "No switching" and "active switching" configurations

In the standard configuration of the model (Dutkiewicz et al., 2009), the Holling type II formulation describes ingestion (I_{jk}) of phytoplankton type j by zooplankton type k depending on the biomass concentration of phytoplankton type j (P_j)

$$I_{jk} = g_{max} \frac{\rho_{jk} P_j}{\kappa_k^P + \sum_r \rho_{rk} P_r} \quad . \tag{2.2}$$

Each of the two zooplankton types k is assigned different, but fixed preferences (ρ_{jk}) for each phytoplankton type j which are set to values between 0 and 1 according to the body sizes of both zooplankton and phytoplankton as well as the phytoplankton functional type (e.g. diatoms, prochlorococcus).

This setup relies on the assumption that the impact of the entire grazer community can be represented by two functional types with fixed food preferences. An explicit representation of the predator community response would require adding a large number of state variables. Instead, we here parameterize the grazer community response implicitly by assuming that consumers covary with the resources on which they are specialized. Such a community response can be captured by replacing the fixed food preferences (ρ) by selectivities (σ), which are calculated from ρ and scaled by the biomass of each phytoplankton type j (Fasham et al., 1990) relative to total phytoplankton biomass available for grazing

$$\sigma_j = \frac{\rho_j P_j}{\sum_r \rho_r P_r} \quad . \tag{2.3}$$

When a food type declines, the corresponding selectivity, and hence ingestion, decreases, while an increasing food type will be selected more strongly and thus suffer from more intense predation.

This grazing formulation is referred to as active switching (Gentleman et al., 2003), while constant food preferences imply no switching. Switching is an effective means for promoting coexistence (Hutson, 1984) and stability in simulated ecosystems (Murdoch and Oaten, 1975) and has been implemented in several ecosystem models (Fasham et al., 1990, 1993; Aumont et al., 2003; Aumont and Bopp, 2006). At the same time, this formulation can cause total ingestion to decrease although total available food increases, which was thought to be unbiological behavior (Gentleman et al., 2003). A recent modeling approach demonstrates, however, how reduced ingestion rates at higher prey concentrations can arise from copepods switching feeding strategies in the face of predation risk (Mariani and Visser, 2010). Active switching between similar kinds of prey was observed in microzooplankton (see references in Strom et al. (2000)) and copepods (Paffenhöfer, 1984). Copepods also actively switch between kinds of prey by shifting to different feeding strategies (Jonsson and Tiselius, 1990; Saiz and Kiørboe, 1995; Kiørboe et al., 1996). Here we interpret active switching not only as behavioral change of one predator type, but as a compound effect of the unresolved predator community.

2.3.2 Grazing pressure

The choice of the grazing formulation is known to determine the simulated dynamics of simple nutrient-phytoplankton-zooplankton (NPZ) systems. Density dependent phytoplankton growth or loss terms, which depend on the phytoplankton concentration with an exponent > 1, as introduced by the active switching formulation, can promote coexistence of several phytoplankton types (Gross et al., 2009). Density independent formulations (exponent $= 1$), for example for the no switching formulation in our model, lead to competitive exclusion. For grazing formulations this criterion for coexistence mathematically implies a positive slope of the clearance rate, I/P, as a function of P. This measure can also be used to characterize the effect of grazing formulations on the stability of simple NPZ systems with one phytoplankton (Gentleman and Neuheimer, 2008). Here we employ this measure to better understand the effect of switching behavior on phytoplankton diversity in a multi-phytoplankton type system. Instead of the term "clearance rate", which refers to the volume of water which zooplankton would entirely clear of prey given a certain ingestion rate, we use the term "specific grazing pressure" for the same quantity to stress the effect of grazing on the phytoplankton.

The specific grazing pressure ($G_{jk} = I_{jk}/P_j$) of zooplankton k for each phytoplankton type j provides a measure of the strength of predation aside from effects of predator concentration. If preferences (ρ_{jk}) are constant, i.e. for no switching (Eq. 2.2), it is given by

$$G_{jk} = \frac{I_{jk}}{P_j} = g_{max} \frac{\rho_{jk}}{\kappa_k^P + \sum_r \rho_{rk} P_r} \quad . \tag{2.4}$$

For selectivities changing with phytoplankton concentration (Eq. 2.3), i.e. for active switching, it is

$$G_{jk} = g_{max} \frac{\rho_{jk} P_j}{\kappa_k^P \sum_r \rho_{rk} P_r + \sum_r \rho_{rk} P_r^2} \quad . \tag{2.5}$$

The slope of G_{jk} is calculated as the first derivative with respect to the phytoplankton concentration of type j ($\partial G_{jk}/\partial P_j$). For no switching, $\partial G_{jk}/\partial P_j$ is negative for all P_j

$$\frac{\partial G_{jk}}{\partial P_j} = -g_{max} \frac{{\rho_{jk}}^2}{\left(\kappa_k^P + \sum_r \rho_{rk} P_r\right)^2} \quad < 0 \tag{2.6}$$

For active switching, $\partial G_{jk}/\partial P_j$ is given by

$$\frac{\partial G_{jk}}{\partial P_j} = g_{max} \frac{\rho_{jk} \left(\sum_{r \neq j} \rho_{rk} P_r^2 - \rho_{jk} P_j^2 + \kappa_k^P \sum_{r \neq j} \rho_{rk} P_r\right)}{\left(\sum_r \rho_{rk} P_r^2 + \kappa_k^P \sum_r \rho_{rk} P_r\right)^2} \tag{2.7}$$

and can be positive or negative depending on ρ_{rk} and P_j.

The initial slope at $P_j = 0$ can be calculated from

$$\frac{\partial}{\partial P_j}\left(\frac{I_{jk}}{P_j}\right)\Big|_{P_j=0} = g_{max}\frac{\rho_{jk}\left(\sum_{r\neq j}\rho_{rk}P_r^2 + \kappa_k^P\sum_{r\neq j}\rho_{rk}P_r\right)}{\left(\sum_r \rho_{rk}P_r^2 + \kappa_k^P\sum_r\rho_{rk}P_r\right)^2} \tag{2.8}$$

$$\overset{P_j=0}{=} g_{max}\frac{\rho_{jk}}{\sum_r \rho_{rk}P_r^2 + \kappa_k^P\sum_r\rho_{rk}P_r} \quad > 0 \tag{2.9}$$

and is always positive. This indicates that G_{jk} increases up to a critical phytoplankton concentration P_j^{crit} which can be determined by

$$\frac{\partial G_{jk}}{\partial P_j} = 0 \Leftrightarrow \quad P_j^{crit} = \sqrt{\frac{1}{\rho_{jk}}\left(\sum_{r\neq j}\rho_{rk}P_r^2 + \kappa_k^P\sum_{r\neq j}\rho_{rk}P_r\right)} \quad . \tag{2.10}$$

For a sigmoidal type III grazing functional response, as used for instance by Yool et al. (2011), a similar result is obtained.

Active switching and no switching thus imply qualitatively different behavior when phytoplankton concentrations change. Active switching can promote coexistence by damping changes in individual phytoplankton concentration as long as phytoplankton concentrations do not exceed P_j^{crit}. No switching may promote dominance of individual phytoplankton types because it amplifies changes in phytoplankton concentration. In the context of stability of NPZ models, a positive slope reduces oscillations and creates refuges from predation for the phytoplankton (Gentleman and Neuheimer, 2008). A negative slope causes a positive feed-back between phytoplankton concentration and growth and destabilizes the system. Below, we show that the slope of the grazing pressure can also explain how active switching helps to generate niches for less abundant phytoplankton types and thereby enhance phytoplankton diversity. We compare results of the active and the no-switching formulations (Section 2.3.1), each with low and high grazing rates from the original configuration and the mechanistic grazing model (Section 2.2.2), respectively, yielding four configurations: *low grazing&no switching* (LGNS), *low grazing&active switching* (LGAS), *high grazing&no switching* (HGNS), and *high grazing&active switching* (HGAS; Table 2.1).

2.4 Results and Discussion

2.4.1 Phytoplankton diversity patterns

For LGNS (essentially the same as Barton et al. (2010a)), phytoplankton diversity, measured as the number of types exceeding P_{th} = 10^{-8} mmol P m^{-3}, averages 6.5 in the upper 55 m of the water column (Fig. 2.1a). Diversity increases by 62% to an average of 10.5 in LGAS (Fig. 2.1b). For HGAS, diversity rises more than three-fold to an average of 21.3 (Fig. 2.1d). Simply increasing grazing rates, however, does not necessarily increase diversity as can be seen in HGNS for which diversity decreases

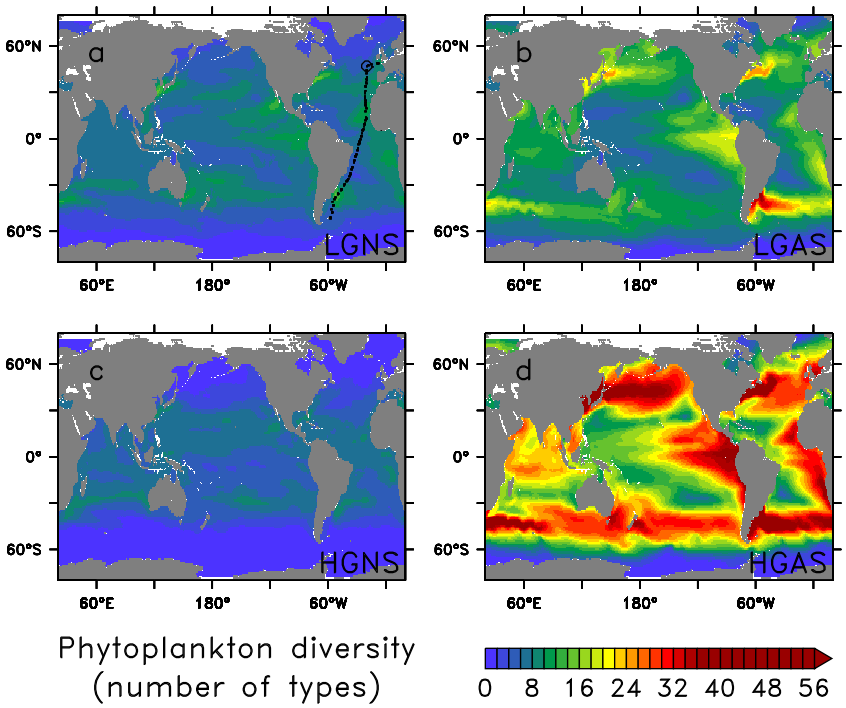

Figure 2.1: Phytoplankton diversity. Annual average number of phytoplankton types exceeding a threshold concentration for **a,** LGNS **b,** LGAS **c,** HGNS **d,** HGAS. See Table 2.1 for abbreviations. The dots and circle in **a** mark the Atlantic Meridional Transect (AMT) and the site of the North Atlantic Bloom Experiment (NABE), respectively.

compared to LGNS to an average of 4.6 species present (Fig. 2.1c).

All configurations show low diversity at high latitudes, and higher diversity at low and intermediate latitudes (Fig. 2.2, 2.3). Maximum zonal average diversity at around 45° latitude arises from hot spots in the western boundary currents (Barton et al., 2010a), where waters with different phytoplankton types mix, thereby increasing local diversity. In these turbulent regions, vertical transport processes associated with frontal dynamics maintain a high nutrient supply to the surface ocean which can promote diversity by allowing both well and less well adapted phytoplankton types to grow. In the simulations with higher diversity, switching prevents weaker competitors from being excluded. Mixing of different water masses thus brings together even larger numbers of phytoplankton types, and the predator-mediated diversity increase is highest. In contrast, in the oligotrophic gyres, a number of phytoplankton types equally well adapted to low nutrient levels coexist (Barton et al., 2010a) and switching enhances diversity only weakly.

Particularly for HGAS, the simulated latitudinal pattern of phytoplankton diversity appears broadly consistent with observational estimates along the Atlantic Meridional Transect (AMT; Fig. 2.2c; Cermeño et al., 2008). However, comparing simulated and observed diversity is not straight forward and any apparent agreement or disagreement might be coincidental. Maximum simulated diversity is obviously limited by the number of phytoplankton types with which the model is initialized. In addition, these results might be sensitive to the choice of the threshold concentration, P_{th}. The sensitivity with

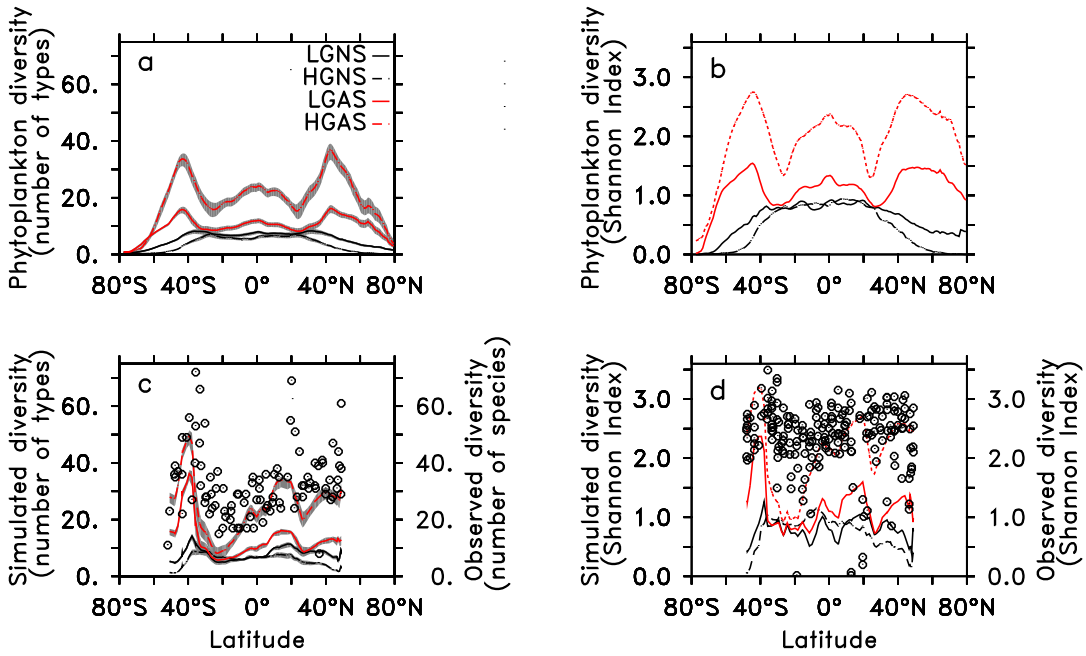

Figure 2.2: Latitudinal diversity gradient. Simulated surface layer diversity as **a,c,** number of phytoplankton types and **b,d** Shannon Index. Diversity is shown in **a,b** as zonal average and in **c,d** along the Atlantic Meridional Transect (AMT). Observed taxonomic diversity shown in **c,d** as number of species (surface data) and as Shannon Index (right y-axes) is calculated from biomass of diatoms, dinoflagellates and coccolithophores along the AMT (circles; Cermeño et al., 2008). Model estimates of functional diversity do not necessarily compare quantitatively to observational estimates of taxonomic diversity. Observational estimates of the Shannon Index may include data from the surface as well as from greater depths (P. Cermeño, personal communication). The uncertainty bands in **a** and **c** denote the diversity range between the ensemble averages of simulations with increased and decreased threshold concentration P_{th} compared to the standard configuration ($P_{th} \cdot 10$ and $P_{th}/10$, respectively).

respect to P_{th} appears to be minor, since changing P_{th} by a factor of 10 results in diversity differences small compared to those due to switching (Fig. 2.2, Table 2.1). Observational estimates of the Shannon Index (H) along the AMT appear to be in general higher than the simulations (Fig. 2.2d). No latitudinal gradient in H can be inferred from the observations along the AMT, possibly because these values include observations at different depths (Cermeño et al., 2008). In addition, both observational diversity measures might be biased particularly at low latitudes since picophytoplankton were neglected (Aiken et al., 2009). This bias is, however, difficult to assess due to the unclear notion of "species" for this group.

2.4.2 Mechanisms of diversity increase

The mechanism by which active switching promotes phytoplankton diversity is illustrated by a simplified example with two equally preferred ($\rho_1 = \rho_2$) phytoplankton types. When the concentration of type 1 (P_1) increases from 0 to 0.01 mmol P m^{-3} with the concentration of type 2 (P_2) fixed at 0.001 mmol P m^{-3}, selectivity for type 1 (σ_1) increases with increasing P_1, while σ_2 decreases (Eq. 2.3, Fig. 2.4a). Increasing P_1 leads to higher specific grazing pressure (G_1) for small concentrations of P_1 as

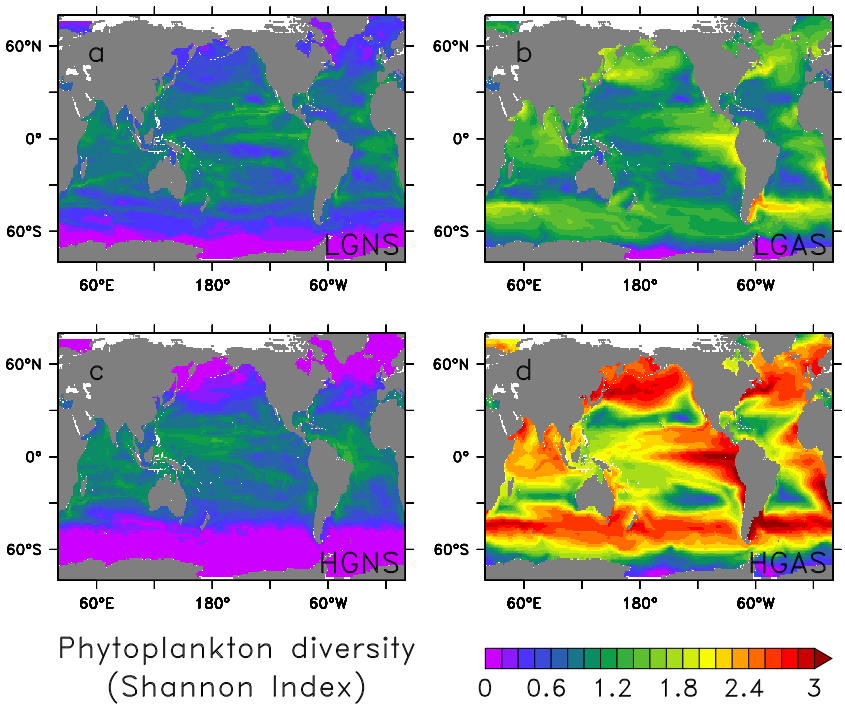

Figure 2.3: Phytoplankton diversity. Annual average Shannon Index for **a,** LGNS **b,** LGAS **c,** HGNS **d,** HGAS. See Table 2.1 for abbreviations.

σ_1 increases, but reduces G_2 for the less abundant type P_2 by increasing total phytoplankton available for grazing ($\sum_r [\sigma_r P_r]$; Fig. 2.4b). In this example, when $P_1 > P_1^{crit}$ (= 0.006 mmol P m^{-3}) any further increase of $\sum_r [\sigma_r P_r]$ leads to a reduction of G for both types. In contrast, under no switching, G for both types always decreases with increasing concentration of P_1 (Eq. 2.6).

By increasing the specific grazing pressure on the most abundant phytoplankton types, active switching makes the less abundant types more competitive. The initial slope of G ($\partial G_{jk}/\partial P_j$) determines whether zooplankton predation can increase diversity in this way. For no switching, $\partial G_{jk}/\partial P_j$ is always negative (Eq. 2.6) and therefore rewards growth of competitive types with reduced grazing pressure, thereby increasing competitiveness and promoting dominance of already successful types. In contrast, the active switching formulation has a positive initial slope at $P_j = 0$ (Eq. 2.9) and G_{jk} thus increases if concentrations of type j increase up to a critical concentration (see Section 2.3.2), so that growth of this type is damped.

The strength of this increase in competitiveness is related to the initial slope of G and depends on the values of g_{max} and κ_k^P. For small g_{max} or large κ_k^P (compared to $\sum_r [\sigma_r P_r]$; LGAS) the initial slope is small (Fig. 2.4b) and the predator-mediated diversity increase is weaker than for HGAS (Fig. 2.1b,d). In contrast, no switching favors the most resource-competitive type by reducing specific grazing pressure with increasing concentration for all phytoplankton types and across all concentrations. In a model ecosystem with one phytoplankton, this reduction in grazing pressure with increasing phytoplankton biomass was shown to cause oscillations and thus reduces the stability of the system (Gentleman and

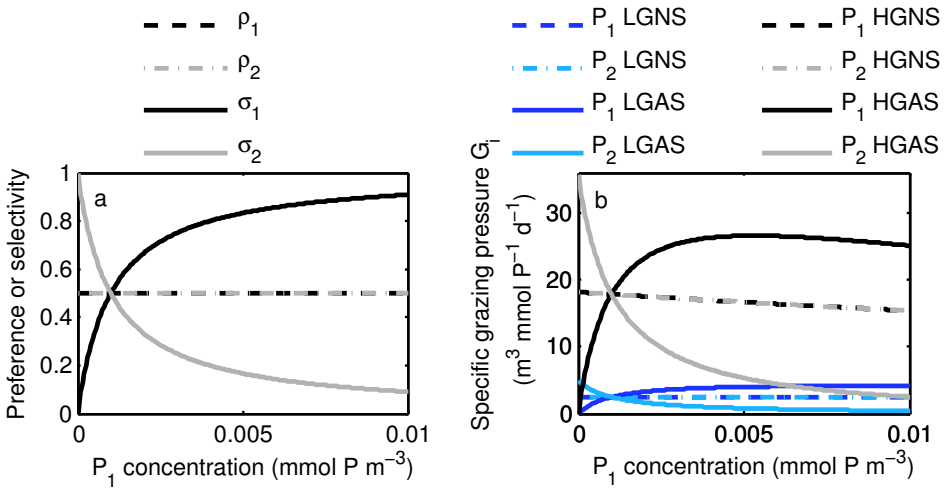

Figure 2.4: Idealized two-phytoplankton system with equal preferences. **a,** Preference (ρ) for *no switching* (dashed lines) or selectivity (σ) for *active switching* (solid lines). Phytoplankton P_1 increases from 0 to 0.01 mmol P m^{-3}, phytoplankton P_2 remains at 0.001 mmol P m^{-3}. **b,** Corresponding specific grazing pressure for *high grazing* and *low grazing* (see Table 2.1 for parameter values).

Neuheimer, 2008). The same property of the grazing function tends to favor coexistence when applied to competing phytoplankton species. The variable grazing pressure creates additional limiting factors for each phytoplankton type individually and thereby enhances the number of competing phytoplankton types that can coexist (Levin, 1970; Chase et al., 2002). Switching thus constitutes one of many potential pathways (Roy and Chattopadhyay, 2007, and references therein) to resolve the "paradox of the plankton" (Hutchinson, 1961), which addresses the apparent contradiction between observed coexistence and theory predicting that the number of coexisting species cannot exceed the number of limiting factors (Levin, 1970).

2.4.3 Primary production and net community production

In the following, we discuss differences in simulated total phytoplankton biomass, primary production (PP) and net community production (NCP) between the different model configurations. NCP is defined as the difference between gross primary production and community respiration within the euphotic zone. Interestingly, NCP is not only controlled bottom-up by physical transport processes supplying nutrients, but it also changes in response to different grazing parameterizations. In fact, the total phytoplankton biomass, PP and NCP differ by as much as a factor of two in the annual mean among the different model simulations (Figs. 2.5-2.7; Table 2.1). The regional patterns of change relative to LGNS differ between both *low* and *high grazing* switching setups. The effects of switching can be seen when comparing LGAS to LGNS. A detailed discussion of regional differences between configurations and the underlying mechanisms is presented in Appendix 2.6.3. In the following, we summarize the main findings.

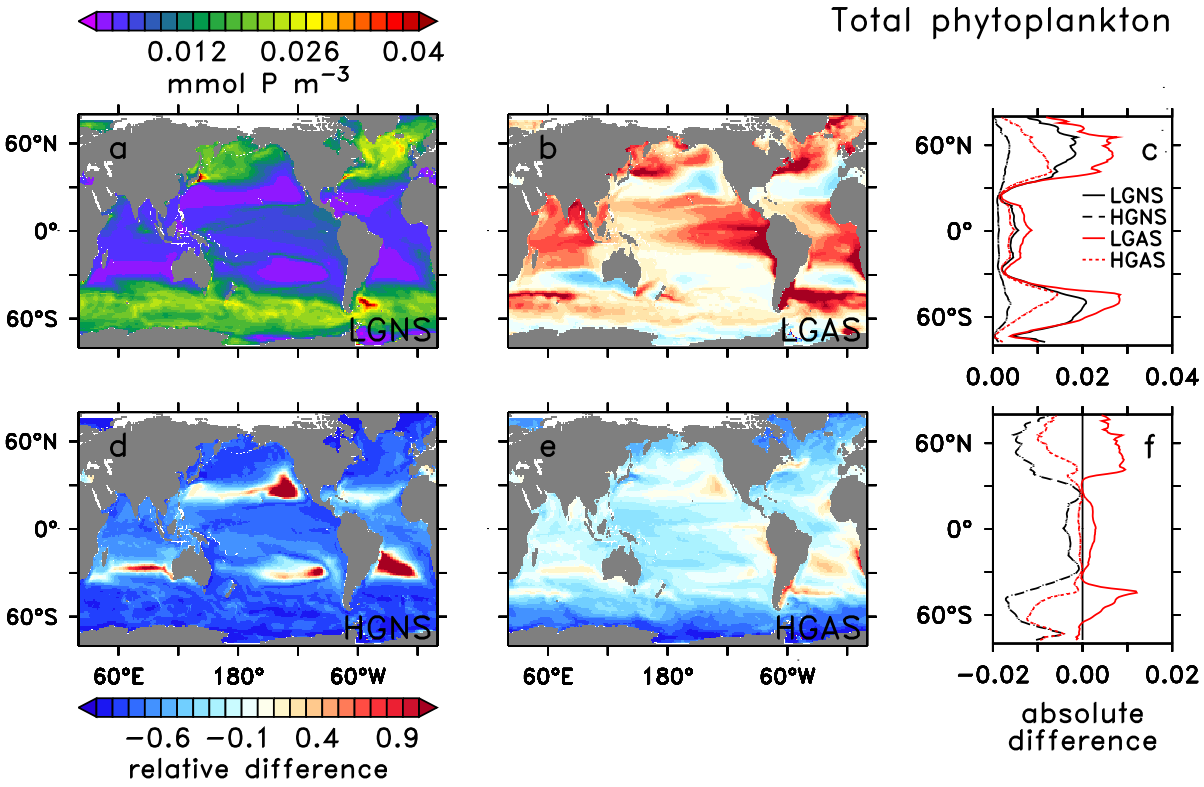

Figure 2.5: Total phytoplankton biomass. **a** Annual average total phytoplankton biomass (0-55 m depth) for LGNS is compared to **b** LGAS, **d** HGNS, and **e** HGAS as relative difference to LGNS. Zonal averages of total phytoplankton biomass are shown in **c** as absolute values and in **f** as absolute difference to LGNS for all configurations.

For both LGAS and HGAS, total phytoplankton biomass and PP increase compared to LGNS and HGNS, respectively, in the productive higher latitudes and in the tropics (shown for LGAS in Fig. 2.5b, 2.6b). For LGAS compared to LGNS, at higher latitudes higher uptake of nutrients intensifies the vertical nutrient gradients. It thereby enhances the mixing-driven input of nutrients from deeper layers which mostly fuels the PP increase. In combination with less grazing, higher phytoplankton biomass results, part of which is exported, thereby enhancing NCP. In contrast, in the permanently stratified low latitude regions (25°S-25°N) dominated by small phytoplankton types, higher total phytoplankton biomass enhances a "fast recycling loop" via dissolved organic matter (DOM) which sustains higher PP.

If grazing rates are increased (HGAS), a smaller phytoplankton standing stock leads to lower export, and thus lower NCP, in the productive regions. Less PP predominantly reflects lower nutrient inputs by vertical mixing. Opposing changes of PP and NCP in some regions (e.g., eastern tropical Atlantic and Pacific) indicate a reduction in community respiration. Less DOM production in the adjacent productive higher latitudes might reduce advective transport into these regions and thus decrease respiration. For HGNS, high grazing rates without switching generally reduce total phytoplankton biomass significantly compared to LGNS and increase nutrient concentrations with the exception of the subtropical gyres where total phytoplankton biomass is very small.

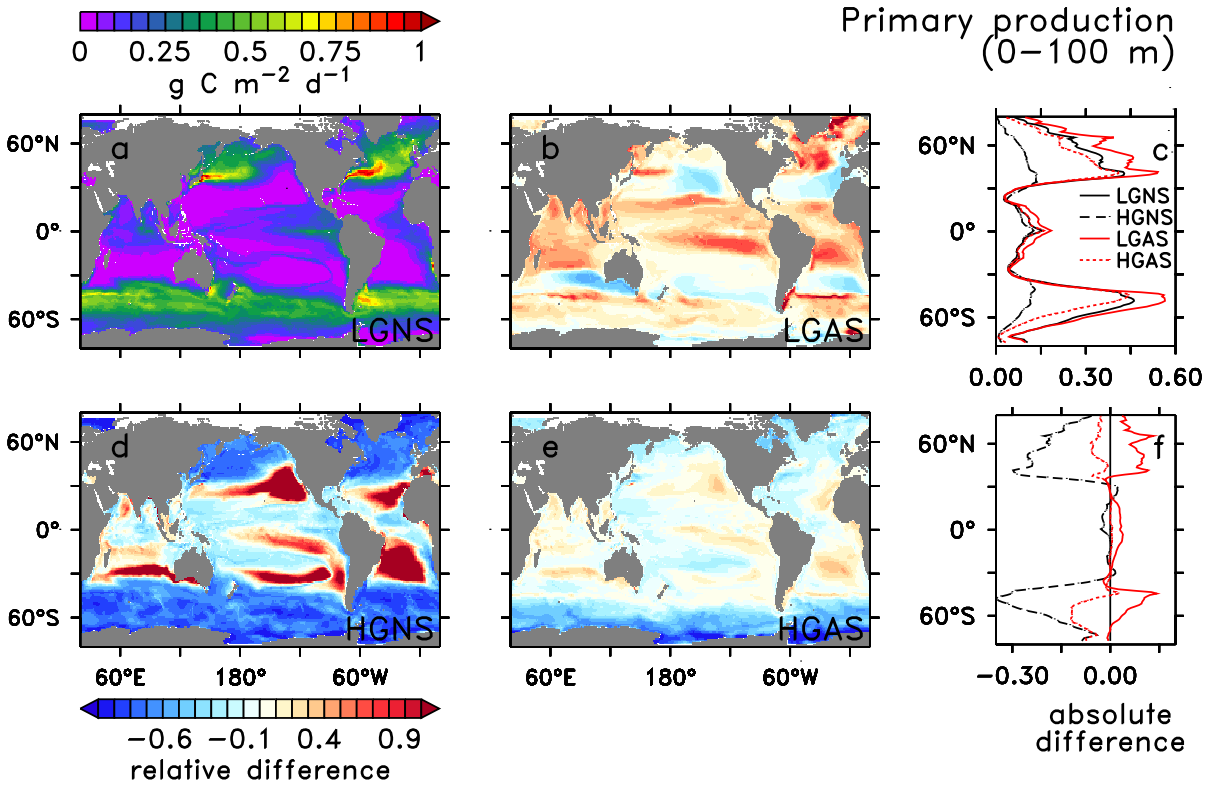

Figure 2.6: Primary production (PP). **a** Annual average PP (0-100 m depth) for LGNS is compared to **b** LGAS, **d** HGNS, and **e** HGAS as relative difference to LGNS. Zonal averages of PP are shown in **c** as absolute values and in **f** as absolute difference to LGNS for all configurations.

Our simulations demonstrate that a predator-mediated increase in phytoplankton diversity can coincide with an increase or a decrease in simulated productivity. An ecosystem with a more diverse phytoplankton community (LGAS) sustains higher PP and export production because of higher total phytoplankton biomass than a less diverse community (LGNS). However, this effect is sensitive to changes in model parameterization, as mechanisms that increase diversity can also result in lower productivity (HGAS). Changes in productivity are fueled by differences in nutrient distributions relative to the standard configuration, and thus differ regionally depending on the physical regime. However, these differences reflect the state of the ecosystem after only short (10 year) integrations from the same initial conditions. Longer term adjustments within the ecosystem might modify the results.

The HGAS configuration reduces simulated differences in PP between eastern and western North Atlantic. This is potentially an improvement in the models results: Observational estimates of PP at BATS (Bermuda Atlantic Time-series Study site) and at ESTOC (European Station for Time series in the Ocean) show little difference (0.38 versus 0.4 g C m^{-2} d^{-1}; Mouriño-Carballido and Neuer, 2008). On a global scale, however, the significance of the differences in PP and NCP is difficult to assess, as they are comparable with the uncertainties attached to the observational estimates. Differences in export production (not shown) between the different configurations are comparable to differences found for different multi-prey grazing formulations by Anderson et al. (2010). Our results support their study

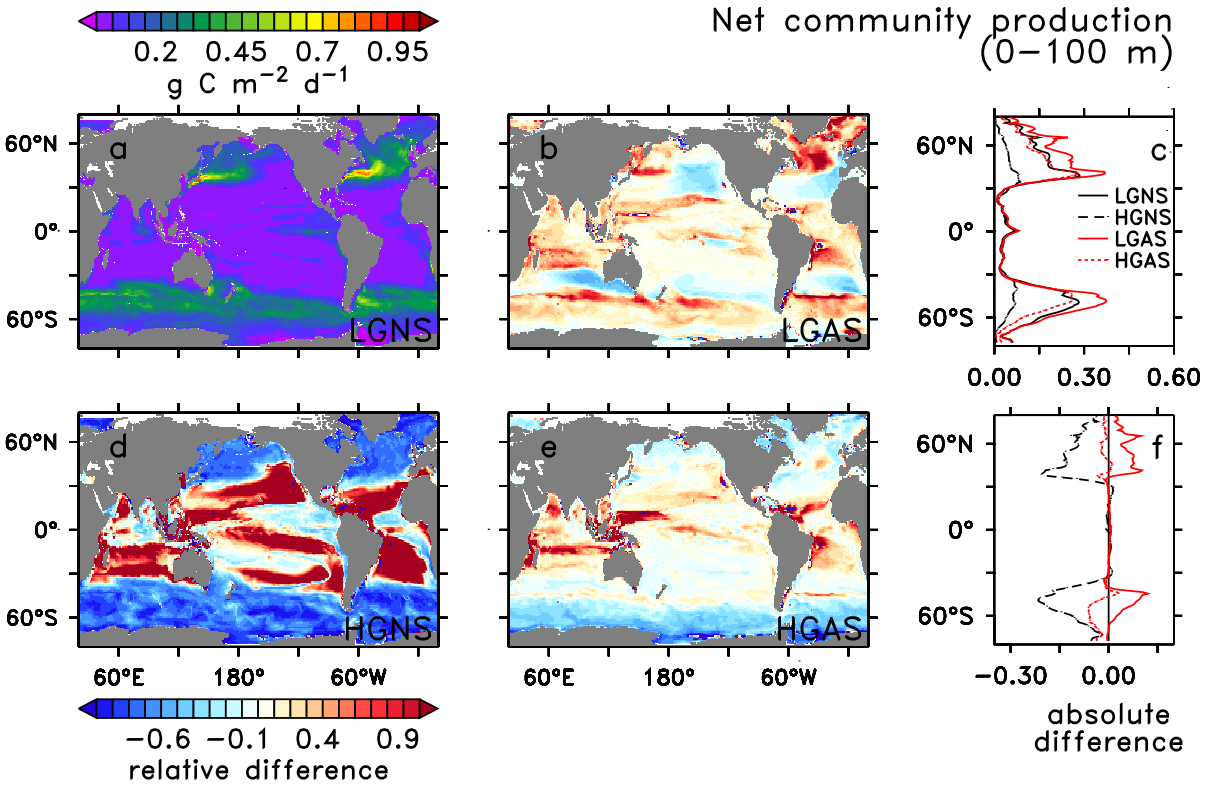

Figure 2.7: Net community production (NCP). **a** Annual average NCP (0-100 m depth) for LGNS is compared to **b** LGAS, **d** HGNS, and **e** HGAS as relative difference to LGNS. Zonal averages of NCP are shown in **c** as absolute values and in **f** as absolute difference to LGNS for all configurations.

in confirming that multi-prey grazing functional responses have a large influence on simulated model dynamics. A more detailed comparison addressing phytoplankton community structure, specifically regarding the effect of explicitly representing phytoplankton diversity within plankton functional types, is to be reported elsewhere.

2.4.4 Seasonal phytoplankton dynamics

The seasonal pattern of simulated phytoplankton diversity is illustrated for the site of the North Atlantic Bloom Experiment (NABE), where active switching sustains a more diverse phytoplankton community. For HGAS, the first phytoplankton spring bloom is followed by a second, lower biomass peak and moderate concentrations for the remainder of the year (Fig. 2.8a). This double peak agrees well with observed phytoplankton biomass (converted from carbon to phosphorus units using C:P=106 mol C (mol P)$^{-1}$ or from chlorophyll a data using P:Chl=0.7 g P (g Chl)$^{-1}$). The first peak (days 100 to 150) is dominated by large phytoplankton types which had high winter biomass (types L1, L3 in Fig. 2.8c) and high growth rates (Fig. 2.8e) in their environment. However, the type with the highest concentration also feels the highest grazing pressure ($G \cdot Z$, Fig. 2.8i), which reduces its growth more strongly than that of other types (Fig. 2.8g) which then bloom consecutively. The second peak

(day 175) is dominated by small phytoplankton types with lower maximum growth rates and higher nutrient affinity (S1, S2). Low grazing pressure allows them to survive the early spring and to finally displace the fast growing species (e.g. L1, L3) once nutrient concentrations decline at the end of the first bloom peak. This succession of smaller types following the larger types dominating the bloom is in good agreement with observations at NABE (Lochte et al., 1993; Sieracki et al., 1993).

In contrast, the standard configuration (LGNS) produces only one bloom peak (Fig. 2.8b) with one dominating small and one large phytoplankton type (Fig. 2.8d; S2 and L3, respectively). It overestimates observed peak biomass by a factor of 3 for the conversion assumed (see caption of Fig. 2.8). Here again types with high winter biomass (Fig. 2.8d) and high growth rates (Fig. 2.8f) dominate the peak. Without switching, grazing pressure is comparably high on all four phytoplankton types present until the bloom peak (Fig. 2.8j) and the types less adapted to winter conditions (S1, L8) cannot survive the bloom in sufficient concentrations to take over afterwards. As a consequence of the lower grazing pressure at high food concentrations, the bloom peaks later and is more pronounced for LGNS compared to HGAS. The bloom is ended bottom up by nutrient limitation on growth rates and top-down effects are of minor importance (Fig. 2.8f,h). For LGAS, results are between those for LGNS and HGAS: the model simulates seasonal succession of 3 types during the first bloom peak, but overestimates observed phytoplankton biomass and captures only one bloom peak. HGNS yields abrupt dynamics which seem unrealistic and overestimates observed phytoplankton biomass to a larger extent than does LGNS.

In previous modeling studies at NABE, the double peak was thought to result from co-limitation of diatoms by silicate (Fasham and Evans, 2000) or from single-phytoplankton-single-zooplankton interactions (Schartau and Oschlies, 2003). In our simulations with active switching, the double peak is a consequence of a phytoplankton community shift driven by both bottom-up and top-down mechanisms.

The simulated community dynamics at BATS mirror the differences from configurations at NABE. At BATS, the bloom is less clearly defined and total phytoplankton biomass is lower, but broadly consistent with chlorophyll observations. For HGAS, two bloom peaks are formed through a succession of large and small phytoplankton types, albeit less clearly than at NABE. For LGNS, one dominant phytoplankton type generates two less distinct bloom peaks. For both configurations, the bloom period is ended bottom-up by declining growth rates and top-down control by grazing is not important during this time of the year.

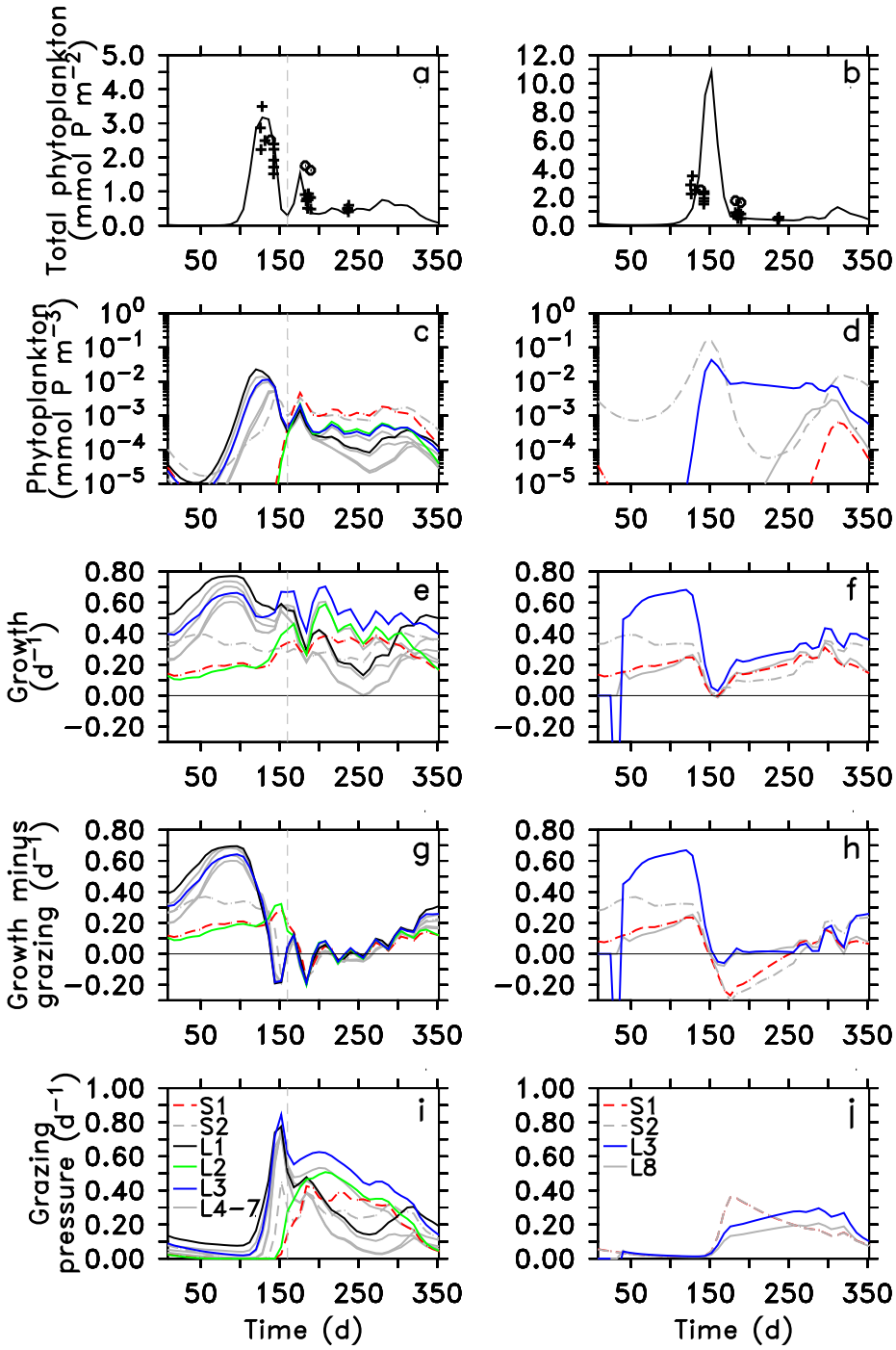

Figure 2.8: Phytoplankton dynamics at the NABE site (47°N, 20°W). For HGAS (left) and LGNS (right) **a,b,** Total phytoplankton concentration from simulations (line) and from observations of total phytoplankton biomass using C:P=106 mol C (mol P)$^{-1}$ (circles) and of chlorophyll a using P:Chl=0.7 g P (g Chl)$^{-1}$ (crosses). For all phytoplankton types present (S: small; L: large) averages of **c,d,** concentrations, **e,f,** growth (nutrient uptake minus sinking minus mortality), **g,h,** growth minus grazing, and **i,j,** total grazing pressure by both zooplankton types. Results are from a representative integration since specific phytoplankton composition differs between the five integrations of the ensemble.

2.5 Conclusions

Our results indicate that grazing pressure can be a key factor in shaping phytoplankton succession and community structure during blooms. Prey-ratio based predation, e.g. a type III or active switching formulation, increases diversity and better captures the observed succession. Significant changes in primary and net community production occur between simulations with different grazing formulations. Regional differences highlight the role of recycling of organic matter in models. We have shown here top-down mechanisms to have the potential for being essential drivers of phytoplankton diversity in global ecosystem models. In addition to the ongoing attempts to relate phytoplankton diversity to physiological variances in the phytoplankton population, the intricate interplay between top-down and bottom-up controls on shaping marine phytoplankton diversity patterns will require more attention in future studies.

Acknowledgements FP gratefully acknowledges the technical help from Oliver Jahn. The authors thank Pedro Cermeño for providing data for his observational diversity estimate. Constructive comments by three anonymous reviewers helped to improve the manuscript. FP is supported by the Kiel Cluster of Excellence "The Future Ocean". SD and MF acknowledge the support of the Gordon and Betty Moore Foundation, the National Oceanic and Atmospheric Administration, and the National Science Foundation.

Role of the funding source The funding sources had no involvement in study design, analysis and interpretation of data, writing of the report or the decision to submit the paper for publication.

2.6 Appendix

2.6.1 Derivation of the *high grazing* parameter set

The grazing parameters in the *high grazing* configuration are derived from a mechanistic predation model for zooplankton. The model is based on size-dependent encounter rate formulations (Visser, 2007) for a generic cruise or current feeder. Encounter rates (r_{kj}; see Table 2.2 for symbols and units) between a zooplankton predator k and its phytoplankton prey j are calculated from the volume the predator can search given its detection area ($\pi R_{det,k}^2$), its swimming velocity (v_k^Z), the phytoplankton sinking speed ($v_{snk,j}$), the phytoplankton abundance (N_j^P), and the selectivity (σ) or preference (ρ), here shown for no switching

$$r_{kj} = \pi R_{det,k}^2 \rho_{jk} N_j^P \sqrt{{v_k^Z}^2 + {v_{snk,j}^P}^2} \quad . \tag{2.11}$$

Detection distance ($R_{det,k}$) and v_k^Z are assumed to scale linearly with predator size (expressed as equivalent spherical diameter ESD_k^Z). The $v_{snk,j}^P$ are interpolated from observations (Smayda, 1970).

The ingestion rate is calculated from the encounter rates considering a handling time (t_H) per successful encounter between predator and prey

$$I_{jk} = \frac{M_j^P}{M_k^Z} \frac{r_{kj}}{1 + t_H r_{kj}} \quad . \tag{2.12}$$

The handling time is set by the handling time constant (t_H^0) and assumed to vary proportionally with the predator-prey size ratio (M_j^P/M_k^Z; Pahlow and Prowe, 2010)

$$t_H = t_H^0 M_j^P / M_k^Z \quad . \tag{2.13}$$

Effects of turbulence, in the form of an additional turbulent velocity increasing the encounter rates, are not considered here to enhance comparability with the original predation model.

The mechanistic predation model (Eq. 2.11, 2.12) reduces to a type II formulation for both active and no switching, here shown for no switching

$$I_{jk} = \frac{1}{t_{H_0}} \frac{\rho_{jk} P_j}{\frac{M_k^Z}{t_{H_0} F} + \rho_{jk} P_j} \quad , \tag{2.14}$$

where $F = \pi R_{det,k}^2 \sqrt{{v_k^Z}^2 + {v_{snk,j}^P}^2}$. The maximum ingestion rate is given by $g_{max} = 1/t_{H_0}$ and the half-saturation concentration is $\kappa_k^P = M_k^Z/(t_{H_0} F)$. This qualitatively corresponds to the traditional grazing formulation implemented in the original model (Eq. 2.2).

Parameters for the mechanistic predation model were estimated from literature data. Zooplankton swimming speed generally increases with body size. For this application, $v_k^Z = 2.9\ ESD_k^Z$ s^{-1} according to data on different zooplankton groups ranging from 4 μm ESD to 1.3 mm ESD (Hansen et al., 1997; Broglio et al., 2001; Strom and Morello, 1998; Tiselius and Jonsson, 1990). The t_{H_0} is set to yield a maximum ingestion rate of about 1 d^{-1} (Hansen et al., 1997), which is used for both the small and the large zooplankton type to be consistent with the original model. Body masses of phytoplankton and zooplankton (M_j^P and M_k^Z, respectively) are calculated from volumes (V_j^P and V_k^Z, respectively) based on cell or body size (ESD) for phytoplankton (Menden-Deuer and Lessard, 2000)

$$M_j^P\,[pg\ C] = 0.288 \cdot V_J^P \left[\mu m^3\right]^{0.811} \tag{2.15}$$

and for zooplankton (Verity and Langdon, 1984)

$$M_k^Z\,[pg\ C] = 0.445 + 0.053 \cdot V_k^Z \left[\mu m^3\right] \tag{2.16}$$

and converted to model units (mmol P cell^{-1}) using Redfield stoichiometry. The detection distance is set

to $R_{det,k} = 1ESD_k^Z$ for simplicity, which is within the range of values calculated for hydromechanical detection of different types of prey (Visser, 2001). While for the *low grazing* configurations $g_{max} = 0.5\ \mathrm{d}^{-1}$ and $\kappa_k^P = 0.1$ mmol P m^{-3} (Table 2.1), the above parameter choices for the mechanistic model imply $g_{max} = 1\ \mathrm{d}^{-1}$ and $\kappa_k^P = 0.027$ mmol P m^{-3}, thus generally resulting in higher ingestion rates in the *high grazing* configurations. Differences in κ_k^P arising from the different size of the two zooplankton types (cf. Table 2.2) are negligible and an intermediate κ_k^P is employed for both zooplankton types in accordance with the original model.

Table 2.2: Symbols used in the text and parameter values used with the mechanistic predation model to derive the *high grazing* parameter set. j and k denote specific phytoplankton and zooplankton types, respectively. Cell or body sizes are given as equivalent spherical diameter (ESD).

variable	value	unit	description
ESD_s^P	1 μm	μm	cell size (ESD) of small phytoplankton
ESD_l^P	10 μm	μm	cell size (ESD) of large phytoplankton
ESD_s^Z	30 μm	μm	body size (ESD) of small zooplankton
ESD_l^Z	300 μm	μm	body size (ESD) of large zooplankton
G_{jk}		mmol P^{-1} d^{-1}	specific grazing pressure of zooplankton k for phytoplankton j
g_{max}	0.5 or 1	d^{-1}	maximum grazing rate (small and large zooplankton)
I_{jk}		d^{-1}	ingestion rate of zooplankton k for phytoplankton j
κ_s^P	0.1 or 0.027	mmol P m^{-3}	half-saturation concentration for grazing (small zooplankton)
κ_l^P	0.1 or 0.027	mmol P m^{-3}	half-saturation concentration for grazing (large zooplankton)
M_j^P		mmol P cell^{-1}	phytoplankton body mass
M_k^Z		mmol P pred^{-1}	zooplankton body mass
N_j^P		cells m^{-3}	phytoplankton abundance
P_j		mmol P m^{-3}	phytoplankton concentration
$R_{det,k}$	1 ESD_k^Z	m	zooplankton detection distance
r_{jk}		cells pred^{-1} d^{-1}	encounter rate of zooplankton k and phytoplankton j
ρ_{jk}			preference of zooplankton k for phytoplankton j
σ_{jk}			selectivity of zooplankton k for phytoplankton j
t_H		d	handling time
t_H^0	$8 \cdot 10^4$ s	d	handling time constant
$v_{snk,j}^P$		m d^{-1}	phytoplankton sinking velocity
v_k^Z	2.9 ESD_k^Z s^{-1}	m d^{-1}	zooplankton swimming velocity
V_j^P		μm^3	phytoplankton cell volume (from ESD)
V_k^Z		μm^3	zooplankton body volume (from ESD)
Z_k		mmol P m^{-3}	zooplankton concentration

2.6.2 Diversity between different integrations of the ensemble

Results presented in this study are the average of an ensemble of five integrations each with a different set of phytoplankton parameters randomly chosen within a given range. Phytoplankton diversity differs only slightly between different integrations (Fig. 2.9). The geographical patterns for all integrations (not shown) are similar and differ less between integrations with the same configuration than between different configurations.

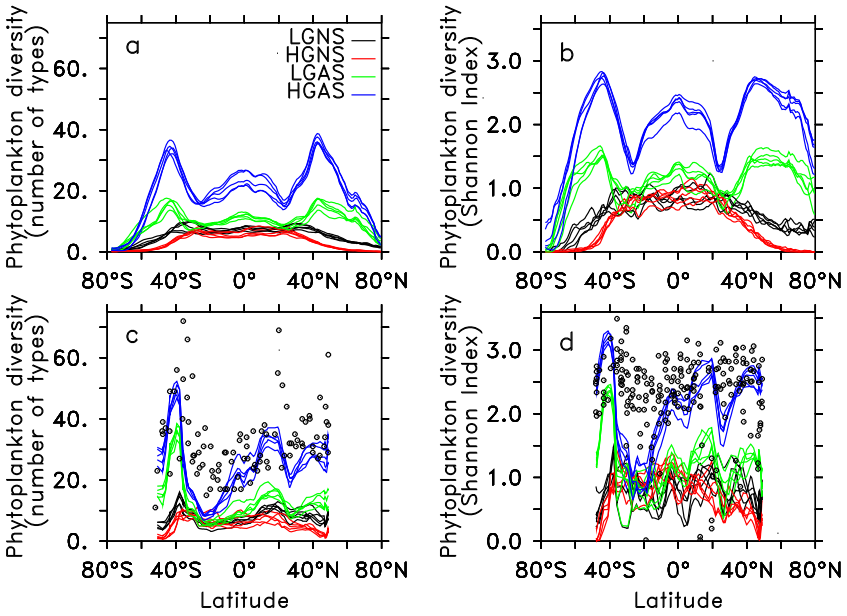

Figure 2.9: Diversity in individual integrations of the ensemble. Simulated annual average phytoplankton diversity as **a,c,** number of phytoplankton types exceeding a threshold concentration of $P_{th} = 10^{-8}$ mmol P m^{-3} and **b,d,** as Shannon Index. The ensemble of five integrations for LGNS, LGAS, HGNS, and HGAS is presented **a,b,** as zonal average and **c,d,** along the Atlantic Meridional Transect (AMT) in comparison to diversity calculated from biomass observations for diatoms, dinoflagellates and coccolithophores (circles) along the AMT as number of species (surface data) and Shannon Index (Cermeño et al., 2008).

2.6.3 Changes in primary production and net community production between configurations

For both LGAS and HGAS, total phytoplankton biomass and PP increase compared to LGNS and HGNS, respectively, in the productive higher latitudes and in the tropics (shown for LGAS in Fig. 2.5b, 2.6b). For LGAS, in higher latitudes lower nutrient concentrations in the surface mixed layer (not shown) lead to a stronger vertical nutrient gradient, and thereby cause higher input of nutrients from the deeper layers by processes like deep winter mixing (Fig. 2.10h). This enhanced nutrient input fuels the largest part of the PP increase, while only a small fraction is due to higher recycling of dissolved organic matter (DOM). Together with less grazing (Fig. 2.10e), higher total phytoplankton biomass remains (Fig. 2.10b). In contrast, in the permanently stratified low latitude regions (25°S-25°N) with little nutrient input by vertical eddy diffusion, enhanced recycling of DOM via phytoplankton mortality is mostly responsible for higher PP and appears to enhance a "fast recycling loop" (Fig. 2.10h). With switching, the damped growth of dominant types and the reduced grazing pressure on phytoplankton types less successful in the competition for nutrients allows the latter types to grow, albeit slowly, at low nutrient concentrations. This increases not only diversity, but also total phytoplankton biomass. At higher latitudes, a fraction of this phytoplankton biomass is exported to greater depths as particulate organic matter (POM; Fig. 2.10n) which is thus not available for remineralization in the surface layer but enhances NCP instead (Fig. 2.7). The lower latitudes are dominated by small phytoplankton

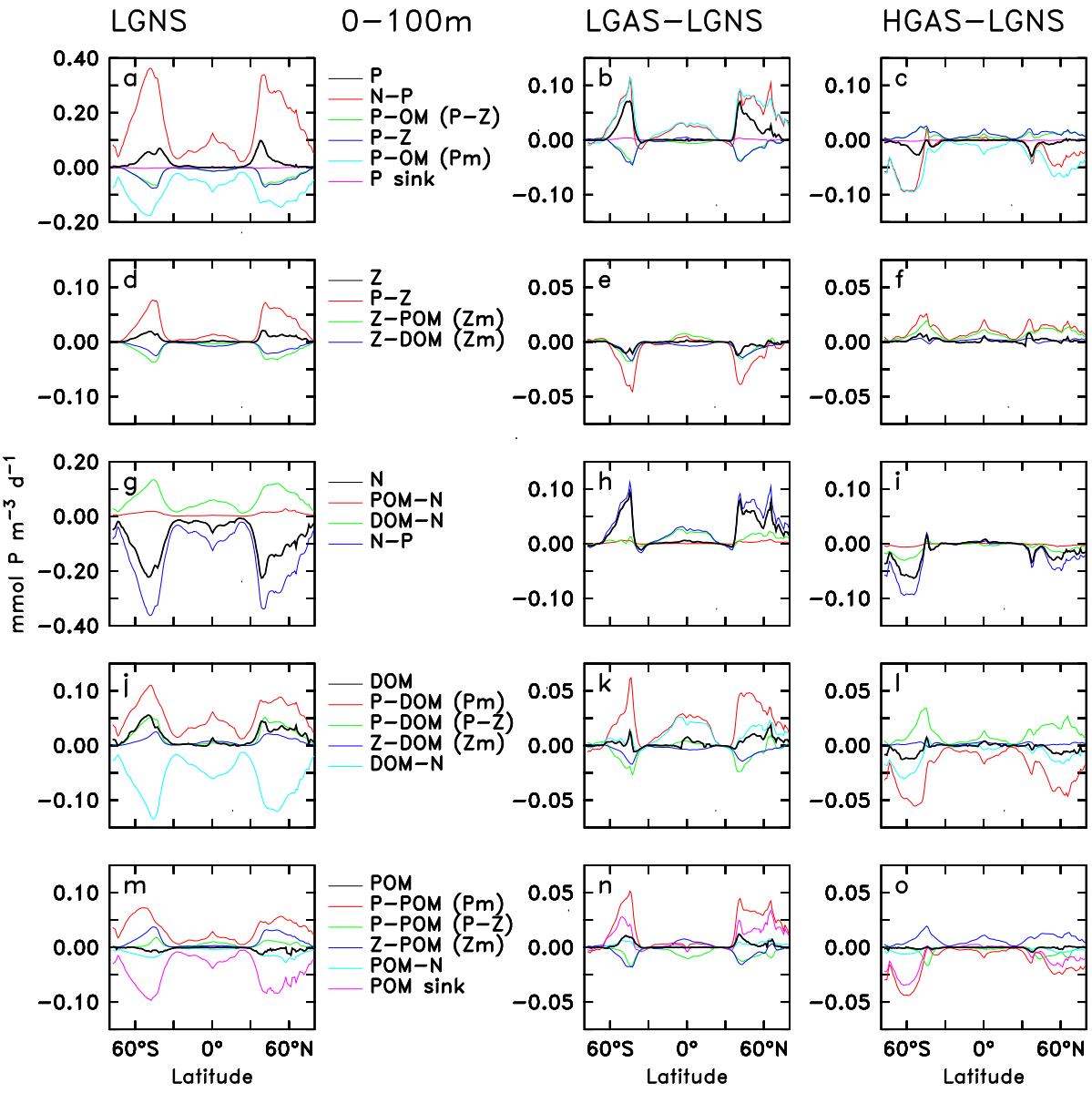

Figure 2.10: Differences in model dynamics between configurations. Fluxes between state variables in the model are shown integrated over the top 100 m as zonal average. Left panels: For LGNS, the black line represents the balance between source (positive) and sink (negative) fluxes. For LGAS and HGAS (middle and right panels, respectively), all lines are absolute changes relative to LGNS, with positive and negative values denoting increases and decreases of the respective flux. State variables for which fluxes are presented from top to bottom are phytoplankton (P), zooplankton (Z), nutrient (phosphate; N), dissolved organic matter (DOM) and particulate organic matter (POM). Fluxes are primary production (N-P), sloppy feeding losses (P-OM (P-Z)), grazing (P-Z), phytoplankton mortality (P-OM (Pm)), phytoplankton sinking (P sink), zooplankton losses to DOM (Z-DOM (Zm)) and POM (Z-POM (Zm)), recycling of DOM (DOM-N) and POM (POM-N) from phytoplankton mortality (P-DOM (Pm) and P-POM (Pm)) and sloppy feeding (P-DOM (P-Z) and P-POM (P-Z)), sinking of POM (POM sink). The black line in **g** shows that nutrients taken up by phytoplankton cannot be supplied by recycling of DOM and POM, and thus indicate physical supply by mixing.

types, for which higher mortality leads to more DOM but little more POM (Figs. 2.10k,n). If grazing rates are increased (HGAS), the phytoplankton standing stock is reduced compared to LGAS, causing lower recycling of nutrients via phytoplankton mortality (Fig. 2.10c). The simultaneous decrease in PP,

however, predominantly reflects lower nutrient inputs by vertical mixing caused by higher nutrient concentrations in the surface layer (Fig. 2.10i). Lower phytoplankton mortality also leads to lower export of POM, and thus lower NCP (Fig. 2.7), in the productive regions, and is only partly compensated by increased fecal pellet production by the zooplankton (Fig. 2.10o).

3 Controls on the diversity-productivity relationship in a marine ecosystem model

This chapter is a submitted manuscript by A. E. F. Prowe, M. Pahlow, and A. Oschlies.

Abstract Species diversity influences the productivity of ecosystems across habitats, and may influence their susceptibility to environmental changes. More diverse communities are often found to be more productive because selection and complementarity effects allow more efficient use of available resources. However, which principles promote coexistence in pelagic model ecosystems is only beginning to be understood as are controls on the diversity-productivity relationship. Here we show that the diversity-productivity relationship of phytoplankton in a global self-assembling ocean ecosystem model depends on the simulated nutrient supply. Increasing productivity with increasing diversity can be found in regions with high nutrient supply. Using a simple idealized model we show that a more diverse community can be more productive if different phytoplankton types utilize complementary niches, here created by preferential zooplankton grazing, thereby increasing resource use. In our model context, total nutrient supply determines a maximum diversity sustained by the ecosystem. Systems with a low nutrient supply cannot sustain high productivity of more diverse communities and produce a neutral or even negative diversity-productivity relationship. Our model results suggest links between diversity, productivity and export production in marine pelagic ecosystems, with the potential for feedbacks of diversity on productivity in response to expected future environmental changes.

3.1 Introduction

Diversity loss is likely to affect the functioning of ecosystems across habitats (McCann, 2000; Isbell et al., 2011). In marine ecosystems, diversity loss could threaten the supply of goods and services of the ocean to humankind (Worm et al., 2006). The notion that high diversity can make ecosystems less vulnerable to environmental changes and sustain its functioning provides an important perspective in the discussion about potential effects of ongoing and future change (Naeem and Li, 1997; Yachi and Loreau, 1999). Diversity affects the functioning of ecosystems via a variety of mechanisms in different ways depending on ecosystem type or environmental conditions (Hooper et al., 2005). Previous studies addressing the relationship between marine biodiversity and ecosystem functioning have often focused on benthic communities or higher trophic levels (Stachowicz et al., 2007; Worm et al., 2006). Evidence

of what governs the effect of diversity on productivity in pelagic ecosystems is still scarce (Duffy and Stachowicz, 2006; Cardinale et al., 2011; Ptacnik et al., 2008, 2010).

The relationship between diversity and ecosystem functioning can take many different shapes (see references in Hooper et al., 2005). One pertaining pattern is an increase in productivity with higher diversity of primary producers. To explain this increase, two mechanisms are commonly proposed: (1) Higher productivity might reflect a selection effect, where the likelihood of a highly productive species being present increases with species richness, or (2) complementarity through niche partitioning or facilitation can lead to higher productivity in more diverse systems (Tilman et al., 1997; Loreau, 1998). In contrast, diversity might not influence productivity if, for example, the system is dominated by one key species present also at low diversity.

These mechanisms were derived mainly for terrestrial and benthic ecosystems (Hooper et al., 2005; Cardinale et al., 2011), which differ from the pelagic realm in that they are structured by spatial constraints, e.g., settling space. Although indications exist that some of these mechanisms might also play a role in the pelagic ocean (Duffy and Stachowicz, 2006), what shapes the relationship between phytoplankton diversity and productivity is only beginning to be understood (Ptacnik et al., 2008, 2010). Ecosystem models are one important tool to investigate and ultimately predict effects of diversity on marine pelagic ecosystem functioning. One way to resolve diversity in large-scale ocean ecosystem models is via formulating a variety of plankton functional types (Le Quéré et al., 2005). An alternative approach explicitly formulates a trait-based phytoplankton community (Follows et al., 2007). In this model, a large number (n=78) of phytoplankton types with different randomly assigned trait values for traits like size and nutrient requirements compete for a number of different limiting nutrients in a global model ocean. The phytoplankton community assembles as a result of physical environmental constraints and competition between the phytoplankton types. In oligotrophic regions with low seasonality and thus stable conditions, the outcome of competition between phytoplankton types can be interpreted using resource competition theory (Dutkiewicz et al., 2009; Barton et al., 2010a). In this model community, phytoplankton diversity can be increased by replacing the standard Holling type 2 zooplankton grazing formulation with a sigmoidal Holling type 3 functional response (Prowe et al., subm., Chapter 2). The sigmoidal grazing response is known to promote coexistence (Murdoch, 1969; Murdoch and Oaten, 1975) by generating individual limiting factors for each phytoplankton type and thereby allowing more types to coexist (Levin, 1970; Chase et al., 2002). We are thus beginning to understand how two important governing forces of coexistence and diversity, namely competition for resources and predation, can shape ecosystem structure in marine ecosystem models.

But what are the consequences and hence the relevance of phytoplankton diversity for the functioning of the simulated ecosystem on a global scale? In order to approach this question we examine global averages of total primary production (PP) and total phytoplankton biomass ($\sum$P) in simulations exhibiting different phytoplankton diversity performed with a 3-dimensional coupled ocean ecosystem model. Starting from two reference model configurations characterized by low and high diversity for the same physical environment (Prowe et al., subm., Chapter 2) we configure simulations with reduced and ele-

vated diversity and investigate the resulting relationships between diversity and productivity. In order to examine what governs the shape of the diversity-productivity relationship in the 3-dimensional global model, we construct a simplified 0-dimensional model of resources, phytoplankton and zooplankton representative of commonly applied marine ecosystem models. We interpret idealized 0-D simulations in terms of competition theory and identify mechanisms governing the diversity-productivity relationship captured by the model. These are then used to explain the regional patterns in the 3-D global ecosystem model.

3.2 Methods

3.2.1 The 3-dimensional global ecosystem model

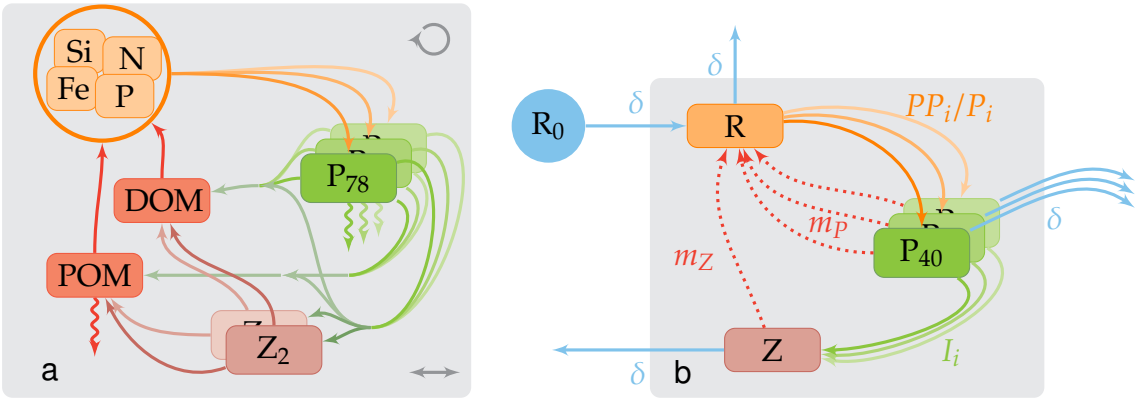

Figure 3.1: The 3-D and the simplified 0-D ecosystem models. (a) The 3-D model includes several nutrients containing elements N, P, Si, and Fe, 78 phytoplankton (P) and 2 zooplankton (Z) types, remineralization via dissolved and particulate organic matter (DOM and POM, respectively), sinking, advection, and mixing processes. (b) The 0-D model has only one nutrient (R), 40 phytoplankton types, and 1 zooplankton type. In the standard chemostat configurations, nutrient input (R_0) and dilution (δ) of all state variables (blue arrows) are in effect and remineralization fluxes (red dotted arrows) are omitted. In the batch culture configurations, remineralization fluxes (m_P and m_Z) compensate for omitted nutrient input and dilution. PP_i and I_i are primary production and ingestion of the individual phytoplankton types.

The relationship between productivity and diversity in a global model ocean is examined in simulations using the 3-D global ecosystem model presented by Follows et al. (2007) in the configuration used by Prowe et al. (subm., Fig. 3.1a, Chapter 2). The model contains the nutrients phosphate, nitrate, nitrite, ammonium, iron, and silicate, 78 phytoplankton types, a small and a large zooplankton type, dissolved and particulate organic matter. Temperature-dependent phytoplankton growth takes into account limitation by light, including effects of self shading and, via a Liebig-type minimum function, by the most limiting nutrient according to a Michaelis-Menten formulation. Phytoplankton losses include a linear mortality, sinking and zooplankton predation, which in the standard configuration is formulated as a Holling type II functional response. Both zooplankton types have the same maximum grazing rate

and half-saturation concentration for grazing. Their grazing rates differ only in the preferences for the different phytoplankton types, which are assigned according to size and palatability.

We compare results of two of the configurations used by Prowe et al. (subm., Chapter 2) which differ only in the zooplankton grazing functional response, namely *low grazing&no switching* (LGNS) with a Holling type 2 response and *low grazing&active switching* (LGAS) with a Holling type 3 response generated by active switching (cf. also Section 3.2.2). In this study, we use as the standard simulation one representative simulation of their ensemble of five simulations with a seed population of n=78 phytoplankton types with randomly assigned trait values for nutrient uptake, light-limited growth, optimal temperature, size (small and large) and sinking speed (see Dutkiewicz et al., 2009, for details on randomization and imposed trade-offs). For this designated phytoplankton community, we create less diverse communities by selecting random sub-groups of seed populations of 15, 30, and 55 phytoplankton types. Adding another n=78 phytoplankton types increases the size of the seed population to n=156 types and provides simulations with further elevated diversity. For each level of reduced initial diversity, five different phytoplankton sub-populations are selected randomly. Realized diversity is measured as the number of phytoplankton types whose concentration exceeds a threshold concentration P_{th} (Table 3.1). Total phytoplankton primary production (PP) is used as a proxy for ecosystem productivity. Annual average realized diversity and PP in the top 0-100 m of the water column are averaged globally for the 10th year of a simulation, by which time diversity and PP have stabilized.

3.2.2 The 0-dimensional model

The 0-D model used in this study is simplified from the 3-D ecosystem model and in its structure represents a typical ecosystem model used in marine modelling studies from small to global scale (Fig. 3.1). It describes the dynamics of a single resource (R), between 1 and 40 phytoplankton types (P_i), and a single zooplankton grazer (Z; Eqs. 3.1-3.3) in a chemostat setup.

$$\frac{\partial R}{\partial t} = -\sum_{r=1,n}\left(\mu\frac{R}{R+k_{R_r}}P_r\right)+\delta(R_0-R) \tag{3.1}$$

$$\frac{\partial P_i}{\partial t} = \mu\frac{R}{R+k_{R_i}}P_i - I_iZ - \delta P_i \tag{3.2}$$

$$\frac{\partial Z}{\partial t} = \sum_{r=1,n}(I_rZ) - \delta Z \tag{3.3}$$

Continuous nutrient input of a fixed concentration (R_0) and losses to all state variables are determined by the dilution rate (δ). Nutrient uptake is formulated as a Michaelis-Menten function with maximum resource uptake rate μ. Phytoplankton types are distinguished by their half-saturation concentrations for nutrient uptake (k_{R_i}). Predation is formulated alternatively as a Holling type 2 or a Holling type 3

Table 3.1: Parameters for model configurations. Parameter values of the standard simulations, initial conditions and diversity threshold P_{th} for all simulations. r is a random number between 0 and 1.

	unit	chemostat		batch culture (basic type 3)		
		type 2, type 3 (basic)	type 3 (active switching)	high R supply	medium R supply	low R supply
R_0	mmol P m^{-3}	1.0	1.0	–	–	–
δ	d^{-1}	0.3	0.3; 0.125	–	–	–
μ	d^{-1}	1.4	1.4	1.4	1.4	1.4
k_R	μmol P m^{-3}	15+r·20	15+r·20	15+r·20	15+r·20	15+r·20
g	d^{-1}	0.5	0.5	0.5	0.5	0.5
k_P	mmol P m^{-3}	0.1	0.1	0.1	0.1	0.1
ρ		0.5	0.5	0.5	0.5	0.5
m_P	d^{-1}	–	–	0.2	0.1	0.0
m_Z	d^{-1}	–	–	0.3	0.3	0.3
R_{ini}	mmol P m^{-3}			0.1		
$(\sum P)_{ini}$	mmol P m^{-3}			0.6		
Z_{ini}	mmol P m^{-3}			0.3		
P_{th}	mmol P m^{-3}			10^{-8}		

(basic or active switching) functional response (Eqs. 3.4-3.6; Holling, 1959a; Gentleman et al., 2003)

$$\text{type 2:}\quad I_i = g\frac{\rho P_i}{k_P + \sum_{r=1,n}(\rho P_r)} \tag{3.4}$$

$$\text{type 3 (basic):}\quad I_i = g\frac{\rho P_i^2}{k_P^2 + \sum_{r=1,n}(\rho P_r^2)} \tag{3.5}$$

$$\text{type 3 (active switching):}\quad I_i = g\frac{\sigma_i P_i}{k_P + \sum_{r=1,n}(\sigma_r P_r)}\ ,\ \sigma_i = \frac{\rho P_i}{\sum_{r=1,n}(\rho P_r)} \tag{3.6}$$

with maximum predation rate (g), half-saturation concentration (k_P), and the fixed or variable preferences for each phytoplankton type (ρ or σ, respectively). The basic type 3 and active switching responses are qualitatively equivalent but differ in the half-saturation constants (Fig. 3.2; Appendix 3.6.1). In the active switching formulation, feeding preferences of the predator for different phytoplankton types depend on the relative abundances of the respective phytoplankton types (prey-ratio based preferences, Eq. 3.6). This formulation is thus based on a more intuitive behavioral description than the basic type 3 with constant preferences, and is therefore also included in the comparison.

The three functional responses, the type 2 and the type 3 basic and active switching responses (Eqs. 3.4-3.6), provide three standard configurations that generate two fundamentally different model ecosystems: with a type 3 functional response, the individual PP of each phytoplankton type (PP_i) and the individual phytoplankton biomass (P_i) are (for typical parameter values) limited by grazing at levels $PP_{i,0}$ and $P_{i,0}$, respectively ("predation-limited PP_i"; Fig. 3.2b). The $PP_{i,0}$ and $P_{i,0}$ depend on the nutrient concentration via resource uptake, but also on the biomass of the other coexisting types via the grazing formulation.

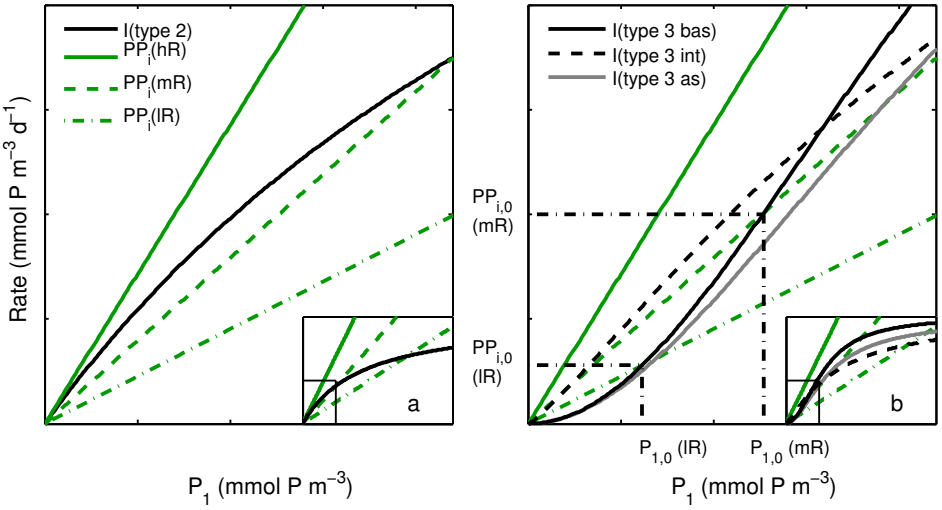

Figure 3.2: Zooplankton grazing functional responses. Primary production (PP$_i$) at high (hR), medium (mR) and low (lR) nutrient concentration and ingestion rate (I) for different functional responses in a hypothetical 2-phytoplankton system with type 1 increasing in concentration (P_1), while P_2 is held constant at 0.21 mmol P m^{-3}. (a) Holling type 2 functional response; (b) Holling type 3 responses: basic type 3 (bas), active switching (as), and with an intermediate exponent of prey concentration of 1.2 (int). P$_{1,0}$ and PP$_{i,0}$ denote the levels at which biomass and primary production of P_1, respectively, are limited by a type 3 functional response (here basic type 3) at medium and low nutrient concentration. Insets display an extended axis range.

With a type 2 response and typical parameter values, PP$_i$ is not limited by losses, but only by nutrient availability ("resource-limited PP$_i$"; Fig. 3.2a).

The model contains seven parameters per phytoplankton type, six of which (μ, g, k_P, ρ, h, δ) are uniform for all phytoplankton types to obtain the simplest model configuration which captures the mechanisms at work in the 3-D model (Table 3.1). Standard parameter values are taken from the 3-D model configuration for small phytoplankton types (Prowe et al., subm., Chapter 2). Feeding preferences are set to an intermediate value. The dilution rate δ substitutes mixing processes and recycling in the surface mixed layers. Preliminary simulations were performed with different δ values. Results shown below use an intermediate value of $\delta = 0.3$ d^{-1}. Random assignment of the nutrient half-saturation concentration (k_{R_i}) based on a uniform distribution within a prescribed range is used to distinguish different phytoplankton types, but sets of random values differ between the 3-D and 0-D models.

A set of simulations with different initial phytoplankton diversity (a diversity series) is obtained by initializing the number of phytoplankton types as either 1, 2, 3, 5, 10, 20, 30, or 40 different types. Random parameter assignment for k_{R_i} uses the same series of random numbers so that, e.g., in the simulations with 20 phytoplankton types the first 10 types are identical to the 10-phytoplankton-type setup. Simulations are integrated for 1000 days from initial conditions, where initial nutrient, initial biomass of zooplankton, and total initial biomass of all phytoplankton types are uniform across simulations (Table 3.1). Each diversity series is repeated with 5 different sets of random values for assigning

k_{R_i}, with results averaged over all ensemble members. Results are only used for analysis if, at the end of the integration, the system is at steady state (approx. 93% of all simulations). In oscillating systems, we assume steady state when the ratio of amplitude to average of the oscillating predator or total phytoplankton concentrations is smaller than 0.1 or when the amplitude decreases below 0.5% of the total initial resources (nutrient and biomass) in the system. The standard simulations are obtained using the standard parameter set (Table 3.1) with a type 2 response, a basic type 3 response and a type 3 response employing active switching.

For the 0-D model, the term "diversity" refers to the realized phytoplankton diversity at steady state, which is taken as the number of coexisting phytoplankton types, i.e., types with a concentration exceeding P_{th} (Table 3.1), at the end of the integration. Total primary production (PP) serves as proxy for ecosystem productivity. Critical resource levels for each phytoplankton type (R_i^*) are calculated by solving Eq. 3.2 for R at steady state

$$\frac{\partial P_i}{\partial t} = 0 \Leftrightarrow R_i^* = \frac{k_{R_i} m_i}{\mu - m_i} \quad , \quad m_i = \frac{I_i Z}{P_i} + \delta \tag{3.7}$$

(Tilman, 1977). They reflect differences in both resource uptake and grazing for the individual phytoplankton types, the latter of which is influenced by the concentrations of all coexisting phytoplankton types (Eqs. 3.4-3.6). Taking grazing into account, the R_i^* of each phytoplankton type i thus becomes a property of the entire system rather than solely reflecting individual phytoplankton traits like the traditional R^* concept developed for chemostat systems without grazers (Tilman, 1977).

The sensitivity of the model results to the shape of the functional response is further examined for a type 3 response with an exponent of 1.2 instead of 2. A sensitivity analysis for all other parameters except ρ is performed by varying parameters in turn by $\pm 10\%$ and $\pm 20\%$ with all other parameters set to their standard values (Table 3.1). All sensitivity simulations are performed as described above. In order to investigate the role of nutrient supply in more detail, we also employ simulations with a batch culture setup (Fig. 3.1), where the dilution rate is set to 0 and zooplankton mortality (m_Z) constitutes the closure of the system (see 3.6.2 for model equations). Mortality of phytoplankton (m_P) and zooplankton (m_Z) compensates for the input of "new" nutrients by providing remineralized nutrients. The strength of this nutrient supply is varied by changing m_P. Also for the batch culture simulations, PP in steady state (at the end of the simulation) serves as proxy for the productivity of the system.

3.3 Results

3.3.1 The diversity-productivity relationship

In our 3-D simulations, the relationship between globally averaged diversity and PP differs notably for the two grazing formulations. In simulations with a type 3 functional response (based on the LGAS configuration), both realized diversity and PP increase with increasing initial diversity. Realized diver-

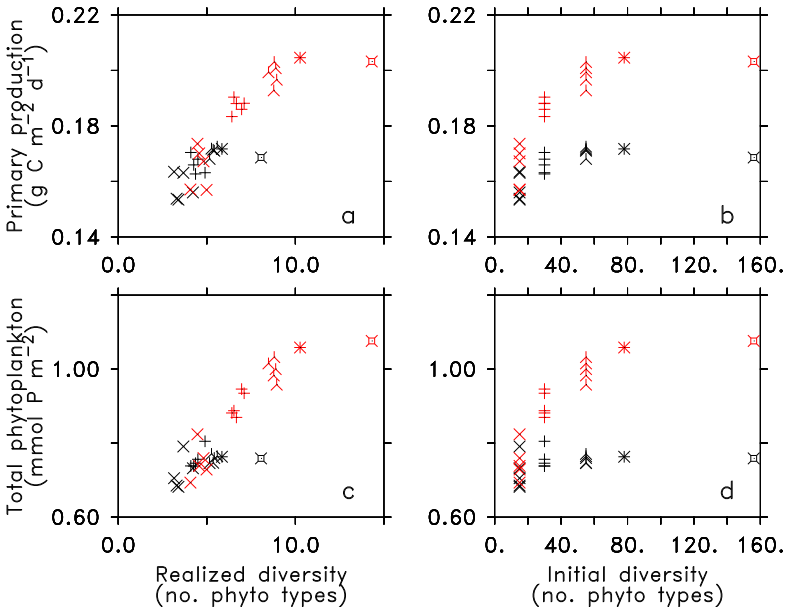

Figure 3.3: The global diversity-productivity relationship. Average global primary production (a-b) and total phytoplankton biomass (c-d) in Year 10 in the upper 0-100 m of the water column for different realized (a,c) and initial (b,d) phytoplankton diversity. Simulations are performed for a type 2 (black) and type 3 (active switching; red) functional response. The reference simulations ($*$) employ a seed population of 78 phytoplankton types (Prowe et al., subm., Chapter 2). The additional simulations employ three different sub-populations of 15 ($\times$), 30 ($+$) and 55 ($\curlywedge$) phytoplankton types selected randomly from the original seed population of 78 types, as well as a configuration with 156 types (78 additional types; $\boxplus$).

sity and PP saturate above an initial diversity of about 80 types (Fig. 3.3). For a type 2 response (the LGNS configuration), diversity levels are equally low irrespective of the chosen initial diversity levels, and a relationship between diversity and PP cannot be identified. The behavior of $\sum$P is very similar to that of PP for both configurations.

Our 0-D simulations with a type 2 and a type 3 functional response capture the two different relationships between diversity and PP found in the 3-D global model. For type 2 grazing, within a diversity series diversity ranges from one to less than five coexisting species, $\sum$P is approximately constant and PP increases only very little at higher diversity (Fig. 3.4). Employing a basic type 3 response, up to 30 types coexist and both PP and $\sum$P increase with increasing diversity. There appears to be a limit to realized diversity, and PP saturates at high diversity. The results for the active switching configuration are qualitatively similar to those using the basic type 3 response, although diversity is generally lower for active switching. As the ingestion is lower than for the basic type 3 response (Fig. 3.2), diversity increases when δ is reduced compared to the standard configuration (Fig. 3.4).

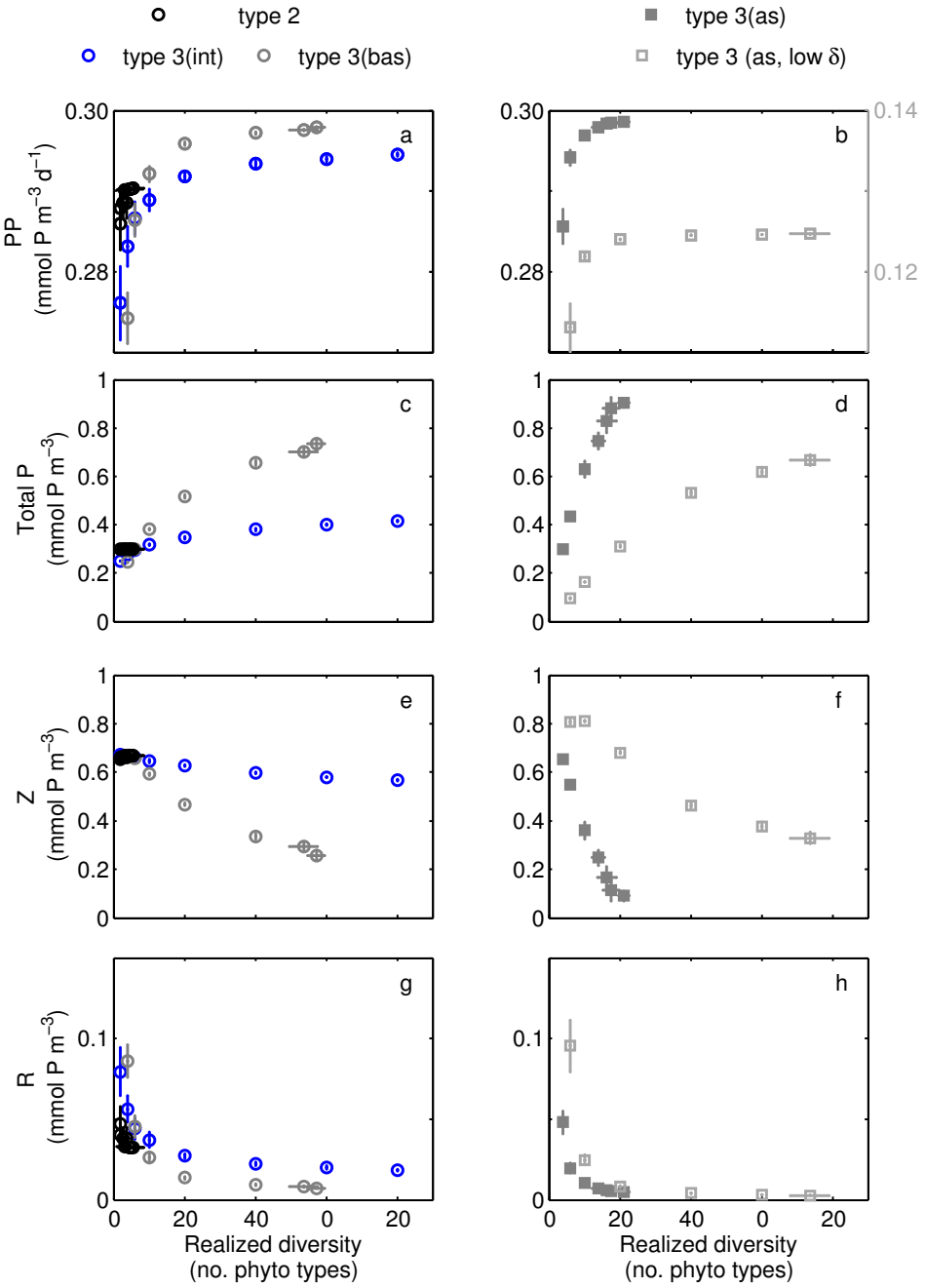

Figure 3.4: 0-D primary production, biomass and nutrient concentration at different diversity. Steady state (a,b) total primary production (PP); (c,d) total phytoplankton biomass ($\sum$P: Total P); (e,f) zooplankton biomass (Z); (g,h) nutrient concentration (R) for ensemble averages with different initial diversity in a chemostat. Left panels: diversity series with a type 2, a basic type 3 functional response, and a type 3 response with an intermediate exponent of prey concentration of 1.2; Right panels: diversity series with a type 3 response (active switching) for standard (filled squares; panel b: left y-axis) and low (open squares; panel b: right y-axis) dilution rate (δ). As the ingestion rate is lower for the active switching than for the basic type 3 response (Fig. 3.2), diversity increases when δ is reduced compared to the standard parameter value (Table 3.1). Error bars denote $\pm$ one standard deviation for five ensemble members for realized diversity, PP, total P, Z, and R.

The simulations employing a type 2 response are dominated by one or few phytoplankton types, while in the type 3 simulations the majority of types initialized coexist. In all 0-D simulations, the final community composition largely assembles on time scales of days.

3.3.2 Grazing controls

The stabilizing nature of the active switching response on simulated ecosystem dynamics is well known (Murdoch and Oaten, 1975) and has been employed in marine ecosystem models of different scales (Fasham et al., 1993; Aumont et al., 2003; Aumont and Bopp, 2006; Prowe et al., subm.). The active switching formulation promotes coexistence via an increase in predation pressure with phytoplankton concentration (e.g., Prowe et al., subm., Chapter 2), which arises from the quadratic functional response to phytoplankton concentration. In this respect, active switching is qualitatively equivalent to the basic type 3 response, although the shapes of the two curves differ (Fig. 3.2b; Appendix 3.6.1).

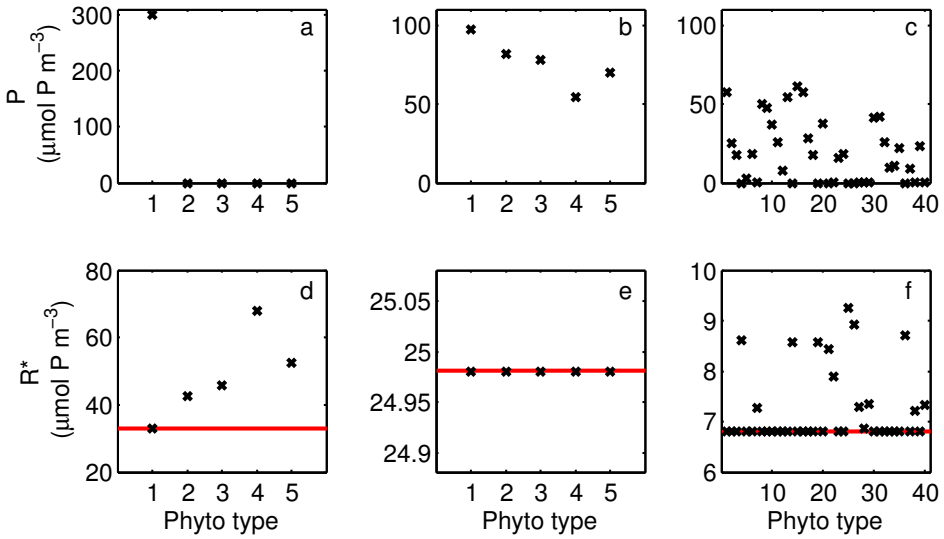

Figure 3.5: R* of coexisting phytoplankton types. Steady state (a-c) phytoplankton concentrations and (d-f) critical resource levels (R*) for all phytoplankton types in one chemostat simulation with five initial phytoplankton types for (a,d) a type 2, (b,e) a basic type 3 functional response, and (c,f) with 40 initial types for a basic type 3 response. The red lines in panels d-f indicate the steady state nutrient concentration.

Resource competition theory characterizes a fundamental difference between the two systems. For the type 2 system, steady state R* values differ for the different phytoplankton types (Fig. 3.5). Resource levels are reduced to the lowest R* value, and the respective phytoplankton type with this R* is the dominant type. Since the resource level determines the phytoplankton types' potential for net growth, less successful phytoplankton types suffer competitive exclusion by the types with the highest growth rate at lowest resource level. In few cases where R* values of different types are very similar, more than one type appear to coexist and exclusion is completed on time scales longer than the simulation time. In contrast, for the type 3 systems, the R* of each phytoplankton type depends on the abundance of the

other types. In our simulations, up to about 30 types all R* values become equal and all phytoplankton types coexist, albeit with different biomass. In this case, predation eliminates the basis for competitive exclusion by adapting to a level for which growth and losses balance for each phytoplankton type individually. If 40 types are initialized, some types do not achieve the low R* displayed by the majority of types and are excluded from the system (Fig. 3.5c,f; see section 3.3.3). This effect causes diversity to approach an apparent upper limit of about 30 coexisting types in our simulations with a basic type 3 functional response (Fig. 3.4).

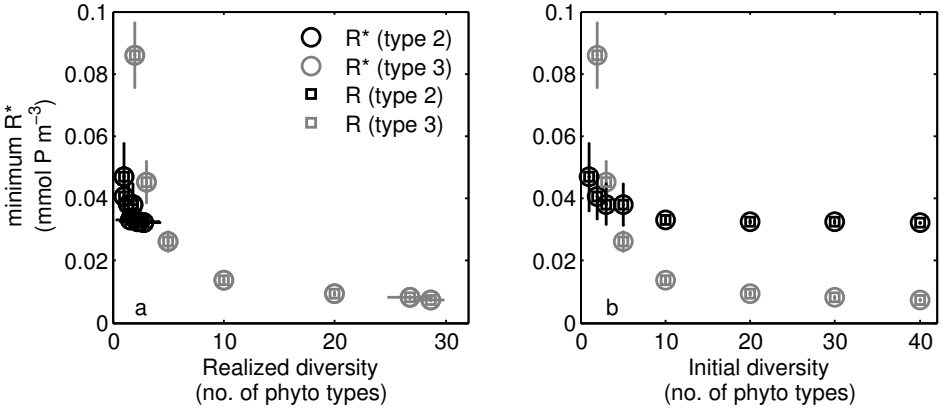

Figure 3.6: Nutrient use at different diversity. Minimum critical resource level (R*) over realized (a) and initial (b) phytoplankton diversity for the ensemble average of the diversity series with type 2 and basic type 3 in a chemostat. Error bars denote ± one standard deviation of five ensemble members for realized diversity and minimum R*.

In simulations with a type 2 response, the minimum R* of all types initialized decreases with increasing diversity within a diversity series (Fig. 3.6). This reflects a selection effect, which is one of two possible explanations for a positive diversity-productivity relationship: systems with higher diversity are more productive because they are more likely to contain a highly productive species (Tilman et al., 1997). In the simulations using a type 3 response, the grazing formulation reduces the minimum R* with increasing diversity because the higher number of phytoplankton types reduces the grazing pressure for each type in spite of the higher ∑P (Eq. 3.5; e.g. Prowe et al., subm., Chapter 2). In the chemostat system, the more complete use of nutrients directly translates into higher primary production, as $PP = \delta(R_0 - R)$ (Eq. 3.1, Fig. 3.4). As R* values are similar for all types present, increasing diversity results in a more productive community, which is able to draw down nutrients to lower levels. The variability seen in the minimum R* and the realized diversity (Fig. 3.6) can thus be explained by the effect of complementarity of niches, here distinguished by predation rather than resources, which thus can also lead to a positive diversity-productivity relationship (Trenbarth, 1974; Loreau, 1998). In our simplified type 2 model system, complementary niches do not occur since only one phytoplankton type dominates irrespective of the number of initialized types. Among our type 2 simulations, the selection effect is not significant as the R* values for each diversity level of the diversity series are within ± one standard deviation of each other (Fig. 3.6). The limited range of realized diversity within this diversity series and not sufficiently pronounced differences in k_{R_i} between the phytoplankton types might preclude identification of a significant selection effect in our simulations.

3.3.3 Nutrient controls

In our simulations, more diverse model ecosystems are able to utilize nutrients more completely (Tilman et al., 1997). For the type 2 configuration, the best competitor can take up nutrients until nutrient levels are reduced to its R^*. In a system with a type 3 functional response, at higher diversity the lower grazing pressure allows nutrients to be drawn down to lower levels. At some diversity level, the nutrient concentration falls below the R^* of the phytoplankton types with the highest k_{R_i}. For these types, growth then cannot balance dilution losses and they are excluded from the system. For the given nutrient supply, in our chemostat model with a type 3 response the ecosystem appears to approach a maximum diversity when close to 30 phytoplankton types coexist.

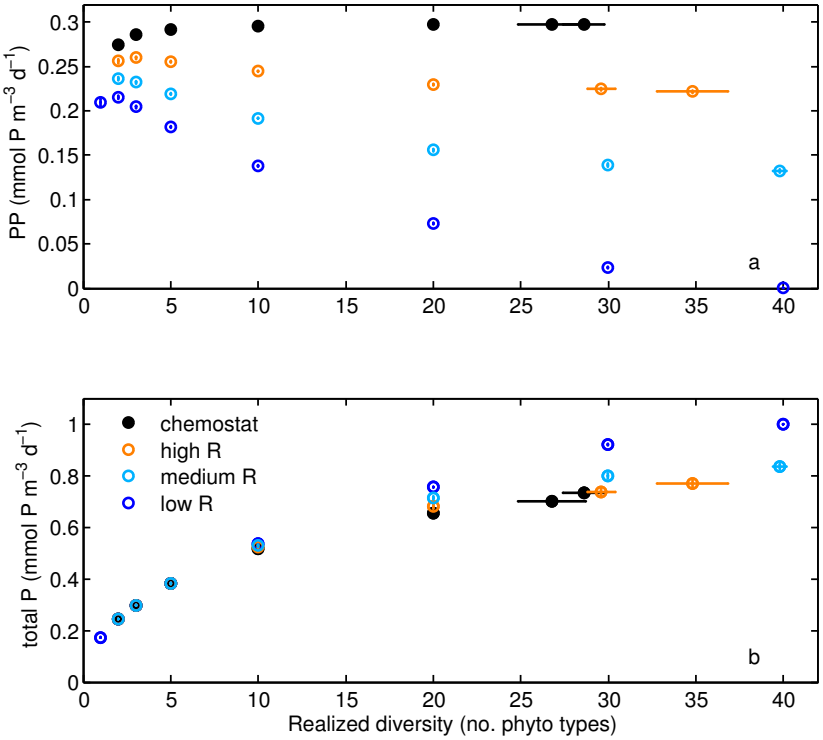

Figure 3.7: Productivity and diversity for different nutrient supply. Total primary production (a) and total phytoplankton biomass (b) over realized phytoplankton diversity for the ensemble average with basic type 3 functional response in a chemostat (filled circles) and in a batch culture 0-D model with three different levels of nutrient supply via remineralization (open circles). Error bars denote ± one standard deviation for five ensemble members.

The diversity-productivity relationship is also sensitive to the strength of the nutrient supply in the 0-D model. A positive relationship between diversity and both PP and $\sum$P is obtained for systems with a type 3 response using a chemostat model with constant nutrient input and continuous losses by dilution. In contrast, in a type 3 batch culture model without inputs and losses to the system and weak supply of remineralized nutrients, PP decreases at higher diversity while $\sum$P increases (Fig. 3.7). In this system, each phytoplankton type cannot exceed a maximum biomass $P_{i,0}$. $P_{i,0}$ depends on the biomass of the other coexisting types via the grazing formulation (Eq. 3.5), and $\sum$P thus increases if more types coexist. Without sufficiently high nutrient supply via remineralization or external inputs,

the more types coexist, the stronger they reduce the nutrient concentration, and thereby also PP. If no phytoplankton mortality other than grazing is considered, in our model all nutrient accumulates as phytoplankton biomass, PP ceases and zooplankton goes extinct when 40 types coexist. Increasing the supply of nutrients via enhanced remineralization of phytoplankton biomass (higher m_P) leads to a weaker decline of PP with increasing diversity. Increasing zooplankton mortality (m_Z) promotes higher PP at low diversity only, since simulated zooplankton biomass is diminished at higher diversity due to lower grazing with increasing number of phytoplankton types. Sufficiently strong remineralization can compensate for the external input of nutrients in terms of sustaining high productivity of diverse communities in this model.

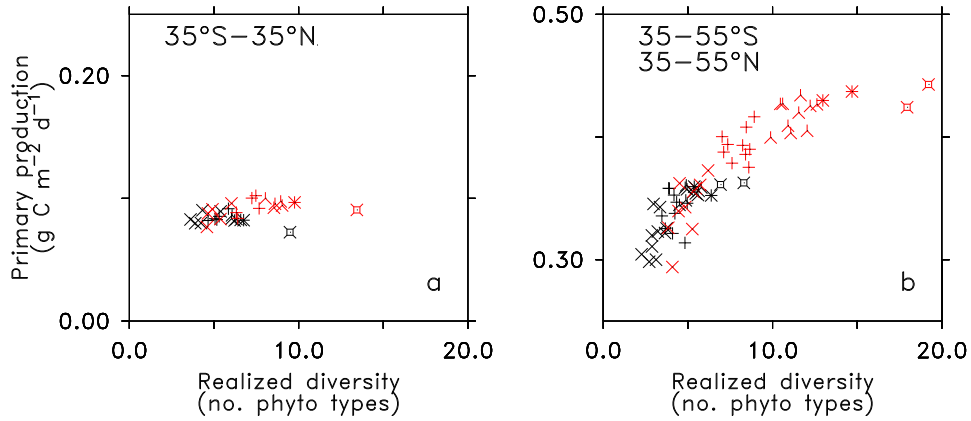

Figure 3.8: Regional diversity-productivity relationship in the 3-D model. Average global primary production in Year 10 in the upper 0-100 m of the water column over realized phytoplankton diversity (a) between 35°S-35°N and (b) between 35°N-55°N and 35°S-55°S. Simulations are performed for a type 2 (black) and a type 3 (active switching; red) functional response. Symbols as in Fig. 3.3.

In the global ocean, the nutrient supply via physical processes like, e.g., mixing and upwelling distinguishes different biogeographical provinces. Indeed, in our global model these different regions display different relationships between diversity and productivity: in the temperate latitudes with generally pronounced seasonal nutrient supply, more diverse communities are substantially more productive than less diverse communities (Fig. 3.8). In contrast, in the more oligotrophic tropical ocean, the effect of diversity on productivity is much less pronounced, as the range of both PP and realized diversity is notably smaller among simulations with different initial diversity. In these regions, one or few simulated key phytoplankton types dominate the community and are responsible for the major part of PP. Niches provided by the physical and ecological environment are scarce and the complementarity effect is small compared to the more productive regions.

3.3.4 Sensitivity to parameters

The shape of the diversity-productivity relationship is mainly sensitive to the shape of the grazing functional response, i.e. type 2 or type 3. Changing other parameters of the model, namely g, k_P, μ, k_R, δ and R_0, does not affect the nature of the diversity-productivity relationship: diversity series

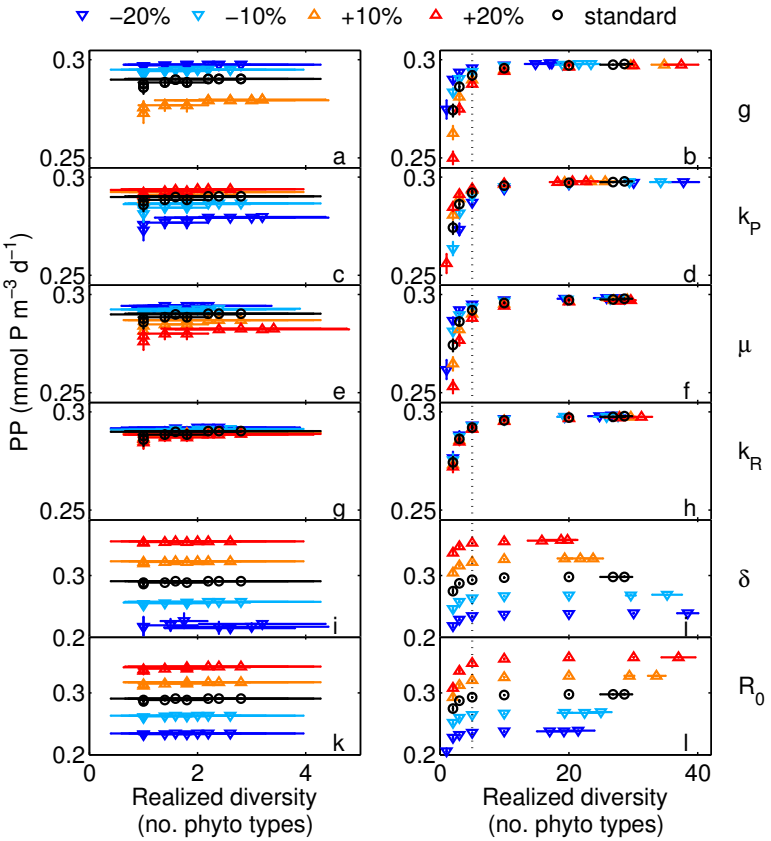

Figure 3.9: Sensitivity of the 0-D diversity-productivity relationship. Sensitivity of total primary production (PP) in steady state to changes of parameter values by ±10% and ±20% for the ensemble average with a type 2 (left panels) and a basic type 3 (right panels) functional response in a chemostat: (a,b) maximum grazing rate (g); (c,d) grazing half-saturation concentration (k_P); (e,f) phytoplankton maximum growth rate (μ); (g,h) half-saturation concentration for nutrient uptake (k_R); (i,j) dilution rate (δ); (k,l) input nutrient concentration (R_0). Horizontal and vertical error bars for each average of five ensemble members with the same initial diversity denote ± one standard deviation for realized diversity and for PP, respectively. The dotted vertical lines in the right panels indicate the approximate range of realized diversity for ensemble members with a type 2 response for orientation. Simulations for a 20% increase in g for the type 2 response (a) did not reach steady state and are omitted.

with type 2 functional response are all characterized by a small diversity range and low variability of PP; for all diversity series with a type 3 response, PP increases with increasing diversity in our chemostat simulations (Fig. 3.9). Here, the variability of PP up to a diversity of about five types (the range displayed for the simulations employing type 2) is notably larger than in simulations employing a type 2 response. The parameters directly affecting nutrient supply, the dilution rate δ and the inflow nutrient concentration R_0, have the most pronounced effect on PP of all the parameters tested in the sensitivity study, and a change by up to 20% causes an approximately proportional change of PP in simulations with both a type 2 or a type 3 functional response. At the same time, a lower δ allows the coexistence of more phytoplankton types at high diversity, particularly in the type 3 simulations, since it reduces losses and allows more types with high half-saturation concentrations for nutrient uptake (k_R) to grow. A similar effect on diversity is found for higher grazing rates (i.e., higher maximum grazing rate g or lower half-saturation concentration k_P). A higher nutrient supply (higher R_0) facilitates higher

diversity if PP_i is predation-limited (type 3). Drawing down nutrients to levels as low as in the standard run requires more coexisting phytoplankton types compared to the standard run, and the diversity limit induced by nutrient depletion becomes effective at higher diversity. All other parameters mostly affect the slope of the increase in PP at low diversity for simulations with a type 3 functional response, or the absolute level of PP in the type 2 simulations. Increasing or decreasing k_R does not significantly influence PP.

3.4 Discussion

In this study we employ a simplified 0-D model to examine what shapes the relationship between diversity and productivity in a global coupled ocean ecosystem model. We have deliberately chosen a simple model of resource-consumer-predator interaction, well aware that these models do not represent the full range of interactions present in natural ecosystems. Ecosystem models of little more structural complexity, however, are commonly used in large-scale ocean biogeochemical models (Le Quéré et al., 2005; Aumont et al., 2003; Aumont and Bopp, 2006; Follows et al., 2007) and are beginning to be applied to questions of plankton diversity (Follows et al., 2007; Dutkiewicz et al., 2009; Barton et al., 2010a; Prowe et al., subm.; Göthlich and Oschlies, subm.).

3.4.1 Grazing: Equivalent R^* and niche complementarity

We compare two different 0-D systems where the phytoplankton types are either characterized in their environment by a range of different R^* values or display similar R^* values. We employ two different grazing functional responses, type 2 and type 3, to create these systems: (i) a concave type 2 functional response that does not limit the primary production PP_i of phytoplankton type i at an individual level. For this configuration, the best competitor for the nutrient, i.e., the type with the lowest R^*, excludes other types. (ii) a sigmoidal type 3 functional response limits the PP_i. This grazing scheme equalizes the R^* values for all types, which allows coexistence. Similarity of R^* values was also put forward as basis for coexistence in oligotrophic regions with low seasonality in the 3-D coupled model (Barton et al., 2010a; Dutkiewicz et al., 2009). These simulations employed a type 2 functional response, and coexisting types were thus inherently equivalent in terms of their nutrient requirements under constant loss rates through grazing. Such inherently R^*-equivalent phytoplankton species are rarely found in competition experiments where competitive exclusion usually dominates in a stable environment (e.g., Passarge et al., 2006). In our study, types with inherently different nutrient requirements are made effectively R^*-equivalent by the type 3 grazing formulation. This kind of R^* equivalence is difficult to infer from the experimental literature, since the majority of competition experiments are performed in the absence of predators (e.g., Miller et al., 2005; Passarge et al., 2006; Sommer, 1985). In our model, the R^* equivalence reduces fitness differences in terms of resource competitiveness among the phytoplankton types and parallels the notion that neutral theory is applicable to niche-governed communities

because of mechanisms equalizing fitness differences (Hubbell, 2001).

With a type 3 functional response, lower grazing on any individual type in a more diverse community reduces its R^* compared to less diverse systems. A more diverse phytoplankton community can thus draw down nutrients to a lower level because of niche complementarity and thereby increase PP in this chemostat system. This more efficient use of resources in more diverse communities is evident in natural phytoplankton assemblages (Ptacnik et al., 2008). For algal communities in spatially heterogeneous stream habitats, higher resource uptake was found to result predominantly from a complementarity effect of different niches which enhanced algal biomass (Cardinale, 2011). The effect of diversity on resource uptake disappeared in homogeneous habitats, which became dominated by the superior competitor. There, the selection effect predominantly explained the biomass increase. These experimental findings agree very well with the results obtained with our two model configurations. This suggests that in our model plankton community the type 2 grazing function might produce a system which is too homogeneous in terms of niches to sustain high diversity. The variable grazing pressure induced by a type 3 functional response creates different niches in a habitat in which spatial structuring plays a minor role, thus promoting diversity. Additional niches can be created, e.g., through trade-offs in and differential nutrient use between the phytoplankton types (Göthlich and Oschlies, subm.).

3.4.2 Nutrient supply and regional patterns

Our model predicts a limit to the diversity of R^*-equivalent phytoplankton types the ecosystem can sustain, which is ultimately determined by nutrient availability. The maximum number of species supported by a system is determined by the potential productivity, i.e. the resource supply, of the system (Loreau et al., 2001). Whether such a diversity limit can be identified in natural systems and if so, what determines whether the maximum diversity is realized, remains an open question.

In our model, the correlation of productivity and phytoplankton diversity depends on the nutrient supply to the system. A system with sufficiently high supply of either "new" or remineralized nutrients allows more diverse communities to be more productive in terms of both PP and $\sum$P than less diverse communities. In a system with low nutrient supply, the higher nutrient uptake owing to the greater $\sum$P of the more diverse community exacerbates the nutrient limitation of PP for a larger number of coexisting species. These regimes are then characterized by a high phytoplankton standing stock ($\sum$P), but very low PP. Such a potentially inverse relationship between PP and standing stock caused by resource limitation has been found for macroalgal communities in marine benthic systems (Carpenter, 1986). The driving mechanism, lower R^* of more diverse communities, is the same for systems with low and high nutrient supply, but the response in PP is different. In the pelagic realm, the phytoplankton standing stock is affected by various loss processes like aggregation, vertical mixing or horizontal transport by currents. Our results emphasize that in marine ecosystems, standing stock and PP should be seen as separate ecosystem functions (Stachowicz et al., 2007).

The significance of the nutrient supply for the diversity-productivity relationship evident in the 0-D

model helps to interpret the 3-D ocean ecosystem model results. In this complex ecosystem model, which takes into account phytoplankton trait trade-offs as well as constraints by the physical environment, productivity and diversity depend on the supply of nutrients by recycling within the surface mixed layer or via physical processes like mixing. In productive regions, a variety of niches facilitated by ample nutrient supply and mediated by grazing are occupied by a diverse community. Here, a loss of diversity leads to a less efficient resource use and thus a significant reduction in productivity. In oligotrophic regions, few key species can persist and dominate the few available niches provided by the low nutrient supply. Diversity loss does not affect productivity here, as the effect of phytoplankton type identity is small.

A recently presented framework of resource supply, diversity and ecosystem functioning suggests that the supply of resources determines the potential productivity, which would be achieved under optimal resource use, as well as the diversity in terms of species richness (Gross and Cardinale, 2007). In regions with suffient nutrient supply to allow complementary resource use of a phytoplankton community, diversity then increases ecosystem functioning through the complementarity effect. In regions with a very low or very high nutrient supply the most successful competitors determine the productivity, and higher diversity in the regional species pool (metacommunity) may increase ecosystem functioning only via the sampling effect (Gross and Cardinale, 2007). A similar distinction might be underlying the regional patterns in our global model ocean. In the oligotrophic gyres, the influence of diversity from adjacent regions might be limited by an overall low regional diversity and low transport, in contrast to the more productive regions with high lateral transport. An imbalance in the supply of different resources compared to the needs of the community might be expected for instance in the Southern Ocean, where primary production is generally assumed to be limited by light and iron. Stoichiometrically imbalanced nutrient supply is expected to decrease both diversity and productivity (Cardinale et al., 2009), thereby possibly affecting the shape of the diversity-productivity relationship. Observations across sites with different resource supply indicate an increase of the resource-use efficiency with resource supply and suggest an effect of the resource supply on the diversity-productivity relationship (Ptacnik et al., 2008; Cardinale et al., 2009). Investigating regional and stoichiometric controls on this relationship in our model in detail would go beyond the scope of this study and remains a subject for future work.

A reduced supply of nutrients predicted for the future ocean (e.g., Sarmiento et al., 2004; Steinacher et al., 2010) might thus limit any potential, beneficial effect of high diversity in mitigating a potential productivity decline (Bopp et al., 2005; Behrenfeld et al., 2006) in a changing climate, and thus exacerbate the impact of diversity loss on ecosystem functioning in the ocean (Worm et al., 2006). The effect of a reduced supply of "new" nutrients might also be offset by enhanced recycling related to reduced export production (EP; e.g., Bopp et al., 2005; Manizza et al., 2010) or elevated heterotrophic rates at higher temperature (Pomeroy and Wiebe, 2001; Wohlers et al., 2009). Modelling studies link changes in PP and EP to floristic shifts in the phytoplankton community and emphasize the role of model structure in these predictions (Bopp et al., 2005; Manizza et al., 2010). Most of these models, however, formulate only few phytoplankton functional types and do not resolve phytoplankton diversity. How diversity will interact with reduced nutrient supply in driving future PP and EP changes poses an interesting question

for future studies.

3.4.3 Modelling predator-mediated diversity

Our model captures the two ends of a continuum axis from pure dominance of a key species to even coexistence of species (Loreau et al., 2001) depending on the functional response. With type 3 grazing, phytoplankton types coexist at fairly similar biomass levels, i.e. at high evenness, since they are picked randomly from a uniform distribution and thus display fairly similar characteristics. In addition, the sigmoidal functional response creates dynamic niches of flexible size for all types, which adjust to yield a balanced community. Simulating a larger variety in the degree of dominance might require including more detailed formulations of processes affecting community dynamics, such as trade-offs between growth and predation (e.g., Tirok and Gaedke, 2010).

Recent approaches indicate that coexistence can also be achieved without this trade-off by implementing trophic complexity. In a complex model food web, herbivory notably enhances coexistence compared to a simple consumer-resource model without explicitly formulating preferential predation on the most abundant consumer type (Brose, 2008). Their ensemble simulations employ a variety of herbivore functional responses including type 2 and type 3 by sampling different values for the exponent of prey concentration between 1 (type 2) and 2 (basic type 3). Sensitivity experiments with our 0-D model demonstrate that in a model with a simple trophic structure, an exponent of 1.2 can already promote considerably higher diversity than a type 2 response (exponent = 1; Fig. 3.4). Such weakly density-dependent loss terms allow coexistence of producers even for an exponent approaching, but not equal to 1 (Gross et al., 2009).

In our model, we have deliberately neglected details concerning resource use and focused on predator-mediated diversity for the sake of simplicity. Differential resource use also promotes coexistence in a 1-trophic level system without predators. There, complementarity of niches in resource use leads to a positive productivity-diversity relationship (Gravel et al., 2011). How this relationship is affected by the interaction of complementarity and predator mediation will be the subject of future research.

3.5 Conclusions

In our model, diversity of phytoplankton types with different nutrient requirements is maintained through a grazing formulation which eliminates resource-competition driven differences in R^* between the phytoplankton types and thus prevents competitive exclusion. In such a model community, the nutrient availability ultimately sets a limit to the diversity sustainable by the system. Whether such a limit to diversity exists in natural marine pelagic ecosystems remains a focus of future research. Irrespective of the particular mechanism promoting diversity, our study demonstrates that in marine ecosystem models of different scale more diverse phytoplankton communities are more productive if they succeed

in using nutrients to a larger degree. Pathways facilitating such a larger nutrient use potentially employ trade-offs between predation and nutrient uptake, differential resource use, or complex trophic interactions. How much an increase or decrease in diversity might affect productivity will differ for different oceanic provinces distinguished by nutrient availability and diversity. A positive diversity-productivity relationship is evident in productive regions with high nutrient supply only. The central role of the nutrient supply for the diversity-productivity relationship links diversity to projected changes in productivity and export production and argues for diversity to be considered in future studies about the role of marine ecosystems at times of environmental change.

Acknowledgements We would like to thank two anonymous reviewers for constructive comments which helped to improve the manuscript. FP was supported by the Kiel Cluster of Excellence "The Future Ocean".

Role of the funding source The funding source had no involvement in study design, analysis and interpretation of data, writing of the report or the decision to submit the paper for publication.

3.6 Appendix

3.6.1 Comparison of functional responses

The three functional responses for zooplankton grazing employed in the 0-dimensional model can be simplified if feeding preferences of the zooplankton for each phytoplankton type i are uniform across types ($\rho_i = \rho$, $i = 1,...,n$)

$$\text{type II:} \quad I_i = g\frac{\rho P_i}{k_P+\sum_r(\rho P_r)} = g\frac{P_i}{k_P/\rho+\sum_r P_r} \tag{3.8}$$

$$\text{type III (basic) :} \quad I_i = g\frac{\rho P_i^2}{k_P^2+\sum_r(\rho P_r^2)} = g\frac{P_i^2}{k_P^2/\rho+\sum_r P_r^2} \tag{3.9}$$

$$\text{type 3 (active switching):} \quad I_i = g\frac{\sigma_i P_i}{k_P+\sum_r(\sigma_r P_r)} \;,\; \sigma_i = \frac{\rho P_i}{\sum_r(\rho P_r)}$$

$$= g\frac{P_i^2}{k_P\sum_r P_r+\sum_r P_r^2} \tag{3.10}$$

In this case, the basic type 3 and the active switching formulation are generally equivalent, but differ in the effective value of the half-saturation concentration.

3.6.2 The batch culture model

In the batch culture model, external nutrient input (δR_0, Eq. 3.1) and dilution of all state variables (Eqs. 3.1-3.3) are omitted ($\delta = 0$). Instead, remineralization of zooplankton and phytoplankton losses, here formulated as a linear mortality term, provides remineralized nutrients and closes the system (Fig. 3.1).

$$\frac{\partial R}{\partial t} = -\sum_{r=1,n}\left(\mu\frac{R}{R+k_{R_r}}P_r\right)+m_P P+m_Z Z \tag{3.11}$$

$$\frac{\partial P_i}{\partial t} = \mu\frac{R}{R+k_{R_i}}P_i - I_i Z - m_P P_i \tag{3.12}$$

$$\frac{\partial Z}{\partial t} = \sum_{r=1,n}(I_r Z) - m_Z Z \tag{3.13}$$

4 Model of optimal current feeding in zooplankton

This chapter is reprinted from the original paper "Model of optimal current feeding in zooplankton" published in the journal Marine Ecology Progress Series with permission by Inter-Research.
Citation: M. Pahlow and A. E. F. Prowe (2010). Model of optimal current feeding in zooplankton. Marine Ecology Progress Series 403:129-144, doi:10.3354/meps08466.

Abstract Zooplankton feeding formulations in plankton models have exclusively focused on the relation between food concentration and ingestion, with respiration and excretion being treated separately, despite experimental evidence for strong links among these processes. We present an optimal current-feeding model linking ingestion, respiration, and assimilation efficiency to foraging activity. The Ivlev model is a special case of our optimal current-feeding model, which applies for static feeding behaviour. We validate our model with experimental data for copepods, ciliates, and dinoflagellates. Parameter estimates suggest that phylogenetic grouping is more important than predator size in determining feeding behaviour. Respiratory costs of foraging, e.g., for generating a feeding current, may be much larger than previously thought, are larger in smaller organisms, and might explain the independent development of feeding thresholds in different micro- and mesozooplankton groups. Both preferential feeding on, and lower feeding thresholds for, larger food particles are predicted to derive from greater capture efficiency owing to enhanced detectability of larger particles. The relation between feeding threshold and prey size appears to depend on feeding strategy but not on predator size, as a common relationship seems to apply for current feeders (ciliates and copepods) spanning a vast size range. Our model exhibits an inverse relationship between ingestion and assimilation efficiency, reducing the contribution of copepods to export of organic matter relative to remineralisation at low food concentrations. Export ratio variations previously thought to require strong shifts in community composition can be generated by changes in feeding behaviour predicted by our model.

4.1 Introduction

Marine zooplankton forms the first gateway in the processing of organic matter derived from primary production in the surface ocean. The fate of this organic matter is thus to a large part a function of three quantities which define zooplankton feeding behaviour and growth: (1) specific ingestion rate I is the total food intake, (2) assimilation efficiency E defines the assimilated and excreted fractions

of the ingested material, and (3) respiration and exudation separate remineralisation from growth, i.e., accumulation of biomass available for utilisation by higher trophic levels. Net growth rate g can be defined as the balance between assimilation EI and respiration R:

$$g = EI - R, \tag{4.1}$$

where R represents respiration of CO_2 and exudation of nutrients (all symbols are summarised in Table 4.1). Sloppy feeding and risk of higher predation will not be considered in this study. Excretion in the form of fecal pellets can be exported to the deep ocean and thereby contribute to the biological carbon pump. Consequently, the zooplankton formulation strongly affects the behaviour of plankton models both directly via its role in the food web and indirectly via its impact on vertical nutrient profiles (Steele and Henderson, 1992). Nevertheless, although many zooplankton models exist (Gentleman et al., 2003), they focus almost exclusively on ingestion and they do not usually allow for dynamic adjustments in feeding behaviour (Paffenhöfer et al., 2007).

Behaviours effecting prey encounter can broadly be categorised into several foraging strategies. The simplest possible behaviour is simply waiting for random prey encounters (ambush feeding), which is efficient for moving prey only (Gerritsen and Strickler, 1977). The most effective means of increasing prey encounters is cruise feeding, i.e., swimming in various patterns, but in addition to metabolic costs, this strategy also inevitably increases encounters with higher predators (Visser et al., 2009). A feeding current can enhance prey encounters as well, albeit somewhat less effective, owing to its limited spatial extent. Because the predator itself is not moving, this strategy does not suffer the increased risk of higher predation incurred by cruise feeding, however. Filter feeders direct their feeding currents through a filter sieving out prey particles, which works most efficiently with very large filters (Gerritsen et al., 1988). Suspension-feeding copepods have often been considered filter feeders (e.g., Conover, 1968; Frost, 1972; Lehman, 1976; Vidal, 1980a) but one important yet still often ignored aspect of this feeding mode is that a copepod's feeding current does not pass through but actually around its feeding appendages (Koehl and Strickler, 1981), which act to detect and capture prey organisms from the feeding current (Visser and Stips, 2002). Therefore, we refer to this feeding mode as current feeding.

Grazing functions commonly applied in plankton models include the Holling types, based on the disk equation, which in turn was derived for insect feeding (Holling, 1959b, 1973) and the Ivlev equation, derived for fish (Ivlev, 1961). Application to zooplankton was empirically motivated (Conover, 1968; Fujii et al., 1986) and has no mechanistic basis. Aside from the inappropriateness of the term filter feeder to describe suspension feeding by copepods, this lack of a mechanistic foundation means that it is difficult to generalise these models and analyse disagreements between models and observations. For example, Parsons et al. (1967) noted the necessity to introduce a feeding threshold into the Ivlev equation in order to describe the behaviour of copepods. Vidal (1980a) and Kiørboe et al. (1982, 1985) introduced entirely new empirical formulations to describe their observations, which fit their data better but could "not be interpreted in biological terms" (Kiørboe et al., 1982, p. 185).

Almost all existing zooplankton feeding models describe ingestion as a function of food concentration,

without any inherent link to respiration or assimilation efficiency, despite many observations that these processes co-vary in a systematic manner (e.g., Landry et al., 1984; Kiørboe et al., 1985). Respiration can be considered the sum of three components, (1) a constant maintenance respiration thought to sustain standard (resting) metabolism, (2) the cost of foraging, and (3) the metabolic cost of assimilation, termed specific dynamic action (Steele and Mullin, 1977). The increase of respiration with increasing growth rate is usually attributed mostly to specific dynamic action (Steele and Mullin, 1977; Kiørboe et al., 1985), whereas the cost of foraging has been suggested to give rise to feeding thresholds in order to save energy in the absence of food (Frost, 1975). Zooplankton assimilation efficiency appears to decrease with increasing growth rate (Steele and Mullin, 1977; Kiørboe et al., 1985), yet it is usually treated as constant in plankton models (Lam and Frost, 1976; Steele, 1998). The only existing feeding model utilising mechanistic relationships among ingestion, respiration, and assimilation efficiency is the optimal-foraging description of filter feeding by Lehman (1976). However, this model has never been validated and, because it cannot be written in closed form, is not suitable for use in larger plankton models.

Optimal-foraging theory has been used previously to construct models of filter and cruise feeding (Lam and Frost, 1976; Lehman, 1976; Gerritsen and Strickler, 1977), but these formulations were never validated or employed in the formulation of plankton models. Current developments in optimal-foraging theory of zooplankton are geared mostly towards food and patch selectivity (Pyke, 1984; Garcia et al., 2007). Visser et al. (2009) recently included a trade-off between prey encounters and risk of higher predation in their optimal-foraging model. In the following we derive, largely from first principles, a zooplankton optimal current feeding (OCF) model based on the idea that zooplankton optimise their growth by balancing the costs and benefits of foraging and assimilation. Because we will assume the cost of foraging to comprise increased respiration and reduced assimilation capacity, this approach produces a model with inherent links among ingestion, respiration, and excretion, suitable for inclusion in larger plankton models.

4.2 Model

The formulation of net growth rate in Eq. (4.1) implies that assimilation comprises two steps, (1) capture and ingestion of prey, I, and (2) the subsequent assimilation as reflected in E. Both specific foraging activity A_f necessary for capturing and ingesting prey as well as digestion and anabolic processes needed for assimilation require energy, which must be supplied by respiration R. Thus, at least two trade-offs can be explored to construct an optimal feeding model: (1) a trade-off between foraging activity and assimilation efficiency, and (2) the balance between assimilation, as defined by foraging activity and assimilation efficiency, and respiration (Fig. 4.1). We derive both of these trade-offs for our OCF model on the basis of the following assumptions:

1. Both feeding current and handling rate (inverse of handling time, h) result from foraging activity

and can be described as simple linear functions of specific foraging activity A_f.

2. The difference between specific total and foraging activities (expressed as $A_t - A_f$) is available for digesting and assimilating ingested material.

3. A fixed proportion (c_a) of assimilated food is respired during assimilation of predator biomass.

4. Foraging activity incurs both direct costs in the form of additional respiration ($c_f A_f$) and indirect costs due to the necessary allocation of potential total specific predator activity A_t to foraging.

5. Foraging activity is regulated so as to maximise predator net growth rate g under steady-state conditions.

Respiration

Assumptions 3 and 4 define respiration as the sum of energy requirements for foraging, assimilation, and maintenance:

$$R = c_f A_f + c_a EI + R_M \tag{4.2}$$

where c_f is a cost coefficient relating foraging activity to respiration, $c_a EI$ specific dynamic action, and R_M specific maintenance respiration.

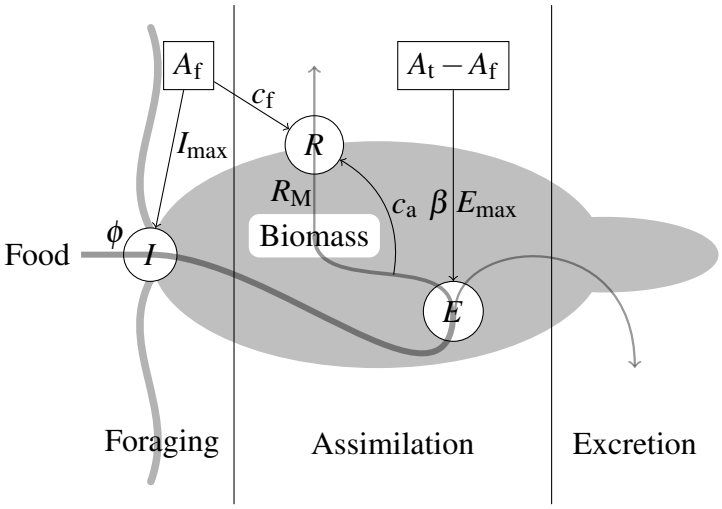

Figure 4.1: Optimal current feeding of zooplankton balances opposing effects of specific foraging activity A_f on specific ingestion rate I and assimilation efficiency E, and ingestion and assimilation against respiration R. Foraging activity leads to capture and ingestion of food as determined by food concentration, maximum specific ingestion rate I_{max} and prey capture coefficient ϕ, but also incurs respiration costs (cost of foraging coefficient, c_f). Assimilation efficiency is a function of digestion (coefficient β) and governs the partitioning of ingested material into assimilated biomass and excretion. It is reduced by allocation of part A_f of potential total specific activity A_t to foraging activity and can reach values up to E_{max}. The cost of assimilation coefficient c_a and specific maintenance energy requirements R_M also affect respiration.

Ingestion

Current feeding, i.e., ingestion via detecting and capturing prey from a feeding current, can be considered analogous to light harvesting by the photosynthetic apparatus of a phytoplankton cell, where the prey stream (product of feeding current F_0 and prey abundance n_P) corresponds to light intensity, the handling time needed for prey detection and capture (h_0) to the reaction time of the photosynthetic reaction center, and prey detectability coefficient (ε) to the light absorption coefficient. Detectability here is supposed to reflect factors, such as size, which could affect a predator's ability to detect and ingest prey, and thus is as much a property of the predator as of the prey. Baumert's (1996) derivation for photosynthesis as a function of light thus leads to the following interpretation of Ivlev's (1961) equation for current feeding:

$$I_0 = \frac{1}{h_0}\left(1 - \mathrm{e}^{-\varepsilon F_0 h_0 n_\mathrm{P}}\right) \tag{4.3}$$

where I_0 is ingestion rate as number of prey ingested by a predator per day and n_P prey abundance. Eq. (4.3) can be transformed in terms of biomass(carbon)-specific quantities by assuming that handling time varies proportionally with predator-prey size ratio and feeding-current strength scales with predator size:

$$I = I_0\frac{m_\mathrm{P}}{m_\mathrm{Z}} = \frac{1}{h}\left(1 - \mathrm{e}^{-\varepsilon F h P}\right), \qquad h = h_0\frac{m_\mathrm{Z}}{m_\mathrm{P}}, \qquad F = \frac{F_0}{m_\mathrm{Z}}, \qquad P = n_\mathrm{P} m_\mathrm{P} \tag{4.4}$$

where I is biomass-specific ingestion rate, F is biomass-specific feeding-current strength, h is biomass-specific handling time, P is prey concentration, m_P is prey size, and m_Z is predator size. The assumptions in Eq. (4.4) may be rather pragmatic, but the above derivation shows that they are implicit in applying the Ivlev equation to current feeding in mass-specific units. The strength of a feeding current does not necessarily mean its velocity, but can also refer to the fraction of time in which the feeding current (with constant velocity) is active (Price and Paffenhöfer, 1986). Since both velocity and temporal fraction of activity of a feeding current are obviously linearly related to prey-encounter rate, any difference between these two mechanisms of varying feeding-current strength F will only affect the value of the prey detectability coefficient ε in Eq. (4.4).

According to Eq. (4.4) and Assumption 1, specific ingestion rate can be formulated in terms of specific foraging activity A_f:

$$I = \alpha A_\mathrm{f}\left(1 - \mathrm{e}^{-\phi P}\right), \qquad \frac{1}{h} = \alpha A_\mathrm{f}, \qquad \varepsilon F = \frac{\phi}{h} = \phi\alpha A_\mathrm{f} \tag{4.5}$$

where α and ϕ are the handling and prey capture coefficients, respectively, relating foraging activity to feeding current, detectability, and prey handling, and εF is effective feeding-current strength. α and ϕ are compound parameters comprising efficiency, size, and geometry of the detection and ingestion apparatus as well as prey size. It is convenient to define $\hat{I}$ as:

$$\hat{I} = 1 - \mathrm{e}^{-\phi P} \tag{4.6}$$

whence specific ingestion rate becomes

$$I = \alpha A_\mathrm{f} \hat{I} \tag{4.7}$$

Table 4.1: Optimal current-feeding model variables and parameters

Symbol	Standard units	Description
A_f	d^{-1}	Specific foraging activity
$A_{\mathrm{f,\,max}}$	d^{-1}	Maximum specific foraging activity
A_t	d^{-1}	Maximum total specific activity
α	–	Prey handling coefficient
β	–	Digestion (assimilation) coefficient
c_a	–	Cost of assimilation coefficient
c_f, c_f^*	–	Cost of foraging activity coefficient[a]
E	–	Assimilation efficiency
$\tilde{E}_\mathrm{g}$	–	Modified gross growth efficiency[b]
E_max	–	Maximum assimilation efficiency
E_min	–	Minimum assimilation efficiency
ε	–	Prey detectability coefficient
F_0	$\mathrm{m^3 d^{-1}}$ predator^{-1}	Feeding current strength
εF	$\mathrm{m^3\,g\,C^{-1}d^{-1}}$	Effective feeding current strength
F	$\mathrm{m^3\,g\,C^{-1}d^{-1}}$	Specific feeding current strength
g	d^{-1}	Net growth rate
g_max	d^{-1}	Maximum net growth rate
h_0	d predator prey^{-1}	Handling time
h	d	Specific handling time
I_0	prey predator$^{-1}\mathrm{d}^{-1}$	Ingestion rate
I	d^{-1}	Specific ingestion rate
I_max	d^{-1}	Maximum specific ingestion rate
m_P	g C prey^{-1}	Prey size (biomass)
m_Z	g C predator^{-1}	Predator size (biomass)
n_P	prey m^{-3}	Prey abundance
P	g C m^{-3}	Prey concentration
P_g	g C m^{-3}	Growth threshold prey concentration
P_m	g C m^{-3}	Prey concentration at peak clearance
P_th	g C m^{-3}	Feeding threshold prey concentration
ϕ	$\mathrm{m^3\,g\,C^{-1}}$	Prey capture coefficient
Π	g C m^{-3}	Effective prey concentration
R_M	d^{-1}	Specific maintenance respiration

[a] c_f^* is effective c_f (see Eq. 4.10)
[b] as defined by Hansen (1992)

Assimilation efficiency

Digestion is modelled as exponential decay of ingested material in the gut (Lehman, 1976), which depends on gut-passage time (assumed proportional to handling time h and hence inverse of specific foraging activity, $1/A_\mathrm{f}$) and decay rate (proportional to $A_\mathrm{t} - A_\mathrm{f}$, Assumption 2). Thus, we describe the decay rate as $\beta(A_\mathrm{t}/A_\mathrm{f} - 1)$, where β is a coefficient of proportionality, relating activity to digestion, i.e., assimilation. A negative relation between decay rate and foraging activity could become manifest in a decrease in digestive enzymes with increasing food concentration, as reported by Hassett and Landry (1983). Assimilation efficiency E can thus be written as a function of specific foraging activity A_f:

$$E = E_\mathrm{max}\left[1 - \mathrm{e}^{-\beta\left(\frac{A_\mathrm{t}}{A_\mathrm{f}} - 1\right)}\right] \tag{4.8}$$

We define β here such that $\alpha\beta A_\mathrm{t}$ is the potential rate of assimilation. Eq. (4.8) follows from the assumption that handling time and gut-passage time are directly related to each other, i.e., the rate at which food passes through the gut adjusts to the speed at which food enters the gut.

Optimal foraging

Substituting Eqs. (4.2) and (4.5) to (4.8) into Eq. (4.1) yields:

$$g = EI - R = \underbrace{E_\mathrm{max}\left[1-\mathrm{e}^{-\beta\left(\frac{A_\mathrm{t}}{A_\mathrm{f}}-1\right)}\right]\alpha A_\mathrm{f}\hat{I}(1-c_\mathrm{a})}_{=EI(1-c_\mathrm{a})} - c_\mathrm{f}^*\alpha A_\mathrm{f} - R_\mathrm{M} \tag{4.9}$$

where the effective cost of foraging coefficient,

$$c_\mathrm{f}^* = \frac{c_\mathrm{f}}{\alpha} \tag{4.10}$$

was introduced for notational convenience. Eq. (4.9) indicates that both above-mentioned trade-offs, between foraging and digestion, and between assimilation and respiration, are related to specific foraging activity. The behaviour of net assimilation $EI(1-c_\mathrm{a})$ and net growth rate g in Eq. (4.9) as functions of foraging activity is illustrated in Fig. 4.2 for several levels of food concentration. Clearly, the optimal level of foraging is positive if and only if food concentration P is above some threshold concentration P_th. For $P = P_\mathrm{th}$ net assimilation $EI(1-c_\mathrm{a})$ just recovers the energy expended for the cost of foraging $c_\mathrm{f}A_\mathrm{f}$ at very small foraging activity (Fig. 4.2A), resulting in an initial slope of zero in g as a function of A_f (Fig. 4.2B). Thus, no net energy gain can be achieved by foraging when food concentration is at or below the feeding threshold, hence the maximum in g occurs at $A_\mathrm{f} = 0$ for $P \leq P_\mathrm{th}$. In this case, the slope of net growth rate g as a function of A_f is always equal to 0 or less (Fig. 4.2B). It follows that solving for a zero derivative of g with respect to specific foraging activity A_f (Assumption 5) will maximise net growth rate only for food concentrations above P_th:

$$\frac{\mathrm{d}\,g}{\mathrm{d}\,A_\mathrm{f}} = \alpha\left\{E_\mathrm{max}\hat{I}(1-c_\mathrm{a})\left[1-\left(1+\beta\frac{A_\mathrm{t}}{A_\mathrm{f}}\right)\mathrm{e}^{-\beta\left(\frac{A_\mathrm{t}}{A_\mathrm{f}}-1\right)}\right] - c_\mathrm{f}^*\right\} \stackrel{!}{=} 0, \qquad A_\mathrm{f} > 0 \tag{4.11}$$

$$\Rightarrow \qquad \alpha A_\mathrm{f} = \begin{cases} \dfrac{\alpha\beta A_\mathrm{t}}{-1-\mathrm{W}_{-1}\left\{-\left[1-\dfrac{c_\mathrm{f}^*}{E_\mathrm{max}\hat{I}(1-c_\mathrm{a})}\right]\mathrm{e}^{-(1+\beta)}\right\}} & \text{if} \quad P > P_\mathrm{th}, \\ 0 & \text{if} \quad P \leq P_\mathrm{th}, \end{cases} \tag{4.12}$$

where W_{-1} is the -1-branch of the Lambert-W function, defined as the inverse function of $x\mathrm{e}^x$: $\mathrm{W}(x\mathrm{e}^x) = x$. A simple and accurate closed-form approximation for W_{-1} is given in Barry et al. (2000). Eq. (4.12) describes optimal regulation of specific foraging activity, balancing specific ingestion rate I, assimilation efficiency E, and respiration R which results in the maximal net growth rate given external (food concentration P) and internal (trade-offs among I, E, and R) limitations.

Feeding threshold

The threshold concentration P_{th} required for feeding can be obtained from the condition that the initial slope of g as a function of A_{f} must be greater than zero, which is equivalent to the requirement that the limit of Eq. (4.11) as $A_{\mathrm{f}} \to 0$ is positive:

$$\lim_{A_{\mathrm{f}} \to 0} \frac{\mathrm{d}\, g}{\mathrm{d}\, A_{\mathrm{f}}} > 0 \qquad \Leftrightarrow \qquad c_{\mathrm{f}}^{*} < E_{\max} \left(1 - c_{\mathrm{a}}\right) \left(1 - \mathrm{e}^{-\phi P}\right) \tag{4.13}$$

$$\Leftrightarrow \qquad P > \frac{1}{\phi} \ln \frac{1}{1 - \dfrac{c_{\mathrm{f}}^{*}}{E_{\max} \left(1 - c_{\mathrm{a}}\right)}} \equiv P_{\mathrm{th}}. \tag{4.14}$$

Thus, the feeding threshold P_{th} is independent of the digestion coefficient β and specific maintenance respiration R_{M}. Digestion cannot interfere with the feeding threshold because it sets in only at food concentrations higher than the feeding threshold, and R_{M} only affects the threshold for positive net growth but not the feeding threshold. A food concentration exceeding P_{g}, which is substantially higher than P_{th}, is needed to achieve positive net growth (Fig. 4.2), as maintenance energy requirements have to be covered in addition to the cost of foraging.

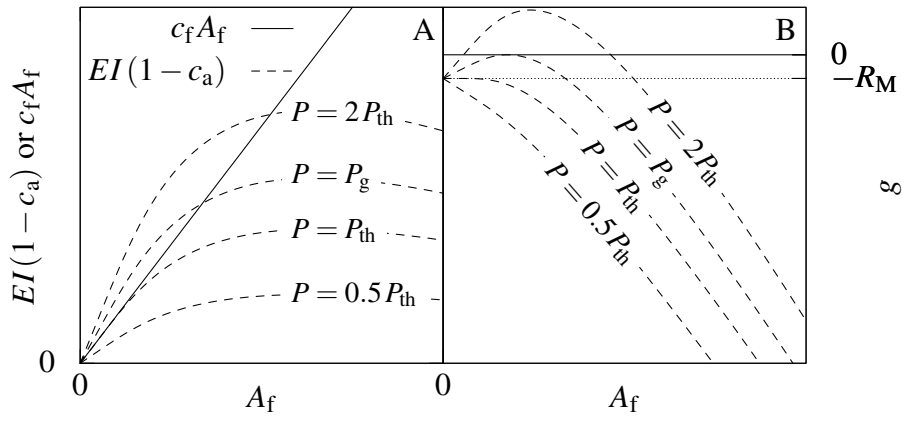

Figure 4.2: Model behaviour. (A) Net assimilation and cost of foraging, $EI\left(1 - c_{\mathrm{a}}\right)$ and $c_{\mathrm{f}} A_{\mathrm{f}}$, and (B) net growth rate, g, as functions of foraging activity A_{f} for different food concentrations P relative to the feeding threshold P_{th}. P_{g} is the food concentration required for assimilation to cover maintenance energy requirements (growth threshold) and R_{M} is maintenance respiration.

Model parameters

Total predator activity A_{t} can be specified as a function of the readily measured maximum specific rate of ingestion $I_{\max}$, which is related to maximum specific foraging activity $A_{\mathrm{f,\,max}}$ via $I_{\max} = \alpha A_{\mathrm{f,\,max}}$ at saturating food concentration ($\hat{I} = 1$, Eq. 4.7). Substituting $\alpha A_{\mathrm{f}} = I_{\max}$ and $\hat{I} = 1$ in Eq. (4.12) and

solving for αA_t gives:

$$\alpha A_t = \frac{I_{max}}{\beta}\left\{-1 - W_{-1}\left[-\left(1 - \frac{c_f^*}{E_{max}(1-c_a)}\right)e^{-(1+\beta)}\right]\right\}. \quad (4.15)$$

Thus, model behaviour is specified by the seven parameters β, c_a, c_f^*, E_{max}, I_{max}, ϕ, and R_M (Fig. 4.3). Maximum assimilation efficiency E_{max}, prey capture coefficient ϕ, and effective cost of foraging coefficient c_f^* determine the initial increase in net growth rate beyond the feeding threshold. Cost of assimilation coefficient c_a, c_f^*, and maximum specific ingestion rate I_{max} set the maximum growth rate (Fig. 4.3A). The initial rise in respiration with food concentration is mostly a function of c_f^* and ϕ, whereas c_a and I_{max} exert strong control on maximum respiration (Fig. 4.3B). The feeding threshold increases with c_a and c_f^* and decreases with increasing E_{max} and ϕ. c_f^* and ϕ are the main determinants of the effective strength of the feeding current (εF, Fig. 4.3C). Whereas foraging activity, and hence also the strength of the feeding current, monotonically increase with food concentration, clearance declines as food concentrations increase beyond a certain food concentration P_m (Fig. 4.3C), as ingestion saturates towards its inherent maximum (Fig. 4.3A). When the cost of foraging is negligible ($c_f^* = 0$ in Fig. 4.3C) then $P_{th} = 0$ and E and A_f become independent of food concentration, such that εF is constant and optimal current feeding reduces to a simple Ivlev model (Eq. 4.5 with constant maximum specific rate of ingestion αA_f), which thus describes static feeding behaviour with constant specific foraging activity. c_a also exerts some influence on the initial decline of assimilation efficiency, which is otherwise mostly controlled by the digestion coefficient β and E_{max} (Fig. 4.3D).

Temperature

Observations indicate that the minimum food concentration required for positive net growth P_g increases with temperature (Vidal, 1980a) but the feeding threshold P_{th} and the food concentration at peak clearance P_m do not (Wlodarczyk et al., 1992). Since I and P_{th} are non-linear functions of β, c_a, c_f^*, E_{max}, and ϕ (Eqs. 4.5 and 4.14), the simplest assumption in accordance with temperature-independent P_{th} and P_m is that none of these five parameters depends on temperature. It follows from this assumption that only two model parameters, I_{max} and R_M, are temperature dependent, as neither P_{th} nor I depend on R_M and I is linear in I_{max} (Eqs. 4.7 and 4.12).

Multiple food sources

The OCF model could be extended to multiple food species in at least two ways, depending on whether the predators are supposed to be specialists or omnivores. A specialist community could be represented by adding individual rates of ingestion, respiration, and excretion for all species. No modification of the OCF equations is necessary in this case. Supposing that several kinds of food of an omnivorous predator differ only in ϕ, we modify Eqs. (4.6) and (4.14) to include all food species P_i and then divide

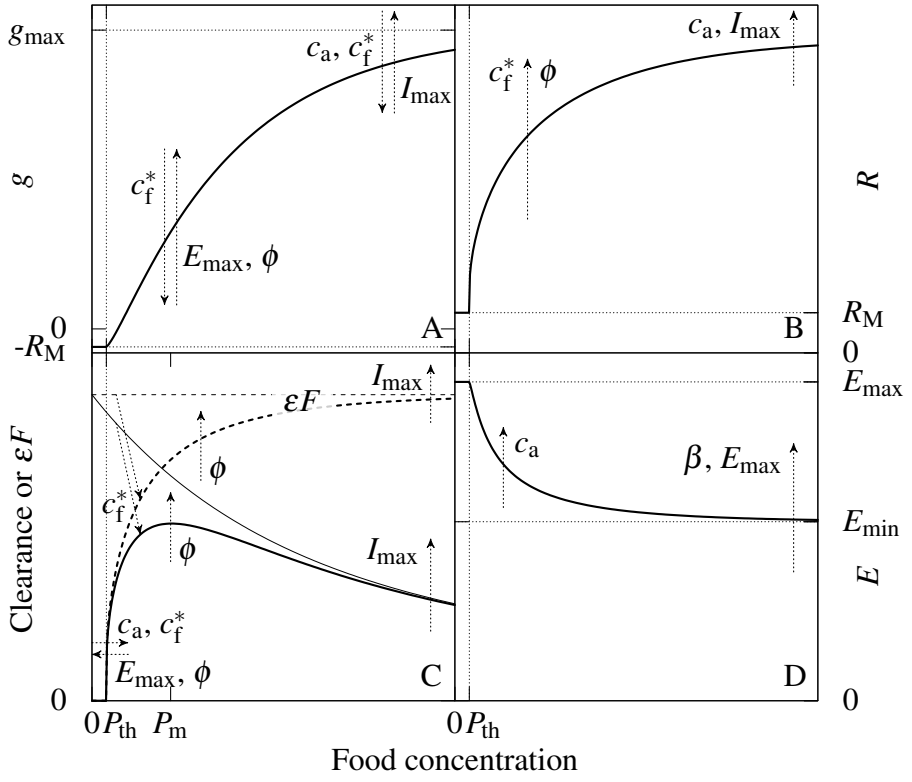

Figure 4.3: Major effects of parameter variations on optimal current-feeding model behaviour as a function of food concentration. (A) net growth rate (g); (B) respiration (R); (C) clearance ($= I/P$; solid lines) and effective strength of feeding current (εF, dashed lines); and (D) assimilation efficiency (E). Arrow heads indicate effects of increasing parameter values. Thin lines in (C) indicate model behaviour for $c_f^* = 0$. Increasing E_{max} and ϕ reduces the feeding threshold P_{th}. Effects of E_{max} and R_M are indicated on the y-axes in (A), (B), and (D). g_{max}: maximum net growth rate; E_{min}: minimum assimilation efficiency; P_m: food concentration at peak clearance.

specific ingestion rate proportionally among all the P_i:

$$\hat{I} = 1 - e^{-\Pi}, \qquad \Pi > \ln \frac{1}{1 - \dfrac{c_f^*}{E_{max}\,(1 - c_a)}}, \qquad \Pi = \sum_i \phi_i P_i, \qquad I_i = \frac{\phi_i P_i}{\Pi} I \tag{4.16}$$

where Π is the effective food concentration (Ambler, 1986). Such a formulation is supported by observations that late-stage and adult *Paracalanus* responded identically to mixed and mono-algal food with the same effective food concentration (Paffenhöfer, 1984; Ambler, 1986). Omnivorous feeding should not be used to represent a community of specialists in this conceptual model, because Eq. (4.16) would underestimate both feeding thresholds and assimilation efficiencies. Application of Eq. (4.16) would also fail in cases where the predator switches feeding behaviour when eating different kinds of prey, e.g., current feeding for phytoplankton and ambush feeding for ciliates (Kiørboe et al., 1996).

4.3 Validation

Model behaviour is illustrated and compared with observations from laboratory studies for copepods, ciliates, and dinoflagellates in Figs. 4.4 to 4.7. We tuned the OCF model parameters by hand so as to obtain as good as possible an agreement with the observations, as assessed by visual inspection.

4.3.1 Copepods

Kiørboe et al. (1985) presented a budget of feeding, respiration, excretion, and growth for the copepod *Acartia tonsa* (Fig. 4.4). Although *A. tonsa* is an ambush feeder when preying on ciliates, this species switches to suspension feeding and generates a feeding current when feeding on phytoplankton (Jonsson and Tiselius, 1990; Kiørboe et al., 1996). The specific rate of egg production was used as a proxy for net growth rate g (Fig. 4.4A), and assimilation efficiency E (Fig. 4.4D) was estimated assuming that ingestion is the sum of egg production, respiration, and excretion. Both egg production and respiration appear to be approximately linearly related to ingestion, except that respiration is reduced at zero ingestion, which is well reproduced by the model (Fig. 4.4A, B, open symbols and dashed lines). Linear relationships between ingestion and growth are frequently observed across a wide range of zooplankton organisms, ranging from protozoa to copepods (e.g., Kiørboe et al., 1985; Hansen, 1992).

According to our model, the effective strength of the feeding current ($\varepsilon F = \phi \alpha A_\mathrm{f}$, see Eq. 4.5) can be computed from ingestion as:

$$\varepsilon F = \frac{\phi I}{1 - \mathrm{e}^{-\phi P}} \tag{4.17}$$

Figs. 4.3C and 4.4C show that feeding current and specific foraging activity A_f increase monotonically with prey concentration, whereas clearance ($= I/P$, Fig. 4.4C) exhibits a maximum at about $150\,\mathrm{mg\,C\,m^{-3}}$ and then decreases with increasing food concentration. Clearance most clearly reveals the feeding threshold, below which clearance must be zero. Without a feeding threshold, clearance would approach its maximum toward a food concentration of zero (Fig. 4.3C, thin solid line). The predicted threshold for growth ($37.4\,\mathrm{mg\,C\,m^{-3}}$, Fig. 4.4A, thick solid line) is somewhat higher than the feeding threshold ($20.2\,\mathrm{mg\,C\,m^{-3}}$, Table 4.2, Fig. 4.4C), due to maintenance respiration. Increasing foraging activity and specific ingestion rate with food concentration are accompanied by decreasing assimilation efficiency (Fig. 4.4D). Declining assimilation efficiency with increasing food concentration was also reported by Landry et al. (1984).

The slope of the approximately linear relationship between growth and ingestion can be interpreted as a modified gross growth efficiency ($\tilde{E}_\mathrm{g}$) as defined by Hansen (1992):

$$\tilde{E}_\mathrm{g} = \frac{g + R_\mathrm{M}}{I} \approx \frac{g_\mathrm{max} + R_\mathrm{M}}{I_\mathrm{max}} = E_\mathrm{min}\,(1 - c_\mathrm{a}) - c_\mathrm{f}^*, \tag{4.18}$$

where g_max and I_max are maximum net growth rate and specific ingestion rate, respectively, and E_min is

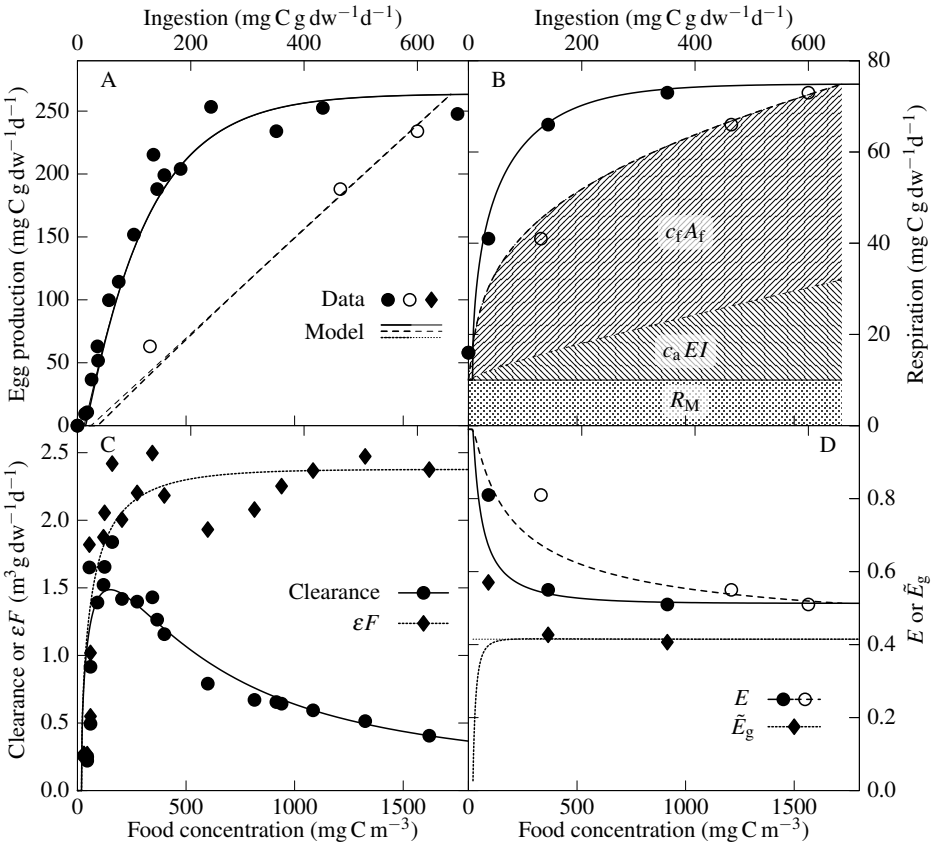

Figure 4.4: Validation of the optimal current-feeding model with data of *Acartia tonsa* feeding on *Rhodomonas baltica*. Closed symbols and solid and dotted lines indicate relationships with food concentration (bottom axes), open symbols and dashed lines with specific ingestion rate (top axes). Thin lines in (A) and (D) are for the linear approximation of the relationship between egg production (g) and specific ingestion rate. εF in (C) is effective feeding-current strength. Shaded areas in (B) outline the contributions of the costs of foraging ($c_f A_f$), specific dynamic action ($c_a EI$), and maintenance (R_M) to total respiration in relation to specific ingestion rate. $\tilde{E}_g$ is a modified gross growth efficiency (see Eq. 4.18 for details), E is assimilation efficiency. DW: copepod dry weight. Data from Kiørboe et al. (1985). Parameters are detailed in Table 4.2.

the minimum assimilation efficiency (for $I = I_{max} = \alpha A_{f,\,max}$):

$$g_{max} = E_{min} I_{max} (1 - c_a) - c_f^* I_{max} - R_M \tag{4.19}$$

$$E_{min} = E_{max} \left[1 - e^{-\beta \left(\frac{\alpha A_t}{\alpha A_{f,\,max}} - 1 \right)} \right]. \tag{4.20}$$

$\tilde{E}_g$ is mostly constant except at the lowest prey concentrations in Fig. 4.4D, where the model diverges from the observations. However, the regression of egg production on ingestion presented by Kiørboe et al. (1985) has a positive y-axis intercept, indicating that the copepods were still producing some eggs after ingestion ceased, which the model cannot reproduce, due to the steady-state assumption (Assumption 5). This phenomenon also implies that Kiørboe et al. (1985) might have overestimated assimilation efficiencies by assuming constant copepod weight in the course of a feeding experiment, and hence explain at least part of the discrepancy between modelled and observed assimilation efficiency at the

Table 4.2: Parameter settings, predator size, feeding thresholds, and maximum growth rates

Taxon	β	c_a	c_f^*	E_{max}	I_{max} (d^{-1})	ϕ ($m^3 gC^{-1}$)	R_M (d^{-1})	Size ($\mu gC\,pred^{-1}$)	P_{th} ($mgC\,m^{-3}$)	g_{max} (d^{-1})
Copepods										
Acartia tonsa	0.2	0.065	0.065	0.99	1.65[a]	3.6	0.025	2.96[c]	20.2	0.66[a]
Calanus pacificus	0.2	0.065	0.065	0.99	0.49	4.5-14.4[b]	-	68[d]	5.1-16.2[b]	-
Ciliates										
Strobilidium spiralis	0.2	0.3	0.3	0.99	5	20	0.15	0.013[e]	28.4	1.11
Strombidium sp.	0.2	0.3	0.3	0.99	2.5	20	0.05	0.0054[e]	28.4	0.58
Lohmanniella oviformis	0.2	0.35	0.3	0.99	3.4	20	0.3	0.00072[e]	31.3	0.46
Dinoflagellate										
Gymnodinium sp.	0.2	0.33	0.25	0.99	2.9	220	0.05	180-360 $\cdot 10^{-6}$[f]	2.15	0.7

[a] assuming a carbon content of 40% of dry wt (Kiørboe et al., 1985)
[b] calculated from cell diameter D of food algae: $\phi = (20 \cdot D)/(D + 40\,\mu m)$
[c] calculated from average cephalothorax length according to Kiørboe et al. (1985)
[d] calculated from average dry wt assuming a carbon content of 40% of dry wt (Frost, 1972)
[e] calculated from cell volume according to Gismervik (2005)
[f] calculated from a range of cell volumes assuming a carbon density of $0.3\,pgC\,\mu m^{-3}$ (Strom, 1991)

lowest food concentration in Fig. 4.4D.

Fig. 4.5 shows the model fit to observations on the copepod *Calanus pacificus* feeding on diatoms of different cell size. Since only ingestion was reported by Frost (1972), the model could not be fully constrained by this data set, hence we used values obtained for *A. tonsa* for β, c_a, c_f^*, and E_{max}. When fitting the model to these data, the differences among the feeding responses to the different food algae could be described by varying the prey capture coefficient ϕ only. Expressing ϕ as a simple saturating function of cell diameter (Table 4.2) produced a reasonable agreement between model and observations, which implies a straight-forward interpretation of ϕ as the efficiency of detecting and capturing food from the feeding current: Food particles too small to be detected by the feeding appendages can also not be captured, setting a lower size-limit to particles which can be utilised (Frost, 1972); larger particles are more easily detected and hence captured, leading to increasing ϕ with increasing particle size. While it is clear that there must also be an upper size-limit above which food particles become difficult and eventually impossible to handle (implying decreasing ϕ with increasing size), food algae of this size were not used in the study by Frost (1972). The prey-size dependence of ϕ generates an inverse relationship between prey size and feeding threshold, which appears to hold across all current feeders considered in the present study (Fig. 4.5, inset).

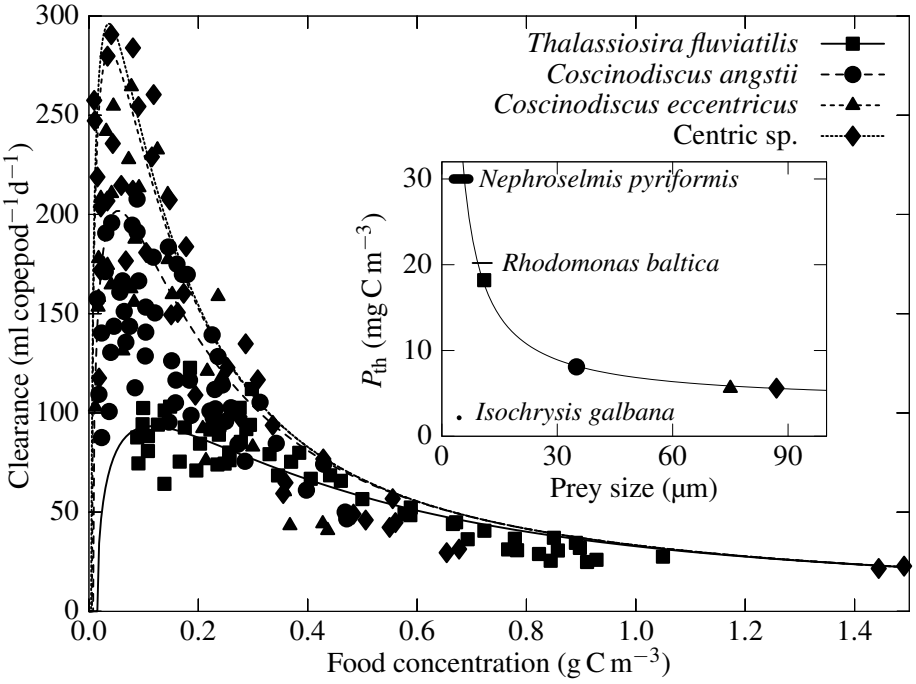

Figure 4.5: Validation of the optimal current-feeding model with data of *Calanus pacificus* feeding on centric diatoms. The model was first fitted to the largest prey (Centric sp., dotted line) and then ϕ was reduced as a saturating function of prey size (see Table 4.2) to obtain fits for the smaller diatom species (solid and dashed lines). Data from Frost (1972). Parameters are detailed in Table 4.2. Inset: relationship between feeding threshold P_{th} and prey size resulting from the prey-size dependence of ϕ. Symbols correspond to the legend in the outer figure. Thickness of horizontal lines indicates range of feeding thresholds for *A. tonsa* and ciliates in Table 4.2, and length of horizontal lines indicates minimum and maximum cell dimensions (e.g., width and length) of *Rhodomonas baltica* and *Nephroselmis pyriformis* used as prey by Kiørboe et al. (1985) and Gismervik (2005), respectively. Dot indicates size of *Isochrysis galbana* (Strom, 1991) and corresponding feeding threshold for *Gymnodinium* sp. from Table 4.2. Dimensions of *N. pyriformis* from the Swedish Meteorological and Hydrological Institute (www.smhi.se).

4.3.2 Ciliates

Copepod and ciliate feeding behaviour exhibit several common features, such as generating a feeding current and releasing fecal aggregates (Jørgensen, 1983; Stoecker, 1984). The OCF model is compared to observations of three ciliate species feeding on small phytoplankton in Fig. 4.6. All three species seem to have similar feeding thresholds and clearance peaks at similar food concentrations. These data also do not fully constrain the model, as no assimilation efficiencies were reported, such that β and E_{max} were set to their estimates for *A. tonsa* (Table 4.2). Nevertheless, it appears noteworthy that all three species, feeding on the same or very similar prey using a feeding current, could be fitted with the same c_{f}^{*} and ϕ, which are the parameters characterising the feeding current (Fig. 4.3C), and which are responsible for the similarities in feeding thresholds and food concentrations at peak clearance. Strong differences in parameter estimates were found only in maximum ingestion I_{max} and specific maintenance respiration R_{M} (Table 4.2, reflecting the differences among net growth rates at zero and saturating food concentrations, see Fig. 4.3A).

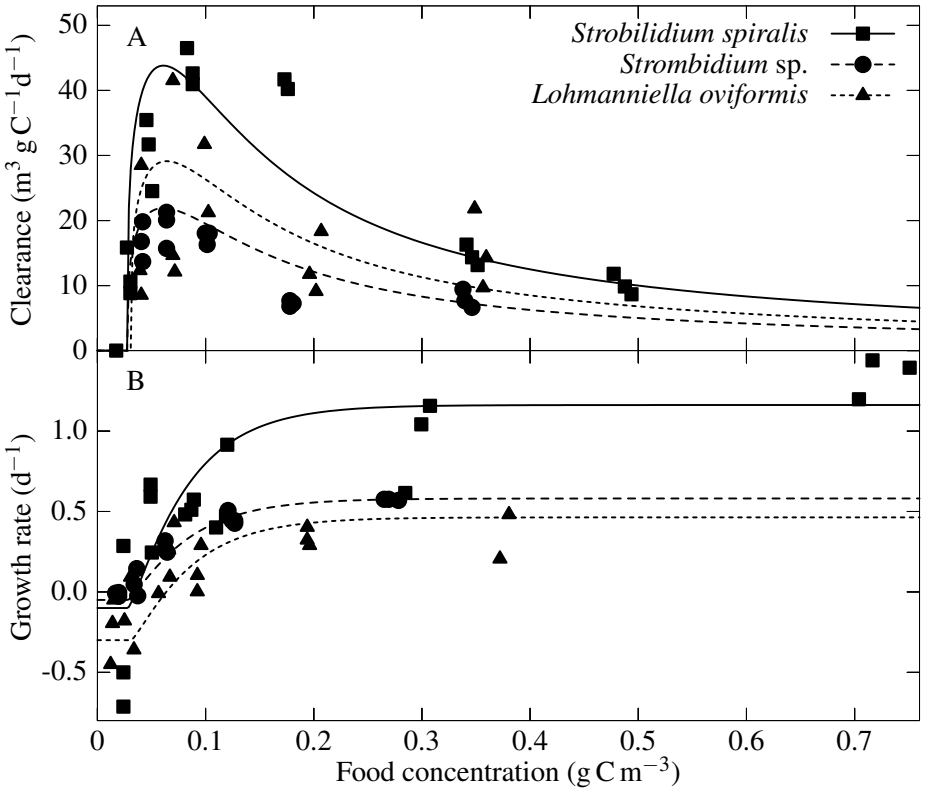

Figure 4.6: Validation of the optimal current-feeding model with data of three planktonic ciliates grazing on *Nephroselmis pyriformis* (*Strombidium* sp. and *L. Oviformis*) or *N. pyriformis* and *Hemiselmis* sp. (*Strobilidium spiralis*). Data from Gismervik (2005). Parameters are detailed in Table 4.2.

4.3.3 Dinoflagellates

The feeding behaviour of dinoflagellates is quite different from that of copepods and ciliates in that they do not generate feeding currents but acquire food by means of cruise feeding. Since it does not matter in terms of encounter rate whether a predator moves through water or water moves past a predator, this mode of foraging should follow the same functional relationship with food concentration as current feeding (Eqs. 4.3 to 4.5). Indeed, flagellate feeding behaviour as observed by Strom (1991) appears to concur qualitatively with that of copepods and ciliates shown above (Fig. 4.7). As with Fig. 4.6, β and $E_{\max}$ could not be constrained. The modelled relationship between net growth rate and specific ingestion rate deviates more strongly from a straight line in Fig. 4.7A than in Fig. 4.4A because of the larger costs of assimilation and foraging estimated for the dinoflagellate (Table 4.2). However, in the region where net growth is positive, i.e., for $I \gtrsim 0.6\,\mathrm{d}^{-1}$, the predicted relationship is again an almost perfectly straight line. Although the data are less clear in this respect than those in Figs. 4.4 to 4.6, clearance peaks well above the lowest food concentrations for both days of the experiment shown in Fig. 4.7B, which indicates the presence of a feeding threshold.

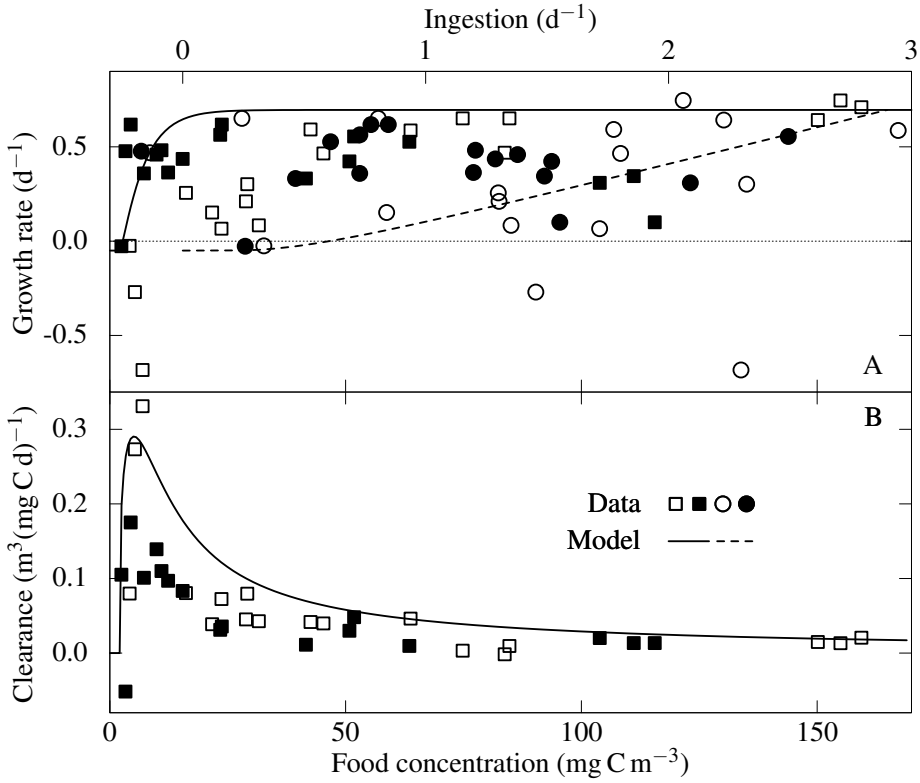

Figure 4.7: Validation of the optimal current-feeding model with data of the heterotrophic dinoflagellate *Gymnodinium* sp. feeding on *Isochrysis galbana* in a two-day experiment. Open symbols: Day 1; closed symbols: Day 2. Squares and solid lines indicate relationships with food concentration (bottom axis), circles and dashed line with specific ingestion rate (top axis). Data from Strom (1991). Parameters are detailed in Table 4.2.

4.4 Discussion

4.4.1 Respiration

The composition of respiration (shaded areas in Fig. 4.4B) draws a picture which differs qualitatively from those proposed earlier (e.g., Steele and Mullin, 1977; Vidal, 1980b), in which the cost of foraging is relatively small and decreases with increasing growth rate, and total respiration is dominated by specific dynamic action. The idea that the cost of foraging should decline with increasing growth rate is based on the observed reduction in clearance (Vidal, 1980b), which in turn is based on the implicit assumption that clearance can be used as a proxy for foraging activity. However, our optimal current feeding (OCF) model demonstrates that this is not necessarily the case (Fig. 4.4A,B), and predicts that the cost of foraging ($c_\mathrm{f} A_\mathrm{f}$) increases with growth rate and also dominates total respiratory energy loss except very close to the feeding threshold, whereas specific dynamic action (metabolic cost of assimilation, $c_\mathrm{a} EI$) becomes significant only at intermediate to high rates of net production (Fig. 4.4B). The low energy requirement of a feeding current calculated from theoretical considerations has been used to suggest that the associated respiratory cost should be very low compared to total respiration

(Fenchel, 1980). However, these calculations only consider very crude estimates of the actually very low efficiency with which the feeding current is generated (Riisgård, 2007). Svetlichny and Hubareva (2005) interpreted observations of very low gross efficiencies of locomotion in copepods as indicating that energy dissipation in feeding currents contributes only negligibly to the overall energy requirement of a feeding current. Generating a feeding current comprises not only muscle activity in legs, feeding appendages, mouth parts, etc., but also increased activity of the animal's circulatory system needed for supplying energy and oxygen and collecting and removing waste products. While more research is needed to elicit the actual contributions of these processes to the total energy demand of foraging activity, it is nevertheless clear that, therefore, a low energy requirement of the feeding current itself does not necessarily imply a low energetic cost of foraging, covering the energy demand of all required metabolic, circulatory, and muscle activity.

Another argument in favour of the large contribution of foraging to total respiratory costs can be derived from the observation that feeding thresholds have developed independently in several different organism groups, e.g., in copepods, ciliates, and apparently also dinoflagellates (Figs. 4.4 to 4.7). Although a feeding threshold might appear trivial at first sight, it requires a capacity to measure food concentration independently from the actual feeding process, since otherwise the organisms could not know when to start foraging again once feeding ceased. Thus, the development and conservation of such a complex feeding behaviour indicates that the possibility of down-regulating their feeding current must represent a strong advantage for these organisms, which is difficult to imagine if the costs of foraging were really insignificant. Only if the contribution of foraging activity to total respiration costs is large, as suggested by the OCF model (Fig. 4.4B), zooplankton animals could significantly extend their ability to survive prolonged periods without food by down-regulating foraging activity at low food concentration.

The assumed linear relationships between strength of feeding current F and foraging activity A_f in Eq. 4.5 and between respiration R and A_f in Eq. 4.2 imply a linear relation between feeding-current intensity and energy requirement of foraging, which contrasts with assumptions of quadratic or cubic relationships in previous optimal-foraging models (Lam and Frost, 1976; Lehman, 1976; Gerritsen and Strickler, 1977; Visser et al., 2009). The assumption of a quadratic relationship was based on the quadratic dependence of energy dissipation on velocity in laminar flow (Lehman, 1976). However, copepods regulate the intensity of their feeding current by varying the fraction of time in which the feeding current is active rather than varying its velocity, implying a linear relationship with energy consumption (Price and Paffenhöfer, 1986). Similarly, a linear dependence of respiration on swimming speed in copepods was observed by Buskey (1998). Thus, linear energetic costs of both swimming and feeding-current generation could explain why the OCF model could describe the feeding behaviour of a (cruise-feeding) dinoflagellate (Fig. 4.7). As noted by Price and Paffenhöfer (1986), the assumption of a quadratic dependence could lead to overestimating energy requirements for high feeding-current intensities. More importantly with respect to feeding thresholds, however, an assumed quadratic relationship would severely underestimate energy requirements of very weak current-feeding activity, which is why none of the previous optimal-foraging models predicted feeding thresholds. The OCF model predicts that a peak in clearance at a food concentration above zero is indicative of a feeding threshold. Minimal

food concentrations applied in most laboratory studies are well above the feeding thresholds predicted by the OCF model. Hence, direct evidence for feeding thresholds, i.e., zero clearance at above-zero food concentration, is scarce but can be found (e.g. Durbin and Durbin, 1992; Gismervik, 2005, Fig. 4.6A).

4.4.2 Feeding thresholds

The lack of clear evidence for feeding thresholds in microzooplankton has presented a problem for our understanding of the ecology of oligotrophic and HNLC (high-nutrient-low-chlorophyll) regions, as the zooplankton communities in these regions are thought to be dominated by microzooplankton (Strom et al., 2000; Paffenhöfer et al., 2007). As clarified by Strom et al. (2000), the relatively stable lower limit for chlorophyll concentrations in these regions appears to require a community grazing threshold. Such a grazing threshold of the whole zooplankton community has indeed been reported by Lessard and Murrell (1998) for the Sargasso Sea, which is difficult to reconcile with the idea that small microzooplankton, which dominate the zooplankton community there, have no feeding threshold. Recently, Gismervik (2005) has presented clear evidence for feeding thresholds in ciliates (Fig. 4.6). Data from an earlier study for the heterotrophic dinoflagellate *Gymnodinium* sp. feeding on *I. galbana* (Strom, 1991) reveal a clearance peak above the lowest food concentrations (Fig. 4.7B), indicating the presence of a feeding threshold. Strom (1991) also found that *Gymnodinium* sp. exhibited a feeding threshold for *Synechococcus* sp. when initial food concentration was low ($< 20\,\mu g\,C\,l^{-1}$), which was not observed when initial food concentration was higher. Such an apparently inconsistent behaviour with different initial conditions could point to insufficient acclimation of the organisms to the experimental setup. This does not appear unlikely, considering that it can take heterotrophic flagellates well in excess of 100 h to adapt to a change in food supply (Fenchel, 1982), whereas the animals are typically allowed to acclimate to new experimental conditions for only two to three days (e.g., Strom, 1991; Hansen, 1992).

The relationship between ϕ and cell diameter of food algae (Table 4.2) implies an inverse relationship between prey size and feeding threshold (Eq. 4.14, Fig. 4.5 inset), although the lowest food concentrations applied by Frost (1972) were apparently still too high in order to observe the feeding thresholds directly. Such a relationship between food particle size and feeding threshold suggests that the frequently-reported preference for larger food items (Frost, 1972; Rollwagen Bollens and Penry, 2003) could actually be passively determined by the ability of the predator to detect these particles in its feeding current. Passive food preferences could justify the use of the concept of effective food concentration (Ambler, 1986) manifest in Eq. 4.16, but probably only so long as the predator employs the same feeding mode for all kinds of prey involved (e.g. in Paffenhöfer, 1984). At least some copepods can switch between current and ambush feeding (Kiørboe et al., 1996) and also the mode of detection can vary between chemoreception of phytoplankton (e.g., Gill and Poulet, 1988; Paffenhöfer and Lewis, 1990) and mechanoreception of large and motile prey (DeMott and Watson, 1991). Hence, more elaborate formulations will probably be required for accurate representation of omnivory involving phytoplankton and zooplankton as prey in plankton models.

The functional relationship between prey size and feeding threshold P_{th} appears to be valid for both copepods and ciliates but not for dinoflagellates (Fig. 4.5 inset). Given the vast size range among the ciliates and copepods (Table 4.2), a common prey size-P_{th} relationship is a rather surprising finding, as it implies that the feeding threshold has very little to do with predator-prey size ratio. Although dinoflagellates are smaller than copepods and ciliates, the *Gymnodinium* sp. used in Strom (1991) reaches about half the size of *Lohmanniella oviformis*, whereas the sizes of the ciliates and copepods considered here span five orders of magnitude (Table 4.2). Thus, it appears very unlikely that the difference in the prey size-dependence of P_{th} between the dinoflagellate on the one hand and the copepods and ciliates on the other is due to the difference in predator size. This leaves only the difference in feeding behaviour, i.e., swimming as opposed to generating a feeding current, as explanation for the different functional relationships of P_{th} and prey size between the dinoflagellate and the current feeders. Nevertheless, the feeding threshold of about $20\,\text{mg C m}^{-3}$ observed by Strom (1991) for *Gymnodinium* feeding on *Synechococcus*, is much larger than the threshold suggested by our model fit for *Isochrysis galbana* (Fig. 4.7), which is much larger than *Synechococcus*. Hence, inverse relationships between food particle size and feeding threshold, albeit different from the one for current feeders, could also apply to dinoflagellates and other microzooplankton groups with similar feeding behaviour.

4.4.3 Cost of foraging

Interestingly, the cost of foraging appears to be much lower in copepods than in ciliates and dinoflagellates, as is the case for the cost of assimilation (Table 4.2), yet the feeding thresholds of copepods are comparable to those of ciliates and dinoflagellates. This is due to the much larger value of ϕ (relating foraging effort to potential clearance) in the smaller organisms, resulting in much higher maximal clearance rates than are achieved by larger organisms. These high rates of clearance in small organisms have been interpreted as indicating efficient feeding at low food concentrations and, accordingly, lower food concentrations were used for predators with smaller body size (see Table 4.2) in the feeding experiments with copepods (0 to $1.7\,\text{g C m}^{-3}$, Figs. 4.4 and 4.5), ciliates (0 to $0.8\,\text{g C m}^{-3}$, Fig. 4.6), and dinoflagellates (0 to $0.17\,\text{g C m}^{-3}$, Fig. 4.7). Nevertheless, copepods reach about the same maximal growth rate of about $0.5\,\text{d}^{-1}$ (Table 4.2) as the smaller organisms used in this study, except *Strobilidium spiralis* (Fig. 4.6B), and they seem to be adapted to a similar range of food concentrations as ciliates and dinoflagellates. Owing to their lower cost of foraging and assimilation, however, copepods should be able to transfer biomass more efficiently from one trophic level to the next than microzooplankton.

4.4.4 Assimilation efficiency

The predicted relationship between food concentration and assimilation efficiency in the OCF model (Fig. 4.4D), when representing copepods in a plankton model, would cause an increase in remineralisation relative to export of fecal pellets towards low food concentrations, such as are characteristic of oligotrophic systems. Steele (1998) suggested that microzooplankton, forming part of the microbial

loop, is mostly responsible for nutrient remineralisation, whereas metazooplankton contributes to export production by releasing fecal pellets. Steele (1998) accordingly separated grazing between (implicit) microzooplankton and (explicit) metazooplankton in his implicit microbial loop formulation (IML). This model is similar to OCF in that it effectively increases the assimilation efficiency of the zooplankton community at low food concentrations, although the underlying mechanism is very different: OCF theory predicts that changes in assimilation efficiency result from dynamic adjustments in feeding behaviour within species, whereas the IML model implies that assimilation efficiency varies due to strong shifts in community composition with static feeding behaviour of individual species. Steele (1998) implemented his IML in a nutrient-phytoplankton-zooplankton (NPZ) model simulating the spring bloom and subsequent transition to stratified summer conditions for the Bermuda Atlantic Time-series Study (BATS) site (Steele and Henderson, 1993; Steele, 1998). The IML model produces much higher ammonium concentrations and much lower export ratios in a simulation for BATS, and is thus more realistic than a control simulation with fixed assimilation efficiency (Steele, 1998).

4.4.5 Plankton dynamics

In order to analyse the effects of the novel features of the OCF model on plankton model behaviour, we have reproduced the simulations by Steele (1998), and implemented our OCF model in the same simple NPZ environment (Appendix in section 4.5). Fig. 4.8 compares the behaviour of the IML and OCF models for the BATS simulation described in Steele and Henderson (1993) and Steele (1998). The high ammonium concentrations and low export ratios predicted by the IML model are connected to strong changes in zooplankton community composition, reflected in the ratio of total grazing to copepod grazing G_N^{-1} (Fig. 4.8A, B), which is the mechanism behind the variations in effective assimilation efficiency in the IML model. The OCF parameters were tuned to obtain an approximate match of the behaviour of the IML model without modifying any of the parameters defining primary production and predation on metazooplankton by higher trophic levels (Table 4.3). The parameter settings are supposed to represent a zooplankton community and are thus not directly comparable to those in Table 4.2, which are for individual species. Nevertheless, the parameter estimates are most similar to those for ciliates in Table 4.2. Overall, the OCF model behaves much more similarly to the IML than to the control simulation shown in Steele (1998), both in terms of phytoplankton and nutrient dynamics and, most importantly, also export ratios (Fig. 4.8A, C), although the OCF model has more pronounced oscillations and somewhat higher export ratios than the IML. Export ratio variations are linked to variations in assimilation efficiency in both the OCF and IML (not shown) models. However, since assimilation efficiency responds to adjustments in feeding behaviour within the existing zooplankton community in the OCF model (Fig. 4.8D), much smaller shifts in community composition would be required than for the IML model to explain the difference in export ratio between bloom and non-bloom conditions.

The main advantage of the OCF model over previous formulations lies in its inherent links among ingestion, respiration, assimilation efficiency, and feeding threshold. Feeding thresholds appear to be a

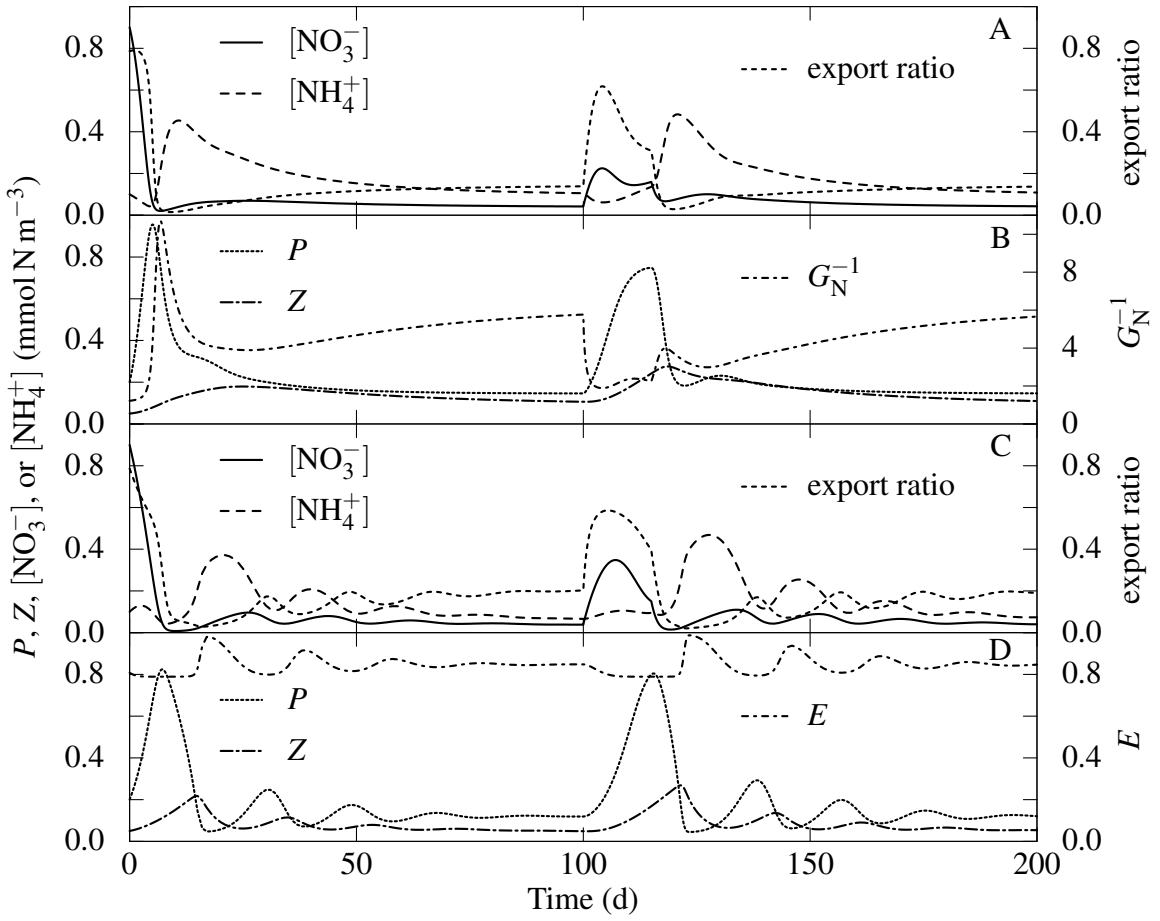

Figure 4.8: (A,B) Simulations with the implicit microbial loop model (see Appendix in section 4.5) presented by Steele (1998). (C,D) Simulations with the implicit microbial loop and copepods replaced by an optimal current feeder. P and Z are phytoplankton and zooplankton concentration, respectively, G_N^{-1} the ratio of total to copepod grazing, export ratio the ratio of export to total primary production, and E assimilation efficiency. Parameter settings are listed in Table 4.3.

general requirement for stability in plankton systems (Strom et al., 2000). Lessard and Murrell (1998) found a feeding threshold for the zooplankton community at BATS of about 0.035 mg Chl m^{-3}, which would correspond to the lowest feeding threshold in Table 4.2 if the C:Chl ratio was about 60. Feeding thresholds seem to follow a similar relationship with prey size for ciliates and copepods, with much lower feeding thresholds in dinoflagellates probably due to their different feeding behaviour. In addition, most parameter estimates in Table 4.2 are much more similar within than among systematic groups. Therefore, we suggest that phylogenetic grouping is more appropriate than predator size for classifying zooplankton into functional groups in multiple-functional-type models.

Assimilation efficiency declines as a predator allocates more of its energy to foraging and increases as more energy is allocated for assimilation. Growth is maximised in the OCF model by allocating less energy to foraging and more towards assimilation as food becomes scarce. The consequent increase in assimilation efficiency increases respiration (remineralisation) at the expense of excretion (export).

Table 4.3: Parameter settings used for Fig. 4.8.

	Parameter setting		Description
A_1	2		phytoplankton preference for NH_4^+
A_4	0.04		light attenuation coefficient for water
A_5	0.03	$m^3\,mmol\,N^{-1}$	light attenuation coefficient for phytoplankton
A_6	0.05	d^{-1}	phytoplankton respiration rate
A_k	0.005	d^{-1}	mixing rate at the base of the mixed layer
B_1	0.5	d^{-1}	maximum grazing rate
B_2	0.3	$mmol\,N\,m^{-3}$	half saturation concentration for grazing
C_2	0.3		assimilation efficiency
D_3	0.3	$m^3\,mmol\,N^{-1}\,d^{-1}$	higher predation on zooplankton
f_r	0.3		recycled fraction of higher predation
f_x	0.3		excreted fraction (export to deep water)
K_N	0.2	$mmol\,N\,m^{-3}$	half saturation concentration for phytoplankton
N_0	2[a]	$mmol\,N\,m^{-3}$	NO_3^- concentration below mixed layer
ψ	2	$m^3\,mmol\,N^{-1}\,d^{-1}$	NH_4^+ inhibition of NO_3^- uptake
V_{max}	0.04	d^{-1}	maximum phytoplankton growth rate
V_s	0.03	d^{-1}	sinking loss rate out of the mixed layer
β	0.2		assimilation coefficient
c_a	0.3		cost of assimilation coefficient
c_f^*	0.3		effective cost of foraging coefficient
E_{max}	0.99		maximum assimilation efficiency
I_{max}	1.2	d^{-1}	maximum specific ingestion rate
ϕ	13	$m^3\,mmol\,N^{-1}$	prey capture coefficient
R_M	0.16	d^{-1}	specific maintenance respiration

[a] N_0 was set to 20 $mmol\,N\,m^{-3}$ during days 100 to 115 (Steele, 1998)

Thus, optimal current feeding could explain at least to a large part the differences between recycling and export production, which implies that the required changes in community composition between subsequent seasonal regimes could be less extreme than previously thought.

Acknowledgements We thank J. H. Steele for prompt help with the reconstruction of the IML simulations. We are very grateful to A. Oschlies, G.-A. Paffenhöfer, and two anonymous reviewers for helpful comments and discussions on the manuscript.

4.5 Appendix: Equations to reconstruct Steele's microbial loop formulation

We used the following equations for reconstructing Steele's (1998) implicit microbial loop formulation (see Fig. 4.8, Table 4.3) and comparing its behaviour with that of the OCF model (modified from Steele and Henderson, 1993; Steele, 1998):

$$\frac{\mathrm{d}\,[\mathrm{NO_3^-}]}{\mathrm{d}t} = -\frac{\mathrm{e}^{-\psi[\mathrm{NH_4^+}]}[\mathrm{NO_3^-}]F_1}{V_\mathrm{N}} + A_\mathrm{k}\left(N_0 - [\mathrm{NO_3^-}]\right) \tag{4.21}$$

$$\frac{\mathrm{d}\,[\mathrm{NH_4^+}]}{\mathrm{d}t} = -\frac{A_1[\mathrm{NH_4^+}]F_1}{V_\mathrm{N}} + A_6P + r_{\mathrm{NH_4^+}}Z + D_3 f_\mathrm{r} Z^2 \tag{4.22}$$

$$\frac{\mathrm{d}\,P}{\mathrm{d}t} = V_\mathrm{N} - A_6P - IZ - (V_\mathrm{s} + A_\mathrm{k})\,P \tag{4.23}$$

$$\frac{\mathrm{d}\,Z}{\mathrm{d}t} = (EI - R)Z - D_3Z^2 \tag{4.24}$$

where $[\mathrm{NO_3^-}]$, $[\mathrm{NH_4^+}]$, P, and Z are nitrate, ammonium, phytoplankton, and zooplankton concentrations, respectively, in mmol N m^{-3}, V_N is nitrogen uptake (phytoplankton gross growth rate), defined as

$$V_\mathrm{N} = \left(\mathrm{e}^{-\psi[\mathrm{NH_4^+}]}[\mathrm{NO_3^-}] + A_1[\mathrm{NH_4^+}]\right)F_1, \qquad F_1 = \frac{V_\mathrm{max}\,P}{\left(K_\mathrm{N} + [\mathrm{NO_3^-}] + A_1[\mathrm{NH_4^+}]\right)(A_4 + A_5P)}, \tag{4.25}$$

$r_{\mathrm{NH_4^+}}$ is ammonium remineralisation, N_0 nitrate concentration at the base of the mixed layer, and A_k and V_s the phytoplankton sinking and vertical mixing coefficients (see Table 4.3 for a summary of the remaining parameters). The implicit microbial loop of Steele (1998) is obtained by substituting E, I, R, and $r_{\mathrm{NH_4^+}}$ with

$$E = C_2G_\mathrm{N}, \qquad I = G_\mathrm{N}^{-1}F_2, \qquad R = 0, \tag{4.26}$$

$$r_{\mathrm{NH_4^+}} = \left(G_\mathrm{N}^{-1} - f_\mathrm{x} - C_2\right)F_2, \qquad G_\mathrm{N}^{-1} = 1 + \frac{K_\mathrm{N}}{\mathrm{NO_3^-}}, \qquad F_2 = B_1\frac{P^2}{B_2^2 + P^2}, \tag{4.27}$$

where G_N^{-1} is the ratio of total grazing to copepod grazing and F_2 is copepod grazing, and the OCF model is implemented with the definitions for E, I, and R from Eqs. (4.7) and (4.8), and

$$r_{\mathrm{NH_4^+}} = R\,. \tag{4.28}$$

5 Feeding of sympagic meiofauna: experiments reveal carnivory, functional response, competition, and high predation impact

This chapter is a manuscript in preparation by M. Kramer and F. Prowe.

Abstract Sympagic meiofauna are assumed to recycle part of the ice-algal production within the sea-ice system. Estimates of their grazing impact are rough due to the lack of experiments. The predation impact within the meiofaunal community has not been assessed yet. We conducted grazing and predation experiments with Arctic and Antarctic sympagic meiofauna to investigate diets and determine ingestion rates. Together with carbon biomass data, we estimated the feeding impact of sympagic meiofauna for different regions and seasons. Several taxa fed on both ciliates and algae. Cnidarians (Arctic) and ctenophores (Antarctic) preyed on metazoans. Cannibalism was recorded in Arctic harpacticoid copepods. Carbon-based grazing rates of the harpacticoids *Tisbe* spp. of 1–36 % d^{-1} were lower than maximum potential ingestion rates from allometric equations and could be described by a rectilinear functional response. Predation rates were highest in the ctenophore *Euplokamis* sp. preying on copepods (191 % d^{-1}). Competition was observed in the harpacticoids *Halectinosoma* spp. and the cnidarian *Sympagohydra tuuli* preying on ciliates and nauplii, respectively. The experimentally derived grazing impact on the ice-algae standing stock (< 2 % d^{-1}) was by one order of magnitude lower than allometric estimates. The predation impact on ciliates and nauplii was remarkably high at some stations (up to > 200 % h^{-1} and 37 % h^{-1}, respectively). Cilivory, carnivory, and flexible feeding strategies probably enable sympagic meiofauna to survive periods of low ice-algal production. Competition might be important in constraining the feeding impact in sea ice. Carnivorous meiofauna presumably constitute competition to under-ice and sub-ice predators and thus influence cryo-pelagic coupling.

5.1 Introduction

Sea ice covers large parts of the polar oceans with 5–45 % of the total Southern Ocean area and 9–100 % of the total Arctic Ocean area (Comiso, 2010). Ice algae, inhabiting the brine channels in sea ice,

contribute substantially to total primary production in ice-covered regions—up to 28 % in certain parts of the Southern Ocean (Arrigo and Thomas, 2004) and up to 57 % in the Central Arctic (Gosselin et al., 1997)—and thus constitute an important base of the polar marine food webs (Legendre et al., 1992). However, it is still unknown to what extent this primary production is available to under-ice grazers and, after release from the ice, to zooplankton and zoobenthos. Since sympagic meiofauna—proto- and metazoans $\geq 20\,\mu$m inhabiting the brine channels—are assumed to also utilise ice algae as a food source (Gradinger, 1995; Arrigo and Thomas, 2004), part of the primary production may be recycled within the system.

Estimates of the extent of such recycling are still very rough, though. Due to the lack of experimental studies, the feeding impact of sympagic meiofauna on ice algae has up to now only been estimated using ingestion rates from allometric equations, which had originally been developed for filter-feeding zooplankton (Moloney and Field, 1989). In most cases, these estimates indicate a low feeding impact (Gradinger, 1999a; Nozais et al., 2001; Michel et al., 2002; Gradinger et al., 2005), but some studies suggest that sympagic meiofauna may in certain situations control accumulation of ice algae and compete with under-ice grazers for this food source (Gradinger et al., 1999; Kramer et al., 2011).

Besides lacking experimental support of ingestion rates, these estimates of the feeding impact neglect the fact that most sympagic meiofauna taxa are not strictly herbivorous, but rather omnivorous, detritivorous, cilivorous or carnivorous (Kramer et al., subm.). Cilivorous or carnivorous feeding and flexible feeding strategies (such as omnivory, diet switches, starvation periods) may substantially reduce the grazing pressure on ice algae. At the same time, predation by sympagic meiofauna may alter the composition of the meiofaunal community and limit the availability of certain prey species to carnivorous sub-ice and under-ice fauna, such as the Arctic amphipods *Themisto libellula* and *Gammarus wilkitzkii* (Werner et al., 2002; Auel and Werner, 2003).

We conducted feeding experiments with various Arctic and Antarctic sympagic meiofauna taxa to

- confirm the cilivorous and carnivorous feeding in certain meiofauna taxa which Kramer et al. (subm.) deduced from fatty acid and stable isotope analyses,
- determine grazing and predation rates,
- investigate and quantify factors influencing ingestion rates (food composition, food density, grazer / predator density) by means of statistics and linear modelling,
- obtain more realistic estimates of the grazing impact on ice algae as well as first estimates of the predation impact on sympagic ciliates and metazoan meiofauna.

5.2 Materials and methods

Sampling and sample processing

Sea ice was sampled during four expeditions to different Arctic and Antarctic regions in summer, spring and winter (Table 5.1). Ice cores for determination of biomass of ice algae and abundance and biomass of sympagic meiofauna were taken and cut according to Kramer et al. (2011). Sympagic meiofauna and ice algae for experiments were gained from non-quantitative sea-ice samples—i. e. from chunks of ice sampled with the aid of a cage on the ship's crane (Kiko et al., 2008) or sawn from ice floes, or from pooled bottom-ice sections from cores.

All ice samples were melted in the dark at $+4\,^{\circ}$C (Gradinger, 1999a), for meiofauna samples after addition of filtered sea water (Garrison and Buck, 1986; Gradinger, 1999a). Melted algae core sections were processed for chlorophyll *a* (chl *a*) analyses according to Gradinger (1999b) and Kramer et al. (2011). Organisms from melted meiofauna core sections were enriched over a 20 μm gauze and fixed with formaldehyde for abundance and biomass determination (Gradinger, 1999a; Kramer et al., 2011). Organisms from non-quantitative samples were enriched likewise and transferred into petri dishes or beakers. Metazoan meiofauna and larger ciliates for feeding experiments were sorted from these samples and either used directly, or kept in the dark at $0\,^{\circ}$C and reared on a mixed sympagic protist diet until the start of the experiments. Parts of the samples from which metazoan meiofauna and larger ciliates had been withdrawn completely were used as stocks for mixed protist cultures, reared on F / 2 culture media based on filtered sea water (S = 30–35).

In addition, ice *in situ* temperature and bulk salinity were determined as described in Horner et al. (1992) and Kramer et al. (2011) for calculation of the brine volume fraction according to Frankenstein and Garner (1967).

Grazing experiments

We modified established methods of grazing experiments (Frost, 1972) specifically for application to sympagic meiofauna, as described in the following.

Experimental setup

Quantitative grazing experiments were conducted with the Arctic sympagic harpacticoid copepods *Tisbe* spp. as grazer and mixed cultures of sea-ice protists as food. Non-quantitative grazing experiments were conducted with Arctic sympagic red and white acoel platyhelminthes, nematodes, harpacticoid copepods (*Halectinosoma* spp. and an unidentified species) and cyclopoid copepods, as well as with Antarctic sympagic white acoels as grazers.

Table 5.1: Expeditions with sea-ice sampling to obtain sympagic meiofauna for feeding experiments (Exp), and to determine abundance and carbon biomass of sympagic meiofauna taxa (Abun, Biom) as well as chlorophyll *a* concentration and ice-algae biomass (Chl) for estimation of the feeding impact. + samples taken for this study; (+)[1] meiofauna abundance already published in Marquardt et al. (2011) and Marquardt (2010); (+)[2] temperature, salinity, chl *a*, meiofauna abundance / carbon biomass already published in Kramer et al. (2011); (+)[3] temperature, salinity provided by G. Carnat, B. Delille, N.-X. Geilfus and G. Song, chl *a* provided by B. Philippe, C. J. Mundy and M. Gosselin; — samples not taken.

Region	Coverage		Time		Campaign	Samples			
	Latitudes	Longitudes	Season	Dates		Symp meiofauna		Algae	
						Exp	Abun, Biom	Exp	Chl
Central Arctic	82°01' N–88°09' N	33°58' E–134°55' W	Summer	Jul 29–Oct 7 2007	ARK–XXII / 2 (RV *Polarstern*)	+	+	+	+
Western Canadian Arctic: Beaufort Sea, Amundsen Gulf	69°57' N–71°34' N	119°36' W–126°10' W	Spring	Mar 13–Jun 5 2008	CFL legs 7–8 (CCGS *Amundsen*)	+	(+)[1]	+	(+)[3]
Antarctic: Southern Ocean: Western Weddell Sea	59°50' S–65°07' S	40°47' W–57°24' W	Winter	Aug 24–Oct 29 2006	ANT–XXIII / 7 (RV *Polarstern*)	+	(+)[2]	+	(+)[2]
Antarctic: Southern Indian Ocean	64°08' S–65°21' S	116°29' E–128°36' E	Winter	Sep 5–Oct 17 2007	SIPEX voyage 1 (RSV *Aurora Australis*)	—	(+)[2]	—	(+)[2]

The 13 treatments in the quantitative experiments differed in initial protist composition and biomass (Appendix 5.6 Fig. 5.6). Each treatment was run with triplicate grazer setups *g* and triplicate protist-only setups *p*. The well-mixed suspensions of protist cultures for each treatment were distributed into 6-well plates (5 mL per well). 10 grazers were added to three of the wells *g* without prior starvation, while no grazers were added to the remaining three wells *p*. Initial protist biomass (Appendix 5.6 Fig. 5.6), determined from linear regressions, ranged between 1 $mg\,L^{-1}$ and 18 $mg\,L^{-1}$ in total and was thus within the range of algae biomass in sea-ice brine (Table 5.2).

It was impossible, with reasonable effort, to simulate all aspects of *in-situ* conditions inside the brine channel system potentially relevant to feeding behaviour, including temperature, light, nutrients and brine-channel geometry. Following a commonly employed approach in experiments with polar organisms (Metz and Schnack-Schiel, 1995; Schnack-Schiel et al., 1995; Werner, 1997; Friedrich and Hendelberg, 2001; Meyer et al., 2010), we conducted the grazing experiments in the dark at 0 °C to avoid freezing of the sea water in the wells. In order to better approximate *in-situ* conditions, experiments were conducted in well-plates instead of in a plankton wheel, so that protists could settle and meiofauna could graze on surfaces. Possible impacts of brine channel geometry, which could not be simulated by the wells, on feeding behaviour are discussed.

The grazing experiments were run for 1–12 weeks to obtain robust estimates of average grazing rates in spite of the low and potentially variable individual ingestion rates. Changes in food quality due to the long duration cannot be ruled out, but the influence on grazing rates is expected to be sufficiently small to nevertheless allow for good estimates. Ciliates present in the protist food cultures might have ingested part of the smaller size fraction of algae, but this did not affect the calculated taxon-specific grazing rates: since ciliates were not a preferred food of *Tisbe* spp. in our experiments (cf. section 5.3 Fig. 5.2), their influence on the algal composition was probably comparable in grazer and protist-only

setups and thus accounted for in our calculation.

By the end of the experiments, the grazers were removed and photographed for determination of volumes and calculation of carbon contents from length and width (Gradinger et al., 1999; Kramer et al., 2011). In few grazing experiments, *Tisbe* spp. grazers reproduced during the experiments; in these cases nauplii were included in carbon content determination and further evaluations, since they were probably feeding stages according to gut colouration. The protists from grazer triplicates and protist-only triplicates were re-suspended from the bottom of the wells, fixed in formaldehyde or Lugol solution, identified based on Tomas (1997) and counted according to Utermöhl (1958). Protist carbon contents were likewise determined from size measurements (Hillebrand et al., 1999), which, for each treatment, were conducted for at least one of the grazer triplicates and one of the protist-only triplicates. The carbon content determination, particularly for metazoan meiofauna, is based on many assumptions (Gradinger et al., 1999) and therefore inaccuracy is estimated to be at least 10 %, which might bias the calculated feeding impact due to non-linear error propagation. However, it is the best estimate possible since direct measurements are not available.

Determination of grazing rates of *Tisbe* spp.

Grazing rates were calculated from the decrease of protist biomass in each of the 13 treatments, determined as the biomass difference between protist-only and grazer setups at the end of the experiments, assuming that this difference had been ingested and that grazing rates were constant over time. In the following, all rates are expressed based on carbon biomass, if not explicitly stated otherwise. Total grazing rates were determined from total protist biomass by linear regression (see Appendix 5.5 for details). Likewise, taxon-specific grazing rates as well as abundance-based grazing rates were calculated for 16 different protist taxa (Appendix 5.5 Table 5.8), the latter needed for determination of selectivity.

The treatments were grouped according to protist composition identified by cluster analysis and SIMPROF test (see Appendix 5.5 for details; significance level of all statistic tests in this study 5 %). To test whether total and taxon-specific grazing rates were significantly positive, a one-tailed test was applied, using the t statistic of the respective regression coefficient as test statistic. All following analyses were performed with only the eight treatments with significantly positive total grazing rates.

We applied a one-way ANOVA to test whether total grazing rates were influenced by protist composition, using the composition groups from cluster analysis. A one-tailed Spearman rank correlation test was performed to test for a positive monotonic relationship between the total grazing rates and the estimated initial total protist biomass. We assumed a rectilinear functional response (Frost, 1972) and thus performed a linear regression of total grazing rates on initial total protist biomass.

A two-way ANOVA was performed on taxon-specific grazing rates to test for the influence of taxon (16 taxa as levels) and protist biomass composition (three groups from cluster analysis as levels). Out of the potential number of grazing rates for 16 taxa in eight treatments, 28 were significantly positive

Table 5.2: Ice-algae and meiofauna abundance and carbon biomass in the brine channels of sea ice for different regions and seasons (including amphipods from melted ice cores). Medians (ranges) are given. — taxon not observed in any sea-ice samples from the respective expedition, *nd* no data. For the western Canadian Arctic, the values were calculated from chl *a* concentration provided by B. Philippe et al., meiofauna bulk abundance obtained from Marquardt (2010) and Marquardt et al. (2011) and sea-ice temperature and bulk salinity provided by G. Carnat et al.. For the Antarctic, the values were calculated from chl *a* concentration, meiofauna bulk abundance and carbon biomass and brine volume fraction obtained from Kramer et al. (2011). Incomplete ice cores (with missing sections) as well as additional bottom-ice sections (meiofauna counted alive) are included.

	Arctic		Antarctic	
	Central Arctic	Western Canadian Arctic	Western Weddell Sea	Southern Indian Ocean
	Summer	Spring	Winter	Winter
Abundance in brine [mL^{-1}]				
Algae	*nd*	*nd*	*nd*	*nd*
Ciliata	1.71 (0.00–26243.54)	0.16 (0.00–230.17)	0.05 (0.00–22.69)	0.07 (0.00–3.23)
Foraminifera	0.00 (0.00–180.38)	—	0.00 (0.00–0.65)	0.03 (0.00–5.75)
Radiolaria	0.00 (0.00–36.88)	—	0.00 (0.00–0.11)	0.00 (0.00–0.89)
Zooflagellata	*nd*	0.00 (0.00–1.17)	*nd*	*nd*
Cnidaria	0.00	0.00 (0.00–0.07)	—	—
Ctenophora	—	—	0.00 (0.00–0.06)	0.00 (0.00–0.05)
Nematoda	0.00 (0.00–445.98)	0.00 (0.00–16.56)	—	—
Acoela	0.00 (0.00–651.81)	0.00 (0.00–1.23)	0.04 (0.00–9.16)	0.00 (0.00–0.47)
Rhabditophora	—	—	0.00 (0.00–0.05)	—
Rotifera	0.04 (0.00–2119.12)	0.04 (0.00–23.89)	—	—
Nemertea	0.00	0.00 (0.00–0.04)	—	—
Nudibranchia juv.	—	—	0.00 (0.00–0.02)	0.00 (0.00–0.02)
Other Mollusca juv.	—	0.00 (0.00–0.19)	—	—
Polychaeta larv. / juv.	—	0.00 (0.00–0.20)	—	—
Cirripedia Nauplii	—	0.00 (0.00–0.01)	—	—
Harpacticoida CI-CVI	0.00 (0.00–1800.62)	0.00 (0.00–0.38)	0.03 (0.00–2.40)	0.00 (0.00–0.04)
Calanoida CI-CVI	0.00	—	0.00 (0.00–0.34)	0.00 (0.00–0.02)
Cyclopoida CI-CVI	0.00 (0.00–52.87)	0.00 (0.00–0.22)	0.00 (0.00–0.04)	—
Copepoda indet. CI-CVI	—	0.00 (0.00–0.03)	—	—
Copepoda Nauplii	0.00 (0.00–240.14)	0.02 (0.00–1.93)	0.00 (0.00–34.64)	0.00 (0.00–1.65)
Amphipoda	0.00	0.00 (0.00–0.03)	—	—
Biomass in brine [$\mu g L^{-1}$]				
Algae (from chl *a*) [$\times 10^3$]	6.14 (0.37–157.00)	3.55 (0.02–4001.53)	2.21 (0.06–241.58)	0.40 (0.00–13.04)
Ciliata	21.82 (0.00–532.11)	4.56 (0.00–8891.98)	5.59 (0.00–1053.59)	0.29 (0.00–397.93)
Foraminifera	0.00 (0.00–98.56)	—	0.00 (0.00–1640.02)	1.56 (0.00–1343.73)
Radiolaria	0.00 (0.00–149.11)	—	0.00 (0.00–214.39)	0.00 (0.00–214.62)
Zooflagellata	*nd*	0.00 (0.00–21.85)	*nd*	*nd*
Cnidaria	0.00	0.00 (0.00–30.62)	—	—
Ctenophora	—	—	0.00 (0.00–19.88)	0.00 (0.00–0.81)
Nematoda	0.00 (0.00–75.96)	0.00 (0.00–1475.74)	—	—
Acoela	0.00 (0.00–295.18)	0.00 (0.00–161.44)	3.99 (0.00–5047.85)	0.00 (0.00–21.31)
Rhabditophora	—	—	0.00 (0.00–496.38)	—
Rotifera	0.29 (0.00–37.56)	0.56 (0.00–402.32)	—	—
Nemertea	0.00	0.00 (0.00–1221.98)	—	—
Nudibranchia	—	—	0.00 (0.00–53.70)	0.00 (0.00–3.25)
Gastropoda / Bivalvia juv.	—	0.00 (0.00–181.10)	—	—
Polychaeta larv. / juv.	—	0.00 (0.00–113.06)	—	—
Cirripedia Nauplii	—	0.00 (0.00–9.53)	—	—
Harpacticoida CI-CVI	0.00 (0.00–1901.61)	0.00 (0.00–573.72)	4.49 (0.00–1309.99)	0.00 (0.00–12.02)
Calanoida CI-CVI	0.00	—	0.00 (0.00–1084.83)	0.00 (0.00–21.79)
Cyclopoida CI-CVI	0.00 (0.00–41.44)	0.00 (0.00–140.63)	0.00 (0.00–23.04)	—
Copepoda indet. CI-CVI	—	0.00 (0.00–22.83)	—	—
Copepoda Nauplii	0.00 (0.00–31.56)	1.65 (0.00–685.98)	0.00 (0.00–3676.59)	0.00 (0.00–34.71)
Amphipoda	0.00	0.00 (0.00–636.56)	—	—
n	99	108	104	105

and thus used in the ANOVA. One-tailed Spearman rank correlation tests were performed to test for a positive monotonic relationship between the taxon-specific grazing rates and the estimated initial biomass of the respective taxon.

Determination of grazing selectivity of *Tisbe* spp.

Selectivity for each protist taxon j in each treatment is presented as electivity index ε ranging from -1 to +1 with 0 representing no preference for the respective taxon (Chesson, 1983). For calculation, we used estimates of protist abundance at the beginning and end of the experiments, which were based on the linear regression applied to determine grazing rates (see Appendix 5.5 for details).

To examine whether selectivity in these mixed-protist grazing experiments differed between the protist taxa or was influenced by protist composition, a two-way ANOVA was performed on the electivity indices. The two factors specified for which of the 16 protist taxa the index had been calculated and which of the three biomass composition clusters the treatment had been assigned to. For each protist taxon, two-tailed Spearman rank correlation tests were performed to test for monotonic relationships of electivity vs. initial abundance and electivity vs. initial biomass of the respective taxon.

Predation experiments

We developed set-up and evaluation of predation experiments specifically for application to sympagic meiofauna, as described in the following. Note the differences to the above-described design of grazing experiments, which made a different approach of evaluation necessary.

Experimental setup

Quantitative predation experiments were conducted with several different combinations of metazoan meiofauna taxa as predators and metazoan meiofauna or ciliates as prey, and with different predator and prey densities (Table 5.3), which were within the range of densities determined for sea-ice brine. These 43 treatments were run in predator triplicates or duplicates (with predators) whenever possible. In 14 cases, replication was not possible due to limited resources. In all but 19 cases, one to three prey-only setups (without predators) were run for each treatment to assess prey reproduction and losses due to handling. Usually animals from several sampling stations had to be pooled for each setup: due to the enormous effort associated with each experiment and to the limited number of animals available from each ice sample, it was impossible to run separate experiments for each sampling event to allow assessment of regional variability in feeding behaviour. Our approach enables us, however, to give an overall picture of the feeding habits of various sympagic meiofauna taxa and to assess general variability and trends in ingestion rates.

For each treatment, a 6-well plate was filled with filtered sea water (5 mL per well), a certain number of prey items were placed into each well, and a certain number of predators were added to the wells of predator setups without prior starvation. As for grazing experiments, it was impossible to simulate all relevant aspects of *in-situ* conditions inside the brine channel system. We thus conducted the predation

experiments in the dark at 0 °C at salinities of 30–35 and in well-plates which were kept still as in the setup of grazing experiments.

In regular intervals (usually 5 hours to 5 days, depending on predator taxa), prey items and predators were transferred individually to well plates with fresh filtered sea water using a pipette and were thereby counted. In contrast to the grazing experiments, we thus assessed both initial and intermediate conditions, which revealed predation rates with respect to temporal variability. Consumed or dead prey as well as dead predators were replaced to enable continuous (and near-constant) predation also at low prey density and in spite of predator and prey mortality. The procedure was conducted under experimental conditions of 0 °C using a stereomicroscope (20–40 × magnification).

The predation experiments were run for usually 3–26 days; only 9 predation experiments were run shorter (Table 5.3). The long duration enabled us to observe temporal variabilities in predation rates and to obtain robust estimates of average predation rates. After each experiment, predators were photographed for determination of volumes and calculation of carbon contents from length and width (Gradinger et al., 1999; Kramer et al., 2011). The carbon content of all prey—as well as of predators in few cases where the size was not measured for the individual experiments—were estimated from carbon contents of the respective taxon from the respective expedition. As mentioned above, the inaccuracy of this method is estimated to be at least 10 %, which might bias the calculated feeding impact; however, it is the best estimate possible since direct measurements are not available.

Determination of predation rates of Arctic and Antarctic sympagic meiofauna

Gains and losses in prey ΔB_{py} attributed to reproduction and handling in predation experiments were determined from prey-only replicates (see Appendix 5.5 for details). To obtain predation rates for each predator replicate and time interval, the change in prey biomass per time was corrected with the respective ΔB_{py} and divided by the predator biomass (averaged over the respective time step). For *Halectinosoma* spp. preying on ciliates, abundance-based predation rates were calculated likewise.

For the following investigations of the influence of prey and predator biomass on predation rates, all time intervals of all predator setups within each predator-prey combination were pooled for further calculations and interpretation. Predation rates varied notably in time, but no systematic temporal trends in predation rates could be detected (Appendix 5.6 Figs. 5.8-5.9) and thus time (or the history of the experiment) obviously had no systematic influence on ingestion rates. Note that this was true for each of the replicates applied for most of the experiments.

In two cases where two- and three-dimensional plots clearly indicated a trend in predation rates with prey and predator biomass, two-dimensional functions were fitted to the data. For *Sympagohydra tuuli* preying on nauplii, a linear function (i. e. a plain) was fitted. For *Halectinosoma* spp. preying on ciliates, we applied an empirical model originally derived for microzooplankton grazing (Peters, 1994), which takes into account both prey and predator abundance. The original equation, which assumes power laws

Table 5.3: Predator and prey taxa used in predation experiments, number of individuals (Ind), number of replicates with predators (Pd repl. = predetor replicates) and without predators (Py repl. = prey-only replicates), duration and experiment identity label (ID).

Region	Predator (Pd)		Prey (Py)		Pd	Py	Duration	Predation
	Taxon	Ind	Taxon	Ind	repl.	repl.		experiment ID
Arctic	Cnidaria: *Sympagohydra tuuli*	1	Ciliata	30	3	0	11 d	Sym-Cil-a
		1	Rotifera	15	3	1	8 d	Sym-Rot-a
		1		20	3	1	14 d	Sym-Rot-b
		2		30	3	1	13 d	Sym-Rot-c
		2		60	3	1	13 d	Sym-Rot-d
		1	Nauplii	15	3	0	9 d	Sym-Nau-a
	Plathelminthes: Acoela indet. red	1	Ciliata	40	3	1	9 d	Aco_r-Cil-a
		1		45	3	1	21 d	Aco_r-Cil-b
		2		6	3	1	10 d	Aco_r-Cil-c
		2		10	3	1	10 d	Aco_r-Cil-d
		2		20	3	1	10 d	Aco_r-Cil-e
		2		50	3	1	10 d	Aco_r-Cil-f
	Harpacticoida: *Tisbe spp.* copepodides	7	*Tisbe spp.* nauplii	77	1	0	9 h	Tis-Nau-a
		8		24	1	0	46 h	Tis-Nau-b
		8		104	1	0	19 h	Tis-Nau-c
		9		114	1	0	46 h	Tis-Nau-d
		15		160	1	0	22 h	Tis-Nau-e
		18		120	1	0	18 h	Tis-Nau-f
	Harpacticoida: *Halectinosoma spp.*	1	Ciliata	65	3	1	8 d	Hal-Cil-a
		2		65	3	1	8 d	Hal-Cil-b
		5		65	3	1	20 d	Hal-Cil-c
		11		55	3	1	9 d	Hal-Cil-d
		11		65	3	1	21 d	Hal-Cil-e
		20		65	3	1	22 d	Hal-Cil-f
	Harpacticoida indet.	5	Ciliata	65	3	1	26 d	Harp-Cil-a
		5		80	3	1	9 d	Harp-Cil-b
		5		100	3	1	19 d	Harp-Cil-c
		5		700	1	1	47 h	Harp-Cil-d
Antarctic	Ctenophora: *Euplokamis sp.*	4	Ciliata	20	1	0	6 d	Eup-Cil-a
		4		40	2	0	17 d	Eup-Cil-b
		4	Ciliata red	40	2	0	10 d	Eup-Cil-c
		4	Acoela indet. white	40	2	0	23 d	Eup-Aco-a
		3	Nauplii	33	1	0	3 d	Eup-Nau-a
		3		60	2	0	4 d	Eup-Nau-b
		4	Harpacticoida	40	1	0	3 d	Eup-Harp-a
		4	Calanoida: *Stephos longipes*	26	1	0	5 h	Eup-Ste-a
		4		40	1	0	9 h	Eup-Ste-b
	Plathelminthes: Acoela indet. white	1	Ciliata	10	3	3	17 d	Aco_w-Cil-a
		2		10	3	3	17 d	Aco_w-Cil-b
		2		20	3	3	17 d	Aco_w-Cil-c
		6		10	3	3	17 d	Aco_w-Cil-d
		10		10	1	0	19 d	Aco_w-Cil-e
		10		20	1	0	10 d	Aco_w-Cil-f

of prey and predator abundance and body volume, was transformed using a base-10 logarithm and fitted to the abundance-based predation rates by multiple linear regression. The exponents for temperature and ciliate body volume were taken from Peters (1994) since ciliate body volumes were estimated as the median from the respective expedition and all experiments were performed at the same temperature, and therefore no range of values was covered in the experiments.

In predator-prey combinations where a relationship between predation rates and prey or predator

biomass was not obvious due to large scatter in the data or an insufficient number of data points, the results for all time intervals in all predator replicates were grouped according to predator and prey biomass by cluster analysis and SIMPROF test (see Appendix 5.5 for details). An average predation rate was then calculated for each cluster, and a *t*-test was applied to test whether it was significantly positive.

Calculation of maximum potential ingestion rates

For both grazing and predation experiments, the individual maximum potential ingestion rate I_{max} was calculated according to Moloney and Field (1989) for the respective range of grazer / predator carbon content to compare with experimental ingestion rates. Temperature correction was performed assuming a Q_{10} value of 2 (Gradinger et al., 1999).

Assessment of feeding impact

Determination of ice-algae biomass and meiofauna abundance and biomass

Carbon biomass of ice algae and abundance and carbon biomass of sympagic meiofauna in the brine channels were determined to adjust densities in feeding experiments to natural conditions and to calculate ingestion rates from experimentally-derived functional response equations. Integrated carbon biomass of ice algae and sympagic meiofauna were determined for estimation of the feeding impact. In the following, the term biomass always refers to carbon biomass.

Bulk concentration of chl *a* in the algae core sections (chl_{bulk}, chlorophyll mass per volume melted ice) was determined fluorometrically according to Gradinger (1999b) and converted to integrated concentration (chl_{int}, mass per area). Furthermore, chl *a* concentration in the brine (chl_{br}, mass per volume brine) was calculated as

$$chl_{br} = \frac{chl_{bulk} \cdot V_{ice_m}}{V_{ice_s} \cdot \delta V_{brine}} \quad , \tag{5.1}$$

where V_{ice_m} is the volume of melted ice, V_{ice_s} is the respective volume of solid ice (core area times section length), and δV_{brine} is the brine volume fraction. Chl *a* concentrations were converted to carbon biomass of ice algae assuming a conversion factor of 52 for the Antarctic in winter (Meiners et al., 2011), of 44 for the Canadian Arctic in spring (B. Philippe, pers. comm.) and 470 for the Central Arctic in summer (own data from ARK–XXII / 2 based on chl *a* and POC measurements, unpubl.; the high ratio might have been caused by high proportions of dinoflagellates and heterotrophic flagellates, Landry et al., 2000). Although the POC:chl ratio might vary considerably between stations and throughout the ice column, the use of average values for each expedition is expected to give sufficiently good estimates of the grazing impact, given the fact that ingestion rates were measured for each taxon irrespective of the sampling station, as described below.

Bulk abundance and integrated abundance of sympagic meiofauna taxa was determined according to Gradinger (1999a). Meiofauna abundance in the brine was calculated as for chlorophyll. Meiofauna abundance was converted to biomass on the base of length and width measurements (Gradinger et al., 1999; Kramer et al., 2011).

Calculation of feeding impact

To estimate *in situ* ingestion rates, functional response and competition equations were derived from the experiments for various combinations of grazers / predators and food / prey. Since grazing experiments were conducted with one grazer taxon only, we applied the respective equation to all proto- and metazoan meiofauna, assuming that it represented the grazing behaviour of the different taxa sufficiently well. For predation on ciliates, we applied the equations derived for certain predator taxa to other predator taxa which we assumed to have similar feeding modes. For predation on metazoans, we assumed that predation took place only for those predator-prey combinations where feeding had actually been observed in quantitative or non-quantitative experiments and, in case of non-quantitative experiments, we applied equations of similar taxa. An exponential term for temperature correction was included in all equations. Details on the equations are given in the results section. Based on these equations, individual *in situ* ingestion rates $I_{ijk,ind}$ were calculated for each pair of grazer or predator i and food type (algae or prey taxon) j, and for each ice-core section k, using the median carbon content of grazer / predator i in section k, the abundance or biomass of predator i and food type j in the brine channels and the sea-ice temperature of section k. For comparison, maximum potential ingestion rates I_{max} were calculated according to the temperature-corrected allometric equation (Moloney and Field, 1989).

Based on these individual *in situ* ingestion rates and maximum potential ingestion rates, we calculated integrated community ingestion rates for each station and food type. From these, we derived the feeding impact of meiofauna on the standing stock of each food type for each station (see Appendix 5.5 for details).

Community ingestion rates and feeding impact for each food type were tested for differences between the expeditions by pairwise application of two-tailed U-tests. For community grazing rates and grazing impact within each region, two-tailed U-tests were applied to test for differences between results from maximum potential ingestion rates and measured grazing rates.

5.3 Results

In the following section, we present the statistically significant results (significance level 5%) from our experiments. The statistical tests applied are described in the Materials and Methods section. Common tests are also mentioned in brackets along with the respective results. Included relevant observations for which no significant results could be obtained are identified in the text.

5.3.1 Grazing rates and selectivity of *Tisbe* spp.

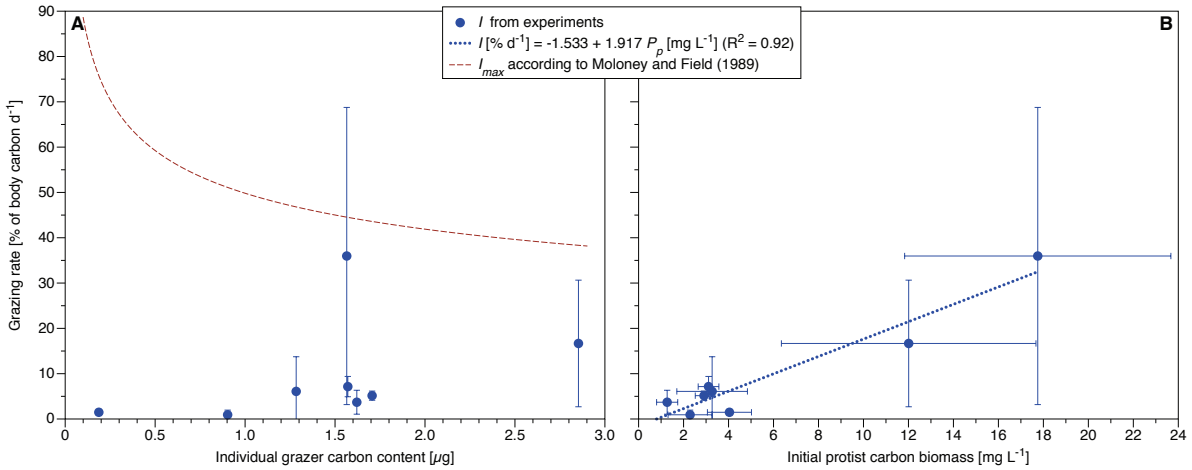

Figure 5.1: Experimentally derived carbon-based grazing rates of *Tisbe* spp. plottet against **A** th e individual grazer carbon content and **B** the initial protist carbon biomass in the respective treatment (blue dots). Grazer carbon contents are means of triplicate grazer setups (i naccuracy estimated to be at least 10 %). Both grazing rate and initial protist carbon biomass were estimated from linear regressions. Error bars show the 95 % confidence intervals of t he regression coefficients. Only significantly positive grazing rates are shown (one-tailed test with t statistics of regression coefficients). For comparison, the maximum potential inges tion rate I_{max}, calculated from an allometric equation (Moloney and Field, 1989), is shown as a dashed red curve (A). The dotted blue line (B) shows a linear regression of experimentall y derived grazing rates on the initial carbon biomass (functional response) used for calculation of the grazing impact.

Replicates in grazing experiments (both grazer setups and protist-only setups) showed a high variability in protist abundance, biomass and, partly, composition. The 13 treatments grouped into three clusters (SIMPROF) according to initial protist biomass compositions (Appendix 5.6 Fig. 5.6).

Positive total grazing rates of the Arctic sympagic harpacticoids *Tisbe* spp. were detected in eight out of 13 treatments (Appendix 5.6 Fig. 5.6; one-tailed test with t statistics of regression coefficients). In these treatments, *Tisbe* spp. ingested between 1 % and 36 % of their body carbon content per day (Fig. 5.1). All experimentally derived grazing rates were lower than the maximum potential ingestion rates calculated from grazer carbon content using an allometric equation (Moloney and Field, 1989); only for the highest experimental value, the confidence interval overlapped with the curve (Fig. 5.1 A). The total grazing rate increased with initial total protist biomass and could be decribed by a linear function (F statistics; Fig. 5.1 B). A feeding threshold below which feeding ceased, as suggested by the linear fit, was not significant. A significant influence of protist composition on total grazing rate could not be detected (one-way ANOVA).

Taxon-specific grazing rates (Appendix 5.6 Fig. 5.7) were highly variable within each protist taxon. Significant differences between taxa or an influence of protist composition could not be detected (two-way ANOVA). The taxon-specific grazing rate increased with biomass only for *Thalassiosira bioculata* (one-tailed Spearman rank correlation test; correlation coefficient 1.0).

Feeding selectivity (Fig. 5.2) differed between protist taxa but was not significantly influenced by protist

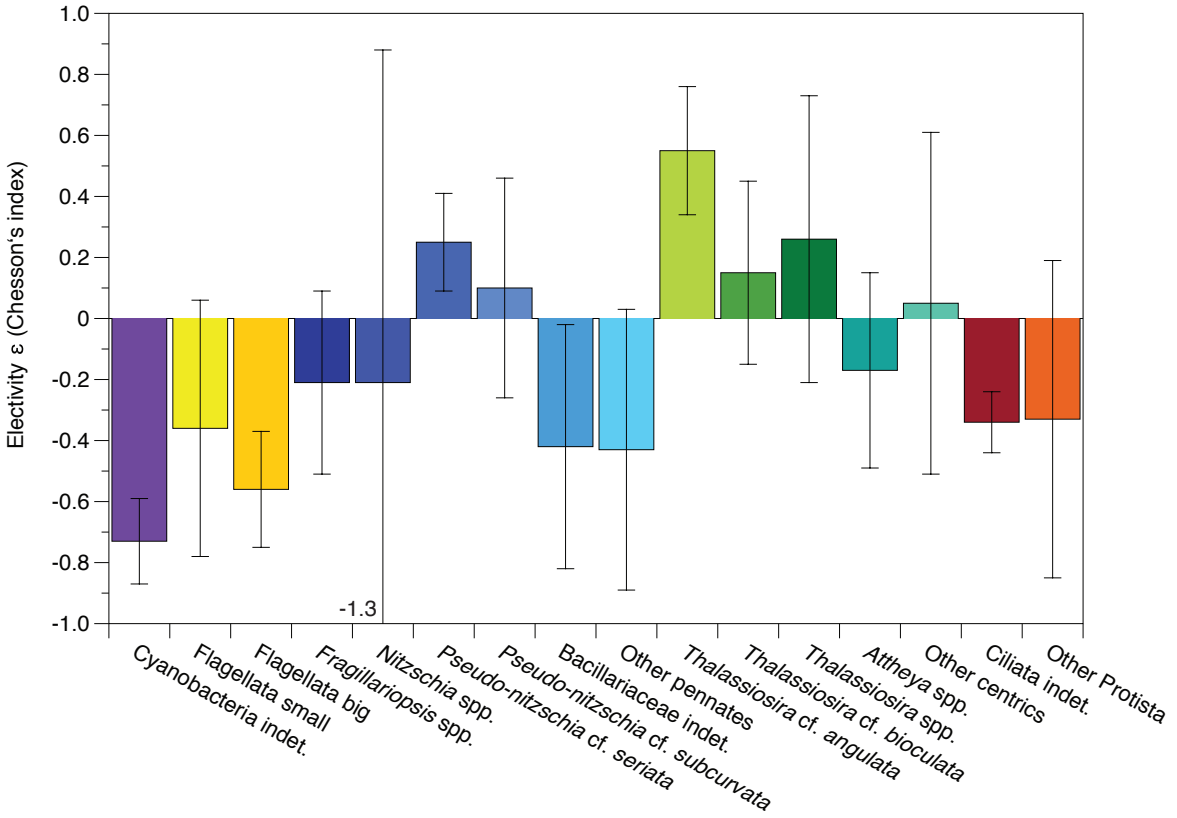

Figure 5.2: Grazing selectivity of *Tisbe* spp. from the electivity index ε (Chesson, 1983) for each protist taxon (mean from 13 treatments, error bars denote standard deviations). Only the range from -1.0 to +1.0 is shown, minima of error bars beyond this range are displayed as numbers.

composition (two-way ANOVA) or the initial abundance or biomass of any of the protist taxa (two-tailed Spearman rank correlation tests). *Tisbe* spp. positively selected the large centric diatom *Thalassiosira angulata* and the pennate diatom *Pseudonitzschia* cf. *seriata*, while negatively selecting cyanobacteria, big flagellates, pennate diatoms (indetermined Bacillariaceae) and ciliates.

5.3.2 Predation rates of Arctic and Antarctic sympagic meiofauna

Predation rates representative of the different predator-prey combinations (Table 5.4) were obtained in different ways according to trends or clusters in the data (Tables 5.5, 5.6). For two predator-prey combinations, predation rates showed distinct trends with predator and prey biomass. For *Sympagohydra tuuli* preying on copepod nauplii, calculated predation rates distinctly decreased with both predator and prey biomass (Appendix 5.6 Fig. 5.14). The relationship was well described by a two-dimensional linear function (F and t statistics):

$$I = 241.836 - 1.06136 B_{py} - 0.114801 B_{pd} \quad (\mathrm{R}^2 = 0.73,\ p < 0.05)\ , \tag{5.2}$$

where I is the carbon-based ingestion rate [$\%\,d^{-1}$] and B_{py} and B_{pd} are the biomass [$\mu g\,L^{-1}$] of prey and predator, respectively.

For *Halectinosoma* spp. preying on ciliates, the relationship could be approximated by a two-dimensional power function according to Peters (1994) fitted to the data (F statistics; Fig. 5.3):

$$I_{ab} = V_{py}^{-0.344} \cdot V_{pd}^{-0.121} \cdot A_{py}^{-1.750} \cdot A_{pd}^{-0.366} \cdot 10^{0.033T} \cdot 10^{3.602} - 0.1 \quad \begin{array}{l}(R^2 = 0.482,\ p < 0.05 \\ \text{for linear regression on} \\ \text{log-transformed data})\ ,\end{array} \tag{5.3}$$

where I_{ab} is the abundance-based ingestion rate [h^{-1}], V_{py} and V_{pd} are the body volumes [μm^3] of prey and predator, respectively, A_{py} and A_{pd} are the abundance [mL^{-1}] of prey and predator, respectively, and T is the temperature (0 °C in this case). The fitted function suggests a decrease of predation rates with prey biomass in addition to the decrease with predator biomass (t statistics). An influence of predator and prey body volume could not be identified, possibly due to the limited size ranges used in the experiments.

No distinct trend in predation rates with prey or predator biomass could be identified for the other predator-prey combinations due to large scatter and, in some cases, too few data points or many negative values. In particular, predation rates exhibited an extreme scatter around zero and were often extremely negative for the predator-prey combinations *Sympagohydra tuuli*—ciliates and Antarctic white acoels—ciliates (Appendix 5.6 Figs. 5.8, 5.10, 5.11). Some distinctly negative values occured for the combinations *Euplokamis* sp.—acoels and *Euplokamis* sp.—ciliates, *S. tuuli*—rotifers and *S. tuuli*—nauplii, and Arctic red acoels—ciliates (Appendix 5.6 Figs. 5.8–5.11, 5.13, refmeio:app:res:pred:fig:symnau). Apart from counting errors, negative values could be caused by higher prey losses in prey-only setups than in predator setups, or by (faster) prey reproduction in predator setups. Predation rates grouped into two or three clusters according to predator and prey biomass (SIMPROF) for a number of predator-prey combinations (Table 5.6). For each cluster, average predation rates were calculated, with some clusters yielding significantly positive predation rates (Table 5.5). For the remaining predator-prey combinations no clusters could be identified (SIMPROF) and one average predation rate was calculated. Consistently positive predation rates were obtained only for *Tisbe* spp. (average 13 $\%\,d^{-1}$; Appendix 5.6 Fig. 5.15).

Predation rates were generally enveloped by the curve of maximum potential ingestion rates (Moloney and Field, 1989; Fig. 5.4). However, measured predation rates declined faster than maximum potential ingestion rates (I_{max}). I_{max} underestimates the highest rates measured for low predator carbon contents, and exceeds measured rates for high predator carbon contents.

5.3.3 Experimental diets and non-quantitative observations

Diets of Arctic and Antarctic sympagic meiofauna in feeding experiments differed between meiofauna taxa (Table 5.4). In nauplii, feeding was not directly observed, but even in early naupliar stages of the Arctic harpacticoids *Tisbe* spp. the guts were brown-coloured and nauplii were often observed on fecal pellets. Grazing effects were not apparent in qualitative grazing experiments with Arctic cyclopoids

Table 5.4: Diets of Arctic and Antarctic sympagic meiofauna in feeding experiments. + feeding observed, + * probably cannibalistic feeding (observed in cultures where nauplii were presumably of the same species), ++ diet obviously preferred (the respec tive prey was reduced more efficiently than alternative prey, or predation rates for the respective prey were much higher than those for alternative prey), — feeding not observed, *nd* not determined (no experiments conducted with this predator-prey combination). In nauplii, feeding was not directly observed, but even in early naupliar stages of the Arctic harpacticoids *Tisbe* spp. the guts were brown-coloured and nau plii were often observed on fecal pellets. Grazing effects were not apparent in qualitative grazing experiments with Arctic cyclopoids and nematodes.

	Observations of feeding on						
	Algae	Ciliata	Rotifera	Polychaeta Trochophora	Copepoda NI-NVI	Harpacticoida CI-CVI	Calanoida CI-CVI
Arctic							
Cnidaria: *Sympagohydra tuuli*	—	—	+	+	++	*nd*	*nd*
Plathelminthes: Acoela (red, white)	—	+	*nd*	*nd*	*nd*	*nd*	*nd*
Harpacticoida indet.	+	++	*nd*	*nd*	+*	*nd*	*nd*
Harpacticoida: *Halectinosoma* spp.	+	+	*nd*	*nd*	*nd*	*nd*	*nd*
Harpacticoida: *Tisbe* spp.	+	—	*nd*	*nd*	+*	*nd*	*nd*
Antarctic							
Ctenophora: *Euplokamis* sp.	—	+	*nd*	*nd*	++	++	++
Plathelminthes: Acoela (white)	+	+	*nd*	*nd*	*nd*	*nd*	*nd*

Table 5.5: Predation rates for predator-prey combinations where significant clusters of predator and prey carbon biomass could be distinguished. B_{pd} = predator carbon biomass range, B_{py} = prey carbon biomass range, I = predation rate (average; marked with $\star$ if significantly positive, t-test, significance level 5 %), n = number of measurements.

Predator—prey	Cluster	B_{pd} [μg L^{-1}]	B_{py} [μg L^{-1}]	I [% d^{-1}]	n
Acoela red—Ciliata	A	0.156–0.874	0.018–0.095	-0.11	27
	B	0.165–1.048	0.141–0.219	2.46 $\star$	44
	C	3.464–4.619	0.173–0.189	0.18	3
Harpacticoida—Ciliata	A	2.278–3.579	0.389–0.656	0.83 $\star$	30
	B	1.365–2.276	0.668–0.786	0.46	15
	C	2.440	5.535	0.34	1
Euplokamis sp.—Ciliata	A	0.085–0.128	0.196–0.204	-20.34	2
	B	0.255–0.340	0.204–0.247	15.18	2
	C	0.255–0.340	0.436–0.611	12.99 $\star$	20
Euplokamis sp.—Copepoda	A	0.255	0.141–0.473	191.22 $\star$	9
	B	0.340	0.690–1.666	503.59	6

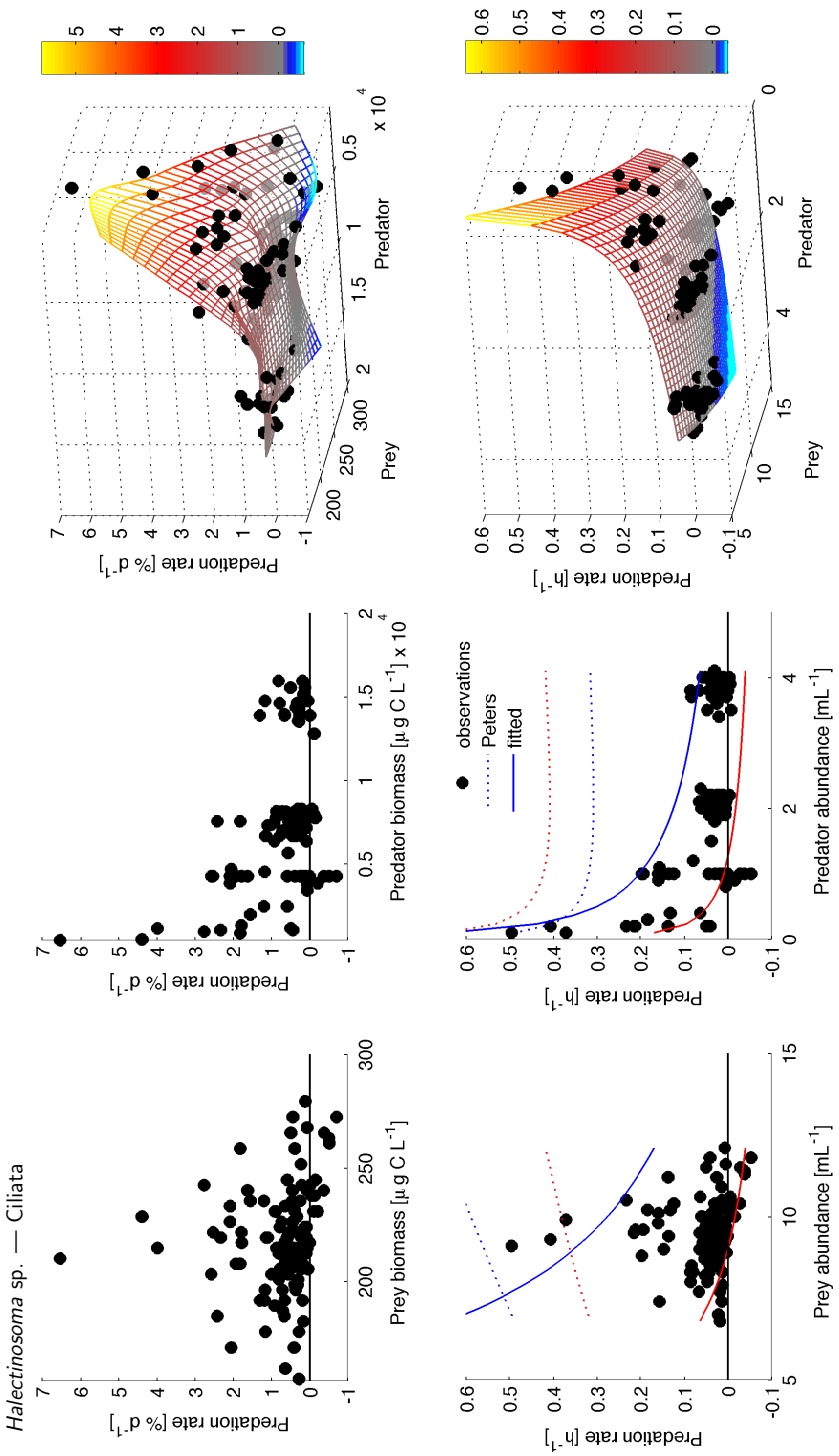

Figure 5.3: **Top** Carbon-based predation rates of the Arctic harpacticoids *Halectinosoma* spp. preying on ciliates, plotted against prey carbon biomass (left), predator carbon biomass (middle) and both prey and predator carbon biomass (right). The mesh in the 3D plot was interpolated using the Matlab gridfit routine (release 2.0, May 23, 2006). **Bottom** Individual-based predation rates of *Halectinosoma* spp. preying on ciliates, plotted against prey abundance (left), predator abundance (middle) and both prey and predator abundance (right). The surface in the 3D plot shows the fitted Peters model (Eq. 5.3). The blue and red lines in the 2D plots show the upper and lower border of the surface within the data range; dotted lines illustrate the original model with the parameters suggested by Peters (1994).

Table 5.6: Equations for calculation of carbon-based grazing and predation rates I [$\%\,d^{-1}$] from algae carbon biomass B_{alg} [$mg\,L^{-1}$], prey carbon biomass B_{py} [$\mu g\,L^{-1}$] or prey abundance A_{py} [mL^{-1}], predator carbon biomass B_{pd} [$\mu g\,L^{-1}$] or predator abundance A_{pd} [mL^{-1}], prey body volume V_{py} [μm^3] and carbon content C_{py} [μg] and predator body volume V_{pd} [μm^3] and carbon content C_{pd} [μg] as well as ice *in-situ* temperature T. All variables were determined for each meiofaunal taxon and ice-core section separately, except for body volumes, where medians of the respective taxon and expedition were used. Since our experiments did not allow conclusions on interspecific competition, we used B_{pd} and A_{pd} of the respective predator taxon, not total meiofauna. Method indicates the method by which predation rates were derived from individual measurements. For *Euplokamis* sp.-Copepoda, results from separate treatments with different prey (nauplii, copepodids of harpacticoids and copepodids of the calanoid *Stephos longipes*) were merged for analyses.

Food / Prey	**Grazer / Predator**	**Ingestion rate [$\%\,d^{-1}$]**	**Determined for pred—prey**	**Method**
Algae	All protozoan and metazoan meiofauna	$I = \begin{cases} 0 \quad \text{for } B_{alg} < \frac{1.533}{1.917} \\ I_{max} \quad \text{for } B_{alg} > \frac{I_{max} \cdot exp(-0.0693T)+1.533}{1.917} \\ (-1.533 + 1.917 B_{alg}) \cdot exp(0.0693T) \quad \text{otherwise} \end{cases}$	*Tisbe* spp.— mixed protists	linear fit
Ciliata	Cnidaria	$I = 0$	*Sympagohydra tuuli*— Ciliata	average
Ciliata	Ctenophora	$I = \begin{cases} 0 \quad \text{for } B_{py} \leq 0.43 \\ 12.99 \cdot exp(0.0693T) \quad \text{for } B_{py} > 0.43 \end{cases}$	*Euplokamis* sp.— Ciliata	cluster
Ciliata	Nematoda, Plathelminthes, Nemertea, Gastropoda	$I = \begin{cases} 0 \quad \text{for } B_{py} \leq 0.14 \text{ or } B_{pd} \geq 1.05 \\ 2.46 \cdot exp(0.0693T) \quad \text{for } B_{py} > 0.14 \text{ and } B_{pd} < 1.05 \end{cases}$	Acoela red— Ciliata	cluster
Ciliata	*Halectinosoma* spp. (all regions), other Harpacticoida (Antarctic, Central Arctic), Cyclopoida, Calanoida, Amphipoda	$I = \begin{cases} 0 \quad \text{for } V_{py}^{-0.344} \cdot V_{pd}^{-0.121} \cdot A_{py}^{-1.750} \cdot A_{pd}^{-0.366} \cdot 10^{0.033T} \cdot 10^{3.602} < 0.1 \\ 0.5 \cdot \frac{C_{py}}{C_{pd}} \cdot 2400 \quad \text{for } V_{py}^{-0.344} \cdot V_{pd}^{-0.121} \cdot A_{py}^{-1.750} \cdot A_{pd}^{-0.366} \cdot 10^{0.033T} \cdot 10^{3.602} > 0.6 \\ (V_{py}^{-0.344} \cdot V_{pd}^{-0.121} \cdot A_{py}^{-1.750} \cdot A_{pd}^{-0.366} \cdot 10^{0.033T} \cdot 10^{3.602} - 0.1) \cdot \frac{C_{py}}{C_{pd}} \cdot 2400 \quad \text{otherwise} \end{cases}$	*Halectinosoma* spp.— Ciliata	trend
Ciliata	Harpacticoida (Canadian Arctic, except for *Halectinosoma* spp.)	$I = \begin{cases} 0.83 \cdot exp(0.0693T) \quad \text{for } B_{py} < 0.66 \\ 0 \quad \text{for } B_{py} \geq 0.66 \end{cases}$	Harpacticoida (CFL)— Ciliata	cluster
Ciliata	Other meiofauna	$I = 0$	No experiments	
Acoela	Ctenophora	$I = 0$	*Euplokamis* sp.— Acoela white	average
Acoela	Other meiofauna	$I = 0$	No experiments	
Rotifera	Cnidaria	$I = 0$	*Sympagohydra tuuli*— Rotifera	average
Rotifera	Other meiofauna	$I = 0$	No experiments	
Nauplii	Cnidaria	$I = \begin{cases} 0 \quad \text{for } 1.06 B_{py} + 0.11 B_{pd} > 241.84 \\ 33.18 \quad \text{for } 1.06 B_{py} + 0.11 B_{pd} < 275.02 \\ (241.84 - 1.06 B_{py} - 0.11 B_{pd}) \cdot exp(0.0693T) \quad \text{otherwise} \end{cases}$	*Sympagohydra tuuli*— Nauplii	trend
Nauplii	*Tisbe* spp., other Harpacticoida (Canadian Arctic, except for *Halectinosoma* spp.)	$I = 13.34 \cdot exp(0.0693T)$	*Tisbe* spp. Copepodides— Nauplii	average
Copepoda	Ctenophora	$I = \begin{cases} 191.22 \cdot exp(0.0693T) \quad \text{for } B_{pd} < 0.26 \\ 0 \quad \text{for } B_{pd} \geq 0.26 \end{cases}$	*Euplokamis* sp.— Copepoda	cluster
Copepoda	*Themisto libellula*	$I = 1.93 \cdot exp(0.0693T)$	*Themisto libellula*— *Calanus* spp. (Auel and Werner, 2003)	
Copepoda	Other meiofauna	$I = 0$	No experiments	
Other meiofauna	All protozoan and metazoan meiofauna	$I = 0$	No experiments	

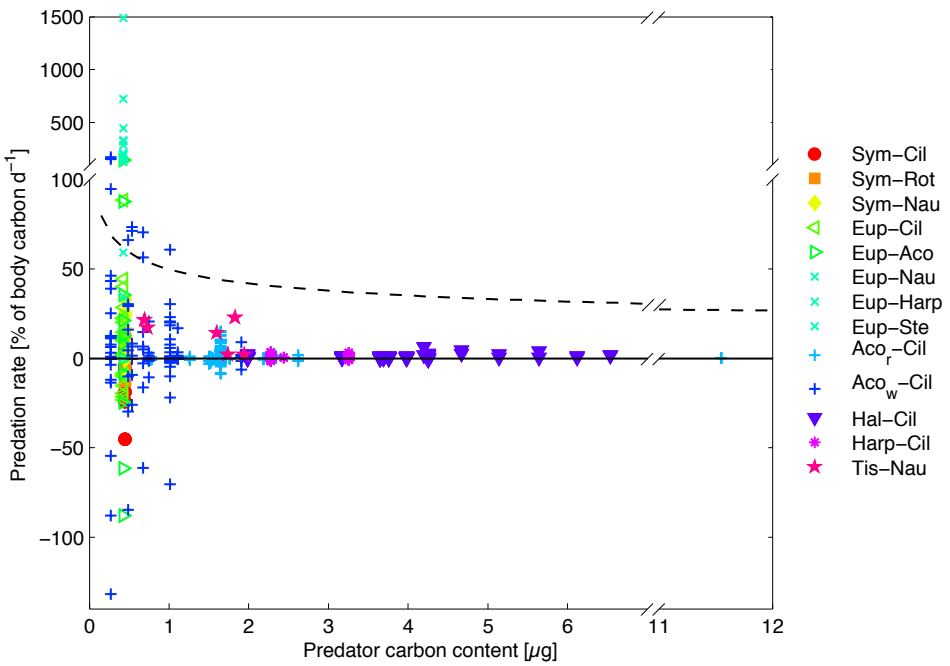

Figure 5.4: Experimentally derived carbon-based predation rates plottet against the median individual predator ca rbon content in the respective setup. For comparison, the maximum potential ingestion rate I_{max}, calculated from an allometric equation (Moloney and Field, 1989), is shown as a dashed curve.

and nematodes. *Tisbe* spp. and other indetermined Arctic harpacticoids as well as Antarctic acoels efficiently grazed on the bottom and in the edges of the experimental vials: at the end of the experiments generally more algae were sticking to the bottom and edges of the vials in protist-only setups than in grazer setups. In the Arctic cnidarian *Sympagohydra tuuli*, budding was often observed shortly after feeding. Also *Tisbe* spp. and *Halectinosoma* spp. as well as Antarctic acoels reproduced during feeding experiments. *Tisbe* spp. also moulted in grazing experiments.

5.3.4 Feeding impact

The *in situ* taxonomic composition of sympagic meiofauna, abundance and biomass of most taxa as well as ice-algae biomass, which were used to calculate the feeding impact, differed between the four regions and seasons investigated (Tables 5.2, 5.7). Thus a range of different communities was covered in this study. It should be noted that some taxa (e. g. the cnidarian *Sympagohydra tuuli* and nemerteans) occurred in bottom-ice sections (Table 5.2) and non-quantitative samples, but not in full cores (Table 5.7), and are thus not included in the estimates of feeding impact given below.

In situ ingestion rates were determined according to experimentally derived equations (Table 5.6) and, for comparison, as maximum potential ingestion rates from an allometric equation (Moloney and Field, 1989). For calculating the grazing rates, we employed a rectilinear functional response (Table 5.6) based on the equation derived from linear regression (Fig. 5.1) in combination with the assumptions

Table 5.7: Integrated ice-algae and meiofauna abundance and carbon biomass (in the whole ice column, expressed in relation to ice area) for different regions and seasons (including amphipods from melted ice cores). Medians (ranges) are given. — taxon not observed in any sea-ice samples from the respective expedition, *nd* no data. For the western Canadian Arctic, chl *a* concentration for calculation of algae carbon biomass was provided by B. Philippe et al.; integrated meiofauna abundance was obtained from Marquardt (2010) and Marquardt et al. (2011). For the Antarctic, chl *a* concentration for calculation of algae carbon biomass as well as integrated meiofauna abundance and carbon biomass were obtained from Kramer et al. (2011). Incomplete ice cores (with missing sections) are included, additional bottom-ice sections (meiofauna counted alive) are excluded.

	Arctic		Antarctic	
	Central Arctic	Western Canadian Arctic	Western Weddell Sea	Southern Indian Ocean
	Summer	Spring	Winter	Winter
Abundance integrated [$\times 10^3$ m^{-2}]				
Algae	*nd*	*nd*	*nd*	*nd*
Ciliata	39.30 (22.79–76.08)	27.74 (1.73–208.43)	19.96 (1.41–84.88)	14.58 (0.18–65.56)
Foraminifera	0.16 (0.00–1.89)	—	0.71 (0.16–3.14)	18.43 (0.00–117.83)
Radiolaria	0.94 (0.00–159.23)	—	0.16 (0.00–0.94)	0.69 (0.00–9.90)
Zooflagellata	*nd*	0.00 (0.00–7.55)	*nd*	*nd*
Cnidaria	0.00	0.00	—	—
Ctenophora	—	—	0.16 (0.00–0.63)	0.00 (0.00–0.56)
Nematoda	0.00 (0.00–0.16)	0.39 (0.00–94.79)	—	—
Acoela	0.94 (0.47–1.41)	1.18 (0.31–11.47)	10.53 (6.29–132.35)	0.81 (0.00–4.46)
Rhabditophora	—	—	0.00 (0.00–0.47)	—
Rotifera	1.89 (1.26–3.77)	2.36 (0.47–153.89)	—	—
Nemertea	0.00	0.00	—	—
Nudibranchia juv.	—	—	0.00 (0.00–0.16)	0.00 (0.00–0.17)
Other Mollusca juv.	—	0.16 (0.00–1.10)	—	—
Polychaeta larv. / juv.	—	0.00 (0.00–0.16)	—	—
Cirripedia Nauplii	—	0.00 (0.00–0.16)	—	—
Harpacticoida CI-CVI	0.79 (0.47–27.19)	0.24 (0.00–2.52)	7.15 (2.67–16.35)	0.00 (0.00–0.34)
Calanoida CI-CVI	0.00	—	0.31 (0.00–0.63)	0.00 (0.00–0.19)
Cyclopoida CI-CVI	0.00 (0.00–0.16)	0.31 (0.00–2.20)	0.00 (0.00–0.63)	—
Copepoda indet. CI-CVI	—	0.00 (0.00–0.16)	—	—
Copepoda Nauplii	0.16 (0.00–0.16)	2.44 (0.16–6.60)	2.83 (0.79–19.33)	0.56 (0.00–49.63)
Amphipoda	0.00	0.00 (0.00–0.16)	—	—
Biomass integrated [mg m^{-2}]				
Algae (from chl *a*) [$\times 10^3$]	0.19 (0.12–0.82)	2.07 (0.01–24.63)	0.26 (0.18–0.48)	0.05 (0.00–0.44)
Ciliata	1.29 (0.33–2.25)	0.75 (0.12–11.30)	2.38 (0.13–6.27)	0.31 (0.00–4.49)
Foraminifera	0.01 (0.00–0.32)	—	1.14 (0.02–2.62)	2.13 (0.00–26.83)
Radiolaria	0.01 (0.00–1.08)	—	0.01 (0.00–2.20)	0.09 (0.00–2.17)
Zooflagellata	*nd*	0.00 (0.00–0.14)	*nd*	*nd*
Cnidaria	0.00	0.00	—	—
Ctenophora	—	—	0.00 (0.00–0.20)	0.00 (0.00–0.01)
Nematoda	0.00 (0.00–0.03)	0.20 (0.00–8.60)	—	—
Acoela	0.22 (0.02–4.06)	0.08 (0.01–0.99)	1.23 (0.26–72.96)	0.04 (0.00–0.21)
Rhabditophora	—	—	0.00 (0.00–3.26)	—
Rotifera	0.03 (0.01–0.06)	0.06 (0.00–2.51)	—	—
Nemertea	0.00	0.00	—	—
Nudibranchia	—	—	0.00 (0.00–0.69)	0.00 (0.00–0.03)
Gastropoda / Bivalvia juv.	—	0.11 (0.00–0.41)	—	—
Polychaeta larv. / juv.	—	0.00 (0.00–0.22)	—	—
Cirripedia Nauplii	—	0.00 (0.00–0.13)	—	—
Harpacticoida CI-CVI	0.59 (0.43–25.03)	0.27 (0.00–5.76)	2.52 (0.32–4.25)	0.00 (0.00–0.10)
Calanoida CI-CVI	0.00	—	0.22 (0.00–0.99)	0.00 (0.00–0.21)
Cyclopoida CI-CVI	0.00 (0.00–0.06)	0.10 (0.00–0.90)	0.00 (0.00–0.33)	—
Copepoda indet. CI-CVI	—	0.00 (0.00–0.10)	—	—
Copepoda Nauplii	0.01 (0.00–0.03)	0.26 (0.02–2.18)	0.19 (0.03–1.83)	0.04 (0.00–1.04)
Amphipoda	0.00	0.00 (0.00–3.25)	—	—
n	5	6	6	12

that grazing rates are zero at low algal concentrations (below the x intercept of the linear function) and constant at I_{max} for high algal concentrations (beyond the intercept of the linear function with I_{max}). Since the grazing experiments did not allow to identify competition, grazer biomass was not included in the equation. For predation, different equations were applied to different predator-prey combinations (Table 5.6). In two cases, predation rates could be calculated using fitted functions (Eqs. 5.2 and 5.3)

describing both functional response and competition. Predation rates were set to zero when the fitted functions returned negative values and set to the maximum measured if the fitted functions exceeded this value. In other cases, based on Table 5.5 and the accompanying paragraphs, predation rates were assumed to be constant over certain ranges of predator and prey biomass; predation rates were assumed to be zero if the average predation rate within the respective range was not significantly positive (t test). In case of white acoels, predation rates were not assumed to be zero (as suggested by the experiments) but the equation for red acoels was applied, since ingestion of ciliates by white acoels had directly been observed. For temperature correction we assumed a Q_{10} value of 2 (Gradinger et al., 1999) with exception of the equation derived from Eq. 5.3, where a Q_{10} of 1.16 is inherent to the original model (Peters, 1994).

Experimentally derived community grazing / predation rates and grazing / predation impact (in the following termed ingestion rates and feeding impact when referring to both grazing and predation) showed some differences (U-test) between the expeditions (Fig. 5.5), which may be regional and / or seasonal. Within the Arctic, community ingestion rates and feeding impact did not differ significantly between the Central Arctic (summer) and the Canadian Arctic (spring), irrespective of the food type. Within the Antarctic, community ingestion rates and feeding impact on ice algae and ciliates were higher in the western Weddell Sea (winter) than in the southern Indian Ocean (winter), but no significant differences were found for predation on copepods.

Comparing Arctic to Antarctic regions, community grazing rates were higher in the Canadian Arctic than in the southern Indian Ocean, but the grazing impact did not differ significantly between any of the Arctic versus Antarctic regions. It never exceeded 2 % of the ice-algae standing stock per day (Fig. 5.5, left panel). Community predation rates and predation impact on ciliates (Fig. 5.5, middle panel) were higher in the western Weddell Sea than in the Central and Canadian Arctic. The predation impact in the western Weddell Sea often exceeded 500 % of the ciliate standing stock per day (20 % per hour) with extremes above 5000 % per day (200 % per hour). In the other regions, extremes were still as high as 80–350 % of the standing stock per day (3–15 % per hour) at some stations. Community predation rates and predation impact on copepods in both Arctic regions were higher than in the southern Indian Ocean. The predation impact in the Arctic sometimes exceeded 10 % of the copepod standing stock per day, while in the Antarctic it was always below 1 % per day. Assuming only nauplii were ingested, the predation impact on the nauplii standing stock in the Canadian and Central Arctic could exceed 280 % and 900 % per day (11 % and 37 % per hour), respectively (Fig. 5.5, right panel).

Experimentally derived community grazing rates were lower (U-test) than estimates based on calculated maximum potential ingestion rates, with exception of the Canadian Arctic in spring, where ice-algae biomass was high and feeding close to the assumed satiation (Fig. 5.5, left panel). The experimentally derived grazing impact was one order of magnitude lower than estimates from maximum potential ingestion rates irrespective of season and region.

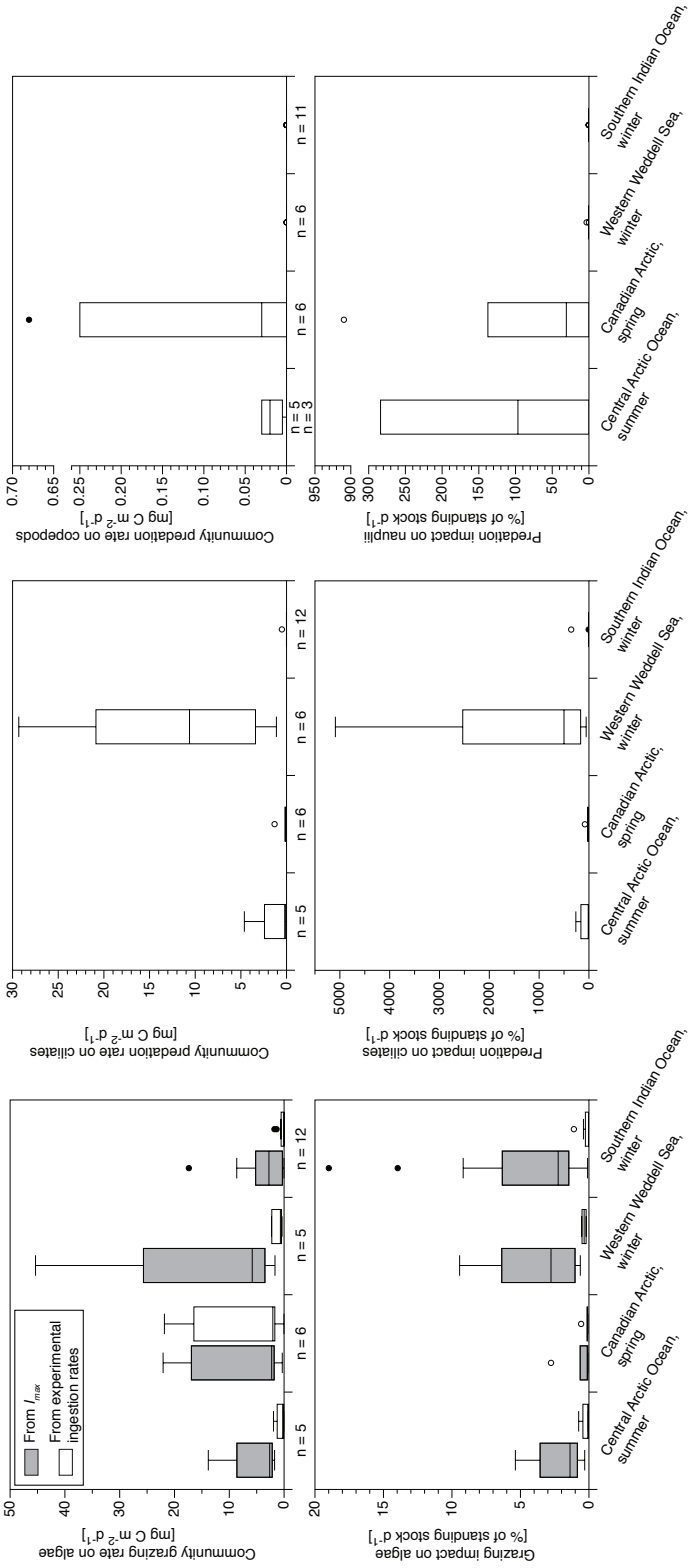

Figure 5.5: Areal ingestion rate (top) of sympagic meiofaunal communities and feeding impact on the standing stock of food organisms (bottom) for ice algae (left), sympagic ciliates (middle) and sympagic copepods (right) as food organisms, based on data from four expeditions (different regions and seasons) and experimentally-derived equations (Table 5.6, white boxes). Grazing rates were also calculated as I_{max} from an allometric equation (Moloney and Field, 1989, grey boxes). Boxplots show medians, quartiles (boxes), ranges (whiskers), outliers (filled circles) and extreme outliers (open circles).

5.4 Discussion

5.4.1 Predation and flexible feeding strategies in sea ice

Our study gives evidence of cilivorous and carnivorous feeding in several Arctic and Antarctic sympagic meiofauna taxa. It is the first experimental study investigating both grazing and predation of various sympagic metazoan meiofauna taxa from both polar regions. Previously, only grazing rates of the Antarctic sympagic calanoids *Paralabidocera antarctica* (Swadling et al., 1997b) and *Stephos longipes* (Schnack-Schiel et al., 1995; Swadling et al., 1997b) were measured in experiments, and predation was investigated only qualitatively in a recent study on the Arctic sympagic cnidarian *Sympagohydra tuuli* (Siebert et al., 2009). Other experimental feeding studies focused on sympagic protozoans (Caron and Gast, 2010). Our study confirms the findings by Kramer et al. (subm.), who deduced from stable isotope and fatty acid data that carnivorous feeding, omnivory and flexible feeding strategies are rather common and that the sympagic food web is therefore more complex than generally assumed. In particular, our experiments confirm the existence of top predators amongst both Arctic and Antarctic sympagic meiofauna (the cnidarian *S. tuuli* and the ctenophore *Euplokamis* sp., respectively), as suggested in recent papers (Bluhm et al., 2007; Piraino et al., 2008; Siebert et al., 2009; Kramer et al., 2011, Kramer et al., subm.). Several sympagic meiofauna taxa exploited various different food sources including algae, ciliates, rotifers, polychaete larvae, copepodites, as well as nauplii of the same taxon. In grazing experiments, the Arctic harpacticoid *Tisbe* spp. ingested various protist taxa, the grazing being independent of protist composition; selectivity was not very pronounced and observed only for few protist taxa. Similar observations of omnivory and flexibility have been reported for various sympagic protozoans (Caron and Gast, 2010) and some under-ice amphipods (Werner and Auel, 2005).

Our experiments support the idea that most sympagic meiofauna taxa apparently do not permanently depend on ice algae as food source (Kramer et al., subm.). They can thus survive also periods of low ice-algal production by switching to alternative diets, as previously reported for some under-ice amphipods (Werner and Auel, 2005). During these periods, meiofauna probably rely on ciliates and other meiofauna as prey, which in turn are supported by bacterial production (Kramer et al., subm.).

This view of flexible feeding strategies is further supported by the temporal variability in predation rates, as observed directly in experiments and suggested by the fluctuations of predation rates over time. Sympagic meiofauna appears to often feed in pulses, followed by periods of starvation. This seems to be particularly pronounced in *S. tuuli*, *Euplokamis* sp. and Antarctic white acoels. In planktonic copepods, high ingestion rates following starvation periods have been interpreted as strategies attributed to predator avoidance (Tiselius, 1998). This explanation is unlikely at least for the sympagic top predators *S. tuuli* and *Euplokamis* sp., but it supports the view that pulse feeding might be a strategy enhancing flexibility.

The ability of meiofauna to utilise different food sources and feed in pulses enables them to live in a habitat with patchy distributions of algae and prey organisms and with high temporal fluctuations, as

suggested also for under-ice amphipods (Werner and Auel, 2005). Such conditions are typical for sea ice (Eicken, 1992; Swadling et al., 1997a). The observed feeding strategies are thus probably adaptations to the sea-ice habitat (Kramer et al., subm.) and hence natural consequences of selection.

5.4.2 Factors influencing ingestion rates: functional response, competition, size and taxa

Grazing rates of the harpacticoids *Tisbe* spp. increase linearly with food biomass, and the relationship can be described by a rectilinear functional response, as previously proposed for various grazers (Frost, 1972; Rothhaupt, 1990). From our data, we cannot identify a threshold food concentration below which *Tisbe* spp. do not graze. Such a threshold, possibly related to a switch to ciliate or animal prey, might be an important factor constraining the grazing impact and preventing the ice-algae stock from exhaustion (Strom et al., 2000). Previous grazing experiments with the Antarctic sympagic calanoid *Stephos longipes* did not indicate a functional response nor a threshold food concentration (Schnack-Schiel et al., 1995), which suggests differences in grazing behaviour between these taxa. However, due to different methods, that study is not directly comparable to ours. Additional grazing experiments with various meiofauna taxa are thus required to investigate these issues.

For predation rates, the influence of prey density was less evident. For the ctenophore *Euplokamis* sp. or red acoels preying on ciliates, predation rates were significantly positive only at high prey biomass, suggesting there might be a functional response which was not evident in our data because of large scatter and because it was possibly concealed by other factors. Other predator-prey combinations showed lower predation rates at higher prey density. This observation might indicate intraguild predation amongst the prey organisms (Lonsdale et al., 1979; Wu et al., 2010). This intraguild predation might be more pronounced in prey-only setups than in predator setups due to predator avoidance strategies of the ciliates (Lima, 1998; Jakobsen, 2002) and thus cause the observed density effect. Experiments with a more extended range of prey densities might help to confirm this hypothesis.

Within the range of predator and prey densities used in our experiments, an influence of predator density on predation rates was more evident than an influence of prey density. For some predator-prey combinations, predation rates declined with increasing predator concentration, possibly indicating intraspecific competition. Although intraspecific competition is part of ecological theory (Begon et al., 2006), it is rarely observed in experiments, therefore generally considered to occur only at extremely high densities beyond the natural range (Fussmann et al., 2005b) and not often included in models (Skalski and Gilliam, 2001). In the sea-ice habitat, however, meiofauna densities in the brine channels are subject to fluctuating temperatures (which control the brine volume fraction) and can temporarily be extremely high (Table 5.2), which might cause intraspecific and possibly also interspecific competition. Such competition might be an important factor constraining the feeding impact at high meiofauna densities. On the other hand, the brine channel geometry might enable meiofaunal predators to avoid each other (Krembs et al., 2000) and thus reduce the effect of competition.

Besides food and grazer / predator density, also the size of both grazer / predator and food particles / prey can influence the ingestion rate (Hansen et al., 1994, 1997). The grazing experiments with *Tisbe* spp. could neither confirm nor contradict the size-dependence of maximum potential ingestion rates I_{max} according to Moloney and Field (1989). The decrease of ingestion rates with predator size suggested for *Halectinosoma* spp. preying on ciliates by the fit of the Peters model was not significant, probably due to the insufficient range in predator size. Likewise, a relationship between predation rate and predator size was not obvious for any other predator-prey combination. Viewing all predation experiments with different predator-prey combinations together (Fig. 5.4), a decrease of predation rates with predator carbon content was indicated by the data, albeit with a steeper slope than suggested by Moloney and Field (1989). This assumes that the measured predation rates were maximum rates, as may be expected due to the high prey densities applied. In some treatments, however, high predator densities may have prevented that maximum rates were reached. The influence of food particle / prey size was not studied in any of the experiments.

The variety of ingestion rates and functional relationships discussed above indicates that different meiofauna taxa apply different capture strategies for different food types. Different strategies of different taxa, as found in zooplankton (Kiørboe, 2011), may contribute in shaping different ecological niches in spite of the generally observed omnivory, thereby sustaining high meiofauna diversity in sea ice. Different strategies of one taxon for different food types, as known for planktonic copepods (Kiørboe et al., 1996) and under-ice amphipods (Werner et al., 2002), are another example of the flexibility of sympagic meiofauna in terms of feeding.

5.4.3 Low grazing and high predation impact

For the first time we were able to give estimates of both grazing and predation impact based on experimental ingestion rates, including the influence of grazer / predator and algae / prey density. Previous studies (Gradinger, 1999a; Gradinger et al., 1999; Nozais et al., 2001; Michel et al., 2002; Gradinger et al., 2005) calculated the grazing impact of sympagic meiofauna exclusively from allometric equations accounting only for the influence of grazer carbon content (Moloney and Field, 1989).

The grazing impact on the ice-algae standing stock calculated from experimental grazing rates was extremely low in all regions and during all seasons studied. It was about one order of magnitude lower than estimates applying allometric equations (Moloney and Field, 1989), indicating that previous studies using these equations (Gradinger, 1999a; Gradinger et al., 1999; Nozais et al., 2001; Michel et al., 2002; Gradinger et al., 2005) probably substantially overestimate the grazing impact.

In contrast to the grazing impact, the predation impact on the ciliate standing stock was often extremely high: our data suggests that in some cases the ciliate standing stock could be grazed down completely within a few hours or even less than one hour, if predation rates were not restricted. The predation impact on ciliates was highly variable with no obvious seasonal or regional differences, but the highest impact was determined for the western Weddell Sea in winter. The estimated predation impact on the

copepod standing stock was extremely low for the Antarctic in winter, of the same order of magnitude as the grazing impact, whereas it was notably higher in the Arctic in spring and summer. When related to the nauplii standing stock only, the predation impact in the Arctic was considerably higher, of the same order of magnitude as the impact on ciliates, suggesting that the standing stock of nauplii could be preyed down completely within a few hours in the absence of constraining factors.

The predation impact on both ciliates and copepods may—at least temporarily or locally—be even higher than we estimated, since even more taxa might feed on ciliates and copepods than we assumed in our calculations. Additionally, also other meiofauna taxa than ciliates and copepods may be preyed on, e. g. rotifers (Siebert et al., 2009). On the other hand, the brine channel geometry might reduce the predation impact, since small meiofaunal prey can probably better avoid predators in the brine channels than in the experimental vials (Krembs et al., 2000). Furthermore, most meiofauna taxa are likely to cover part of their energy demand by grazing on algae (Kramer et al., subm.) at least during times of high ice-algae standing stocks, which probably also lowers the predation impact. We thus hypothesise that the actual predation impact can be particularly high during autumn and winter, when the ice-algae standing stock is low. However, meiofaunal predators probably can alter the meiofaunal community structure on the small scale throughout the year, given the temporal variability of predation rates observed in experiments and the patchy distribution of sympagic meiofauna in the ice (Swadling et al., 1997a).

We conclude that grazing activity by sympagic meiofauna is generally unlikely to restrict the accumulation of ice algae or to limit the availability of ice algae to under-ice and sub-ice grazers. Predation activity by meiofauna, in contrast, can substantially influence the meiofaunal community composition. Furthermore, it is probable that carnivorous meiofauna compete with under-ice and sub-ice predators, such as carnivorous amphipods (Werner et al., 2002; Auel and Werner, 2003) and krill (Wickham and Berninger, 2007), for prey organisms. Carnivorous and omnivorous meiofauna is thus likely to influence the quantity and quality of cryo-pelagic coupling through predation activity within the ice. Carnivorous feeding by sympagic meiofauna should therefore explicitely be included in future investigations and theoretical considerations concerning the role of sea ice in polar marine ecosystems.

5.4.4 Potential of feeding experiments and modelling in sympagic meiofauna studies

The methods we applied in grazing and predation experiments proved well feasible for meiofauna, and future studies using similar methods can help to resolve some of the issues that still remained unclear in this study. The influence of grazer / predator and food particle / prey sizes on ingestion rates should be investigated and the respective parameters better constrained by applying a wide range of grazer / predator and food particle / prey sizes. Likewise, functional response and competition should be further investigated by applying a wide range of grazer / predator and protist / prey densities. Since ingestion rates are likely to be influenced by the geometry of the brine channel system, future studies should also aim to mimic this geometry following the approach by Krembs et al. (2000). Also, it might

be possible to assess ingestion rates *in situ* as described for benthic meiofauna by Decho (1988), but using fluorescent dyes probably more suitable to the sometimes strongly pigmented sympagic meiofauna than the red dye applied by Decho. Future studies should furthermore investigate ingestion of bacteria by sympagic meiofauna with methods successfully applied previously to bacterivorous protists (Sherr and Sherr, 1993; Laurion et al., 1995).

Extended modelling efforts are required to better describe and understand the response of ingestion rates to grazer / predator and protist / prey density and size. Mechanistic models including predator density (Jost, 2000) are based on additional assumptions about the underlying predation process and fitting these models would have been beyond the scope of this work. We thus used the empirical model by Peters (1994) for the harpacticoids *Halectinosoma* spp. preying on ciliates. Both the function fitted to our data and the original model (Peters, 1994) estimated a similar effect of the predator density on predation rates, indicating that the model describes the intraspecific predator behaviour in sea ice quite well. The influence of prey density, in contrast, differed substantially (in magnitude and sign) compared to the original model. This model was derived predominantly from ingestion rates of zooplankton feeding on algae and bacteria, and thus does not take into account effects of intraguild predation. Development of a new model specifically for sympagic meiofauna, including intraguild predation besides competition and functional response, is therefore desirable.

Acknowledgements We first of all thank Iris Werner (Institute for Polar Ecology IPÖ, University of Kiel, Germany) for her constant support during all phases of this study, including constructive comments on the manuscript. Great thanks are also due to Rainer Kiko (IFM-GEOMAR, Kiel, Germany) for excellent collaboration and great support in the field and lab during ANT–XXIII / 7 and ARK–XXII / 2. We further thank Markus Pahlow (IFM-GEOMAR), Dieter Piepenburg (IPÖ) and Wolfgang Ebenhöh (Institute for Chemistry and Biology of the Marine Environment ICBM, University of Oldenburg, Germany) for advice concerning data evaluation, statistics and modelling. Miriam Marquardt, Verena Lieb, Claudia Wittwer and Christin Kleinelanghorst (IPÖ) are thanked for conducting the protist counts in grazing experiments and the carbon content assessment of sympagic meiofauna and algae. We also thank our colleagues for kindly providing unpublished data, particularly Gauthier Carnat (Centre for Earth Observation Science, University of Manitoba, Winnipeg, Canada), Bruno Delille and Nicolas-Xavier Geilfus (Chemical Oceanography Unit, University of Liège, Belgium), Guisheng Song (Institut des sciences de la mer de Rimouski ISMER, University of Quebec at Rimouski, Canada) and Thomas Brown (University of Plymouth, UK) for temperature and salinity data from CFL as well as Benoit Philippe, Christopher John Mundy and Michel Gosselin (ISMER) for chl *a* data from CFL. This research was supported by the Deutsche Forschungsgesellschaft WE 2536 / 11–1,–2 (to MK) and by the Kiel Cluster of Excellence "The Future Ocean" (to FP).

5.5 Appendix I: Methods

Details on the determination of grazing rates

The carbon-based grazing rate I ([μg μg^{-1} d^{-1}] or [d^{-1}]) was assumed to be

$$I = \frac{P_p - P_g}{G \cdot t} \quad , \tag{5.4}$$

where P_p and P_g are the protist carbon biomass in protist-only setups and grazer setups, respectively, G is the grazer carbon biomass and t is the duration of the experiment. Eq. 5.4 was rearranged to calculate one grazing rate for each treatment based on protist biomass from the protist-only triplicates (P_{p_r}, $r = 1,2,3$) and the grazer triplicates (P_{g_q}, $q = 1,2,3$; Eq. 5.5). Linear regression of P_{g_q} against $-G_q \cdot t$ yielded the grazing rate as slope I and an estimated initial protist biomass as intercept P_p

$$\begin{pmatrix} P_{p1} \\ P_{p2} \\ P_{p3} \\ P_{g1} \\ P_{g2} \\ P_{g3} \end{pmatrix} = -I \begin{pmatrix} 0 \\ 0 \\ 0 \\ G_{g1} \\ G_{g2} \\ G_{g3} \end{pmatrix} \begin{pmatrix} 0 \\ 0 \\ 0 \\ t_1 \\ t_1 \\ t_1 \end{pmatrix} + P_p \quad . \tag{5.5}$$

In this way, one protist biomass and one grazing rate per treatment could be calculated without previously averaging between the replicates.

According to Eq. 5.5 total grazing rates (I_{tot}) were calculated for each of the 13 treatments using total protist biomass in protist-only setups and grazer setups. In addition, taxon-specific grazing rates (I_j) for 16 different protist taxa j (listed in Table 5.8) were calculated from the biomass of the respective taxa. Likewise, taxon-specific grazing rates were calculated based on the protist abundances of the 16 taxa for calculating the selectivity index.

Groups of treatments with similar protist composition were identified by cluster analysis (hierarchical agglomerative, group-average linkage) with similarity profile test (SIMPROF, Clarke and Warwick, 2001; 1000 permutations, 999 simulated profiles; significance level of all statistic tests in this study 5 %) applied to the estimated relative initial biomass of the 16 protist taxa in the 13 treatments. In few cases estimates of initial biomass were just slightly negative; these values had to be set to zero prior to analysis.

Details on the determination of grazing selectivity

A selectivity index α_j was calculated for each protist taxon and treatment according to Chesson (1983) assuming that the abundance of a taxon j ($j = 1, ..., 16$, Table 5.8) was reduced by grazing (Manly et al.,

Table 5.8: List of protist taxa in grazing experiments and groups used in plots and calculations.

Protist groups	**Taxa included**	**Remarks**
Cyanobacteria indet.	Cyanobacteria indet.	
Flagellata small	Flagellata indet. 1	small
Flagellata big	*Cryptomonas* spp.	
	Dinoflagellata indet.	
	Chlamydomonas spp.	
	Flagellata indet. 2	big
Fragillariopsis spp.	*Fragillariopsis* species 1	
	Fragillariopsis species 2	similar to *Nitzschia* spp.
Nitzschia spp.	*Nitzschia frigidia*	
	Nitzschia spp.	
Pseudo-nitzschia cf. *seriata*	*Pseudo-nitzschia* cf. *seriata*	
Pseudo-nitzschia cf. *subcurvata*	*Pseudo-nitzschia* cf. *subcurvata*	
Bacillariaceae indet.	Bacillariaceae indet.	
Other pennates	Achnanthaceae indet.	
	Navicula spp.	
	Navicula transistans var. *Derasa f. delicatula*	
	Cylindrotheca closterium	
	Bacillariales indet.	
	Entomoneidaceae indet.	*Entomoneis kjellmannii* or *Amphiprora hyperborea*
Thalassiosira cf. *angulata*	*Thalassiosira* cf. *angulata*	
Thalassiosira cf. *bioculata*	*Thalassiosira* cf. *bioculata*	
Thalassiosira spp.	*Thalassiosira* spp.	
Attheya spp.	*Attheya longicornis*	
	Attheya cf. *longicornis*	
	Attheya septentrionalis	
Other centrics	*Bacteriosira bathymophala*	
	Chaetoceros spp.	
	Coscinodiscineae indet.	similar to *Leptocylindricus* spp.
	Biddulphiales indet.	
Ciliata indet.	Ciliata indet.	
Other Protista	Heliozoa indet.	
	Protista indet. 1	possibly *Phaeocystis pouchetii*
	Protista indet. 2	
	Protista indet. 3	centric shape

1972):

$$\alpha_j = \frac{ln((P_{p,j} - P_{g,j})/P_{p,j})}{\sum_{l=1}^{m} ln((P_{p,l} - P_{g,l})/P_{p,l})} \ , \ j = 1, ..., m = 16 \ . \tag{5.6}$$

The initial abundance of taxon j, $P_{p,j}$, was approximated by the estimated initial protist abundance (Eq. 5.5). Using taxon-specific grazing rates I_j and estimated initial protist abundance $P_{p,j}$, an estimate of the abundance $P_{g,j}$ of taxon j at the end of the experiment was calculated

$$P_{g,j} = -I_j \cdot \bar{G} \cdot t + P_{p,j} \ , \tag{5.7}$$

where $\bar{G}$ is the abundance of the grazer *Tisbe* spp. averaged over the triplicates. Only those taxa were considered for Eq. 5.6 for which the taxon-specific grazing rate in the particular treatment was significantly positive.

The electivity index ε was calculated according to Chesson (1983):

$$\varepsilon_j = \frac{m \cdot \alpha_j - 1}{(m-2) \cdot \alpha_j + 1} \ , \ j = 1, ..., m = 16 \ . \tag{5.8}$$

Details on the determination of predation rates

Gains and losses in prey attributed to reproduction and handling in predation experiments were determined from the average change in prey biomass per time ΔB_{py} in prey-only replicates for each time step in each treatment. For treatments with ciliate prey which were lacking prey-only setups, ΔB_{py} was estimated as average from all prey-only setups with ciliate prey. For experiments with rotifers, nauplii and copepodide prey which were lacking prey-only setups, ΔB_{py} was set to zero, since for these taxa individuals are not likely to be lost during counting and reproduction rates are low compared to those for ciliates.

To identify groups of replicates according to predator and prey biomass, a cluster analyses (hierarchical agglomerative clustering based on Bray-Curtis similarity) and a SIMPROF test (1000 permutations, 999 simulated profiles) were applied to fourth-root transformed biomass data.

Details on the assessment of the feeding impact

Based on individual *in situ* ingestion rates $I_{ijk,ind}$, bulk ingestion rates $I_{ijk,bulk}$ were calculated for each pair of predator / grazer i and food type j, and for each ice-core section k, according to the equation

$$I_{ijk,bulk} = I_{ijk,ind} \cdot B_{ik,bulk} \ , \tag{5.9}$$

where $B_{ik,bulk}$ is the bulk biomass of predator or grazer taxon i in section k—i. e. $I_{ij,bulk}$ is the biomass of a certain food type ingested by a certain predator or grazer taxon per time and volume of melted ice. The bulk community ingestion rate $I_{comm,jk,bulk}$ of total sympagic meiofauna was then calculated for each ice-core section and food type as

$$I_{comm,jk,bulk} = \sum_i I_{ijk,bulk} \ , \tag{5.10}$$

and the integrated community ingestion rate $I_{comm,j,int}$ was calculated for each station and food type as

$$I_{comm,j,int} = \frac{\sum_k (I_{comm,jk,bulk} \cdot V_{ice_m,k})}{A} \ , \tag{5.11}$$

where $V_{ice_m,k}$ is the volume of melted ice-core section k and A is the ice-core cross-sectional area—i. e. $I_{comm,j,int}$ is the biomass of a certain food type ingested by sympagic meiofauna per time and ice area.

The feeding impact $F_{j,st}$ of meiofauna on the standing stock of each food type was then calculated for

each station as

$$F_{j,st} = \frac{I_{comm,j,int}}{B_{j,int}} \quad , \tag{5.12}$$

where $B_{j,int}$ is the integrated biomass of food type j—i. e. $F_{j,st}$ is the fraction of the standing stock of a certain food type ingested by sympagic meiofauna per time.

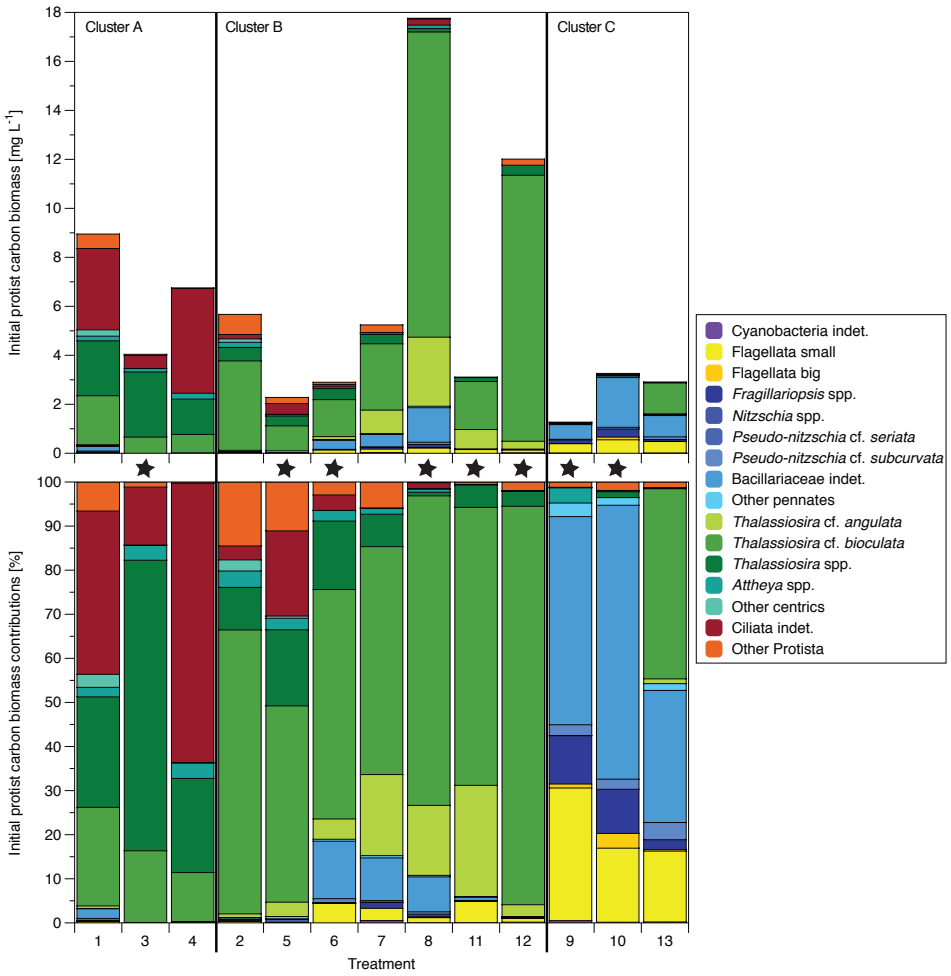

Figure 5.6: Initial protist composition in the 13 treatments of grazing experiments, estimated from linear regressions, with absolute biomass (upper panel) and biomass contributions (lower panel) of the different protist taxa. The treatments are grouped into three significantly different clusters (SIMPROF). Treatments where grazing rates were significantly positive are marked $\star$ (one-tailed test with t statistics of regression coefficients).

5.6 Appendix II: Results

Details on the results of grazing experiments

Initial protist composition in grazing experiments

The 13 treatments grouped into three significantly different clusters (SIMPROF) according to initial protist biomass compositions determined by linear regressions. Treatments 1, 3 and 4 (cluster A) were dominated by the large centric diatoms *Thalassiosira* spp. and *T. bioculata* as well as ciliates, with low contributions of small centric diatoms and other protists (i. e. protists other than flagellates, diatoms and ciliates) and very low contributions of pennate diatoms. Treatments 2, 5, 6, 7, 8, 11 and 12 (cluster B) were dominated by *T. bioculata*, with in part remarkably high contributions of *T. angulata*, *Thalassiosira* spp. or pennate diatoms, usually low contributions of ciliates and other protists and always low contributions of small centric diatoms and small flagellates. Treatments 9, 10 and 13 (cluster C) were dominated by pennate diatoms, with remarkably high contributions of small flagellates, usually low contributions of centric diatoms and very low contributions of big flagellates and other protists. Biomass contributions of cyanobacteria were low in all treatments.

Almost all taxa present in the experimental protist suspensions had been reported from Arctic sea ice previously, pennate diatoms and / or flagellates usually being the dominant groups (Gosselin et al., 1997; Druzhkov et al., 2001; Werner et al., 2007; Poulin et al., 2011; Mundy et al., 2011). Big centric diatoms such as *Thalassiosira* spp. are not very common in Arctic sea ice, but have been reported from this habitat (Druzhkov et al., 2001; Werner et al., 2007; Mundy et al., 2011) and may even dominate the ice-algae assemblage (Ratkova and Wassmann, 2005). The algal suspensions applied in the experiments thus represented natural ice-algal communities pretty well.

Taxon-specific grazing rates

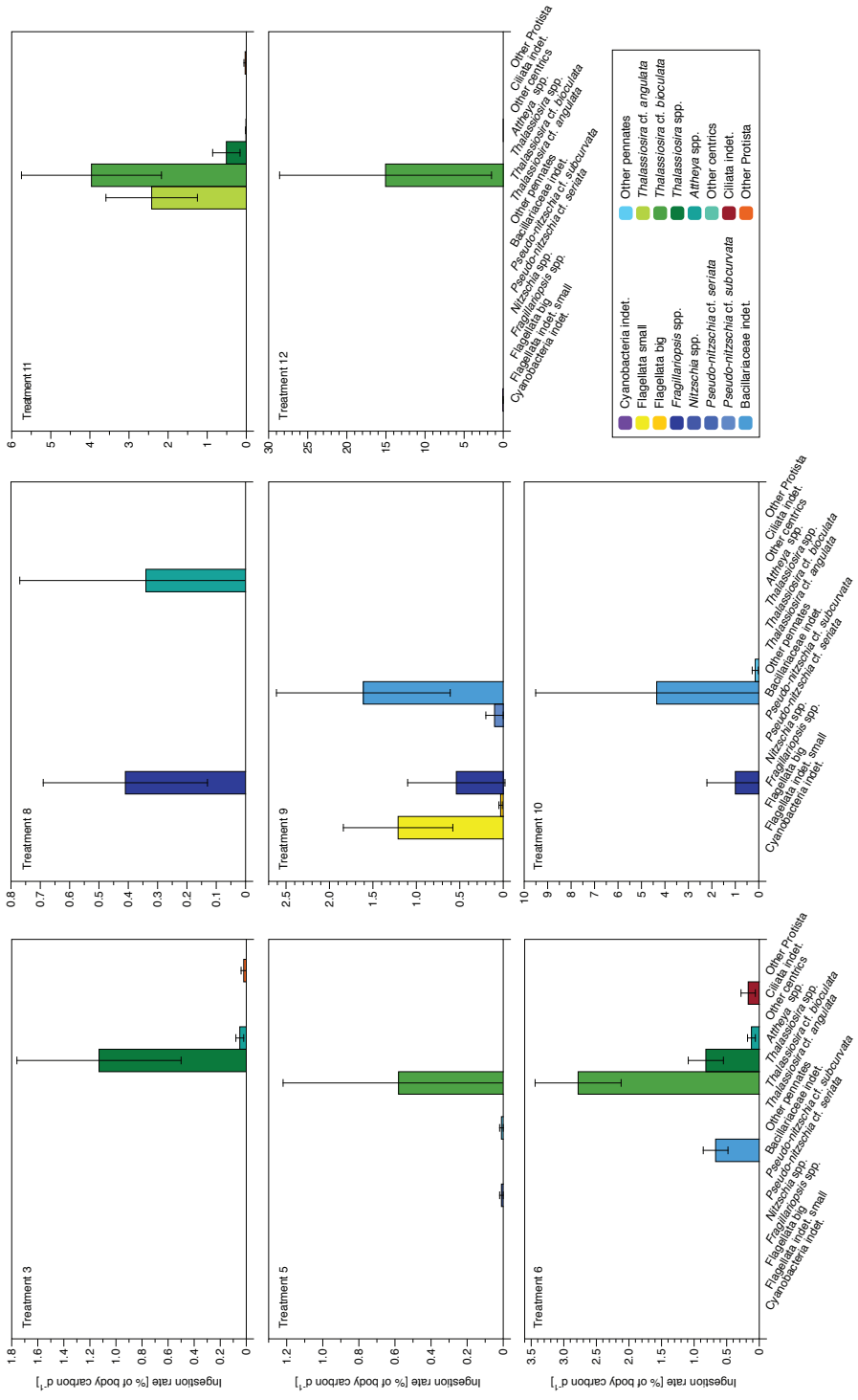

Figure 5.7: Taxon-specific grazing rates of *Tisbe* spp. in the eight treatments with significantly positive total ingestion rates. Only significantly positive taxon-specific grazing rates are shown. Error bars denote 90 % confidence intervals of the regression coefficients.

Details on the results of predation experiments

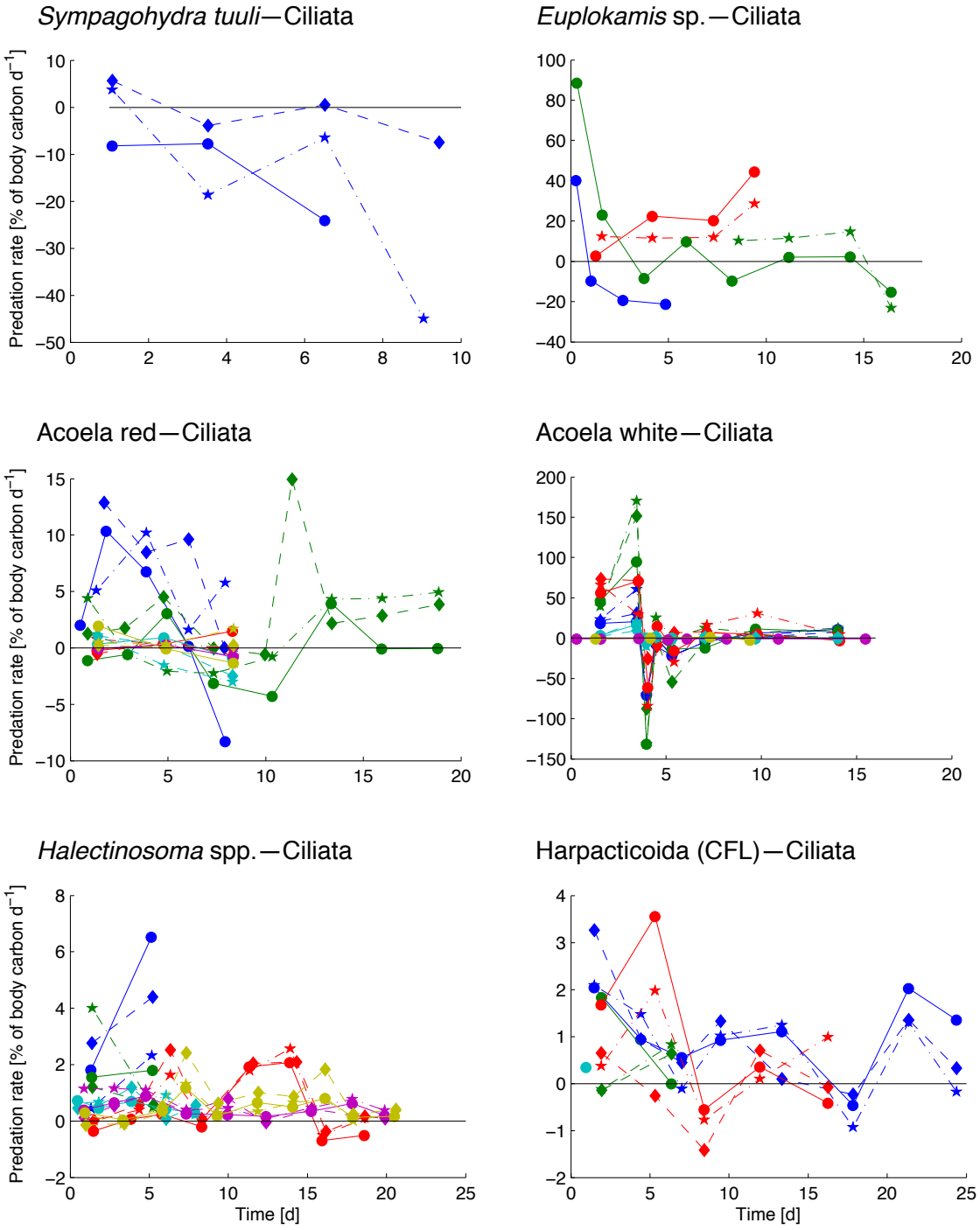

Figure 5.8: Predation rates of different metazoan meiofaunal predators on ciliate prey, plotted over the time from the beginning of the experiment. Replicate predator setups (run simultanously under similar conditions) are indicated by similar colours but different symbols.

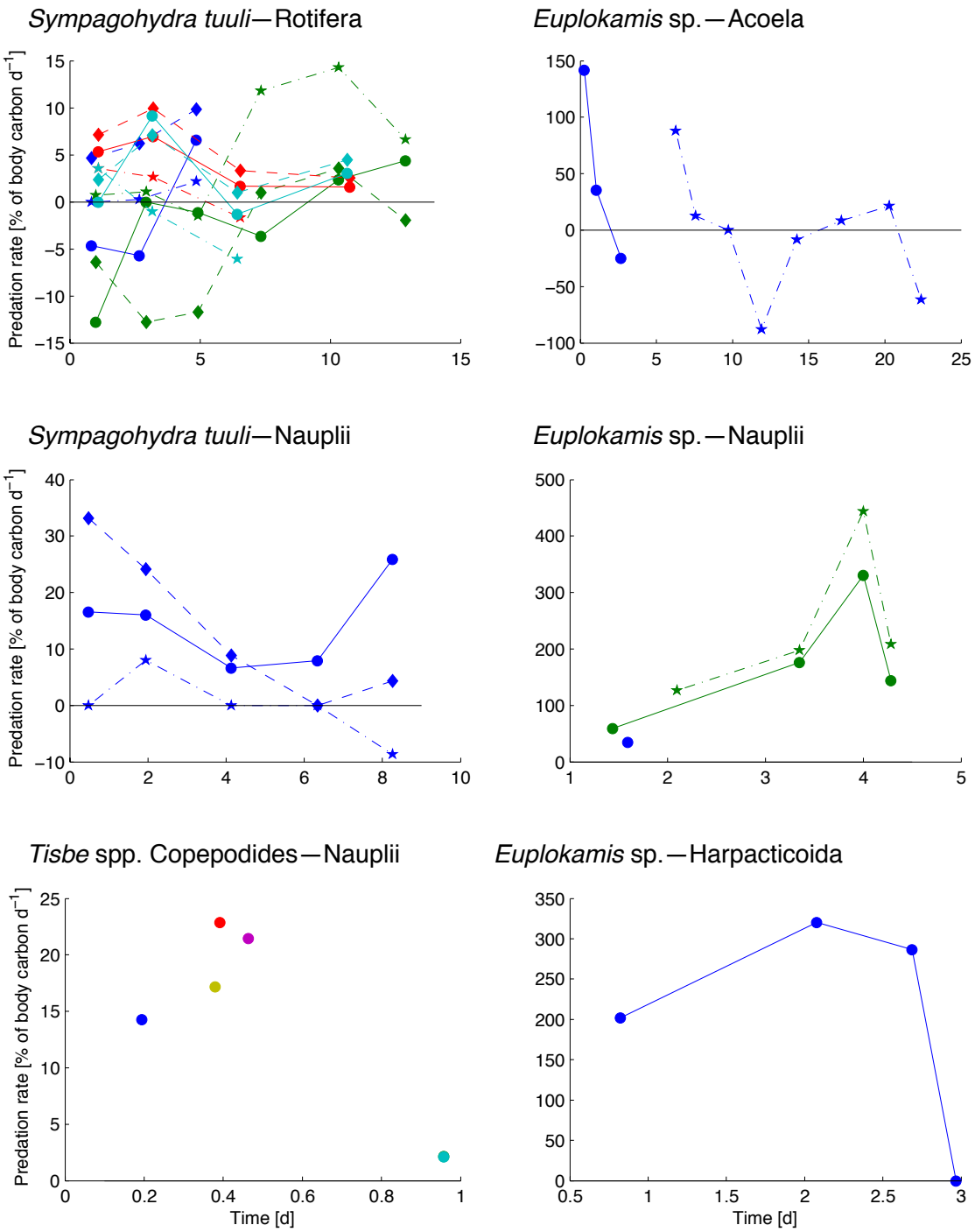

Figure 5.9: Predation rates of different metazoan meiofaunal predators on metazoan prey, plotted over the time from the beginning of the experiment. Replicate predator setups (run simultanously under similar conditions) are indicated by similar colours but different symbols. *Euplokamis* sp. preying on *Stephos longipes* are not shown.

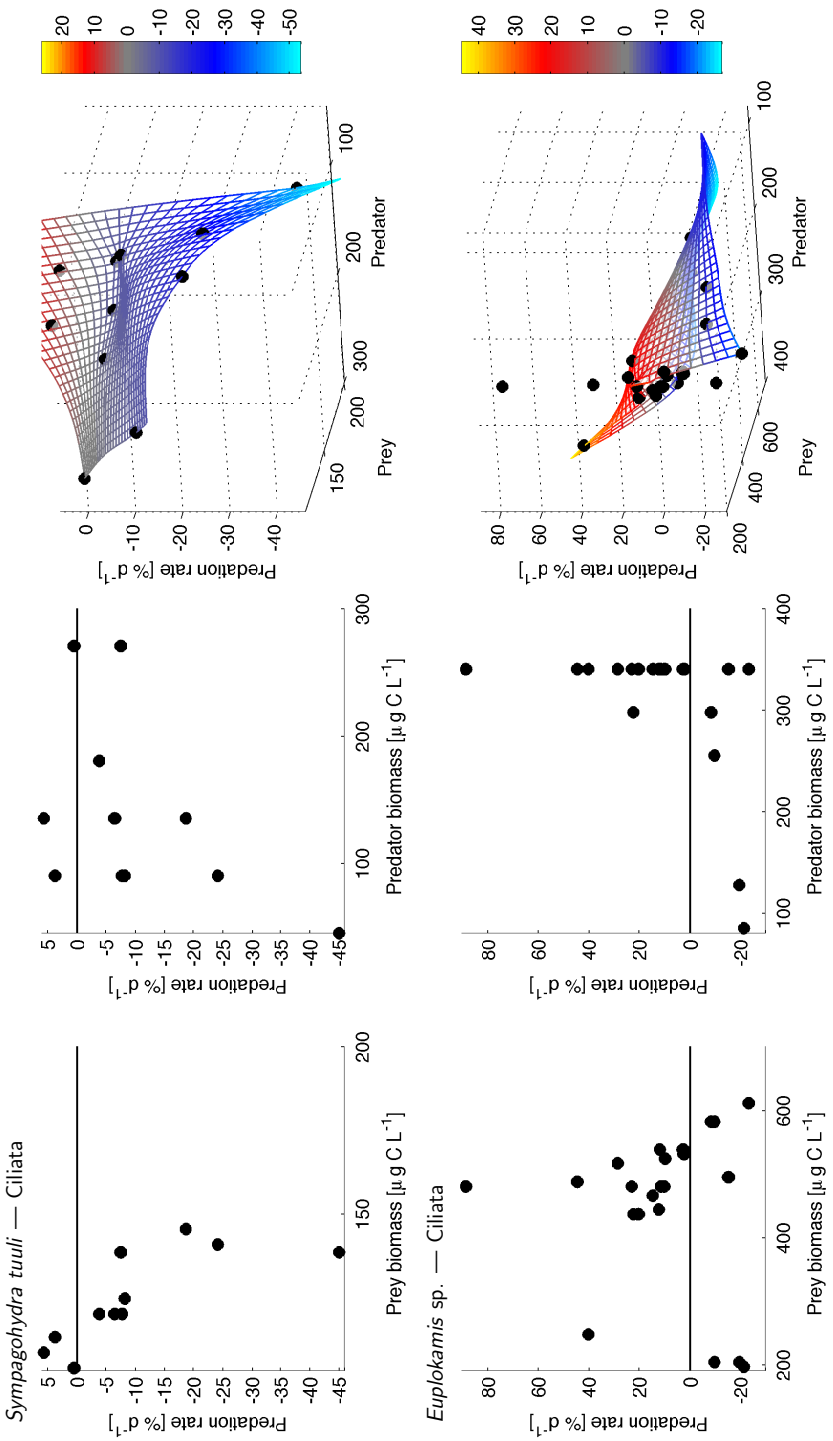

Figure 5.10: Predation rates of the Arctic cnidarian *Sympagohydra tuuli* (top) and the Antarctic ctenophore *Euplokamis* sp. (bottom) preying on ciliates, plotted against prey biomass (left), predator biomass (middle) and both prey and predator biomass (right). The mesh in the 3D plots was interpolated using the Matlab gridfit routine (release 2.0, May 23, 2006).

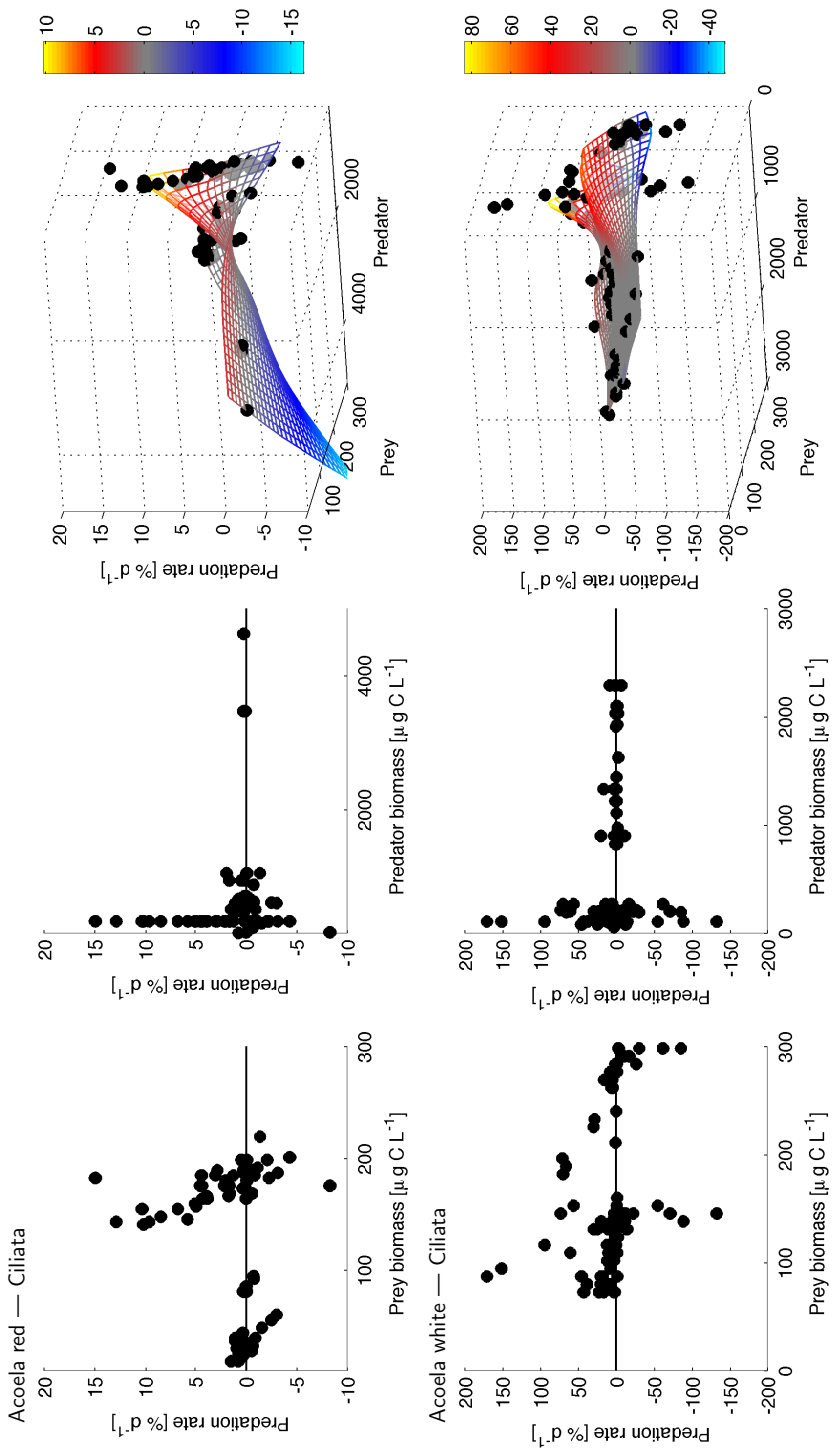

Figure 5.11: Predation rates of Arctic red (top) and Antarctic white (bottom) acoels preying on ciliates, plotted against prey biomass (left), predator biomass (middle) and both prey and predator biomass (right). The mesh in the 3D plots was interpolated using the Matlab gridfit routine (release 2.0, May 23, 2006).

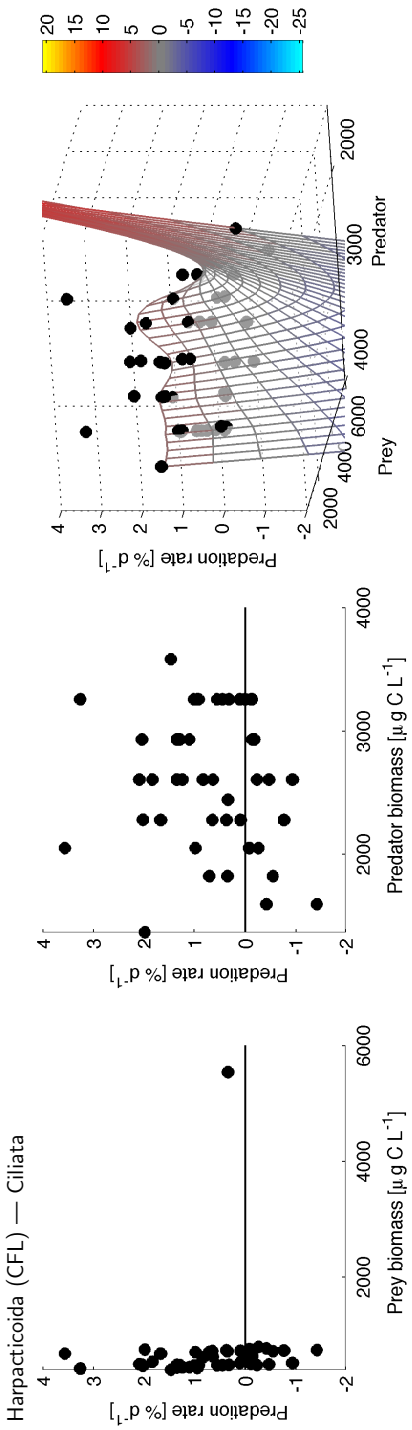

Figure 5.12: Predation rates of indetermined harpacticoids from the Canadian Arctic preying on ciliates, plotted against prey biomass (left), predator biomass (middle) and both prey and predator biomass (right). The mesh in the 3D plots was interpolated using the Matlab gridfit routine (release 2.0, May 23, 2006).

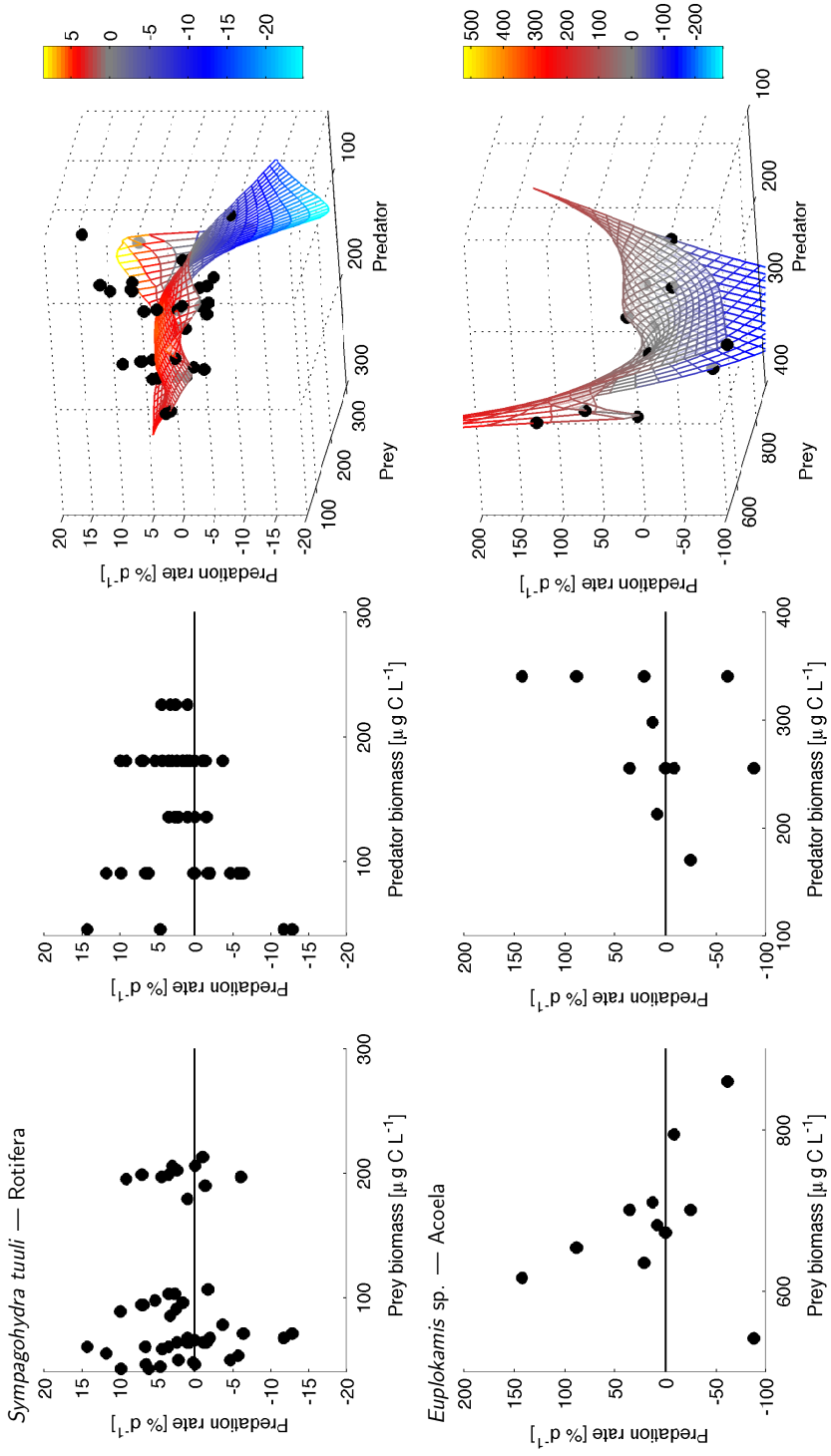

Figure 5.13: Predation rates of the Arctic cnidarian *Sympagohydra tuuli* preying on rotifers (top) and the Antarctic ctenophore *Euplokamis* sp. preying on white acoels (bottom), plotted against prey biomass (left), predator biomass (middle) and both prey and predator biomass (right). The mesh in the 3D plots was interpolated using the Matlab gridfit routine (release 2.0, May 23, 2006).

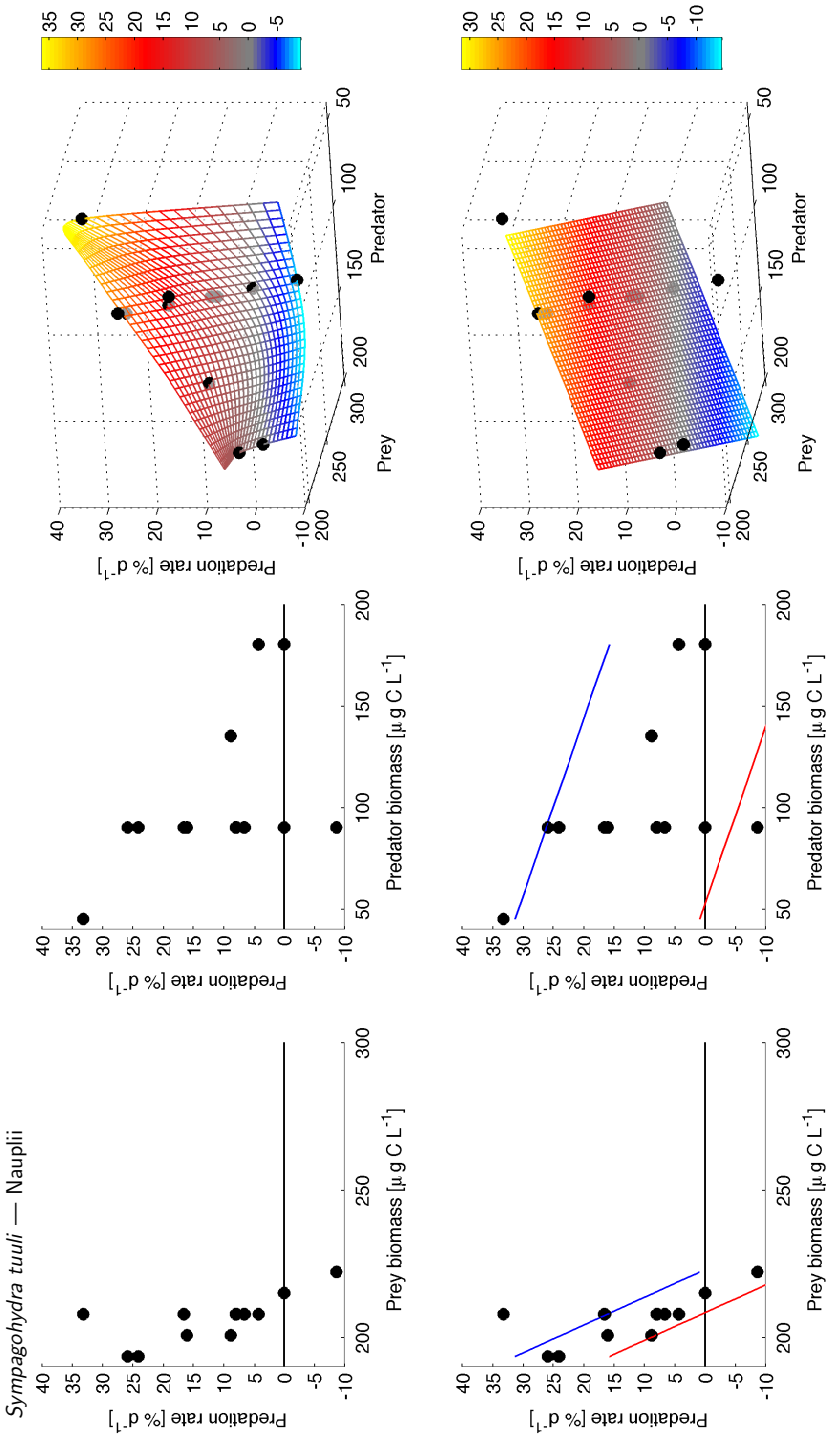

Figure 5.14: **Top** Predation rates of the Arctic cnidarian *Sympagohydra tuuli* preying on nauplii, plotted against prey carbon biomass (left), predator carbon biomass (middle) and both prey and predator carbon biomass (right). The mesh in the 3D plot was interpolated using the Matlab gridfit routine (release 2.0, May 23, 2006). **Bottom** Same as above, the surface in the 3D plot showing a plain fitted to the data (Eq. 5.2) and the red and blue lines in the 2D plots showing the upper and lower borders of the plain within the data range.

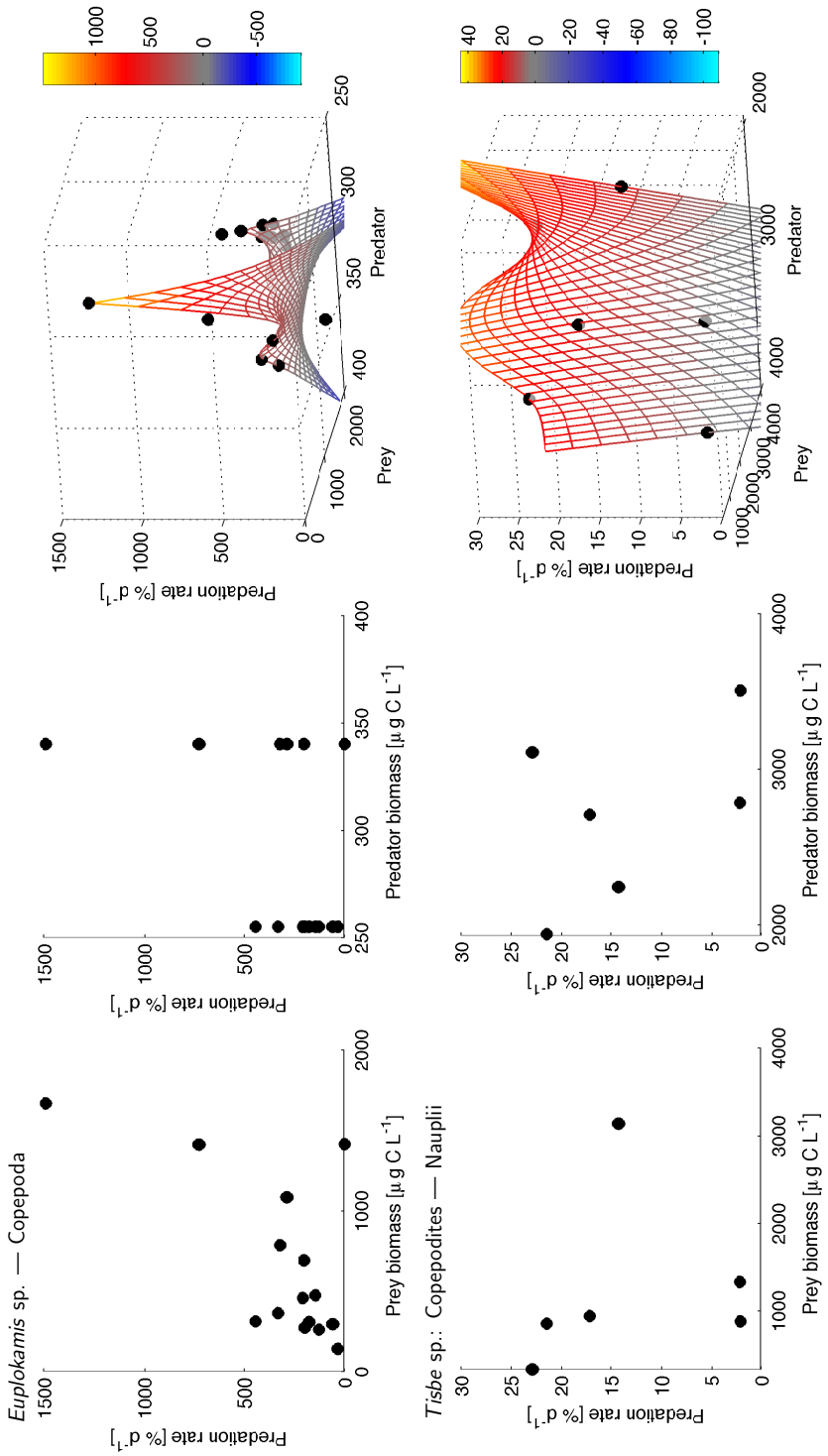

Figure 5.15: Predation rates of the Antarctic ctenophore *Euplokamis* sp. preying on copepods (merged from separate setups with nauplii, harpacticoid copepodides and calanoid copepodides of *Stephos longipes* as prey; top) and of copepodides of the Arctic harpacticoid *Tisbe* spp. preying on nauplii of the same species (bottom), plotted against prey carbon biomass (left), predator carbon biomass (middle) and both prey and predator carbon biomass (right). The mesh in the 3D plots was interpolated using the Matlab gridfit routine (release 2.0, May 23, 2006).

6 Summary and outlook

Research of biodiversity and its influence on ecosystem processes and functioning has traditionally been rooted in terrestrial and benthic ecology. With its large extent, continuously moving fluid and rapid turnover of organic matter, the pelagic ocean poses a challenge to observational studies of marine pelagic diversity and its effects on ecosystem functioning, as indicated for instance by primary production, at large scales. A novel global coupled ocean ecosystem modelling approach (Follows et al., 2007) allows to resolve marine phytoplankton diversity and investigate its effects on community structure and ecosystem functioning without the restrictions of observational and experimental limitations. Using this model, bottom-up controls of diversity by nutrients have been identified, while top-down effects via zooplankton feeding have not yet been investigated.

This thesis focuses on the effects of zooplankton predation on phytoplankton diversity, and the resulting consequences for simulated ecosystem functioning in the framework of the global model presented by Follows et al. (2007). It demonstrates the effects of different predation formulations on diversity and community structure (Chapter 2) and investigates the consequences of phytoplankton diversity for primary production (Chapter 3). Given the large influence of predation formulations on diversity and ecosystem functioning, an alternative predation model, which is less simplistic than commonly employed formulations, is presented in Chapter 4. The complexity of feeding relationships and challenges to understand these community processes experimentally, albeit for a sea-ice ecosystem, are demonstrated in Chapter 5.

In concord with a study employing an ocean ecosystem model with a small number of plankton functional types (PFTs; Anderson et al., 2010), Chapter 2 demonstrates that the choice of zooplankton predation formulation significantly affects simulated ecosystem functioning and community structure. In the diversity-resolving model used in this study, a sigmoidal functional response, which implicitly describes feeding of a zooplankton community, increases diversity and improves the representation of seasonal succession in the model compared to observations at a time-series site. The simulations indicate an interplay between bottom-up and top-down controls on phytoplankton coexistence, and thus diversity. Employing fairly general parameterisations of the zooplankton community allows to demonstrate the relevance of predation controls on diversity. Understanding and representing the underlying principles, however, will require more refined formulations of the feeding process, for instance based on trade-offs or optimality (cf. Chapter 4) and/or an explicit zooplankton community. In the context of such future work, assessing model skill on the global scale will require adequate observations and measures of diversity.

Chapter 3 demonstrates that more diverse phytoplankton communities able to utilise complementary

niches can exhibit a higher primary production on the global scale. The positive diversity-productivity relationship suggests that diversity might feed back on ocean ecosystem functioning. In the model phytoplankton community, differences in competitiveness for resources between the phytoplankton types are negligible when using a type 3 grazing functional response. A type 2 response results in one dominating phytoplankton type and an effect of diversity on primary production cannot be identified. This implies that the way in which coexistence or dominance arise in the model may affect the functioning of the simulated ecosystem. Feeding models which consider trade-offs between traits of phytoplankton and zooplankton and capture community dynamics explicitly might help to further understand how diversity controls ecosystem functioning in natural marine plankton communities.

This analysis focuses on primary production in accordance with the majority of studies in diversity-ecosystem functioning research. For the biogeochemical cycling of elements, in particular carbon, in the ocean, however, the export of organic matter into the deep ocean via the biological pump is important. Fig. 6.1 shows the ratio of export to primary production for the simulations presented in Chapter 3, which were performed with different initial numbers of phytoplankton types, and for a type 2 and a type 3 grazing functional response. The ratio of export to primary production is fairly robust against changes in diversity, with only a slight, insignificant tendency to decrease with higher diversity. The constant export ratio contrasts with a roughly 25% increase in global primary production for a two-fold increase in the average number of phytoplankton types. In the model, the export production mainly consists of particulate organic matter (detritus) produced by zooplankton egestion, sloppy feeding and phytoplankton mortality. Part of this detritus is exported into the deep ocean, the remainder is remineralised in the surface layer. The export thus depends on both secondary production and phytoplankton biomass, and on their partitioning towards either regenerated production or sinking detritus. This partitioning is affected by the size structure of the plankton community which determines the production of dissolved and particulate organic matter. Particularly among the simulations with the smallest phytoplankton assemblage, the size structure may differ notably; each phytoplankton type is assigned a size (small or large) and is best suited to an individual combinations of nutrients, light, and temperature according to its combination of parameters. In a small phytoplankton assemblage with a small number of parameter combinations, the spatial distributions of biomass and related production can vary considerably (see also section 6.2). The simulations with type 3 grazing tend to have a slightly lower export to primary production ratio than the corresponding simulations with type 2 grazing, and thus relatively more regenerated production. This might be linked to the overall more efficient nutrient use in the phytoplankton communities characterised by complementary resource use with type 3 grazing.

Chapter 3 also demonstrates that in the global model ocean, the positive relationship between phytoplankton diversity and productivity is pronounced in regions with high nutrient supply by vertical mixing but not evident in oligotrophic regions. Complementary 0-D simulations indicate that insufficient nutrient supply might limit the number of coexisting phytoplankton types at high diversity levels. The role of nutrient supply for diversity and productivity is examined further in section 6.1.

The global ocean ecosystem model used here employs fairly simplistic formulations of zooplankton

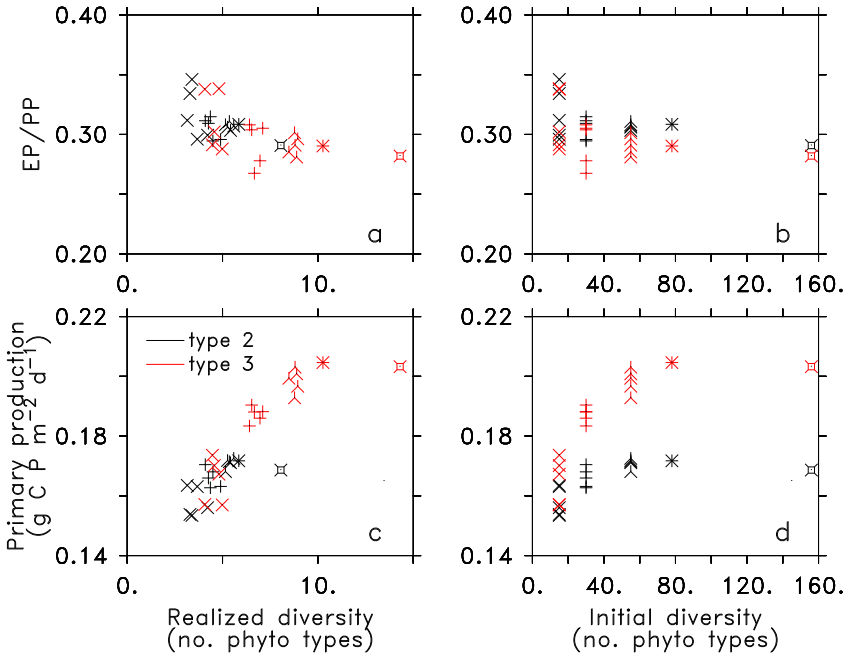

Figure 6.1: Ratio of annual average export production (EP) to primary production (PP; a,b) and PP (c,d) in the top 100 m for global simulations with different initial diversity. For both a type 2 (black symbols) and a type 3 (red symbols) grazing functional response, the standard simulation (n=78 phytoplankton types; $*$) is compared to simulations with smaller subpopulations (n=15 ($\times$), 30 ($+$), 55 ($\curlywedge$) and one simulation with higher diversity (n=156 ($\square$); cf. Chapter 3).

feeding. The classical type 2 functional response with fixed parameters for each type does not take into account behavioural shifts of the zooplankton individual or community. The type 3 functional response parameterises a community response, but the underlying mechanisms are not well defined. A different approach presented in this study formulates feeding for one feeding strategy, namely current feeding, in terms of optimal allocation of energy between generating a feeding current and assimilating food (Chapter 4). The model predicts a feeding threshold which has been suggested to be important, e.g., for allowing a persistent, low phytoplankton standing stock in high nutrient, low chlorophyll regions. It suggests that energetic costs for motion in zooplankton might be much larger than often assumed. This optimality-based approach demonstrates how trade-offs not captured in the traditionally employed feeding formulations may provide explanations for observed paradigms like zooplankton community dynamics in a seasonally stratified surface mixed layer. It remains to be tested how such optimality based formulations of zooplankton feeding compare with the established, more static formulations in larger scale ecosystem models. For this comparison, the model of optimal current feeding needs to be extended for feeding on multiple prey types.

Feeding on multiple and different types of prey is not well known from the experimental literature, since most zooplankton feeding studies necessarily focus on individual predator-prey combinations because conditions are better to control and results are easier to interpret. In the feeding experiments described in Chapter 5, different algal and protist food sources were offered to sea-ice meiofauna in feeding experiments, demonstrating the influence of feeding on the sea-ice community. Conducting

such experiments using mixtures with a stable composition of prey types yet representative of the natural prey environment is difficult. However, such experiments addressing multiple food sources and feeding strategies for zooplankton are needed to better understand feeding ecology in the ocean, and constrain ocean ecosystem models.

6.1 Sensitivity to environmental changes

The results presented in Chapter 3 suggest that nutrient supply might determine whether more diverse communities can be more productive. Aside from the shape of the diversity-productivity relationship, the nutrient supply also sets an upper limit to diversity in the model. In a changing climate, the nutrient supply to the surface ocean via mixing is generally predicted to decrease because of enhanced stratification. In the following section, the effects of a reduction in nutrient supply on the functioning of a diverse model phytoplankton community are investigated.

In the global model, the supply of nutrients to the surface layers from the deep ocean is to a large extent controlled by the vertical eddy diffusivity k_e which determines the strength of vertical mixing processes arising from mixed layer dynamics. To test the influence of the nutrient supply on primary and export production depending on the diversity of the simulated community, we carried out two sets of experiments. In the first set, k_e for all biogeochemical tracers was reduced by 50% and simulations were conducted with different levels of initial diversity. In the second set, an established phytoplankton community experiences a sudden reduction in k_e by 50% after 10 years of simulation. Effects on primary and export production are examined after 10 more simulated years. In both cases, the change in k_e does not affect stratification or the depth of the mixed layer, but only mixing of nutrients, phytoplankton and the other biogeochemical tracers. In the following, at first the results obtained from the first set of simulations are presented.

Fig. 6.2 shows export and primary production for the simulations with different initial diversity and type 3 grazing presented in Chapter 3 together with parallel simulations with reduced mixing. Firstly, with a lower supply of nutrients, the worst competitors for nutrients among the phytoplankton would be excluded from the system because they grow too slowly to balance losses through mortality and predation. Consequently, the number of coexisting types would decrease. In the present simulations, the overall reduced supply of nutrients only results in a minor decrease in realized diversity. Diversity decreases the most for the simulations initialised with the largest number of phytoplankton types. In general, reductions amount to 4% or less of the initial number of species. The magnitude of this nutrient effect on diversity is linked to the choice of parameter values defining the minimum resource level R^* required to compensate losses (cf. section 1.2.3). Reducing k_e potentially both reduces losses by mixing and exacerbates nutrient limitation depending on the physical environment. The lower mortality through mixing reduces R^* and might thus counteract the effect of reduced nutrient supply on coexistence. Given that the phytoplankton assemblages are randomly picked from the standard assemblage with n=78 types, more simulations with other assemblages and regional analyses are needed to assess this

effect more reliably.

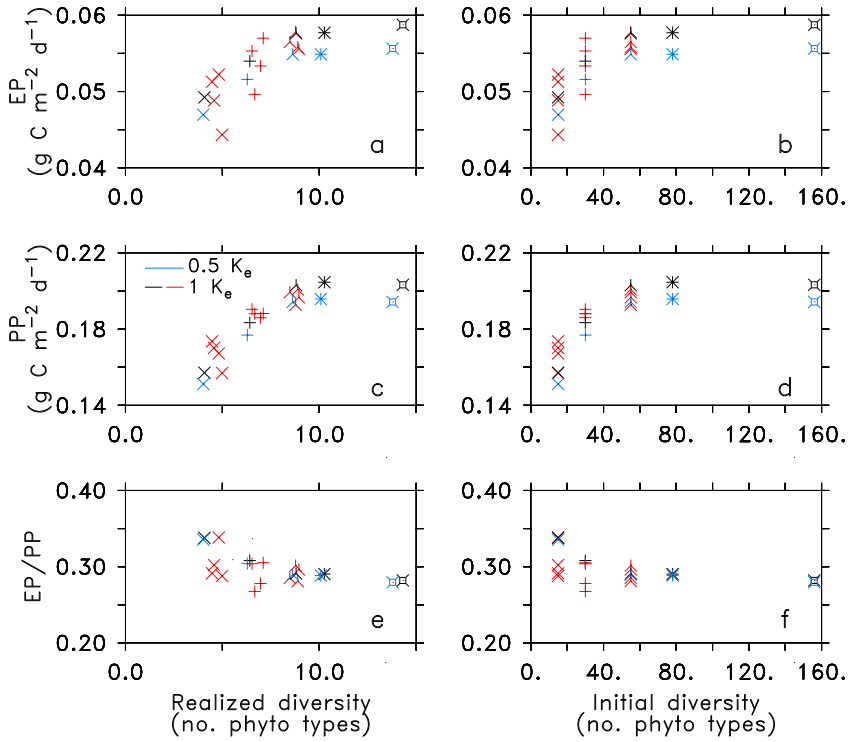

Figure 6.2: Annual average export production (EP; a,b), primary production (PP; c,d) and their ratio (EP/PP; e,f) over realized and initial diversity in the top 100 m for global simulations with different initial diversity (n=15 (×), 30 (+), 55 (⅄), 78 (∗), 156 (¤) phytoplankton types). Simulations are performed for a type 3 grazing functional response. Blue symbols: simulations with reduced mixing; black symbols: corresponding simulations with the same phytoplankton assemblage and standard mixing; red symbols: parallel simulations with different phytoplankton assemblages and standard mixing.

Secondly, both export and primary production decrease as a result of the reduced supply of nutrients from the deep ocean. For the export production, this reduction is expected since the export of organic matter from the surface, aside from atmospheric or terrestrial sources, is ultimately governed by the supply of nutrients from the deep ocean. Primary production decreases to a similar degree, and the ratio between export and primary production is almost identical in the standard and reduced mixing simulations.

Other studies evaluating oceanic changes due to rising atmospheric CO_2 levels predict export production to decline as much as, or more than, primary production on centennial scales, so that the export ratio remains nearly constant or decreases (e.g., Steinacher et al., 2010). The constant export ratio found in our simulations agrees with the results Steinacher et al. (2010) obtained for three out of four large-scale climate models which do not resolve phytoplankton diversity. A significantly reduced export ratio is found only for one of the models. This can be attributed to floristic shifts from diatoms with large sinking speeds and zooplankton to smaller nanophytoplankton which are part of the recycling loop (Bopp et al., 2005). The negative effect of reduced nutrient supply on primary production may be counteracted by an increase in light availability and temperature in a shallower surface mixed layer (Sarmiento et al., 2004), which may be beneficial to phytoplankton growth. In our experiment, the

enhanced light availability is captured by the reduced mixing, but effects of a shoaling mixed layer on temperature are not taken into account. In some regions primary production might therefore decline more strongly here than in simulations simulating enhanced stratification. Our model results show no effect of diversity on the magnitude of changes in export or primary production caused by reduced mixing. In particular, high diversity does not mitigate the reduction of export and primary production induced by nutrient supply in our simulations.

These results relate to the question whether more diverse systems are more robust and less susceptible to environmental changes than systems with lower diversity. Observational and theoretical studies have identified lower temporal variability of production or biomass in more diverse systems (McGrady-Steed et al., 1997; Cottingham et al., 2001). Our results presently only allow to assess variability due to community composition. Temporal variability in ecosystem functioning of communities differing in diversity may arise in this phytoplankton diversity-resolving model since community composition and biomass levels of individual types may vary interannually (cf. simulations at NABE presented in Chapter 2). This variability could be examined, in accord with the above mentioned studies addressing the diversity-variability relationship, for example using primary production averages of different years for simulations with different diversity. Moreover, several other measures of ecosystem stability exist may show different relationships with diversity (Ives and Carpenter, 2007). A different view of the variability within simulations with different diversity is provided by the patterns of different plankton functional types presented in section 6.2.

In addition to the variability and robustness of predictions in relation to diversity, the simulations can help to identify any potential buffering effect of diversity on ecosystem functions under the influence of environmental changes. In order to approach this question, in the second set of simulations one of the standard 10-year simulations used in Chapters 2 and 3 with n=78 phytoplankton types and a type 3 grazing functional response was continued for another 10 years, once with reduced mixing (50% reduced k_e) as above and once without any changes to provide a control simulation. The same setup was applied to three simulations each with a different subpopulation of the original assemblage with n=30 phytoplankton types.

Fig. 6.3 shows the absolute and relative differences of different ecosystem level properties in year 20 between the simulations with reduced k_e and the respective control simulations. For the standard setup with n=78 phytoplankton types, diversity, i.e., the number of coexisting types, overall changes less than 5%, with increases at higher latitudes and decreases for regions from roughly 40°S to 40°N. Changes in total phytoplankton biomass, primary and net community production are larger, with reductions around 10% in the tropics and subtropics and exceeding 20% around 30°S and 30°N. At higher latitudes, changes are generally small, and in the zonal average positive only in the Southern Ocean. Higher productivity in this region has been identified observationally (Behrenfeld et al., 2006) and in coupled ocean ecosystem models (e.g., Bopp et al., 2001), and can be explained by higher light availability in a shoaling surface mixed layer. Lower productivity in the remaining ocean reflects aggravated nutrient limitation. The effect of higher light availability at higher latitudes is reflected at least partly by a lower

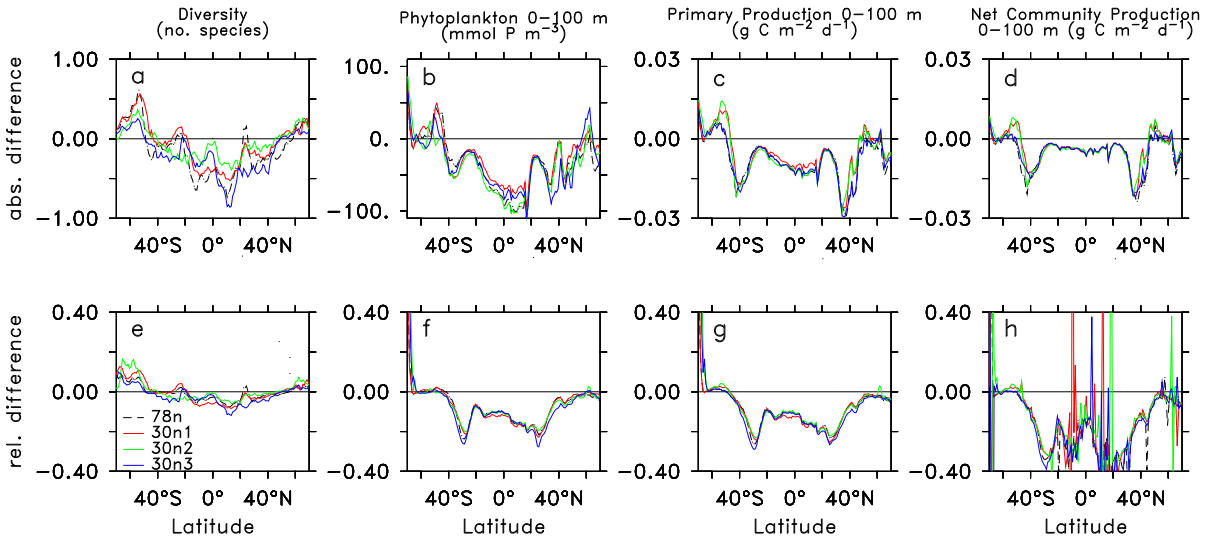

Figure 6.3: Absolute and relative differences between simulations with reduced and standard mixing (e.g., $78n[0.5k_e] - 78n[1k_e]$ and $(78n[0.5k_e] - 78n[1k_e])/78n[1k_e]$, respectively) 10 years after the reduction in mixing. Diversity (a,e), total phytoplankton biomass (b,f), primary production (c,g), and net community production (d,h) are shown for the standard simulation with a type 3 grazing functional response and with 78 phytoplankton types as well as for three subpopulations with 30 types each.

phytoplankton mortality due to mixing in the short-term simulations presented here.

Reduced mixing due to enhanced stratification of the upper ocean and thereby lower input of nutrients into the surface layers is one of the consequences predicted under a warming climate (e.g., Sarmiento et al., 2004; Steinacher et al., 2010). The sudden reduction in nutrient supply implied by this setup is, however, not realistic in the sense of expected time scales of change in the ocean in a changing climate. The resolution and number of state variables in the 3-D model makes longer simulations with more gradual changes not feasible within a reasonable time frame. A more realistic setup would require a model configured to perform climate change simulations, i.e., an online simulation coupled to the physical model, with lower spatial and temporal resolution, and possibly also fewer state variables. However, the resulting reductions in primary production observed after 10 years of reduced mixing are of the same order of magnitude as predictions from century-scale simulations (Steinacher et al., 2010; Taucher and Oschlies, 2011).

Overall, no pronounced difference between the simulations with n=78 types and the three simulations with n=30 types is evident. Relative changes in all properties are of similar order of magnitude and display similar zonal patterns among the simulations. Differences within the ensemble of three simulation with similar initial (n=30) diversity are comparable with differences between simulations with different initial diversity. A regional buffering effect of diversity can likewise not be identified. In the Southern Ocean, for example, primary production shows a small increase as expected from the alleviated light limitation. The relative increase is smaller, however, than the corresponding increase in diversity. A pronounced positive effect of increasing diversity on production is thus not evident. For some latitudes, the simulation with the largest changes in diversity also shows the largest changes in one or several

of the other properties. Taken together, it appears that in our model changes in ecosystem functions and diversity are both ultimately controlled by the physical environment. This view agrees with a recent model of diverse communities in which resource supply governs both diversity and the potential productivity of a system given an optimal use of available resources (Gross and Cardinale, 2007). A positive effect of diversity on productivity under reduced mixing is not predicted by this model at the diversity range tested so far. Simulations covering an extended diversity range and employing a larger variety of different random phytoplankton assemblages are needed to confirm or revise these findings. Results are qualitatively similar for simulations employing a type 2 grazing functional response as well as for an increased light scenario.

6.2 Resolving diversity within plankton functional types

The variability inherent in simulations with different levels of diversity can also be assessed in terms of how variable simulated distributions of different plankton functional types (PFTs) are. In state of the art ocean ecosystem models, the plankton community is represented by a small number of PFTs, such as diatoms, which are characterised by their functional role within the ecosystem (e.g., Le Quéré et al., 2005). Such models are critised for several reasons including unresolved diversity within a PFT (Thingstad et al., 2010). The model employed in this study differs in that it resolves four phytoplankton PFTs, namely *diatom analogues*, *other large phytoplankton*, *Prochlorococcus analogues*, and *other small phytoplankton*, with several phytoplankton types. Large phytoplankton types have high maximum growth rates and high requirements of nutrients, and belong to *diatom analogues* if they use silica, and to *other large phytoplankton* otherwise. Small types have lower maximum growth rates and a higher nutrient affinity, and are *Prochlorococcus analogues* if they cannot use nitrate, and *other small phytoplankton* otherwise. The number of state variables within one PFT depends on the total number of phytoplankton types with which the model is initialised. In this section, I examine how sensitive the distribution of PFTs composed of several different phytoplankton types is to the initial number of types in the model. In the simulations with different initial diversity levels employed before, the biomass of the individual types is summed according to which PFT they belong to. The fraction of total biomass contributed by each PFT is examined as average of ensembles of five simulations with different initial diversity. In addition, in one selected simulation of each ensemble, the dominance of each PFT is calculated.

Fig. 6.4 shows the distribution of diatoms as fraction of total biomass as average of five simulations with different phytoplankton assemblages, and for three levels of initial diversity. The lower panels indicate the standard deviation of the ensemble of five simulations. Similar figures for the other three PFTs can be found in Appendix 7. With an increasing number of state variables resolving each PFT the regional patterns become more clearly defined. The regional distributions obtained for different phytoplankton assemblages become more similar with higher diversity as indicated by the decrease in the standard deviation. The variance of total biomass, which might bias the variance of the average fraction, does

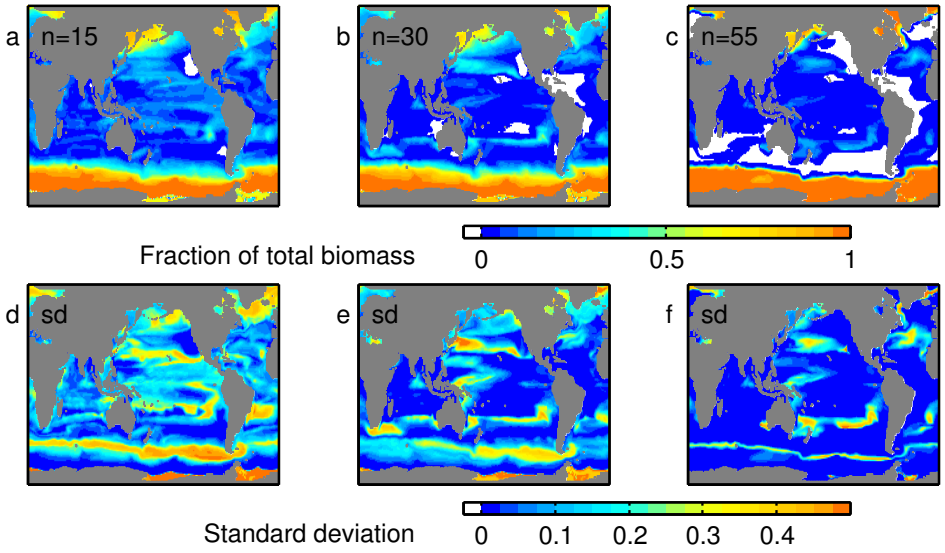

Figure 6.4: Fraction of total biomass contributed by the plankton functional type (PFT) *diatoms analogues* as averages (a-c) and standard deviation (d-f) of five simulations each with different initial diversity n=15 (a,d), n=30 (b,e), n=55 (c,f) phytoplankton types.

not differ systematically between levels of diversity.

In this model, for 55 types initialized the standard deviation of the diatom fraction of total biomass is reduced to about 8% in the diatom-dominated Southern Ocean. The higher variance for PFTs represented by fewer phytoplankton types does not necessarily imply that in simulations with PFTs represented by just one type spatial patterns are associated with a high uncertainty. In these models, parameter values for each PFT typically represent an average of a range of observed values for each trait. In the model experiments presented here, parameter values are selected randomly from a uniform distribution on such a range. A community of few phytoplankton types might therefore include a larger number of types with extreme, atypical parameter values. This might lead to a pronounced occurrence of a PFT in regions where this PFT is rarely observed in notable contributions in nature. Furthermore, the distribution of biomass between PFTs depends on the parameterisation of the other coexisting PFTs in a given location. An experimental setup more relevant to the representation of PFTs by one phytoplankotn type in other PFT-based models might include selecting phytoplankton types from a normal distribution centred around an average parameter value for each phytoplankton trait. In general, these results indicate that care should be taken in parameterising the different PFTs in such models.

An alternative measure to assess the variability of PFT distributions with respect to different diversity levels is to calculate the dominance of each PFT as fraction of the year for which the respective PFT comprises more than 50% of the total biomass while exceeding a small threshold biomass. PFT dominance can be used to compare PFT distributions with satellite observations based on ocean colour (PHYSAT) as demonstrated, e.g., by Anderson et al. (2010) for the North Atlantic and Pacific oceans.

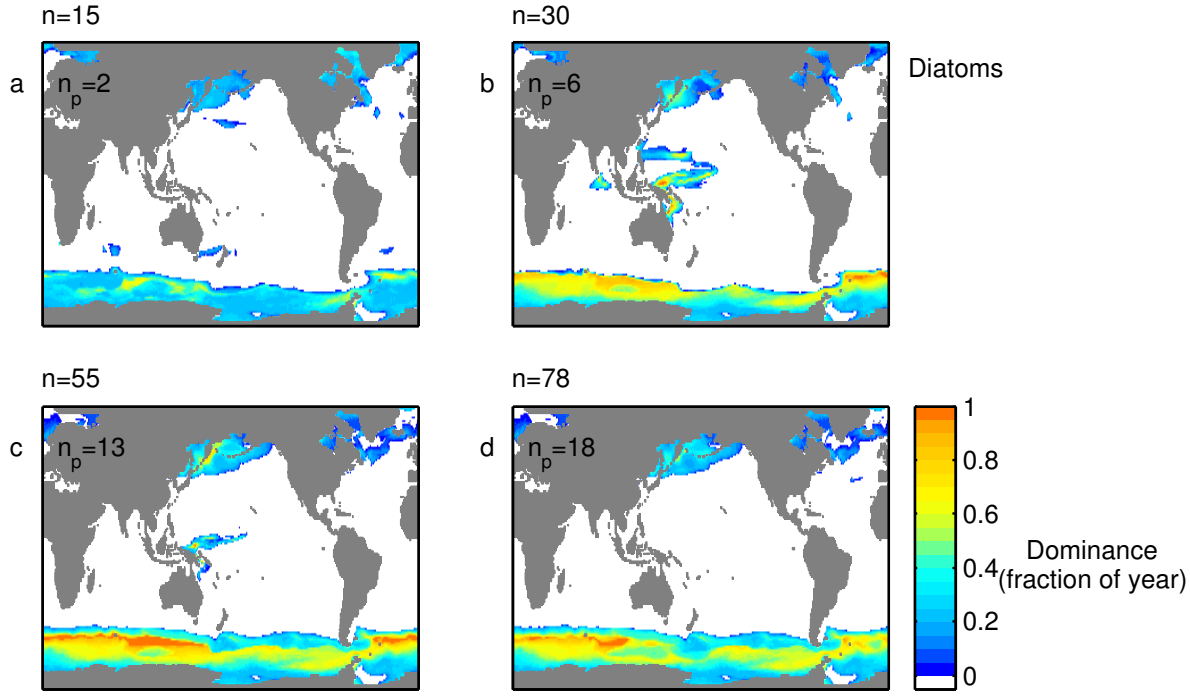

Figure 6.5: Plankton functional type (PFT) dominance for *diatoms analogues* expressed in simulations with different initial diversity (n=15, 30, 55, 78 phytoplankton types initialised). PFT dominance is expressed as fraction of a year for which the PFT comprises more than 50% of the total biomass. In each simulations, n_p phytoplankton types are *diatoms analogues*.

The PFT distributions derived from satellite imagery, e.g., by Alvain et al. (2005, 2008), aim to detect specific phytoplankton groups by characteristic pigments identified from variation in spectral variability. As discussed by Anderson et al. (2010), this assignment relies on small signals compared to the variability due to phytoplankton abundance. Satellite-based PFT distributions might therefore give reliable estimates for specific locations, but robust regional or even global estimates are difficult to obtain. Simulations with the required temporal resolution at four diversity levels are currently only available for one of the five phytoplankton assemblages used above. Nevertheless, these simulations can serve as an example for a more extensive comparison remaining to be performed.

Fig. 6.5 shows the spatial distribution of PFT dominance for diatoms at four levels of initial diversity. Similar figures for the remaining PFTs are shown in Appendix 7. PFT dominance differs notably between the simulations with low diversity (n=15 and n=30 initialised types). For high diversity (n=55 and n=78 types), PFT dominance is more similar. In order to better compare the spatial patterns, in Fig. 6.6 the correlation coefficient calculated from the PFT dominance for each model grid box is shown between adjacent diversity levels. With increasing initial diversity, a greater number of grid boxes fall on the 1:1 line between adjacent diversity levels, indicating that the correlation between the PFT dominance distributions increases. Given that the phytoplankton assemblages are characterised by randomly assigned traits, a lower variability in PFT distributions with higher diversity within a PFT can be expected. With the present model configuration, the number of types within a PFT which still improves

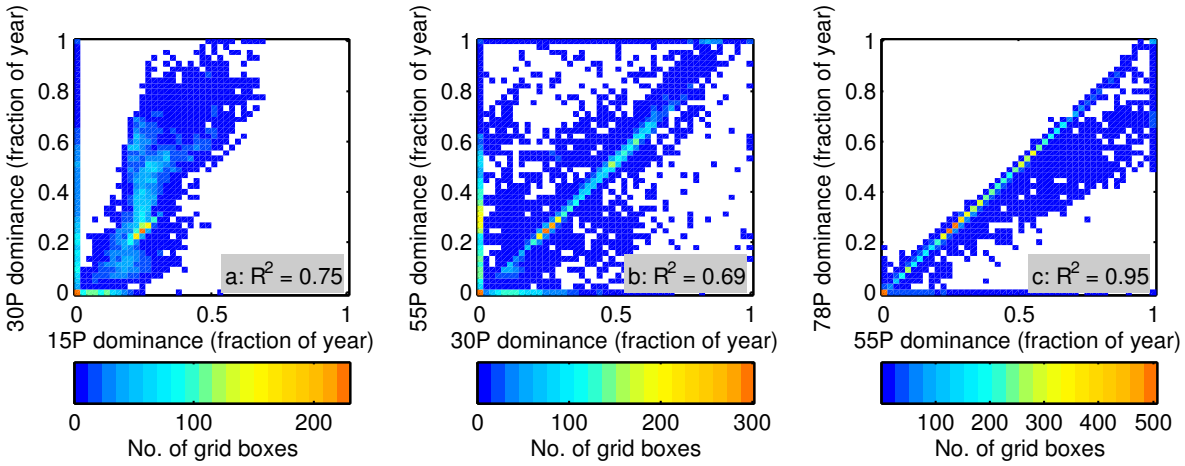

Figure 6.6: Plankton functional type (PFT) dominance for *diatoms analogues* compared per grid box between simulations with different initial diversity (n=15, 30, 55, 78 phytoplankton types). The shading indicates the number of grid boxes in the global model for which the respective combination of dominance values is found. *R* is the correlation coefficient.

the robustness of the PFT distribution compared to fewer types appears to reach a limit at around n=55 types. More simulations with different assemblages are needed to establish a reliable estimate of the variability of PFT distributions, and ultimately allow a comparison with other observational and model estimates, thereby assessing the model skill in simulating the distribution of plankton functional types in the oceans.

6.3 Concluding remarks

This thesis investigates for the first time the control of phytoplankton diversity by top-down processes in the global ocean. It thereby continues from previous work on the bottom-up controls by resource availability and use, employing a global ocean ecosystem model which resolves diversity. This model allows to investigate how theoretical concepts of competition and coexistence developed in idealized models and demonstrated in experiments may apply to ocean phytoplankton communities. While bottom-up processes related to resources are already captured in some detail in the ocean ecosystem model, top-down mechanisms controlling diversity through zooplankton feeding have not been represented in detail to date. This thesis reveals considerable effects of the formulation of top-down processes on phytoplankton diversity, succession, community structure, and mechanisms of competition and coexistence in the model. It motivates the development of mechanistic models of zooplankton feeding which may enhance our ability to capture predator-prey relationships and thereby improve our representation of diverse model plankton communities. Furthermore, it demonstrates that diversity has the potential to influence the functioning of the ecosystem. At the same time, it becomes evident that the mechanisms underlying the relationship between diversity and ecosystem functioning in the ocean are not well understood.

The results presented in this outlook indicate avenues for future work which make use of the unique structure of the diversity-resolving ocean ecosystem model employed here. The influence of resource supply to the surface ocean on phytoplankton diversity and productivity and their potential feedbacks is relevant for scenarios of the ocean and its role in biogeochemical cycling in a future climate. How the resource supply affects diversity and productivity in ocean ecosystems is not well understood. The global model presented here allows to investigate these controls by explicitly relating nutrient fluxes, diversity and productivity under current and expected future conditions. Furthermore, this model system might serve to assess the uncertainties inherent in simulating ocean ecosystems based on plankton functional types. The influence of variability in PFT distributions on ecosystem dynamics and biogeochemical cycling are not well understood. Consequences being discussed include changes in community structure and export production which may affect the role of ocean ecosystems for biogeochemical cycling of carbon now and in the future.

7 Appendix

The ocean ecosystem model employed in this study resolves different plankton functional types (PFTs), which are represented by several phytoplankton types with randomly assigned parameters for nutrient and light requirements, optimum temperature, size and others. In addition to the figure for the PFT *diatom analogues* presented in Chapter 6, the following figures show results for the remaining three PFTs, namely *Prochlorococcus analogues*, *other small phytoplankton* and *other large phytoplankton*.

The sensitivity of the simulated PFT distributions to the initial diversity can be examined using the variability in PFT distributions as fraction of total biomass. Figs. 7.1-7.3 show the distribution of each PFT as fraction of total biomass as average of five simulations with different phytoplankton assemblages, and for three levels of initial diversity.

Another measure to assess PFT variability, which also allows comparison with satellite-based estimates, is the dominance of each PFT. Dominance is expressed as the fraction of time per year for which the PFT comprises 50% or more of the total phytoplankton biomass. Figs. 7.4-7.4 show the spatial distribution of PFT dominance for each PFT at four levels of initial diversity. For easier comparison of the spatial patterns, the correlation of PFT dominance between adjacent diversity levels is shown in Figs. 7.7-7.7.

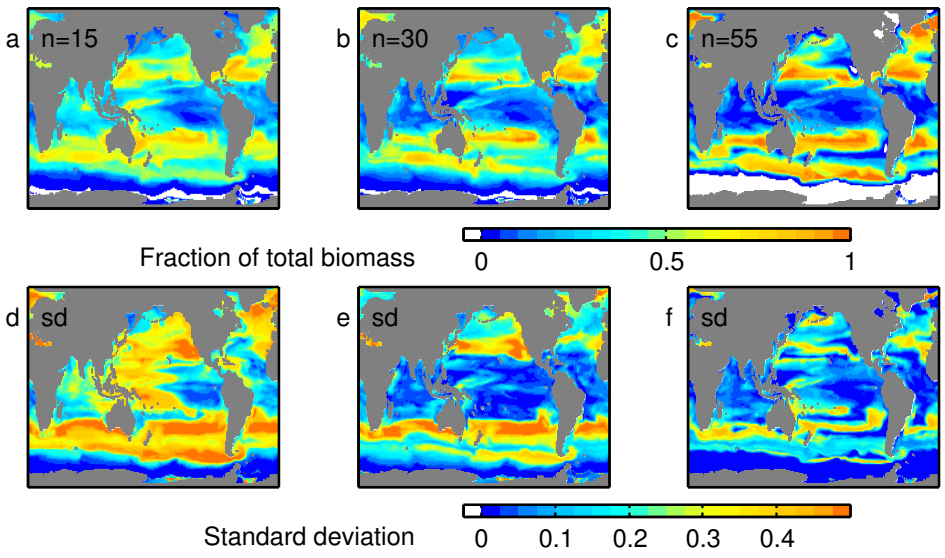

Figure 7.1: Fraction of total biomass contributed by the plankton functional type (PFT) *other large phytoplankton* as averages (a-c) and standard deviation (d-f) of five simulations each with different initial diversity n=15 (a,d), n=30 (b,e), n=55 (c,f) phytoplankton types.

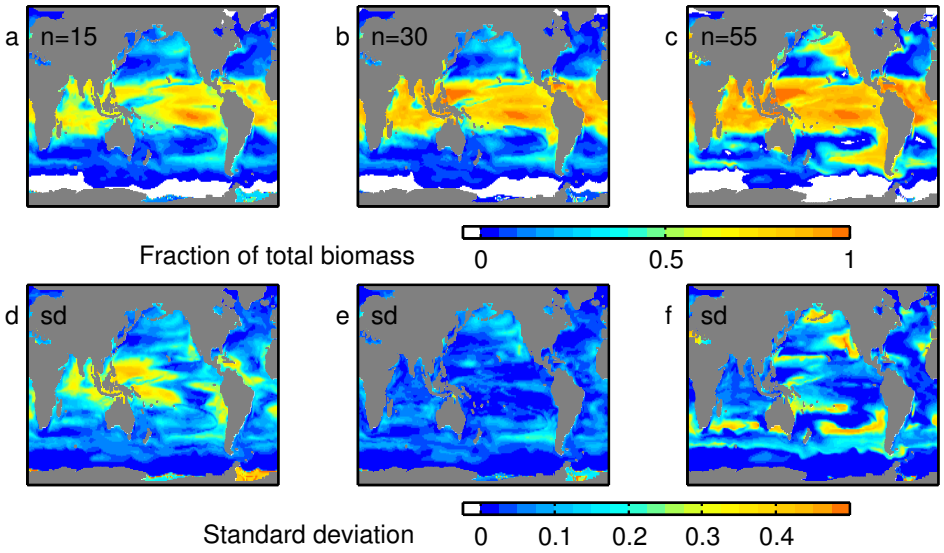

Figure 7.2: As Fig. 7.1, but for *Prochlorococcus analogues*.

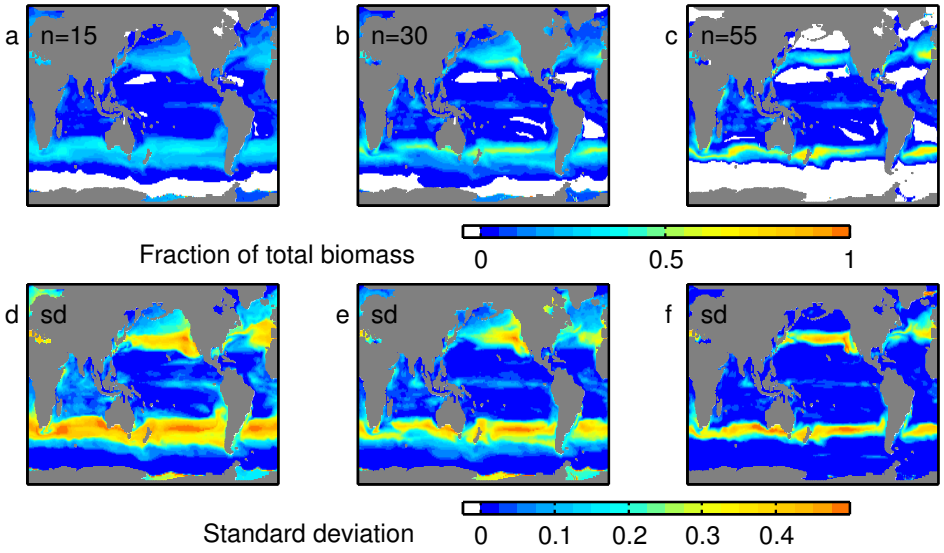

Figure 7.3: As Fig. 7.1, but for *other small phytoplankton*.

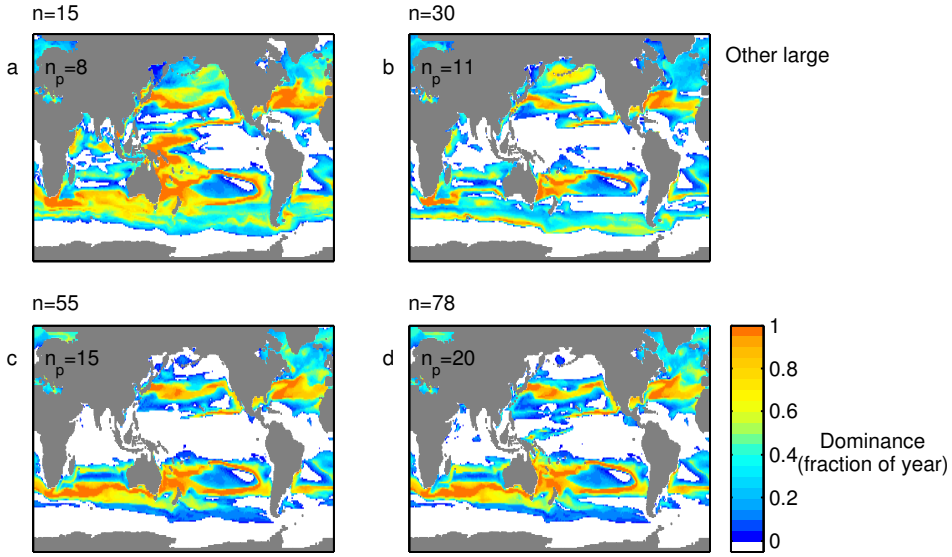

Figure 7.4: Plankton functional type (PFT) dominance for *other large phytoplankton* expressed in simulations with different initial diversity (n=15, 30, 55, 78 phytoplankton types initialized). PFT dominance is expressed as fraction of a year for which the PFT comprises more than 50% of the total biomass. In each simulations, n_p phytoplankton types belong to the PFT *other large phytoplankton*.

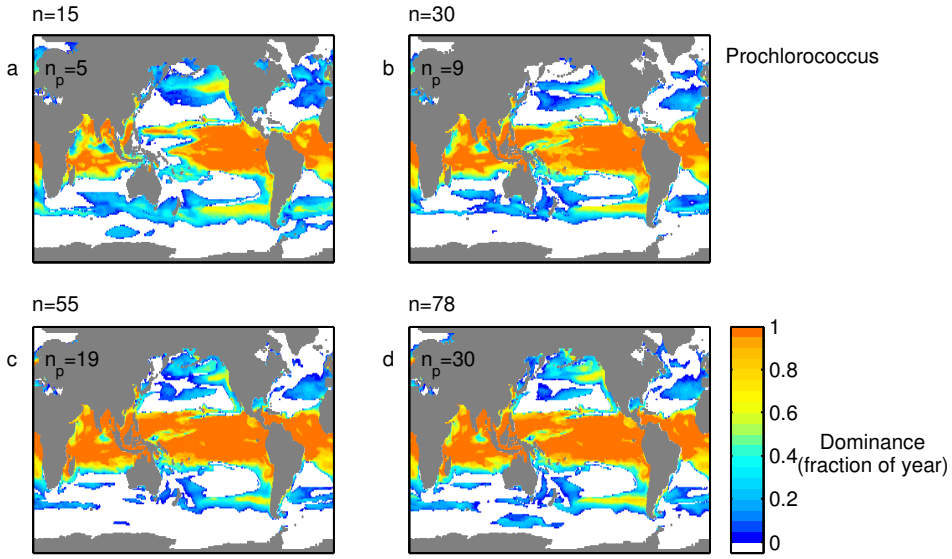

Figure 7.5: As Fig. 7.4, but for *Prochlorococcus analogues*.

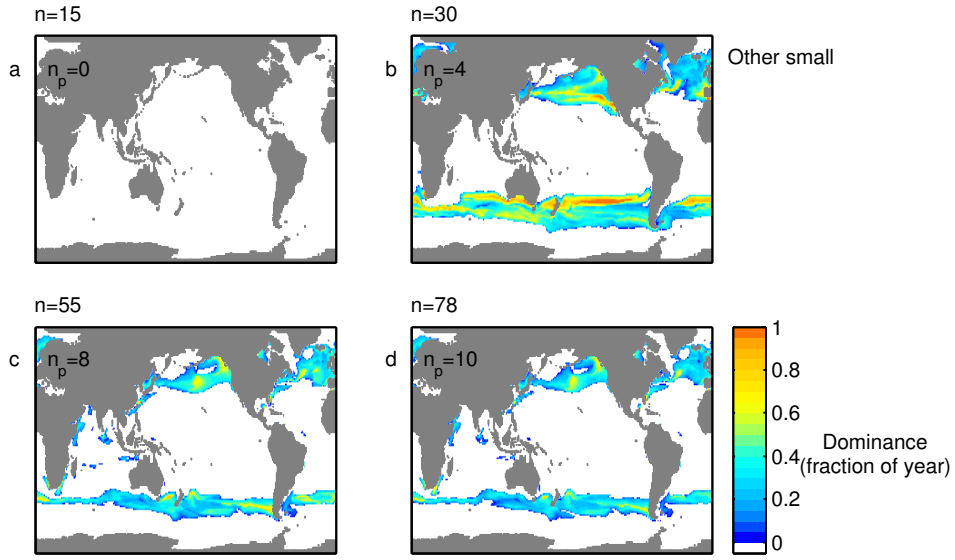

Figure 7.6: As Fig. 7.4, but for *other small phytoplankton*.

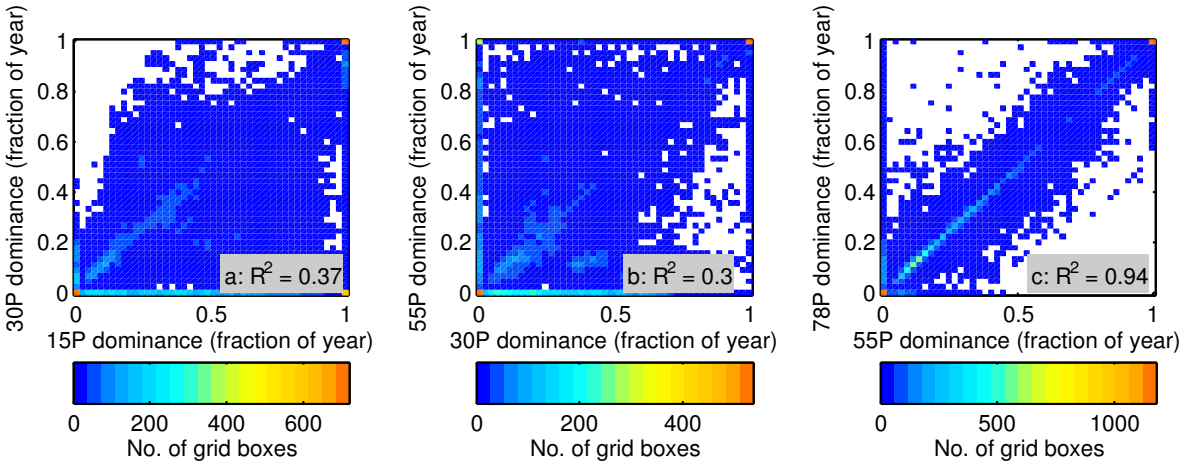

Figure 7.7: Plankton functional type (PFT) dominance for *other large phytoplankton* compared per grid box between simulations with different initial diversity (n=15, 30, 55, 78 phytoplankton types). The shading indicates the number of grid boxes in the global model for which the respective combination of dominance values is found. *R* is the correlation coefficient.

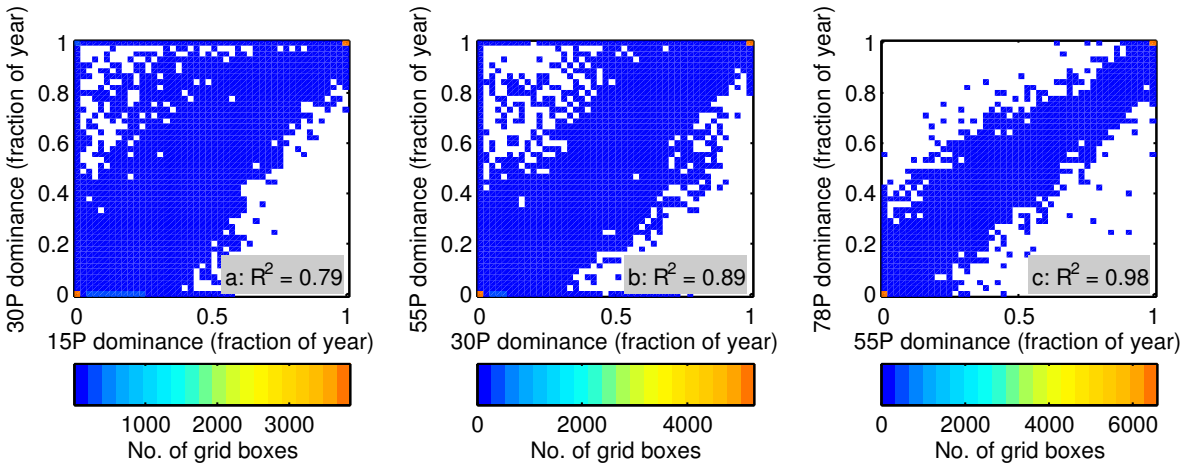

Figure 7.8: As Fig. 7.7, but for *Prochlorococcus analogues*.

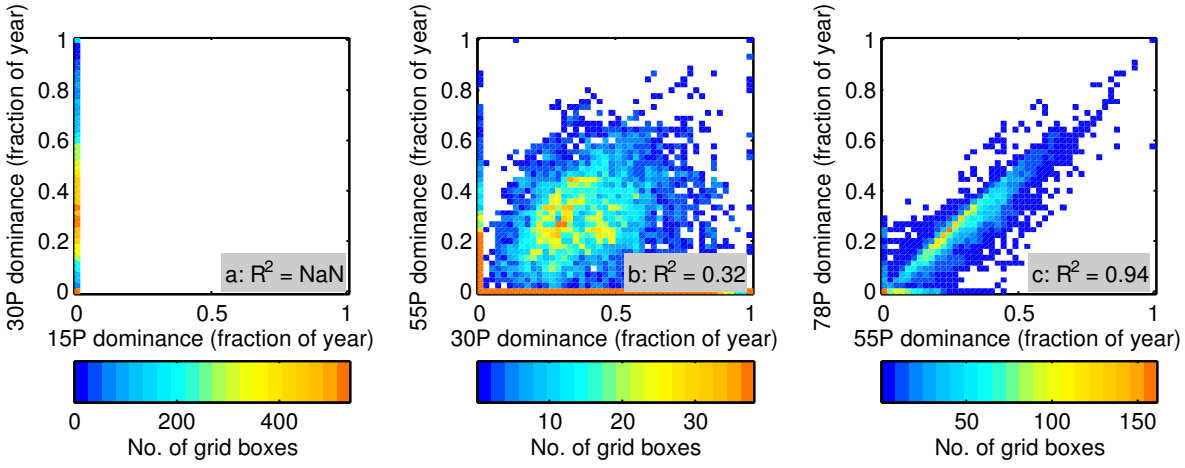

Figure 7.9: As Fig. 7.7, but for *other small phytoplankton*.

Bibliography

L. Aarssen (1997). High productivity in grassland ecosystems: effected by species diversity or productive species? *Oikos*, 80(1): 183–184.

J. Aiken, Y. Pradhan, R. Barlow, et al. (2009). Phytoplankton pigments and functional types in the Atlantic Ocean: A decadal assessment, 1995-2005. *Deep-Sea Res. II*, 56(15): 899–917. doi: 10.1016/j.dsr2.2008.09.017.

C. H. Ainsworth, J. F. Samhouri, D. S. Busch, et al. (2011). Potential impacts of climate change on Northeast Pacific marine foodwebs and fisheries. *ICES J. mar. Sci.*, 68(6): 1217–1229. doi: 10.1093/icesjms/fsr043.

S. Alvain, C. Moulin, Y. Dandonneau, and F. Breon (2005). Remote sensing of phytoplankton groups in case 1 waters from global SeaWiFS imagery. *Deep-Sea Res. I*, 52(11): 1989–2004. doi: 10.1016/j.dsr.2005.06.015.

S. Alvain, C. Moulin, Y. Dandonneau, and H. Loisel (2008). Seasonal distribution and succession of dominant phytoplankton groups in the global ocean: A satellite view. *Global Biogeochem. Cycles*, 22(3): GB3001. doi:10.1029/2007GB003154.

J. W. Ambler (1986). Formulation of an ingestion function for a population of *Paracalanus* feeding on mixtures of phytoplankton. *J. Plankton Res.*, 8(5): 957–972. doi:10.1093/plankt/8.5.957.

T. Anderson (2005). Plankton functional type modelling: running before we can walk? *J. Plankton Res.*, 27(11): 1073–1081. doi:10.1093/plankt/fbi076.

T. R. Anderson, W. C. Gentleman, and B. Sinha (2010). Influence of grazing formulations on the emergent properties of a complex ecosystem model in a global ocean general circulation model. *Prog. Oceanogr.*, 87(1-4): 201–213. doi:10.1016/j.pocean.2010.06.003.

R. Armstrong (1999). Stable model structures for representing biogeochemical diversity and size spectra in plankton communities. *J. Plankton Res.*, 21(3): 445–464.

K. R. Arrigo, D. H. Robinson, D. L. Worthen, et al. (1999). Phytoplankton community structure and the drawdown of nutrients and CO_2 in the Southern Ocean. *Science*, 283(5400): 365–367. doi: 10.1126/science.283.5400.365.

K. R. Arrigo and D. N. Thomas (2004). Large scale importance of sea ice biology in the Southern Ocean. *Antarct. Sci.*, 16(4): 471–486. doi:10.1017/S0954102004002263.

H. Auel and I. Werner (2003). Feeding, respiration and life history of the hyperiid amphipod *Themisto libellula* in the Arctic marginal ice zone of the Greenland Sea. *J. Exp. Mar. Biol. Ecol.*, 296(2): 183–197. doi:10.1016/S0022-0981(03)00321-6.

O. Aumont and L. Bopp (2006). Globalizing results from ocean in situ iron fertilization studies. *Global Biogeochem. Cycles*, 20(2). doi:10.1029/2005GB002591.

O. Aumont, E. Maier-Reimer, S. Blain, and P. Monfray (2003). An ecosystem model of the global ocean including Fe, Si, P colimitations. *Global Biogeochem. Cycles*, 17(2). doi:10.1029/2001GB001745.

F. Azam, T. Fenchel, J. G. Field, et al. (1983). The ecological role of water–column microbes in the sea. *Mar. Ecol. Prog. Ser.*, 10: 257–263.

N. S. Banas (2011). Adding complex trophic interactions to a size-spectral plankton model: Emergent diversity patterns and limits on predictability. *Ecol. Model.*, 222: 2663–2675. doi: 10.1016/j.ecolmodel.2011.05.018.

D. A. Barry, J.-Y. Parlange, L. Li, et al. (2000). Analytical approximations for real values of the Lambert W-function. *Math. Comput. Simulat.*, 53(1–2): 95–103. doi:10.1016/S0378-4754(00)00172-5.

A. D. Barton, S. Dutkiewicz, G. Flierl, J. Bragg, and M. J. Follows (2010a). Patterns of diversity in marine phytoplankton. *Science*, 327(5972): 1509–1511. doi:10.1126/science.1184961.

A. D. Barton, S. Dutkiewicz, G. Flierl, J. Bragg, and M. J. Follows (2010b). Response to comment on "Patterns of diversity in marine phytoplankton". *Science*, 329(5991). doi:10.1126/science.1190048.

H. Baumert (1996). On the theory of photosynthesis and growth in phytoplankton. Part I: Light limitation and constant temperature. *Int. Rev. Gesamten Hydrobiol. Hydrogr.*, 81(1): 109–139. doi: 10.1002/iroh.19960810113.

G. Beaugrand, P. Reid, F. Ibanez, J. Lindley, and M. Edwards (2002). Reorganization of North Atlantic marine copepod biodiversity and climate. *Science*, 296(5573): 1692–1694.

M. Begon, C. R. Townsend, and J. L. Harper (2006). *Ecology: From individuals to ecosystems*. Blackwell Publishing, Malden, Oxford, Victoria, 4 ed.

S. Behl, A. Donval, and H. Stibor (2011). The relative importance of species diversity and functional group diversity on carbon uptake in phytoplankton communities. *Limnol. Oceanogr.*, 56(2): 683–694. doi:10.4319/lo.2011.56.2.0683.

M. J. Behrenfeld, R. T. O'Malley, D. A. Siegel, et al. (2006). Climate-driven trends in contemporary ocean productivity. *Nature*, 444(7120): 752–755. doi:10.1038/nature05317.

B. Beisner (2001). Herbivory in variable environments: an experimental test of the effects of vertical mixing and daphnia on phytoplankton community structure. *Can. J. Fish. Aquat. Sci.*, 58(7): 1371–1379.

J. Blackford, J. Allen, and F. Gilbert (2004). Ecosystem dynamics at six contrasting sites: a generic modelling study. *J. Mar. Syst.*, 52(1-4): 191–215. doi:10.1016/j.jmarsys.2004.02.004.

B. A. Bluhm, R. Gradinger, and S. Piraino (2007). First record of sympagic hydroids (Hydrozoa, Cnidaria) in Arctic coastal fast ice. *Polar Biol.*, 30(12): 1557–1563. doi:10.1007/s00300-007-0316-9.

L. Bopp, O. Aumont, P. Cadule, S. Alvain, and M. Gehlen (2005). Response of diatoms distribution to global warming and potential implications: A global model study. *Geophys. Res. Lett.*, 32(19). doi:10.1029/2005GL023653.

L. Bopp, P. Monfray, O. Aumont, et al. (2001). Potential impact of climate change on marine export production. *Global Biogeochem. Cycles*, 15(1): 81–99.

P. Boyd and S. Doney (2002). Modelling regional responses by marine pelagic ecosystems to global climate change. *Geophys. Res. Lett.*, 29(16). doi:10.1029/2001GL014130.

P. W. Boyd, R. Strzepek, F. Fu, and D. A. Hutchins (2010). Environmental control of open-ocean phytoplankton groups: Now and in the future. *Limnol. Oceanogr.*, 55(3): 1353–1376. doi: 10.4319/lo.2010.55.3.1353.

E. Broglio, M. Johansson, and P. R. Jonsson (2001). Trophic interaction between copepods and ciliates: effects of prey swimming behavior on predation risk. *Mar. Ecol. Prog. Ser.*, 220: 179–186.

U. Brose (2008). Complex food webs prevent competitive exclusion among producer species. *Proc. R. Soc. Lond. B*, 275(1650): 2507–2514. doi:10.1098/rspb.2008.0718.

J. Bruggeman and S. A. L. M. Kooijman (2007). A biodiversity-inspired approach to aquatic ecosystem modeling. *Limnol. Oceanogr.*, 52(4): 1533–1544.

K. O. Buesseler, A. N. Antia, M. Chen, et al. (2007). An assessment of the use of sediment traps for estimating upper ocean particle fluxes. *J. Mar. Res.*, 65(3): 345–416.

K. O. Buesseler and P. W. Boyd (2009). Shedding light on processes that control particle export and flux attenuation in the twilight zone of the open ocean. *Limnol. Oceanogr.*, 54(4): 1210–1232.

E. Buitenhuis, C. Le Quere, O. Aumont, et al. (2006). Biogeochemical fluxes through mesozooplankton. *Global Biogeochem. Cycles*, 20(2). doi:10.1029/2005GB002511.

E. J. Buskey (1998). Energetic costs of swarming behavior for the copepod *Dioithona oculata*. *Mar. Biol.*, 130(3): 425–431. doi:10.1007/s002270050263.

S. H. M. Butchart, M. Walpole, B. Collen, et al. (2010). Global biodiversity: Indicators of recent declines. *Science*, 328(5982): 1164–1168. doi:10.1126/science.1187512.

A. Calbet and E. Saiz (2005). The ciliate-copepod link in marine ecosystems. *Aquat. Microb. Ecol.*, 38(2): 157–167.

J. G. Canadell, C. Le Quere, M. R. Raupach, et al. (2007). Contributions to accelerating atmospheric CO_2 growth from economic activity, carbon intensity, and efficiency of natural sinks. *Proc. Natl. Acad. Sci. USA*, 104(47): 18 866–18 870. doi:10.1073/pnas.0702737104.

B. Cardinale, A. Ives, and P. Inchausti (2004). Effects of species diversity on the primary productivity of ecosystems: extending our spatial and temporal scales of inference. *Oikos*, 104(3): 437–450.

B. Cardinale, M. Palmer, and S. Collins (2002). Species diversity enhances ecosystem functioning through interspecific facilitation. *Nature*, 415(6870): 426–429.

B. J. Cardinale (2011). Biodiversity improves water quality through niche partitioning. *Nature*, 472(7341): 86–U113. doi:10.1038/nature09904.

B. J. Cardinale, H. Hillebrand, W. S. Harpole, K. Gross, and R. Ptacnik (2009). Separating the influence of resource 'availability' from resource 'imbalance' on productivity-diversity relationships. *Ecol. Lett.*, 12(6): 475–487. doi:10.1111/j.1461-0248.2009.01317.x.

B. J. Cardinale, K. L. Matulich, D. U. Hooper, et al. (2011). The functional role of producer diversity in ecosystems. *Am. J. Bot.*, 98(3): 572–592. doi:10.3732/ajb.1000364.

B. J. Cardinale, D. S. Srivastava, J. E. Duffy, et al. (2006). Effects of biodiversity on the functioning of trophic groups and ecosystems. *Nature*, 443(7114): 989–992. doi:10.1038/nature05202.

D. A. Caron and P. D. Countway (2009). Hypotheses on the role of the protistan rare biosphere in a changing world. *Aquat. Microb. Ecol.*, 57(3): 227–238. doi:10.3354/ame01352.

D. A. Caron and R. J. Gast (2010). Heterotrophic protists associated with sea ice. In D. N. Thomas and G. S. Dieckmann (eds.), *Sea ice*, pp. 327–356. Wiley-Blackwell, Oxford, 2 ed.

R. C. Carpenter (1986). Partitioning herbivory and its effects on coral reef algal communities. *Ecol. Monogr.*, 56(4): 345–364.

P. Cermeño, C. de Vargas, F. Abrantes, and P. G. Falkowski (2010). Phytoplankton biogeography and community stability in the ocean. *PLoS ONE*, 5(3): e10 037. doi:10.1371/journal.pone.0010037.

P. Cermeño, E. Marañon, D. Harbour, et al. (2008). Resource levels, allometric scaling of population abundance, and marine phytoplankton diversity. *Limnol. Oceanogr.*, 53(1): 312–318.

J. Chase, P. Abrams, J. Grover, et al. (2002). The interaction between predation and competition: a review and synthesis. *Ecol. Lett.*, 5(2): 302–315.

J. Chesson (1983). The estimation and analysis of preference and its relationship to foraging models. *Ecology*, 64(5): 1297–1304.

P. Chesson (2000). Mechanisms of maintenance of species diversity. *Annu. Rev. Ecol. Syst.*, 31: 343–366.

K. R. Clarke and R. M. Warwick (2001). *Change in marine communities: an approach to statistical analysis and interpretations*. PRIMER-E Ltd, Plymouth, 2 ed.

J. Comiso (2010). *Polar oceans from space*, *Atmospheric and Oceanographic Sciences Library*, vol. 41. Springer, New York, Dordrecht, Heidelberg, London.

J. Connell (1978). Diversity in tropical rain forests and coral reefs - high diversity of trees and corals is maintained only in a non-equilibrium state. *Science*, 199(4335): 1302–1310.

R. J. Conover (1968). Zooplankton—life in a nutritionally dilute environment. *Am. Zool.*, 8: 107–118.

K. Cottingham, B. Brown, and J. Lennon (2001). Biodiversity may regulate the temporal variability of ecological systems. *Ecol. Lett.*, 4(1): 72–85.

A. W. Decho (1988). How do harpacticoid grazing rates differ over a tidal cycle? Field verification using chlorophyll-pigment analyses. *Mar. Ecol. Prog. Ser.*, 45: 263–270.

W. R. DeMott and M. D. Watson (1991). Remote detection of algae by copepods: responses to algal size, odors and motility. *J. Plankton Res.*, 13(6): 1203–1222. doi:10.1093/plankt/13.6.1203.

N. V. Druzhkov, E. I. Druzhkova, and L. L. Kuznetsov (2001). The sea-ice algal community of seasonal pack ice in the southwestern Kara Sea in late winter. *Polar Biol.*, 24(1): 70–72.

J. Duffy and J. Stachowicz (2006). Why biodiversity is important to oceanography: potential roles of genetic, species, and trophic diversity in pelagic ecosystem processes. *Mar. Ecol. Prog. Ser.*, 311: 179–189.

E. G. Durbin and A. G. Durbin (1992). Effects of temperature and food abundance on grazing and short-term weight change in the marine copepod *Acartia hudsonica*. *Limnol. Oceanogr.*, 37(2): 361–378. doi:10.4319/lo.1992.37.2.0361.

S. Dutkiewicz, M. J. Follows, and J. G. Bragg (2009). Modeling the coupling of ocean ecology and biogeochemistry. *Global Biogeochem. Cycles*, 23: GB4017. doi:10.1029/2008GB003405.

H. Eicken (1992). The role of sea ice in structuring Antarctic ecosystems. *Polar Biol.*, 12(1): 3–13.

P. Falkowski, R. Scholes, E. Boyle, et al. (2000). The global carbon cycle: A test of our knowledge of Earth as a system. *Science*, 290(5490): 291–296.

M. Fasham, H. Ducklow, and S. McKelvie (1990). A nitrogen-based model of plankton dynamics in the oceanic mixed layer. *J. Mar. Res.*, 48(3): 591–639.

M. Fasham, J. Sarmiento, R. Slater, H. Ducklow, and R. Williams (1993). Ecosystem behavior at Bermuda Station-S and Ocean Weather Station India - A General-circulation model and observational analysis. *Global Biogeochem. Cycles*, 7(2): 379–415.

M. J. R. Fasham and G. T. Evans (2000). Advances in ecosystem modelling within JGOFS. In R. B. Hanson, H. W. Ducklow, and J. G. Field (eds.), *The Changing Ocean Carbon Cycle*, pp. 417–446. Cambridge University Press.

T. Fenchel (1980). Relation between particle size selection and clearance in suspension-feeding ciliates. *Limnol. Oceanogr.*, 25(4): 733–738. doi:10.4319/lo.1980.25.4.0733.

T. Fenchel (1982). Ecology of heterotrophic microflagellates. III. Adaptations to heterogeneous environments. *Mar. Ecol. Prog. Ser.*, 9: 25–33. doi:10.3354/meps009025.

T. Fenchel (2008). The microbial loop-25 years later. *J. Exp. Mar. Biol. Ecol.*, 366(1-2): 99–103. doi:10.1016/j.jembe.2008.07.013.

C. Field, M. Behrenfeld, J. Randerson, and P. Falkowski (1998). Primary production of the biosphere: Integrating terrestrial and oceanic components. *Science*, 281(5374): 237–240.

Z. V. Finkel, J. Beardall, K. J. Flynn, et al. (2010). Phytoplankton in a changing world: cell size and elemental stoichiometry. *J. Plankton Res.*, 32(1): 119–137. doi:10.1093/plankt/fbp098.

K. J. Flynn and A. Mitra (2009). Building the "perfect beast": modelling mixotrophic plankton. *J. Plankton Res.*, 31(9): 965–992. doi:10.1093/plankt/fbp044.

M. J. Follows and S. Dutkiewicz (2011). Modeling diverse communities of marine microbes. *Annu. Rev. Mar. Sci.*, 3: 427–451. doi:10.1146/annurev-marine-120709-142848.

M. J. Follows, S. Dutkiewicz, S. Grant, and S. W. Chisholm (2007). Emergent biogeography of microbial communities in a model ocean. *Science*, 315: 1843–1846.

J. Fox (2005). Interpreting the 'selection effect' of biodiversity on ecosystem function. *Ecol. Lett.*, 8(8): 846–856. doi:10.1111/j.1461-0248.2005.00795.x.

G. Frankenstein and R. Garner (1967). Equations for determining the brine volume of sea ice from -0.5° to -22.9°C. *J. Glaciol.*, 6(48): 943–944.

P. Franks, J. Wroblewski, and G. Flierl (1986). Behavior of a simple plankton model with food-level acclimation by herbivores. *Mar. Biol.*, 91(1): 121–129.

C. Friedrich and J. Hendelberg (2001). On the ecology of Acoela living in the Arctic sea ice. *Belg. J. Zool.*, 131(Supplement 1): 213–216.

B. W. Frost (1972). Effects of size and concentration of food particles on the feeding behaviour of the marine planktonic copepod *Calanus pacificus*. *Limnol. Oceanogr.*, 17(6): 805–815.

B. W. Frost (1975). A threshold feeding behavior in *Calanus pacificus*. *Limnol. Oceanogr.*, 20: 263–266. doi:10.4319/lo.1975.20.2.0263.

H. L. Fuchs and P. J. S. Franks (2010). Plankton community properties determined by nutrients and size-selective feeding. *Mar. Ecol. Prog. Ser.*, 413: 1–15. doi:10.3354/meps08716.

K. Fujii, C. S. Holling, and P. M. Mace (1986). A simple generalized model of attack by predators and parasites. *Ecol. Res.*, 1(2): 141–156. doi:10.1007/BF02347017.

G. Fussmann and B. Blasius (2005). Community response to enrichment is highly sensitive to model structure. *Biol. Lett.*, 1(1): 9–12. doi:10.1098/rsbl.2004.0246.

G. Fussmann, G. Weithoff, and T. Yoshida (2005a). A direct, experimental test of resource vs. consumer dependence. *Ecology*, 86(11): 2924–2930.

G. F. Fussmann, G. Weithoff, and T. Yoshida (2005b). A direct, experimental test of resource vs. consumer dependence. *Ecology*, 86(11): 2924–2930. doi:10.1890/04-1107.

L. Gamfeldt, H. Hillebrand, and P. Jonsson (2005). Species richness changes across two trophic levels simultaneously affect prey and consumer biomass. *Ecol. Lett.*, 8(7): 696–703. doi:10.1111/j.1461-0248.2005.00765.x.

R. Garcia, F. Moss, A. Nihongi, et al. (2007). Optimal foraging by zooplankton within patches: the case of *Daphnia*. *Math. Biosci.*, 207(2): 165–88. doi:10.1016/j.mbs.2006.11.014.

D. L. Garrison and K. R. Buck (1986). Organism losses during ice melting: a serious bias in sea ice community studies. *Polar Biol.*, 6(4): 237–239. doi:10.1007/BF00443401.

G. Gause (1934). *The struggle for existence*. Williams and Wilkins, Baltimore.

W. Gentleman, A. Leising, B. Frost, S. Strom, and J. Murray (2003). Functional responses for zooplankton feeding on multiple resources: a review of assumptions and biological dynamics. *Deep-Sea Res. II*, 50: 2847–2875.

W. C. Gentleman and A. B. Neuheimer (2008). Functional responses and ecosystem dynamics: how clearance rates explain the influence of satiation, food-limitation and acclimation. *J. Plankton Res.*, 30(11): 1215–1231. doi:10.1093/plankt/fbn078.

J. Gerritsen, K. G. Porter, and J. R. Strickler (1988). Not by sieving alone: observations of suspension feeding in *Daphnia*. *Bull. Mar. Sci.*, 43(3): 366–376.

J. Gerritsen and J. R. Strickler (1977). Encounter probabilities and community structure in zooplankton: a mathematical model. *J. Fish. Res. Board Can.*, 34(1): 73–82.

C. Gill and S. Poulet (1988). Responses of copepods to dissolved free amino-acids. *Mar. Ecol. Prog. Ser.*, 43(3): 269–276.

I. Gismervik (2005). Numerical and functional responses of choreo- and oligotrich planktonic ciliates. *Aquat. Microb. Ecol.*, 40(2): 163–173. doi:10.3354/ame040163.

I. Gismervik and T. Andersen (1997). Prey switching by *Acartia clausi*: experimental evidence and implications of intraguild predation assessed by a model. *Mar. Ecol. Prog. Ser.*, 157: 247–259.

M. Gosselin, M. Levasseur, P. A. Wheeler, R. A. Horner, and B. C. Booth (1997). New measurements of phytoplankton and ice algal production in the Arctic Ocean. *Deep-Sea Res. II*, 44(8): 1623–1644. doi:10.1016/S0967-0645(97)00054-4.

L. Göthlich and A. Oschlies (subm.). Phytoplankton niche generation by stoichiometric plasticity. submitted.

R. Gradinger (1995). Climate change and biological oceanography of the Arctic Ocean. *Phil. Trans. R. Soc. Lond. A*, 352(1699): 277–286. doi:10.1098/rsta.1995.0070.

R. Gradinger (1999a). Integrated abundance and biomass of sympagic meiofauna in Arctic and Antarctic pack ice. *Polar Biol.*, 22(3): 169–177. doi:10.1007/s003000050407.

R. Gradinger (1999b). Vertical fine structure of the biomass and composition of algal communities in Arctic pack ice. *Mar. Biol.*, 133(4): 745–754. doi:10.1007/s002270050516.

R. Gradinger, C. Friedrich, and M. Spindler (1999). Abundance, biomass and composition of the sea ice biota of the Greenland Sea pack ice. *Deep-Sea Res. II*, 46(6-7): 1457–1472. doi:10.1016/S0967-0645(99)00030-2.

R. R. Gradinger, K. Meiners, G. Plumley, Q. Zhang, and B. A. Bluhm (2005). Abundance and composition of the sea-ice meiofauna in off-shore pack ice of the Beaufort Gyre in summer 2002 and 2003. *Polar Biol.*, 28(3): 171–181. doi:10.1007/s00300-004-0674-5.

D. Gravel, T. Bell, C. Barbera, et al. (2011). Experimental niche evolution alters the strength of the diversity-productivity relationship. *Nature*, 469(7328): 89–92. doi:10.1038/nature09592.

K. Gross and B. J. Cardinale (2007). Does species richness drive community production or vice versa? Reconciling historical and contemporary paradigms in competitive communities. *Am. Nat.*, 170(2): 207–220.

T. Gross, A. M. Edwards, and U. Feudel (2009). The invisible niche: Weakly density-dependent mortality and the coexistence of species. *J. Theor. Biol.*, 258(1): 148–155. doi:10.1016/j.jtbi.2009.01.018.

A. Hammer and J. Pitchford (2005). The role of mixotrophy in plankton bloom dynamics, and the consequences for productivity. *ICES J. mar. Sci.*, 62(5): 833–840. doi:10.1016/j.icesjms.2005.03.001.

B. Hansen, P. K. Bjørnsen, and P. J. Hansen (1994). The size ratio between planktonic predators and their prey. *Limnol. Oceanogr.*, 39(2): 395–403.

P. J. Hansen (1992). Prey size selection, feeding rates and growth dynamics of heterotrophic dinoflagellates with special emphasis on *Gyrodinium spirale*. *Mar. Biol.*, 114: 327–334. doi: 10.1007/BF00349535.

P. J. Hansen, P. K. Bjørnsen, and B. W. Hansen (1997). Zooplankton grazing and growth: Scaling within the 2-2,000-μm body size range. *Limnol. Oceanogr.*, 42(4): 687–704.

G. Hardin (1960). The competitive exclusion principle. *Science*, 131: 1292–1297.

R. P. Hassett and M. R. Landry (1983). Effects of food-level acclimation on digestive enzyme activities and feeding behavior of *Calanus pacificus*. *Mar. Biol.*, 75(1): 47–55. doi:10.1007/BF00392629.

H. Hillebrand, C.-D. Dürselen, D. Kirschtel, U. Pollingher, and T. Zohary (1999). Biovolume calculation for pelagic and benthic microalgae. *J. Phycol.*, 35(2): 403–424.

H. Hillebrand, D. S. Gruner, E. T. Borer, et al. (2007). Consumer versus resource control of producer diversity depends on ecosystem type and producer community structure. *Proc. Natl. Acad. Sci. USA*, 104(26): 10 904–10 909. doi:10.1073/pnas.0701918104.

K. M. Hilligsøe, K. Richardson, J. Bendtsen, et al. (2011). Linking phytoplankton community size composition with temperature, plankton food web structure and sea-air CO_2 flux. *Deep-Sea Res. I*, 58(8): 826–838. doi:10.1016/j.dsr.2011.06.004.

C. S. Holling (1959a). The components of predation as revealed by a study of small-mammal predation of the European pine sawfly. *Can. Ent.*, 91: 385–398.

C. S. Holling (1959b). Some characteristics of simple types of predation and parasitism. *Can. Ent.*, 91: 385–398.

C. S. Holling (1973). Resilience and stability of ecological systems. *Annu. Rev. Ecol. Syst.*, 4: 1–23. doi:10.1146/annurev.es.04.110173.000245.

D. Hooper, F. Chapin, J. Ewel, et al. (2005). Effects of biodiversity on ecosystem functioning: A consensus of current knowledge. *Ecol. Monogr.*, 75(1): 3–35.

R. Horner, S. F. Ackley, G. S. Dieckmann, et al. (1992). Ecology of sea ice biota. 1. Habitat, terminology, and methodology. *Polar Biol.*, 12(3-4): 417–427. doi:10.1007/BF00243113.

S. Hubbell (2001). *The Unified Neutral Theory of Biodiversity and Biogeography*. Monographs in Population Biology. Princeton University Press, Princeton.

J. Huisman, R. Jonker, C. Zonneveld, and F. Weissing (1999). Competition for light between phytoplankton species: Experimental tests of mechanistic theory. *Ecology*, 80(1): 211–222.

J. Huisman and F. Weissing (1999). Biodiversity of plankton by species oscillations and chaos generated by multispecies competition. *Nature*, 402: 407–410.

M. Huston (1997). Hidden treatments in ecological experiments: Re-evaluating the ecosystem function of biodiversity. *Oecologia*, 110(4): 449–460.

G. E. Hutchinson (1957). Concluding remarks. *Cold Spring Harbor Symposia on Quantitative Biology*, 22: 415–427.

G. E. Hutchinson (1961). The paradox of the plankton. *Am. Nat.*, 95(882): 137–145.

V. Hutson (1984). Predator mediated coexistence with a switching predator. *Math. Biosci.*, 68: 233–246.

X. Irigoien, J. Huisman, and R. Harris (2004). Global biodiversity patterns of marine phytoplankton and zooplankton. *Nature*, 429(6994): 863–867. doi:10.1038/nature02593.

F. Isbell, V. Calcagno, A. Hector, et al. (2011). High plant diversity is needed to maintain ecosystem services. *Nature*, 477: 199–202. doi:10.1038/nature10282.

A. R. Ives and S. R. Carpenter (2007). Stability and diversity of ecosystems. *Science*, 317(5834): 58–62. doi:10.1126/science.1133258.

V. S. Ivlev (1961). *Experimental ecology of the feeding of fishes*, chap. 3, pp. 19–40. Yale University Press, New Haven.

G. A. Jackson and J. Checkley, David M. (2011). Particle size distributions in the upper 100 m water column and their implications for animal feeding in the plankton. *Deep-Sea Res. I*, 58(3): 283–297. doi:10.1016/j.dsr.2010.12.008.

H. Jakobsen (2002). Escape of protists in predator-generated feeding currents. *Aquat. Microb. Ecol.*, 26(3): 271–281.

J. Jeschke, M. Kopp, and R. Tollrian (2002). Predator functional responses: Discriminating between handling and digesting prey. *Ecol. Monogr.*, 72(1): 95–112.

J. Jeschke, M. Kopp, and R. Tollrian (2004). Consumer-food systems: why type I functional responses are exclusive to filter feeders. *Biol. Rev.*, 79(2): 337–349. doi:10.1017/S1464793103006286.

P. R. Jonsson and P. Tiselius (1990). Feeding behaviour, prey detection and capture efficiency of the copepod *Acartia tonsa* feeding on planktonic ciliates. *Mar. Ecol. Prog. Ser.*, 60: 35–44.

C. B. Jørgensen (1983). Fluid mechanical aspects of suspension feeding. *Mar. Ecol. Prog. Ser.*, 11: 89–103. doi:10.3354/meps011089.

C. Jost (2000). Predator-prey theory: hidden twins in ecology and microbiology. *Oikos*, 90(1): 202–208. doi:10.1034/j.1600-0706.2000.900125.x.

R. Kiko, M. Kramer, M. Spindler, and H. Wägele (2008). *Tergipes antarcticus* (Gastropoda, Nudibranchia): distribution, life cycle, morphology, anatomy and adaptation of the first mollusc known to live in Antarctic sea ice. *Polar Biol.*, 31(11): 1383–1395. doi:10.1007/s00300-008-0478-0.

T. Kiørboe (2008). *A mechanistic approach to plankton ecology*. Princeton University Press.

T. Kiørboe (2011). How zooplankton feed: mechanisms, traits and trade-offs. *Biol. Rev.*, 86(2): 311–339. doi:10.1111/j.1469-185X.2010.00148.x.

T. Kiørboe, A. Andersen, V. J. Langlois, H. H. Jakobsen, and T. Bohr (2009). Mechanisms and feasibility of prey capture in ambush-feeding zooplankton. *Proc. Natl. Acad. Sci. USA*, 106(30): 12 394–12 399. doi:10.1073/pnas.0903350106.

T. Kiørboe, F. Møhlenberg, and K. Hamburger (1985). Bioenergetics of the planktonic copepod *Acartia tonsa*: Relation between feeding, egg production and respiration, and composition of specific dynamic action. *Mar. Ecol. Prog. Ser.*, 26: 85–97. doi:10.3354/meps026085.

T. Kiørboe, F. Møhlenberg, and H. Nicolajsen (1982). Ingestion rate and gut clearance in the planktonic copepod *Centropages hamatus* (Lilleborg) in relation to food concentration and temperature. *Ophelia*, 21(2): 181–194.

T. Kiørboe, E. Saiz, and M. Viitasalo (1996). Prey switching behaviour in the planktonic copepod *Acartia tonsa*. *Mar. Ecol. Prog. Ser.*, 143: 65–75.

M. A. R. Koehl and J. R. Strickler (1981). Copepod feeding currents: Food capture at low Reynolds number. *Limnol. Oceanogr.*, 26(6): 1062–1073. doi:10.4319/lo.1981.26.6.1062.

M. Kramer, U. Struck, A. Schukat, R. Kiko, and I. Werner (subm.). Trophic positions of Arctic and Antarctic sympagic meiofauna and its role in cryo-pelagic coupling identified by stable isotopes and fatty acids. submitted.

M. Kramer, K. M. Swadling, K. M. Meiners, et al. (2011). Antarctic sympagic meiofauna in winter: comparing diversity, abundance and biomass between perennially and seasonally ice-covered regions. *Deep-Sea Res. II*, 58(9-10): 1062–1074. doi:10.1016/j.dsr2.2010.10.029.

P. Kratina, M. Vos, A. Bateman, and B. R. Anholt (2009). Functional responses modified by predator density. *Oecologia*, 159(2): 425–433. doi:10.1007/s00442-008-1225-5.

C. Krembs, R. Gradinger, and M. Spindler (2000). Implications of brine channel geometry and surface area for the interaction of sympagic organisms in Arctic sea ice. *J. Exp. Mar. Biol. Ecol.*, 243(1): 55–80. doi:10.1016/S0022-0981(99)00111-2.

R. K. Lam and B. W. Frost (1976). Model of copepod filtering response to changes in size and concentration of food. *Limnol. Oceanogr.*, 21(4): 490–500. doi:10.4319/lo.1976.21.4.0490.

M. Landry (1981). Switching between herbivory and carnivory by the planktonic marine copepod *Calanus pacificus*. *Mar. Biol.*, 65(1): 77–82.

M. R. Landry, R. P. Hassett, V. Fagerness, J. Downs, and C. J. Lorenzen (1984). Effect of food acclimation on assimilation efficiency of *Calanus pacificus*. *Limnol. Oceanogr.*, 29(2): 361–364. doi:10.4319/lo.1984.29.2.0361.

M. R. Landry, M. E. Ondrusek, S. J. Tanner, et al. (2000). Biological response to iron fertilization in the eastern equatorial Pacific (IronEx II). I. Microplankton community abundances and biomass. *Mar. Ecol. Prog. Ser.*, 201: 27–42. doi:10.3354/meps201027.

I. Laurion, S. Demers, and A. F. Vézina (1995). The microbial food web associated with the ice algal assemblage: biomass and bacterivory of nanoflagellate protozoans in Resolute Passage (High Canadian Arctic). *Mar. Ecol. Prog. Ser.*, 120: 77–87. doi:10.3354/meps120077.

C. Le Quéré, S. Harrison, I. Prentice, et al. (2005). Ecosystem dynamics based on plankton functional types for global ocean biogeochemistry models. *Global Change Biol.*, 11(11): 2016–2040. doi:10.1111/j.1365-2468.2005.01004.x.

L. Legendre, S. F. Ackley, G. S. Dieckmann, et al. (1992). Ecology of sea ice biota. 2. Global significance. *Polar Biol.*, 12(3-4): 429–444. doi:10.1007/BF00243114.

J. T. Lehman (1976). The filter-feeder as an optimal forager, and the predicted shapes of feeding curves. *Limnol. Oceanogr.*, 21(4): 501–516. doi:10.4319/lo.1976.21.4.0501.

M. Leibold (1996). A graphical model of keystone predators in food webs: Trophic regulation of abundance, incidence, and diversity patterns in communities. *Am. Nat.*, 147(5): 784–812.

M. Leibold, M. Holyoak, N. Mouquet, et al. (2004). The metacommunity concept: A framework for multi-scale community ecology. *Ecol. Lett.*, 7(7): 601–613. doi:10.1111/j.1461-0248.2004.00608.x.

E. J. Lessard and M. C. Murrell (1998). Microzooplankton herbivory and phytoplankton growth in the northwestern Sargasso Sea. *Aquat. Microb. Ecol.*, 16(2): 173–188. doi:10.3354/ame016173.

S. A. Levin (1970). Community equilibria and stability, and an extension of the competitive exclusion principle. *Am. Nat.*, 104: 413–423.

S. L. Lima (1998). Stress and decision making under the risk of predation: recent developments from behavioral, reproductive, and ecological perspectives. In A. P. Möller, M. Millinski, and P. J. B. Slater (eds.), *Stress and behavior*, *Advances in the Study of Behavior*, vol. 27, pp. 215–290. Academic Press, San Diego, London. doi:10.1016/S0065-3454(08)60366-6.

E. Litchman, P. d. T. Pinto, C. A. Klausmeier, M. K. Thomas, and K. Yoshiyama (2010). Linking traits to species diversity and community structure in phytoplankton. *Hydrobiol.*, 653(1): 15–28. doi:10.1007/s10750-010-0341-5.

K. Lochte, H. Ducklow, M. Fasham, and C. Stienen (1993). Plankton succession and carbon cycling at 47°N 20°W during the JGOFS North-Atlantic Bloom Experiment. *Deep-Sea Res. II*, 40(1-2): 91–114.

M. L. Longhi and B. E. Beisner (2010). Patterns in taxonomic and functional diversity of lake phytoplankton. *Freshw. Biol.*, 55(6): 1349–1366. doi:10.1111/j.1365-2427.2009.02359.x.

D. J. Lonsdale, D. R. Heinle, and C. Siegfried (1979). Carnivorous feeding behavior of the adult calanoid copepod *Acartia tonsa* Dana. *J. Exp. Mar. Biol. Ecol.*, 36(3): 235–248. doi:10.1016/0022-0981(79)90119-9.

M. Loreau (1998). Biodiversity and ecosystem functioning: A mechanistic model. *Proc. Natl. Acad. Sci. USA*, 95(10): 5632–5636.

M. Loreau and A. Hector (2001). Partitioning selection and complementarity in biodiversity experiments. *Nature*, 412(6842): 72–76.

M. Loreau, S. Naeem, P. Inchausti, et al. (2001). Ecology - biodiversity and ecosystem functioning: Current knowledge and future challenges. *Science*, 294(5543): 804–808.

R. MacArthur and E. Wilson (1967). *The theory of island biogeography*. Princeton Univ Pr.

M. Manizza, E. T. Buitenhuis, and C. Le Quere (2010). Sensitivity of global ocean biogeochemical dynamics to ecosystem structure in a future climate. *Geophys. Res. Lett.*, 37. doi: 10.1029/2010GL043360.

B. F. J. Manly, P. Miller, and L. M. Cook (1972). Analysis of a selective predation experiment. *Am. Nat.*, 106(952): 719–736.

R. Margalef (1978). Life-forms of phytoplankton as survival alternatives in an unstable environment. *Oceanol. Acta*, 1: 493–509.

P. Mariani and A. W. Visser (2010). Optimization and emergence in marine ecosystem models. *Prog. Oceanogr.*, 84: 89–92.

M. Marquardt (2010). *Studies on sympagic meiofauna in fast and pack ice in the southeastern Beaufort Sea (Canadian Arctic)*. Diploma thesis, Institut für Polarökologie, Christian-Albrechts-Universität zu Kiel.

M. Marquardt, M. Kramer, G. Carnat, and I. Werner (2011). Vertical distribution of sympagic meiofauna in sea ice in the Canadian Beaufort Sea. *Polar Biol.*, in press. doi:10.1007/s00300-011-1078-y.

K. McCann (2000). The diversity-stability debate. *Nature*, 405(6783): 228–233.

E. McCauley and F. Briand (1979). Zooplankton grazing and phytoplankton species richness - Field-tests of the predation hypothesis. *Limnol. Oceanogr.*, 24(2): 243–252.

B. McGill, B. Enquist, E. Weiher, and M. Westoby (2006). Rebuilding community ecology from functional traits. *Trends Ecol. Evol.*, 21(4): 178–185. doi:10.1016/j.tree.2006.02.002.

J. McGrady-Steed, P. Harris, and P. Morin (1997). Biodiversity regulates ecosystem predictability. *Nature*, 390(6656): 162–165.

K. M. Meiners, L. Norman, M. A. Granskog, et al. (2011). Physico-ecobiogeochemistry of East Antarctic pack ice during the winter-spring transition. *Deep-Sea Res. II*, 58(9-10): 1172–1181. doi:10.1016/j.dsr2.2010.10.033.

S. Menden-Deuer and E. J. Lessard (2000). Carbon to volume relationships for dinoflagellates, diatoms, and other protist plankton. *Limnol. Oceanogr.*, 45(3): 569–579.

A. Merico, J. Bruggeman, and K. Wirtz (2009). A trait-based approach for downscaling complexity in plankton ecosystem models. *Ecol. Model.*, 220(21): 3001–3010. doi: 10.1016/j.ecolmodel.2009.05.005.

C. Metz and S. B. Schnack-Schiel (1995). Observations on carnivorous feeding in Antarctic calanoid copepods. *Mar. Ecol. Prog. Ser.*, 129: 71–75. doi:10.3354/meps129071.

B. Meyer, L. Auerswald, V. Siegel, et al. (2010). Seasonal variation in body composition, metabolic activity, feeding, and growth of adult krill *Euphausia superba* in the Lazarev Sea. *Mar. Ecol. Prog. Ser.*, 398: 1–18. doi:10.3354/meps08371.

C. Michel, T. G. Nielsen, C. Nozais, and M. Gosselin (2002). Significance of sedimentation and grazing by ice micro- and meiofauna for carbon cycling in annual sea ice (northern Baffin Bay). *Aquat. Microb. Ecol.*, 30(1): 57–68. doi:10.3354/ame030057.

T. Miller, J. Burns, P. Munguia, et al. (2005). A critical review of twenty years' use of the resource-ratio theory. *Am. Nat.*, 165(4): 439–448.

C. L. Moloney and J. G. Field (1989). General allometric equations for rates of nutrient uptake, ingestion, and respiration in plankton organisms. *Limnol. Oceanogr.*, 34(7): 1290–1299.

F. M. Monteiro, M. J. Follows, and S. Dutkiewicz (2010). Distribution of diverse nitrogen fixers in the global ocean. *Global Biogeochem. Cycles*, 24: GB3017. doi:10.1029/2009GB003731.

X. A. G. Moran, A. Lopez-Urrutia, A. Calvo-Diaz, and W. K. W. Li (2010). Increasing importance of small phytoplankton in a warmer ocean. *Global Change Biol.*, 16(3): 1137–1144. doi: 10.1111/j.1365-2486.2009.01960.x.

A. Morozov, E. Arashkevich, M. Reigstad, and S. Falk-Petersen (2008). Influence of spatial heterogeneity on the type of zooplankton functional response: A study based on field observations. *Deep-Sea Res. II*, 55(20-21): 2285–2291. doi:10.1016/j.dsr2.2008.05.008.

A. Y. Morozov (2010). Emergence of Holling type III zooplankton functional response: Bringing together field evidence and mathematical modelling. *J. Theor. Biol.*, 265(1): 45–54. doi: 10.1016/j.jtbi.2010.04.016.

B. Mouriño-Carballido and S. Neuer (2008). Regional differences in the role of eddy pumping in the North Atlantic Subtropical Gyre – Historical conundrums revisited. *Oceanography*, 21(2): 52–61.

C. J. Mundy, M. Gosselin, J. Ehn, et al. (2011). Characteristics of two distinct high-light acclimated algal communities during advanced stages of sea ice melt. *Polar Biol.*, p. 18 pp. doi:10.1007/s00300-011-0998-x.

W. Murdoch, S. Avery, and M. Smyth (1975). Switching in predatory fish. *Ecology*, 56(5): 1094–1105.

W. W. Murdoch (1969). Switching in general predators. Experiments on predator specificity and stability of prey populations. *Ecol. Monogr.*, 39: 335–354.

W. W. Murdoch and A. Oaten (1975). Predation and population stability. *Adv. Ecol. Res.*, 9: 1–131.

M. Myerscough, M. Darwen, and W. Hogarth (1996). Stability, persistence and structural stability in a classical predator-prey model. *Ecol. Model.*, 89(1-3): 31–42.

S. Naeem and S. Li (1997). Biodiversity enhances ecosystem reliability. *Nature*, 390(6659): 507–509.

J. Norberg (2004). Biodiversity and ecosystem functioning: A complex adaptive systems approach. *Limnol. Oceanogr.*, 49(4): 1269–1277.

J. Norberg, D. Swaney, J. Dushoff, et al. (2001). Phenotypic diversity and ecosystem functioning in changing environments: A theoretical framework. *Proc. Natl. Acad. Sci. USA*, 98(20): 11 376–11 381.

C. Nozais, M. Gosselin, C. Michel, and G. Tita (2001). Abundance, biomass, composition and grazing impact of the sea-ice meiofauna in the North Water, northern Baffin Bay. *Mar. Ecol. Prog. Ser.*, 217: 235–250. doi:10.3354/meps217235.

M. Pace, J. Cole, S. Carpenter, and J. Kitchell (1999). Trophic cascades revealed in diverse ecosystems. *Trends Ecol. Evol.*, 14(12): 483–488.

G.-A. Paffenhöfer (1984). Food ingestion by the marine planktonic copepod *Paracalanus* in relation to abundance and size distribution of food. *Mar. Biol.*, 80: 323–333.

G.-A. Paffenhöfer and K. D. Lewis (1990). Perceptive performance and feeding behavior of calanoid copepods. *J. Plankton Res.*, 12(5): 933–946. doi:10.1093/plankt/12.5.933.

G.-A. Paffenhöfer, B. F. Sherr, and E. B. Sherr (2007). From small scales to the big picture: persistence mechanisms of planktonic grazers in the oligotrophic ocean. *Mar. Ecol.*, 28(2): 243–253. doi: 10.1111/j.1439-0485.2007.00162.x.

M. Pahlow and A. E. F. Prowe (2010). Model of zooplankton optimal current feeding. *Mar. Ecol. Prog. Ser.*, 403: 129–144. doi:10.3354/meps08466.

T. R. Parsons, R. J. LeBrasseur, and J. D. Fulton (1967). Some observations on the dependence of zooplankton grazing on the size and concentration of phytoplankton blooms. *J. Oceanogr. Soc. Japan*, 23: 10–17.

J. Passarge, S. Hol, M. Escher, and J. Huisman (2006). Competition for nutrients and light: Stable coexistence, alternative stable states, or competitive exclusion? *Ecol. Monogr.*, 76(1): 57–72.

O. Petchey and K. Gaston (2006). Functional diversity: back to basics and looking forward. *Ecol. Lett.*, 9(6): 741–758. doi:10.1111/j.1461-0248.2006.00924.x.

O. Petchey, E. O'Gorman, and D. Flynn (2010). A functional guide to functional diversity measures. In S. Naeem, D. Bunker, A. Hector, M. Loreau, and C. Perrings (eds.), *Biodiversity, ecosystem functioning, and human wellbeing: an ecological and economic perspective*, chap. 4, pp. 49–59. Oxford Univ Press.

F. Peters (1994). Prediction of planktonic protistan grazing rates. *Limnol. Oceanogr.*, 39(1): 195–206.

S. Piraino, B. A. Bluhm, R. Gradinger, and F. Boero (2008). *Sympagohydra tuuli* gen. nov. and sp. nov. (Cnidaria: Hydrozoa) a cool hydroid from the Arctic sea ice. *J. Mar. Biol. Assoc. U. K.*, 88(8): 1637–1641. doi:10.1017/S0025315408002166.

L. Pomeroy (1974). Oceans food web, a changing paradigm. *BioScience*, 24(9): 499–504.

L. Pomeroy and W. Wiebe (2001). Temperature and substrates as interactive limiting factors for marine heterotrophic bacteria. *Aquat. Microb. Ecol.*, 23(2): 187–204.

M. Poulin, N. Daugbjerg, R. Gradinger, et al. (2011). The pan-Arctic biodiversity of marine pelagic and sea-ice unicellular eukaryotes: A first-attempt assessment. *Mar. Biodivers.*, 41(1): 13–28. doi: 10.1007/s12526-010-0058-8.

H. Price and G. Paffenhöfer (1986). Effects of concentration on the feeding of a marine copepod in algal monocultures and mixtures. *J. Plankton Res.*, 8(1): 119–128.

A. E. F. Prowe, M. Pahlow, S. Dutkiewicz, M. Follows, and A. Oschlies (subm.). Top-down control of marine phytoplankton diversity in a global ecosystem model. submitted.

R. Ptacnik, S. D. Moorthi, and H. Hillebrand (2010). Hutchinson reversed, or why there need to be so many species. *Adv. Ecol. Res.*, 43: 1–43. doi:10.1016/S0065-2504(10)43001-9.

R. Ptacnik, A. G. Solimini, T. Andersen, et al. (2008). Diversity predicts stability and resource use efficiency in natural phytoplankton communities. *Proc. Natl. Acad. Sci. USA*, 105(13): 5134–5138. doi:10.1073/pnas.0708328105.

G. H. Pyke (1984). Optimal foraging theory: A critical review. *Annu. Rev. Ecol. Syst.*, 15: 523–575. doi:10.1146/annurev.es.15.110184.002515.

T. N. Ratkova and P. Wassmann (2005). Sea ice algae in the White and Barents seas: composition and origin. *Polar Res.*, 24(1-2): 95–110. doi:10.1111/j.1751-8369.2005.tb00143.x.

A. Richardson and D. Schoeman (2004). Climate impact on plankton ecosystems in the Northeast Atlantic. *Science*, 305(5690): 1609–1612. doi:10.1126/science.1100958.

U. Riebesell, A. Körtzinger, and A. Oschlies (2009). Sensitivities of marine carbon fluxes to ocean change. *Proc. Natl. Acad. Sci. USA*, 106(49): 20 602–20 609. doi:10.1073/pnas.0813291106.

H. U. Riisgård (2007). Biomechanics and energy cost of the amphipod *Corophium volutator* filter-pump. *Biol. Bull.*, 212(2): 104–114. doi:10.2307/25066588.

G. C. Rollwagen Bollens and D. L. Penry (2003). Feeding dynamics of *Acartia* spp. copepods in a large, temperate estuary (San Francisco Bay, CA). *Mar. Ecol. Prog. Ser.*, 257: 139–158. doi: 10.3354/meps257139.

B. Rost, I. Zondervan, and D. Wolf-Gladrow (2008). Sensitivity of phytoplankton to future changes in ocean carbonate chemistry: current knowledge, contradictions and research directions. *Mar. Ecol. Prog. Ser.*, 373: 227–237. doi:10.3354/meps07776.

K. O. Rothhaupt (1990). Differences in particle size-dependent feeding efficiencies of closely related rotifer species. *Limnol. Oceanogr.*, 35(1): 16–23.

S. Roy and Y. Chattopadhyay (2007). Towards a resolution of 'the paradox of the plankton': A brief overview of proposed mechanisms. *Ecol. Complex.*, 4: 26–33.

E. Saiz and T. Kiørboe (1995). Predatory and suspension feeding of the copepod *Acartia tonsa* in turbulent environments. *Mar. Ecol. Prog. Ser.*, 122: 147–158.

J. Sarmiento, R. Slater, R. Barber, et al. (2004). Response of ocean ecosystems to climate warming. *Global Biogeochem. Cycles*, 18(3). doi:10.1029/2003GB002134.

O. Sarnelle (2005). Daphnia as keystone predators: effects on phytoplankton diversity and grazing resistance. *J. Plankton Res.*, 27(12): 1229–1238. doi:10.1093/plank/fbi086.

V. M. Savage, C. T. Webb, and J. Norberg (2007). A general multi-trait-based framework for studying the effects of biodiversity on ecosystem functioning. *J. Theor. Biol.*, 247(2): 213–229. doi: 10.1016/j.jtbi.2007.03.007.

M. Schartau and A. Oschlies (2003). Simultaneous data-based optimization of a 1D-ecosystem model at three locations in the North Atlantic: Part II - Standing stocks and nitrogen fluxes. *J. Mar. Res.*, 61(6): 795–821.

A. Schmidtke, U. Gaedke, and G. Weithoff (2010). A mechanistic basis for underyielding in phytoplankton communities. *Ecology*, 91(1): 212–221.

S. B. Schnack-Schiel, D. Thomas, G. S. Dieckmann, et al. (1995). Life cycle strategy of the Antarctic calanoid copepod *Stephos longipes*. *Prog. Oceanogr.*, 36(1): 45–75.

T. Schoener (1988). The ecological niche. In J. Cherrett (ed.), *Ecological Concepts: the Contribution of Ecology to an Understand of the Natural World*, chap. 4, pp. 79–113. Oxford Blackwell Scientific.

E. Schulze and H. Mooney (1993). *Biodiversity and ecosystem function*. Springer-Verlag, New York, USA.

C. Shannon and W. Weaver (1949). *The mathematical theory of communication*. University of Illinois Press.

E. Sherr and B. Sherr (2002). Significance of predation by protists in aquatic microbial food webs. *Anton. Leeuw. Int. J. G.*, 81(1-4): 293–308.

E. B. Sherr and B. F. Sherr (1993). Protistan grazing rates via uptake of fluorescently labeled prey. In P. F. Kemp, B. F. Sherr, E. B. Sherr, and J. J. Cole (eds.), *Handbook of methods in aquatic microbial ecology*, pp. 695–701. Lewis Publishers, Boca Raton.

J. Shurin, D. Gruner, and H. Hillebrand (2006). All wet or dried up? real differences between aquatic and terrestrial food webs. *Proc. R. Soc. Lond. B*, 273(1582): 1–9. doi:10.1098/rspb.2005.3377.

S. Siebert, F. Anton-Erxleben, R. Kiko, and M. Kramer (2009). *Sympagohydra tuuli* (Cnidaria, Hydrozoa): first report from sea ice of the central Arctic Ocean and insights into histology, reproduction and locomotion. *Mar. Biol.*, 156(4): 541–554. doi:10.1007/s00227-008-1106-9.

J. M. Sieburth, V. Smetacek, and J. Lenz (1978). Pelagic ecosystem structure: Heterotrophic compartments of the plankton and their relationship to plankton size fractions. *Limnol. Oceanogr.*, 23(6): 1256–1263.

M. Sieracki, P. Verity, and D. Stoecker (1993). Plankton community response to sequential silicate and nitrate depletion during the 1989 North-Atlantic spring bloom. *Deep-Sea Res. II*, 40(1-2): 213–225.

G. Skalski and J. Gilliam (2001). Functional responses with predator interference: Viable alternatives to the Holling Type II model. *Ecology*, 82(11): 3083–3092.

T. J. Smayda (1970). The suspension and sinking of phytoplankton in the sea. *Oceanogr. Mar. Biol. Annu. Rev.*, 8: 353–414.

B. Smith and J. Wilson (1996). A consumer's guide to evenness indices. *Oikos*, 76(1): 70–82.

U. Sommer (1984). The paradox of the plankton - fluctuations of phosphorus availability maintain diversity of phytoplankton in flow-through cultures. *Limnol. Oceanogr.*, 29(3): 633–636.

U. Sommer (1985). Comparison between steady state and non-steady state competition: Experiments with natural phytoplankton. *Limnol. Oceanogr.*, 30(2): 335–346.

U. Sommer (1995). An experimental test of the intermediate disturbance hypothesis using cultures of marine phytoplankton. *Limnol. Oceanogr.*, 40(7): 1271–1277.

U. Sommer (2002). Competition and coexistence in plankton communities. In U. Sommer and B. Worm (eds.), *Competition and Coexistence*, chap. 4, pp. 79–108. Springer-Verlag.

U. Sommer (2008). Trophic cascades in marine and freshwater plankton. *Int. Rev. Hydrobiol.*, 93(4-5): 506–516. doi:10.1002/iroh.200711039.

U. Sommer, H. Stibor, A. Katechakis, F. Sommer, and T. Hansen (2002). Pelagic food web configurations at different levels of nutrient richness and their implications for the ratio fish production: primary production. *Hydrobiol.*, 484(1-3): 11–20.

U. Sommer and B. Worm (2002). *Competition and Coexistence*, *Ecological Studies*, vol. 161. Springer-Verlag.

J. J. Stachowicz, J. F. Bruno, and J. E. Duffy (2007). Understanding the effects of marine biodiversity on communities and ecosystems. *Annu. Rev. Ecol. Evol. Syst.*, 38: 739–766. doi: 10.1146/annurev.ecolsys.38.091206.095659.

J. H. Steele (1998). Incorporating the microbial loop in a simple plankton model. *Proc. R. Soc. Lond. B*, 265(1407): 1771–1777. doi:10.1098/rspb.1998.0501.

J. H. Steele and E. W. Henderson (1992). The role of predation in plankton models. *J. Plankton Res.*, 14(1): 157–172. doi:10.1093/plankt/14.1.157.

J. H. Steele and E. W. Henderson (1993). The significance of interannual variability. In G. T. Evans and M. J. R. Fasham (eds.), *Towards a Model of Ocean Biogeochemical Processes*, *NATO ASI Series*, vol. I 10, pp. 237–260. Springer.

J. H. Steele and M. M. Mullin (1977). Zooplankton dynamics. In E. D. Goldberg, I. N. McCave, J. J. O'Brien, and J. H. Steele (eds.), *Marine Modeling*, *The Sea*, vol. 6, pp. 857–890. Wiley, New York.

M. Steinacher, F. Joos, T. L. Frölicher, et al. (2010). Projected 21st century decrease in marine productivity: A multi-model analysis. *Biogeosciences*, 7(3): 979–1005.

D. K. Steinberg, B. A. S. Van Mooy, K. O. Buesseler, et al. (2008). Bacterial vs. zooplankton control of sinking particle flux in the ocean's twilight zone. *Limnol. Oceanogr.*, 53(4): 1327–1338.

F. M. Stewart and B. R. Levin (1973). Partitioning of resources and the outcome of interspecific competition: A model and some general considerations. *Am. Nat.*, 107: 171–198.

G. Stirling and B. Wilsey (2001). Empirical relationships between species richness, evenness, and proportional diversity. *Am. Nat.*, 158(3): 286–299.

D. K. Stoecker (1984). Particle production by planktonic ciliates. *Limnol. Oceanogr.*, 29(5): 930–940. doi:10.4319/lo.1984.29.5.0930.

M. Striebel, S. Behl, S. Diehl, and H. Stibor (2009). Spectral niche complementarity and carbon dynamics in pelagic ecosystems. *Am. Nat.*, 174(1): 141–147. doi:10.1086/599294.

S. Strom and H. Loukos (1998). Selective feeding by protozoa: model and experimental behaviors and their consequences for population stability. *J. Plankton Res.*, 20(5): 831–846.

S. L. Strom (1991). Growth and grazing rates of the herbivorous dinoflagellate *Gymnodinium* sp. from the open subarctic Pacific Ocean. *Mar. Ecol. Prog. Ser.*, 78: 103–113. doi:10.3354/meps078103.

S. L. Strom, C. B. Miller, and B. W. Frost (2000). What sets lower limits to phytoplankton stocks in high-nitrate, low-chlorophyll regions of the open ocean? *Mar. Ecol. Prog. Ser.*, 193: 19–31.

S. L. Strom and T. A. Morello (1998). Comparative growth rates and yields of ciliates and heterotrophic dinoflagellates. *J. Plankton Res.*, 20(3): 571–584.

L. S. Svetlichny and E. S. Hubareva (2005). The energetics of *Calanus euxinus*: locomotion, filtration of food and specific dynamic action. *J. Plankton Res.*, 27(7): 671–682. doi:10.1093/plankt/fbi041.

K. M. Swadling, J. A. E. Gibson, D. A. Ritz, and P. D. Nichols (1997a). Horizontal patchiness in sympagic organisms of the Antarctic fast ice. *Antarct. Sci.*, 9(4): 399–406. doi:10.1017/S0954102097000515.

K. M. Swadling, J. A. E. Gibson, D. A. Ritz, P. D. Nichols, and D. E. Hughes (1997b). Grazing of phytoplankton by copepods in eastern Antarctic coastal waters. *Mar. Biol.*, 128(1): 39–48. doi:10.1007/s002270050066.

T. Takahashi, S. C. Sutherland, R. Wanninkhof, et al. (2009). Climatological mean and decadal change in surface ocean pCO_2, and net sea-air CO_2 flux over the global oceans. *Deep-Sea Res. II*, 56(8-10): 554–577. doi:10.1016/j.dsr2.2008.12.009.

J. Taucher and A. Oschlies (2011). Can we predict the direction of marine primary production change under global warming? *Geophys. Res. Lett.*, 38: L02 603. doi:10.1029/2010GL045934.

T. F. Thingstad, E. Strand, and A. Larsen (2010). Stepwise building of plankton functional type (PFT) models: A feasible route to complex models? *Prog. Oceanogr.*, 84(1-2): 6–15. doi:10.1016/j.pocean.2009.09.001.

D. Tilman (1977). Resource competition between planktonic algae: An experimental and theoretical approach. *Ecology*, 58: 338–348.

D. Tilman (2001). Functional diversity. In S. A. Levin (ed.), *Encyclopedia of Biodiversity*, pp. 109–120. Academic Press, San Diego, CA.

D. Tilman, C. Lehman, and K. Thomson (1997). Plant diversity and ecosystem productivity: Theoretical considerations. *Proc. Natl. Acad. Sci. USA*, 94(5): 1857–1861.

K. Tirok and U. Gaedke (2010). Internally driven alternation of functional traits in a multispecies predator-prey system. *Ecology*, 91(6): 1748–1762.

P. Tiselius (1998). Short term feeding responses to starvation in three species of small calanoid copepods. *Mar. Ecol. Prog. Ser.*, 168: 119–126.

P. Tiselius and P. R. Jonsson (1990). Foraging behaviour of six calanoid copepods: Observations and hydrodynamic analysis. *Mar. Ecol. Prog. Ser.*, 66: 23–33.

D. P. Tittensor, C. Mora, W. Jetz, et al. (2010). Global patterns and predictors of marine biodiversity across taxa. *Nature*, 466(7310): 1098–U107. doi:10.1038/nature09329.

C. R. Tomas (ed.) (1997). *Identifying marine phytoplankton*. Academic Press, San Diego.

B. B. Trenbarth (1974). Biomass productivity of mixtures. *Adv. Agron.*, 26: 177–210.

H. Utermöhl (1958). Zur Vervollkommnung der quantitativen Phytoplankton-Methodik. *Mitteilungen der Internationalen Vereinigung für Theoretische und Angewandte Limnologie*, 9: 1–38.

P. G. Verity and C. Langdon (1984). Relationships between lorica volume, carbon, nitrogen, and ATP content of tintinnids in Narragansett Bay. *J. Plankton Res.*, 6(5): 859–868.

J. Vidal (1980a). Physioecology of zooplankton. I. Effects of phytoplankton concentration, temperature, and body size on the growth rate of *Calanus pacificus* and *Pseudocalanus* sp. *Mar. Biol.*, 56(2): 111–134. doi:10.1007/BF00397129.

J. Vidal (1980b). Physioecology of zooplankton. III. Effects of phytoplankton concentration, temperature, and body size on the metabolic rate of *Calanus pacificus*. *Mar. Biol.*, 56(3): 195–202. doi:10.1007/BF00645343.

A. W. Visser (2001). Hydromechanical signals in the plankton. *Mar. Ecol. Prog. Ser.*, 222: 1–24.

A. W. Visser (2007). Motility of zooplankton: fitness, foraging and predation. *J. Plankton Res.*, 29(5): 447–461.

A. W. Visser, P. Mariani, and S. Pigolotti (2009). Swimming in turbulence: zooplankton fitness in terms of foraging efficiency and predation risk. *J. Plankton Res.*, 31(2): 121–133.

A. W. Visser and A. Stips (2002). Turbulence and zooplankton production: insights from PROVESS. *J. Sea Res.*, 47(3–4): 317–329. doi:10.1016/S1385-1101(02)00120-X.

T. Volk and M. I. Hoffert (1985). Ocean carbon pumps: Analysis of relative strengths and efficiencies in ocean–driven CO_2 changes. In E. T. Sundquist and W. S. Broecker (eds.), *The Carbon Cycle and Atmospheric CO_2: Natural Variations Archean to Present*, *Geophysical Monograph*, vol. 32. American Geophysical Union.

B. A. Ward, S. Dutkiewicz, A. D. Barton, and M. J. Follows (2011). Biophysical aspects of resource acquisition and competition in algal mixotrophs. *Am. Nat.*, 178(1): 98–112. doi:10.1086/660284.

J. J. Weis, B. J. Cardinale, K. J. Forshay, and A. R. Ives (2007). Effects of species diversity on community biomass production change over the course of succession. *Ecology*, 88(4): 929–939.

I. Werner (1997). Grazing of Arctic under-ice amphipods on sea-ice algae. *Mar. Ecol. Prog. Ser.*, 160: 93–99. doi:10.3354/meps160093.

I. Werner and H. Auel (2005). Seasonal variability in abundance, respiration and lipid composition of Arctic under-ice amphipods. *Mar. Ecol. Prog. Ser.*, 292: 251–262. doi:10.3354/meps292251.

I. Werner, H. Auel, and C. Friedrich (2002). Carnivorous feeding and respiration of the Arctic under-ice amphipod *Gammarus wilkitzkii*. *Polar Biol.*, 25(7): 523–530.

I. Werner, J. Ikävalko, and H. Schünemann (2007). Sea-ice algae in Arctic pack ice during late winter. *Polar Biol.*, 30(11): 1493–1504. doi:10.1007/s00300-007-0310-2.

S. A. Wickham and U.-G. Berninger (2007). Krill larvae, copepods and the microbial food web: interactions during the Antarctic fall. *Aquat. Microb. Ecol.*, 46(1): 1–13.

E. Wlodarczyk, A. G. Durbin, and E. G. Durbin (1992). Effect of temperature on lower feeding thresholds, gut evacuation rate, and diel feeding behavior in the copepod *Acartia hudsonica*. *Mar. Ecol. Prog. Ser.*, 85: 93–106. doi:10.3354/meps085093.

J. Wohlers, A. Engel, E. Zöllner, et al. (2009). Changes in biogenic carbon flow in response to sea surface warming. *Proc. Natl. Acad. Sci. USA*, 106(17): 7067–7072. doi:10.1073/pnas.0812743106.

B. Worm, E. B. Barbier, N. Beaumont, et al. (2006). Impacts of biodiversity loss on ocean ecosystem services. *Science*, 314(5800): 787–790. doi:10.1126/science.1132294.

B. Worm, H. Lotze, H. Hillebrand, and U. Sommer (2002). Consumer versus resource control of species diversity and ecosystem functioning. *Nature*, 417(6891): 848–851.

C.-J. Wu, K.-P. Chiang, and H. Liu (2010). Diel feeding pattern and prey selection of mesozooplankton on microplankton community. *J. Exp. Mar. Biol. Ecol.*, 390(2): 134–142. doi: 10.1016/j.jembe.2010.05.003.

C. Wunsch and P. Heimbach (2007). Practical global oceanic state estimation. *Physica D*, 230(1-2): 197–208. doi:10.1016/j.physd.2006.09.040.

S. Yachi and M. Loreau (1999). Biodiversity and ecosystem productivity in a fluctuating environment: The insurance hypothesis. *Proc. Natl. Acad. Sci. USA*, 96(4): 1463–1468.

A. Yool, E. E. Popova, and T. R. Anderson (2011). MEDUSA: a new intermediate complexity plankton exosystem model for the global domain. *Geosci. Model Dev.*, 4: 381–417. doi:10.5194/gmd-4-381-2011.

E. Zöllner, H.-G. Hoppe, U. Sommer, and K. Jürgens (2009). Effect of zooplankton-mediated trophic cascades on marine microbial food web components (bacteria, nanoflagellates, ciliates). *Limnol. Oceanogr.*, 54(1): 262–275.

List of Figures

List of Tables

Acknowledgements - Danksagung

I am very grateful — Ich bin sehr dankbar —
to Andreas Oschlies for being a Doktorvater to me throughout a long journey.

to Markus Pahlow for always having time for questions, more questions, and the same questions again; for many insights into a complicated world of modelling, marine science, and other things; for guidance, advice, encouragement; and for turning me from a student into a colleague.

to Nora Kemmler for not only being the best office mate I could have ever dreamt of, but for being a friend to share what people don't tell you before what a PhD is about.

to Iris Kriest, Lavinia Patara, Maike Kramer and Nuno Nunes for proof-reading, encouragement, and an open ear.

to Bei Su, Markus Pahlow, Nora Kemmler and Nuno Nunes for lunch.

to Oliver Jahn for answering questions, helping with code, going for lunch, and convincing me that dancing is great.

to Stephanie Dutkiewicz, Mick Follows, and the MIT crew for welcoming me on board, for ideas, answers, and motivation, and for sharing their model ocean.

to Helmuth Thomas for setting a good example not only in science, and for keeping track of the beer dues.

to Björn Fiedler and Paulchen for living the love of the sea with me.

to the Werftteam, Carola and Zuversicht for another life far away from the desk with problems that one can fix with a bit of wood or string or paint.

to my sister Ellen for not doing a PhD just now, hence having all feet on the ground.

meinen Eltern die mit mir viele Jahre im Sommer an die Ostsee gefahren sind.

and to the fg for most of the above, and much of what remains when you subtract a PhD from life. But most of all, for the tigergoose.

Erklärung

Die vorliegende Arbeit ist - abgesehen von der Beratung durch meine Betreuer - nach Inhalt und Form meine eigene Arbeit. Sie hat weder ganz noch in Teilen bereits an anderer Stelle im Rahmen eines Prüfungsverfahrens vorgelegen. Diese Arbeit ist unter Einhaltung der Regeln guter wissenschaftlicher Praxis der Deutschen Forschungsgemeinschaft entstanden.

Kiel, den 11. November 2011

Friederike Prowe